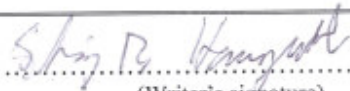




University of
Stavanger

Faculty of Science and Technology

MASTER'S THESIS

Study program/ Specialization: PETROLEUM ENGINEERING / DRILLING	SPRING 2011 RESTRICTED ACCESS
Writer: STIG-BJØRAN HAUGSTAD	 (Writer's signature)
Faculty supervisor: BERNT S. AADNØY, UNIVERSITY OF STAVANGER	
External supervisor(s): MICHAEL COLLINS, SHELL DEVELOPMENT (AUSTRALIA)	
Titel of thesis: WELL DESIGN CONSIDERATIONS FOR CO ₂ INJECTION AT PRELUDE	
Credits (ECTS): 30	
Key words: CO ₂ injection, Prelude, corrosion, CO ₂ corrosion, acid resistant cement, equation of state, elastomers, annulus fluid, Joule- Thomson cooling	Pages:178 Perth, 15th of June 2011 Date/year

Acknowledgment

This thesis was written by:

Stig-Bjørn Haugstad

stig.b.haugstad@gmail.com / stig.haugstad@shell.com

The project advisor was:

Michael Collins

Head of Well Delivery Australia

Shell Development (Australia) Pty. Ltd.

The scientific advisor was:

Bernt Sigve Aadnøy

Professor

University of Stavanger – Department of Petroleum Engineering

I would like to express my sincere gratitude to the University of Stavanger and its staff for providing quality education. Further, the work experience I have received through Shell have been a real motivator and would like to thank all individuals within Shell that have provided feedback and thoughts regarding work presented within this thesis.

Disclaimer

This thesis is an independent work by Stig-Bjørn Haugstad supported and aided by individuals within the Shell group. All possible errors and omissions in this paper are the sole responsibility of the author.

Due to the sensitivity of the data in this report a confidentiality agreement between University of Stavanger, Shell Development Australia Pty Ltd , and the author Stig-Bjørn Haugstad have been signed. This agreement lays a five-year restriction on publishing this thesis or any information contained within it running from 15.06.2011-15.06.2016.

Summary

The global economy is set to grow four-fold by 2050, promising economic benefits and a higher standard of living for millions. At the same time the global community is uniting in an effort to combat global warming. Achieving both goals will require energy to be harvested from sustainable resources. Australia, producing most of its electricity from coal, can achieve this through a switch to natural gas, in which it has a large resource base. However, most natural gas resources contain a portion CO₂ which will cause large emissions. Geo-sequestration is recognized as safe mean of control and through implementation of both; a double environmental benefit can be achieved.

Prelude is a gas condensate field located in Western Australia, operated by Shell Development Australia. The field is planned to be developed as a floating LNG facility. Containing 9% CO₂ it will give significant emission. The sensitivity of the emissions has prompted Shell to look at reduction measures. One such measure is re-injection into the reservoir in which the CO₂ originated.

There is currently much focus on deep saline formation as these offers the largest theoretical storage potential. However, injecting into existing gas fields offer significant advantages through proven capacity and sealing structure, limiting the leak risk to wells penetrating the cap rock.

CO₂ injection is not new to the industry and have been used for EOR since the 1970's. However, injection at Prelude is more complex in two aspects:

- The pressure and temperature is much higher than the current experience with CO₂ injection.
- The well is located subsea in a remote location.

To date there is only one operational subsea CO₂ injector, Snøhvit, and injection generally commences at shallower depth than what is the case at Prelude. Well design at Prelude is thus pushing the envelope and it is necessary to investigate the significance.

Challenges and gaps were identified through investigating the current body of knowledge and by modelling the well through its lifecycle. Most challenges relates to the corrosive environment posed by CO₂ in combination with water. If a water free system cannot be guaranteed, aggressive corrosion of carbon steel will take place, necessitating CRA's.

The degradation of Portland cement is likely slow, being diffusion controlled. However, mechanically induced fractured can cause rapid loss of sealing capability. A more robust solution is obtained through acid resistant cements that are practically inert to CO₂ attack.

Another identified area of concern was elastomers, as they are generally optimized for service with hydrocarbons. To prevent swelling, the solubility parameter of the elastomer and the fluid of which it is in contact, should be 1-2 units. With CO₂ and HC having widely different parameters, this is hard to obtain. Selection of elastomers is therefore a trade-off between physical and chemical properties.

Large temperature drops were observed during operations involving pressure drops. This phenomenon is caused by Joule-Thomson cooling and observed to increase in severity with decreasing reservoir pressure. Massive temperature drops can have serious consequences but can be controlled through operational procedures.

The identified gaps are related to modelling capabilities and measurements at the high pressure and temperatures observed at Prelude. Current modelling software lack capabilities in predicting thermodynamics of CO₂ accurately, which is important for determining the loads exerted on the well and for selection of materials. Because most software are designed and developed for hydrocarbons, they lack a fit-for-purpose equation of state for CO₂ mixtures with impurities. Corrosion modelling is found to be limited to 50 bar partial pressure CO₂, and there is a lack of measurement data beyond this limit.

The challenges and gaps identified are not anticipated to be a showstopper for inclusion of CO₂ injection at Prelude.

Table of Contents

Acknowledgment	III
Disclaimer	III
Summary	IV
List of Figures	XI
List of Tables	XIII
Chapter 1	1
Introduction	1
1.1 Background	1
1.2 Scope of Work.....	2
1.3 Project Boundaries and Assumptions	2
1.4 Shell ORP	2
1.5 Report Rationale and Structure	3
1.6 Prelude Value Drivers.....	4
Chapter 2	5
Prelude CO₂ Geo-Sequestration	5
2.1 Objectives.....	5
2.2 Methodology.....	5
2.3 Prelude Development Overview	5
2.4 Prelude CO ₂ Geo-Sequestration.....	7
2.5 Integrated Geo-Sequestration System.....	9
2.6 Reservoir	10
2.7 Production Wells.....	10
2.8 Subsea System, Riser, Swivel and Turret	10
2.9 Topside.....	11
2.10 Injection System.....	11
2.11 Start-Up & Shut-Down	11
2.12 Well & Reservoir Management.....	12
2.13 Existing Wells	12
2.14 Monitoring	12
2.15 Stakeholders and Regulatory Landscape	12
2.16 Conclusion.....	12

Chapter 3	13
Evaluation of Industry Experience	13
3.1 Objectives.....	13
3.2 Methodology.....	13
3.3 Commercial CO ₂ Geological Storage Operations	13
3.3.1 K12-B	13
3.3.2 Gorgon.....	15
3.3.3 Sleipner.....	16
3.3.4 Snøhvit.....	18
3.3.5 In Salah	18
3.4 Acid-Gas Injection	19
3.5 Enhanced Oil Recovery Projects	19
3.6 Other Injection Schemes.....	21
3.6.1 Natural Gas Storage	21
3.6.2 Liquid Waste Disposal	21
3.7 Conclusion.....	22
Chapter 4	25
Key Parameters.....	25
4.1 Objectives.....	25
4.2 General.....	25
4.3 Injection Fluid Properties.....	25
4.4 Subsurface and Environmental Properties	26
Chapter 5	27
Pressure & Temperature Predictions.....	27
5.1 Objectives.....	27
5.2 Methodology.....	27
5.3 CO ₂ Properties and Behavior	27
5.4 Numerical Simulation of CO ₂ Flows	31
5.4.1 <i>Effect of Impurities</i>	32
5.4.2 <i>Well Performance Simulations</i>	33
5.4.3 <i>Enthalpy Balance</i>	36
5.5 Tubing Size	39

5.6 Deviation	40
5.7 Operating Pressure	41
5.8 Operating Temperature	41
5.9 Operating Envelope	42
5.10 Steady-State Behavior with Time.....	42
5.10.1 <i>Quality Control of Model</i>	43
5.11 Closed In Tubing Head Pressure (CITHP).....	44
5.12 Transient Temperature Analysis	47
5.10.1 <i>Emergency Shut-down</i>	47
5.10.2 <i>Close-In and Start-Up</i>	49
5.13 Injection Under Matrix or Fracturing Conditions.....	50
5.14 Conclusion and Recommendation	51
Chapter 6	52
Material Selection.....	52
6.1 Objectives.....	52
6.2 Methodology.....	52
6.3 The Free Water Issue	52
6.3.1 <i>Hydrates</i>	54
6.4 Cement.....	56
6.4.1 Chemical Degradation of Cement	57
6.4.2 Degradation Rates.....	61
6.4.3 Field Experience	64
6.4.5 Mechanical Considerations	65
6.4.6. Selection of Cement System	66
6.4.7 Conclusion & Recommendation.....	67
6.5 Steel	68
6.5.1 Carbon Dioxide Corrosion	68
6.5.2 Injection Well Metallurgy Assessment.....	76
6.5.3 Selection of Metallurgy	88
6.5.4 Conclusion & Recommendation.....	89
6.6 Elastomers.....	90
6.6.1 Degradation of Elastomers.....	92

6.6.2 Selection of Elastomers	92
6.6.3 Conclusion & Recommendation	93
6.7 Packer Fluid	94
6.7.1 Introduction	94
6.7.2 Selection of Packer Fluid	94
6.7.3 Conclusion & Recommendation	97
6.8 Chapter Conclusion	98
Chapter 7	99
Well Hardware Selection	99
7.1 Objectives	99
7.2 Methodology	99
7.3 Selection of Lower Completion	99
7.3.1 Requirement for Sand Control	99
7.3.2 Screening for Lower Completion	108
7.3 Inverted Well	115
7.4 Packer	116
7.5 PDHG	116
7.6 Safety Valve	117
7.6.1 Safety Valve Testing	117
7.7 X-mas Tree	117
7.8 Conclusion & Recommendation	118
Chapter 8	119
Other Considerations	119
8.1 Objectives	119
8.2 Methodology	119
8.3 Operating the Well	119
8.4 Adjacent Wells	121
8.5 Well Monitoring	121
8.6 Conclusions & Recommendations	124
Chapter 9	125
Tubing Stress Analysis	125
9.1 Objectives	125

9.2 Methodology.....	125
9.3 Design Assumptions.....	125
9.4 Modelling CO ₂ in WellCat.....	126
9.5 Design Load Cases.....	127
9.5.1 Thermal Operations.....	127
9.5.2 Load Cases for Tubing.....	128
9.6 Failure Criteria.....	130
9.7 Results from Load Analysis.....	132
9.8 Safety Factor Plots.....	134
9.9 Conclusion & Recommendation.....	136
Chapter 10.....	137
HSE issues related to CO₂ Injection.....	137
10.1 Objectives.....	137
10.2 Methodology.....	137
10.3 Discussion.....	137
10.4 Conclusion.....	139
Chapter 11.....	140
Conclusion & Recommendations.....	140
Abbreviations.....	142
References.....	143
Appendix A: Software Description.....	147
Prosper.....	147
WellCat.....	147
FIST.....	147
Appendix B: Prosper Input.....	148
Appendix C: Basic Model for Annular Pressure Buildup [78].....	159
Appendix D: Well Schematic.....	163

List of Figures

FIGURE 1.1: THE SHELL OPPORTUNITY REALIZATION PROCESS.	3
FIGURE 2.1: PRELUDE FIELD LOCATION.....	5
FIGURE 2.2: PRELUDE SUBSEA DEVELOPMENT. [4]	6
FIGURE 2.3: PRELUDE, CRUX REF. CASE PRODUCTION PROFILES (CO ₂ CONSTRAINED). [5]	7
FIGURE 2.4: LITO-STRATIGRAPHIC COLUMN FOR THE EAST BROWSE BASIN	8
FIGURE 2.5: INTEGRATED PRELUDE GEO-SEQUESTRATION SYSTEM	9
FIGURE 3.1: TIME LAPSE PIT DEPTH CHART OF THE INJECTION TUBING OF WELL K12-B6 [15].....	13
FIGURE 3.2: MAP OF THE TOP RESERVOIR DEPICTING COMPARTMENTS, INJECTION AND PRODUCTION WELLS DIRECTLY INVOLVED IN THE INJECTION OF CO ₂ AT K12-B [15].	14
FIGURE 3.3: SIMPLIFIED DIAGRAM OF THE SLEIPNER CO ₂ STORAGE PROJECT[17].....	16
FIGURE 3.4: TIME-LAPSE DATASET VISUALIZING THE SPREAD OF THE INJECTED CO ₂ IN THE UTSIRA FORMATION SLEIPNER [17].....	17
FIGURE 3.5: INJECTION WELL DESIGN AND PERFORATION INTERVAL [20].	17
FIGURE 3.6: SCHEMATIC OF CO ₂ STORAGE AT KRECHBA [24].	18
FIGURE 5.1: PHASE DIAGRAM OF CO ₂ . [27].....	28
FIGURE 5.2: CO ₂ DENSITY AS A FUNCTION OF TEMPERATURE AND PRESSURE[27].....	29
FIGURE 5.3: VARIATION IN CO ₂ VISCOSITY AS A FUNCTION OF TEMPERATURE AND PRESSURE[27].	29
FIGURE 5.4: JT COEFFICIENT OF CO ₂ [29].....	30
FIGURE 5.5: SCHEMATIC DESCRIPTION OF IMPURITIES EFFECT UPON WELL DESIGN AND OPERATION.	32
FIGURE 5.6: COMPARISON BETWEEN VALUES CALCULATED BY PROSPER (PR) AND REFPROF FROM NIST.	33
FIGURE 5.7: TUBING SIZE SENSITIVITY MODELLING.	39
FIGURE 5.8: WELL DEVIATION AND INJECTION PRESSURE FOR RATE OF 93 MMSCF/D.	40
FIGURE 5.9: OPERATING ENVELOPE FOR WELL.....	42
FIGURE 5.10: FLUID BOTTOMHOLE TEMPERATURE WITH TIME.....	43
FIGURE 5.11: TEMPERATURE AS FUNCTION OF TIME FOR HYPOTHETICAL CASE OF 1 MMSCF/D INJECTION RATE.....	44
FIGURE 5.12: CITHP VARIATION WITH CHANGE IN RESERVOIR PRESSURE.	45
FIGURE 5.13: LIQUID DEPTH IN THE WELL DURING CLOSED-IN CONDITION FOR DIFFERENT RESERVOIR PRESSURES.	45
FIGURE 5.14: DENSITY VARIATION IN THE WELL DURING CLOSED IN CONDITION FOR DIFFERENT RESERVOIR PRESSURE.	46
FIGURE 5.15: MIXTURE DENSITY AS A FUNCTION OF DEPTH WHEN THE RESERVOIR PRESSURE IS 136 BAR AND HAS A TEMPERATURE OF 155°C.....	47
FIGURE 5.16: CONSERVATIVE APPROACH TO ESD OF JT COOLING IN THE INJECTOR.	48
FIGURE 5.17: EXPECTED CHOKE PERFORMANCE AND CONDITIONS UPSTREAM OF THE CHOKE AT RESERVOIR PRESSURE 136 BAR.....	49
FIGURE 5.18: INJECTION PRESSURE COMPRESSOR MAX.	50
FIGURE 6.1: MUTUAL SOLUBILITIES OF H ₂ O AND CO ₂ AT 35, 40, 60, AND 75°C AND PRESSURES TO 600 BAR[41]. Y-AXIS SHOW Y H ₂ O IN PPM [41].	53
FIGURE 6.2: HYDRATE STABILITY IN THE PRESENCE OF DISTILLED WATER [42]	54
FIGURE 6.3: PRESSURE VS. TEMPERATURE PROFILE OF TUBING FLUID DURING SHUT-IN FOR EARLY AND LATE LIFE PLOTTED AGAINST THE HYDRATE CURVE FOR PURE CO ₂ OBTAINED FROM [42].	55
FIGURE 6.4: SCHEMATIC OF POSSIBLE LEAKAGE PATHWAYS THROUGH AN ABANDONED WELL (A) BETWEEN CASING AND CEMENT (B) BETWEEN CEMENT PLUG AND CASING (C) THROUGH THE CEMENT PORE SPACE (D) THROUGH THE CASING (E) THROUGH FRACTURES IN CEMENT (F) BETWEEN CEMENT AND ROCK [43].....	56
FIGURE 6.5: ILLUSTRATION OF THE DIFFERENT ZONES DUE TO THE CHEMICAL REACTIONS OCCURRING IN THE CEMENT CORE. ZONE 1– DISSOLUTION OF Ca(OH) ₂ . ZONE 2-PRECIPIATION OF CaCO ₃ . ZONE 3-DISSOLUTION OF CaCO ₃ AND DECALCIFICATIONS OF C-S- H. KUTCHKO ET AL. (2007) [23]	58
FIGURE 6.6: CARBONATION DEPTH (MM) VS TIME ^{1/2} (DAYS ^{1/2}) AT 50°C, KUTCHKO EL AL. (2008) [23]	61
FIGURE 6.7: CARBONATION DEPTH (MM) VS TIME (DAYS) AT 50°C, KUTCHKO EL AL. (2008) [23].....	61
FIGURE 6.8: RATE OF CARBONATION FOR PORTLAND CEMENT, BARLET-GOUEDARD ET AL. (2006) [33]	61

FIGURE 6.9: EXPERIMENTAL SETUP FOR TESTING CEMENT AT SUPERCRITICAL CO ₂ CONDITIONS BARLET-GOUEDARD ET AL. (2006) [48]	.61
FIGURE 6.10: THE CARBONATION DEPTH (MM) VERSUS TIME (DAYS) AT 50°C AND 90°C, BASED ON RESULTS FROM KUCHKOV ET AL. (2008) AND BARLET-GOUEDARD ET AL. (2006, 2008) [23]	.62
FIGURE 6.11: THE CARBONATION DEPTH (MM) VERSUS TIME (DAYS) AT 50°C AND 90°C, BASED ON RESULTS FROM KUCHKOV ET AL. (2008) AND BARLET-GOUEDARD ET AL. (2008) [23]	.63
FIGURE 6.12: CORROSION RATE AS A FUNCTION OF CHROMIUM CONTENT [35]	.71
FIGURE 6.13: EFFECT OF H ₂ S CONCENTRATION IN A SLIGHTLY SOUR ENVIRONMENT [56]	.72
FIGURE 6.14: EFFECT OF TEMPERATURE ON CORROSION RATE OF STEELS IN THE SYSTEM. 450G CO ₂ /1000G H ₂ O [64]	.74
FIGURE 6.15: FIRST PASS MATERIAL SELECTION [35]	.76
FIGURE 6.16: NACE MR 0175 SOUR SERVICE DEFINITION [35]	.80
FIGURE 6.17: SAFE OPERATING ENVELOPE FOR 13CR STAINLESS STEEL IN SWEET SERVICE (BASED ON LIMITING CORROSION RATE OF 0,05 MM/YR) [57]	.82
FIGURE 6.18: API L80 13CR; SULPHIDE STRESS CRACKING (RED); RESISTANT (GREEN), AND YELLOW REPRESENTS CONDITIONS REQUIRING FURTHER CHECKING OF ALLOY BEHAVIOR. ISO 151156-3 LIMITS SHOWN BY HEAVY BLACK LINES [57]	.82
FIGURE 6.19: DIMENSIONAL SSC SUSCEPTIBILITY DIAGRAMS OF A SUPER 13% Cr SS (SPECIMENS WERE STRESSED AT 90% AYS) [57]	.83
FIGURE 6.20: LIMITS OF USE OF AISI 316L STAINLESS STEEL IN SWEET ENVIRONMENTS.	.84
FIGURE 6.21: TEMPERATURE LIMITS FOR DUPLEX STAINLESS STEELS AS A FUNCTION OF SODIUM CHLORIDE CONCENTRATION (<0,05 MM/YR CORROSION AND NO SCC OR SSC) [57]	.85
FIGURE 6.22: SAFE OPERATING ENVELOPE OF 22CR DUPLEX STAINLESS STEELS IN CO ₂ ENVIRONMENTS CONTAINING H ₂ S AND CHLORIDE IONS [57]	.86
FIGURE 6.23: SAFE OPERATING ENVELOPE OF 25CR DUPLEX STAINLESS STEELS IN CO ₂ ENVIRONMENTS CONTAINING H ₂ S AND CHLORIDE [57]	.86
FIGURE 7.1: CONCEPTUAL FIST DIAGRAM, SHOWING TENDENCIES FOR SAND AT A SPECIFIC DEPTH [82]	.101
FIGURE 7.2: ILLUSTRATION OF THE SAND PRONE PLOT SHOWING DIFFERENT SANDING TENDENCIES FOR DIFFERENT DEPTHS IN THE COMPLETION INTERVAL [82]	.103
FIGURE 7.3: INITIAL SAND FAILURE PROFILE FOR SIZE EFFECT FACTOR 2. (OPEN HOLE- FIRST YEAR OF INJECTION)[83]	.105
FIGURE 7.4: INITIAL SAND FAILURE PROFILE FOR SIZE EFFECT FACTOR 2 (OPEN HOLE - LATE INJECTIONLIFE) [83]	.105
FIGURE 7.5: INITIAL SAND FAILURE PLOT FOR SIZE EFFECT FACTOR 2.5 (OPEN HOLE - FIRST YEAR OF INJECTION) [83]	.106
FIGURE 7.6: PRELUDE CO ₂ INJECTOR – SANDFACE SCREENING CRITERIA.	.110
FIGURE 7.7: INJECTION PRESSURE FOR DIFFERENT COMPLETIONS FOR GOOD, BAD AND BASE CASE INJECTING AT 93 MMscf/d.	.112
FIGURE 7.8: SENSITIVITY FOR OHGP PARAMETERS.	.114
FIGURE 7.9: AS A FUNCTION OF TEMPERATURE AT 137 BAR [NIST].	.114
FIGURE 8.1: WH COMPONENT TEMPERATURE VARIATION FOR CLOSE-IN AND START-UP SCENARIOS INSTANTANEOUS, 1/2 HOUR, 1 HOUR AND 2 HOURS [92].	.120
FIGURE 8.2: SCHEMATIC OF PRIMARY MIGRATION & SEEPAGE PATHWAYS [93].	.122
FIGURE 9.1: WELLBORE DENSITY WELLCAT VS. NIST.	.127
FIGURE 9.2: DIFFERENTIAL PLOT FOR THE DIFFERENT LOAD CASES.	.132
FIGURE 9.3: 7" SM25-CRW # 34.228 KG/M PRODUCTION TUBING – VME PLOT.	.133
FIGURE 9.4: 7" SM25-CRW # 38.692 KG/M PRODUCTION TUBING – VME PLOT.	.133
FIGURE 9.5: TRIAXIAL SAFETY FACTOR PLOT FOR 25CrW -110 # 26 TUBING.	.134
FIGURE 9.6: BURST SAFETY FACTOR PLOT FOR SM25CRW -125 # 38.691 KG/M TUBING.	.135
FIGURE 9.7: COLLAPSE SAFETY FACTOR PLOT FOR SM25CRW -125 # 38.691 KG/M TUBING.	.135
FIGURE 9.8: AXIAL SAFETY FACTOR PLOT FOR SM25CRW -125 # 38.691 KG/M TUBING.	.136

List of Tables

TABLE 3.1: COMMONLY USED MATERIALS IN CO ₂ INJECTION WELL DESIGN AND CONSTRUCTION – USA PROJECTS [13].	20
TABLE 3.2: COMPARING CHARACTERISTICS OF CO ₂ GEOLOGICAL STORAGE TO OTHER INJECTION TYPES (GREEN = COMPARABLE, RED = NOT COMPARABLE, YELLOW = COMPARABLE IN SOME ASPECTS). WELL NUMBERS, INJECTION RATES AND VOLUMES ARE "SITE SCALE" AND REFER TO A SINGLE OPERATION [17].	24
TABLE 4.1: RESERVOIR PROPERTIES.	26
TABLE 5.1: SUGIANTO (2007) ERROR FOR DENSITY [33].	31
TABLE 5.2: INJECTION PRESSURE. ROUNDED TO NEAREST BAR.	41
TABLE 5.3: INJECTION TEMPERATURE. ROUNDED TO NEAREST °C.	41
TABLE 5.4: JT COOLING.	49
TABLE 6.1: CO ₂ RESISTANT CEMENTS.	60
TABLE 6.2: MAIN DIFFERENCES BETWEEN EXPERIMENTS OF BARLET-GOUEDARD ET AL. (2006) AND KUCHKOV ET AL. (2008) [49].	62
TABLE 6.3: PARTIAL PRESSURE CO ₂ AND H ₂ S.	77
TABLE 6.4: CORROSION MODELS [65, 66].	78
TABLE 6.5: INPUT TO NORSOK M-506.	79
TABLE 6.6: CORROSION RATE AND WALL THICKNESS LOSS ESTIMATION STATIC CONDITION.	79
TABLE 6.7: CORROSION RATE AND WALL THICKNESS LOSS ESTIMATION FLOWING CONDITION.	79
TABLE 6.8: SAFE OPERATING LIMITS 15/12/2007 [57].	84
TABLE 6.9: CORROSION THREATS FOR TUBING AND COMPLETION COMPONENTS.	88
TABLE 6.10: FEASIBILITY OF COMMON METALS.	89
TABLE 6.11: METALLURGY RECOMMENDATION.	89
TABLE 6.12: COMMON ELASTOMERS [35].	91
TABLE 6.13: COMPARISON BETWEEN N ₂ CUSHION OR NOT IN THE A-ANNULUS.	97
TABLE 8.1: SUMMARY OF IN-WELL DIRECT AND INDIRECT MONITORING TECHNIQUES [25].	123
TABLE 10.1: ACUTE HEALTH EFFECTS CAUSED BY HIGH CONCENTRATIONS OF CO ₂ [26].	138

Chapter 1

Introduction

As a conclusion to the master degree in Petroleum Engineering (Master of Science) at the University of Stavanger, the last semester consist of writing an independent master's thesis. This work is finalized and presented in this document.

1.1 Background

The global economy is set to grow four-fold by 2050. This promises economic benefits and a higher standard of living for millions. However, it also brings challenge in terms of greenhouse gas releases. The International Energy Agency has constructed different scenarios forecasting the CO₂ emissions towards 2050. In the Blue scenario (50% reduction) carbon capture and storage (CCS) represent 19% of total reduction.

On a per capita scale, Australia is one of the largest greenhouse gas emitters globally. This is largely due to a heavy reliance on coal for power generation. At the same time Australia aiming at being a heavyweight within CCS, and was the first country in the world to released acreage for commercial CCS (2008). However, politically it has proven hard to get emissions trading through parliament with three unsuccessful efforts by the Kevin Rudd government.

On the 24th of February 2011 the carbon tax was once again put on the agenda by the current Prime Minister, Julia Gillard. Since then the debate on a carbon tax has dominated the news picture. Currently, there is far more opposition to a carbon tax than there is support. A newspoll presented in 'The Australian' newspaper reviled that almost 60% of voters opposed the tax.

Shell is one of the major companies in Australia supporting the carbon tax initiative, with the following statement from Ann Pickard, Country Chair, Shell Australia:

"The company has long been an advocate for progressive policies to tackle climate change, to ensure positive environmental outcomes, while not adversely impacting on Australia's prosperity.

Shell believes a carbon pricing system should encourage investment in the technological developments needed to raise energy efficiency and lower CO₂ emissions, without distorting international competition."

Natural gas fields in Australia contains up to 26% CO₂ thus it is likely that future project will have to implement CCS or other carbon reducing actions. Shell recently passed FID for the Prelude field containing 9% CO₂. Implementing CCS for Prelude was one option considered. However, there are technical and economic barriers for implementing CCS in an offshore-subsea environment. Currently, only one subsea injection well is operated globally, Snøhvit Norway.

Based upon the experience from miscible fluid injection for the purpose of tertiary oil recovery, combined with the general experience of gas re-injection and gas production internationally, there is a tendency in the CCS industry to believe that everything is already known about CO₂ injection wells. Analyses of the technical issues have however identified CO₂ injection wells to be even more challenging in a several aspects. This includes the fluids and pressures that they must handle and the long term duration in which full well integrity is expected.

In designing a well, consideration has to be given to all the different scenarios it will phase during construction, operation, suspension and ultimate abandonment. Similar considerations must given CO₂ injection wells for sequestration. However, with a operational design often 40+ years followed by the need for continued integrity for a planned abandonment for 1000+ years, it is evident that correct design, especially in terms of selected material used in the well is of utmost importance [1].

1.2 Scope of Work

The thesis aims at presenting the main challenges identified for geo-sequestration into the main gas bearing formation at Prelude. After presentation of main challenges, the focus will be shifted to well design, where the objectives are as follows:

- Review current industry experience with CO₂ injection and assess applicability to Prelude.
- Identify and describe challenges related to CO₂ injection.
- Examine the criticality of the challenges identified.
- Give recommendation regarding material selection.
- Give recommendation regarding well hardware selection.
- Identify areas requiring further work.

1.3 Project Boundaries and Assumptions

The focus of this thesis is well design for CO₂ injection. The casing design is considered to be the same as for the Prelude development wells, and have not been given any considerations. Geomechanical and geochemical interactions and the effect on injection have not been considered.

Material selection is a key element in design of CO₂ injection wells. Different projects will have different impurities, depending on source and capture technology. This work only considers impurities observed in the Prelude CO₂ stream, which is described in [Chapter 4](#).

1.4 Shell ORP

The Shell Opportunity Realization Process (ORP) is a framework used by Shell to manage opportunities. It is a management standard to help projects mature towards decision faster, and have on a high level been the framework for the work presented in this thesis.

In the ORP opportunities are developed through six phases (Figure 1.1 below). Each phase has a clear milestones, decision gates, activities, deliverables, and decision requirements. Critical to the ORP is the recognition of processes that are part of divergent thinking, and the process that involves convergent thinking. The first two phases A) Identify, and B) Assess, are part of the divergent thinking and should therefore be wide and shallow, identifying all options. In the later stages (C-F) the focus changes from identification to value delivery. The last phases should select and define the potential outcomes, and

thus requires convergent thinking to eliminate non-feasible options. A complete opportunity realization process will run the full project life, and therefore not all processes of the ORP will be eligible for this thesis. In correspondence with the scope of this thesis, the processes A and B will be the main focus, additionally entering into the select phase (C) for some aspects.

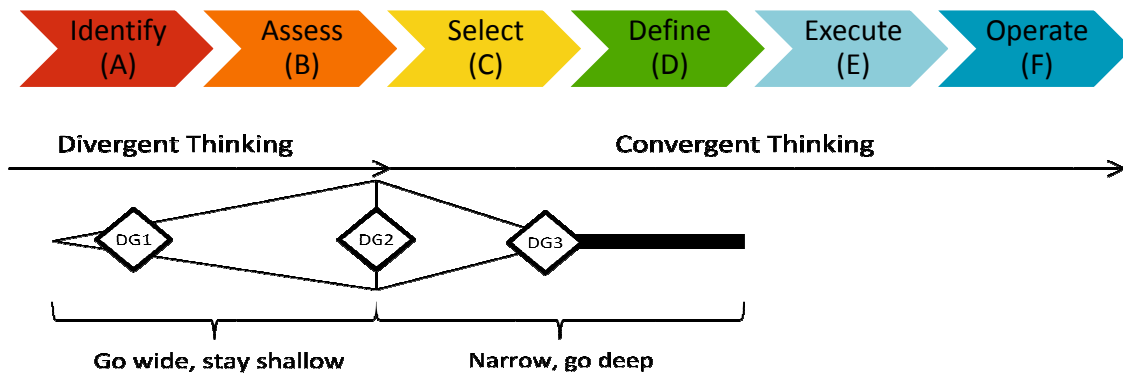


Figure 1.1: The Shell opportunity realization process.

1.5 Report Rationale and Structure

The thesis start by introducing the Prelude field development and identified challenges for geo-sequestration into the gas bearing formation. Then the current industry experience and its applicability to Prelude are reviewed.

Following, the key parameters are used to establish the operating envelope, which is needed for assessment of materials and well hardware in the proceeding chapters.

To assess the accuracy of the well design software used within Shell, a tubing design analysis was performed and results are presented in Chapter 9.

HSE issues are presented in Chapter 10,

Finally in Chapter 11 conclusions on material selection and challenges is offered in conjunction with gaps in current knowledge.

1.6 Prelude Value Drivers

Value drivers for the Prelude project:

- HSE
- Robustness
- Repeatability
- Availability & reliability
- NPV/VIR (driven by cost, schedule, production and availability)
- Flexibility
- Schedule certainty
- Capex certainty
- Ultimate hydrocarbon recovery

Chapter 2

Prelude CO₂ Geo-Sequestration

2.1 Objectives

The objectives of this chapter is to give an introduction to the Prelude development project, the geo-sequestration option for Prelude and a short introduction to the challenges that have been identified,

2.2 Methodology

The adapted methodology was reviewing of Shell internal documents.

2.3 Prelude Development Overview

In early 2007, Shell Development Australia (SDA) discovered a gas-condensate accumulation in Exploration Permit WA-371-P. The permit is located in the northern Browse Basin, approximately 475 km NNE of Broome in water depth of about 250 m. Recoverable reserves is estimated to be between 2-3 TCF, and Shell hold 100 % interest. [2]

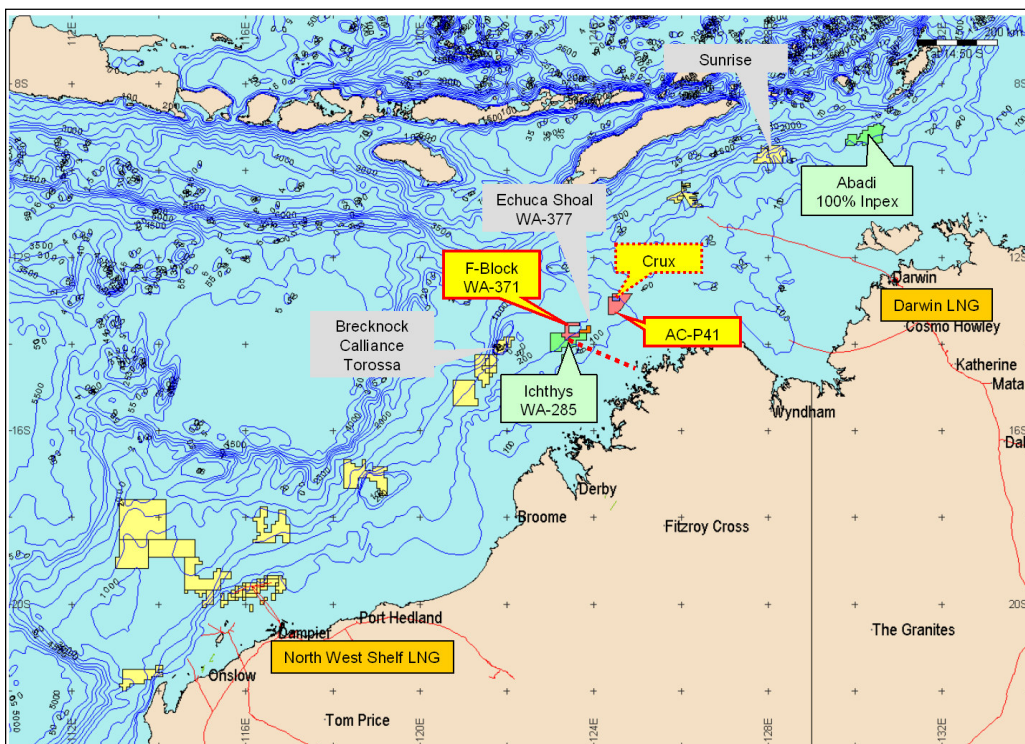


Figure 2.1: Prelude Field Location

The development area is remote, and subject to frequent cyclone activity in the region. In addition, there is limited land based infrastructure within a 1000 km distance of the location. The nearest coastline is the Kimberley wilderness, which is an environmentally sensitive area. [3]

Shell has selected a generic FLNG as the preferred host facility for Prelude which will be connected to a single subsea drill centre with 7 subsea production wells. A three dimensional view of the subsea development is shown in Figure 2.2. The generic FLNG will have a design capacity of 3.5 Mtpa LNG, 0.4 Mtpa LPG and 37,000 bpd condensate. The plateau rate is 565 MMscfd gas including 9 % CO₂ and 38,000 bpd condensate.[3]

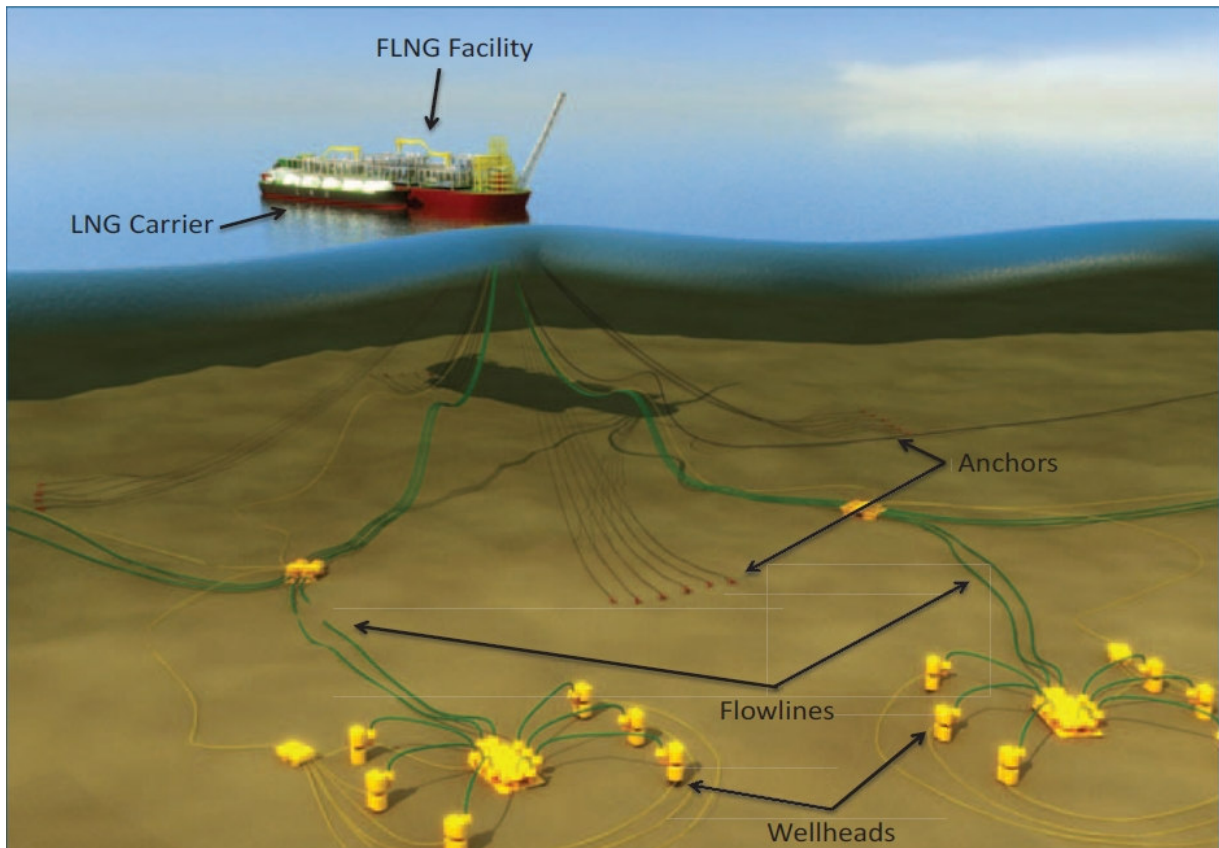


Figure 2.2: Prelude Subsea Development. [4]

The development concepts under consideration also include provision for tie-back of near field development wells. The most notable of these are the Crux discovery, located 160km NE of Prelude. Nexus is currently operator of the Crux Field. In 2006, Nexus sold the gas rights for the AC-P23 block to SDA while retaining all condensate rights. In 2007, Nexus sold 15 % of its remaining rights to Osaka Gas. Nexus plan a condensate stripping project until December 31st 2020, when operatorship of the gas field is transferred to SDA. Following the Nexus condensate stripping project, Shell plan to drill subsea wells producing to an FPSO exporting dry gas to Prelude via a 160 km pipeline tieback to the Prelude FLNG, tentative first gas date is 2022. [3]

Figure 2.3 shows the reference case production profile for the Prelude and Crux gas rates, which plateau just below a total constrained rate of 565 MMscfd. The chart also shows the combined production of CO₂ from the two fields. The CO₂ production increases during gas production from Crux field in about 2022 and plateaus at the constrained rate of 93 MMscfd. The Basis-for-Design document indicates that the acid gas injection system should be designed for required injection rate of 46, 75, and 93 MMscfd,

which represent the minimum, normal and maximum expected acid gas rates, respectively. These required injection rates include 10% design margin. [2]

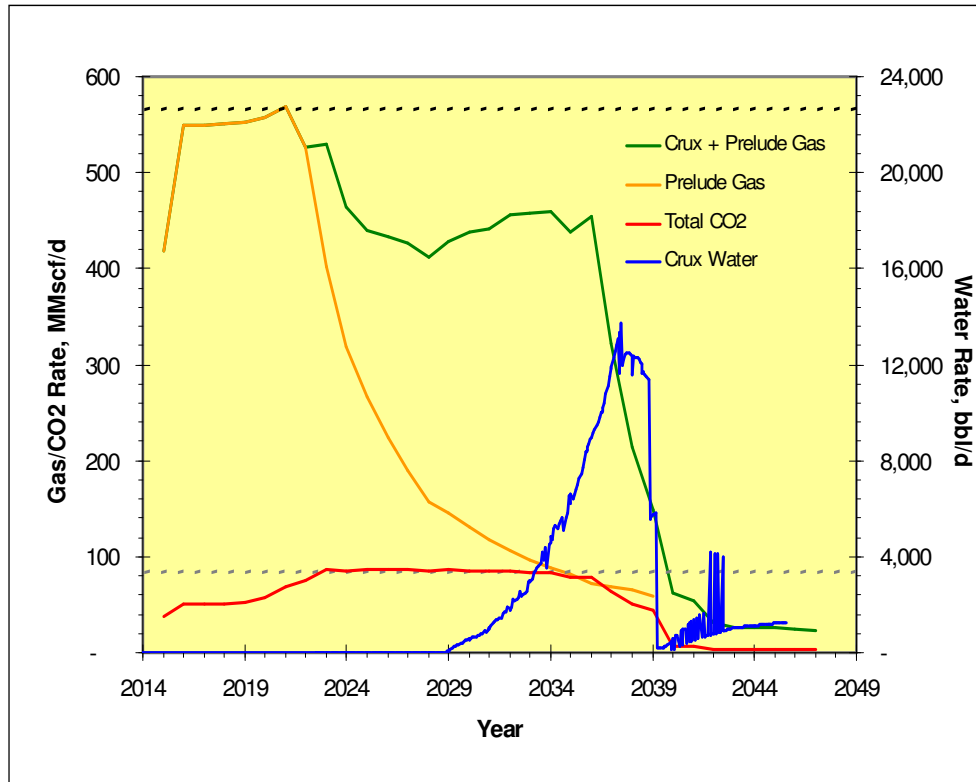


Figure 2.3: Prelude, Crux Ref. Case Production Profiles (CO₂ Constrained). [5]

2.4 Prelude CO₂ Geo-Sequestration

As a component of the Prelude FLNG Development, the stakeholders are considering CO₂ geo-sequestration, which aims at reinjecting more than one million metric tons per annum into the underground through a host facility designed for 93 MMscf/d of acid gas on an operating day basis (excluding availability)[6].

The target formations initially considered for the acid gas reinjection were:

- Puffin
- Swan formation.

The Puffin aquifer is at depth of approximately 1800m TVDSS. Nearly 100 m of net sand is present in the Lower Puffin with an estimated porosity of 23 % and average air permeability of 140 mD – thus providing favorable conditions for CO₂ injection. [7]

The CO₂ could also be reinjected into the producing Swan reservoir at approximately 4000m TVDSS. The Swan formation has a porosity of about 12% and a average air permeability of 40 mD and a gas column of up to 70 m. [7]

**Puffin Fm
2000 mss**

**Swan Fm
4020 mss**

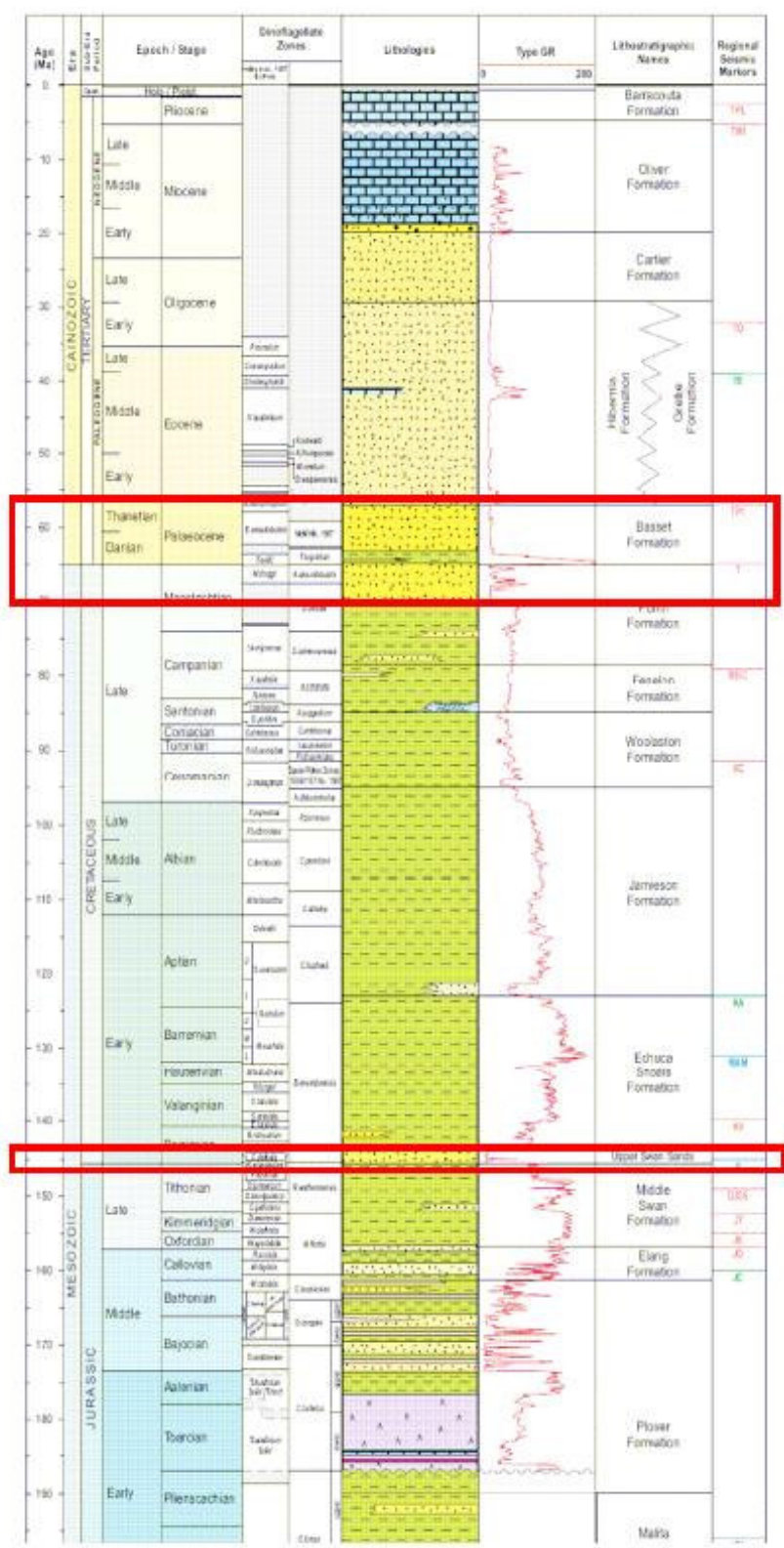


Figure 2.4: Lito-stratigraphic column for the East Browse Basin

Comparing the two options, the Puffin formation is considered the better alternative, owing to the following benefits:

- Lower reservoir pressure and temperature
- More favorable rock properties
- More technical mature in terms of design

However, due to the overlaying Intra Puffin Shale could not be confirmed as a seal, it has been concluded that injection will have to be into the Swan formation. The Swan formation has a proven hydrocarbon seal, assuring CO₂ containment. [7]

The feasibility review of injecting into the Upper Swan Sandstone, the main gas-bearing interval, identified challenges regarding geo-sequestration. The rest of this chapter is designated to give an overview of these challenges.

2.5 Integrated Geo-Sequestration System

In order to make LNG, CO₂ in the feed gas must be stripped out. This is done in the Acid Gas Removal Unit (AGRU) on the FLNG host. H₂S contained in the feed gas will tend to follow the CO₂ stream leading to a higher concentration of H₂S in the CO₂ stream than in the feed gas. The combined stream leaving the AGRU is commonly referred to acid gas and contains trace amounts of hydrocarbons and water in addition to CO₂ and H₂S. [8] The acid gas will be compressed for re-injection into the Swan formation. This will cause the migration of a CO₂ plume towards the production wells, resulting in a gradual increase in concentration of the production stream. It is considered that CO₂ concentration can be limited to 13 mol % (gFLEG limit) for any one well by utilizing blending strategies. This allows recycling CO₂ without significant adverse impact on ultimate recovery [9].

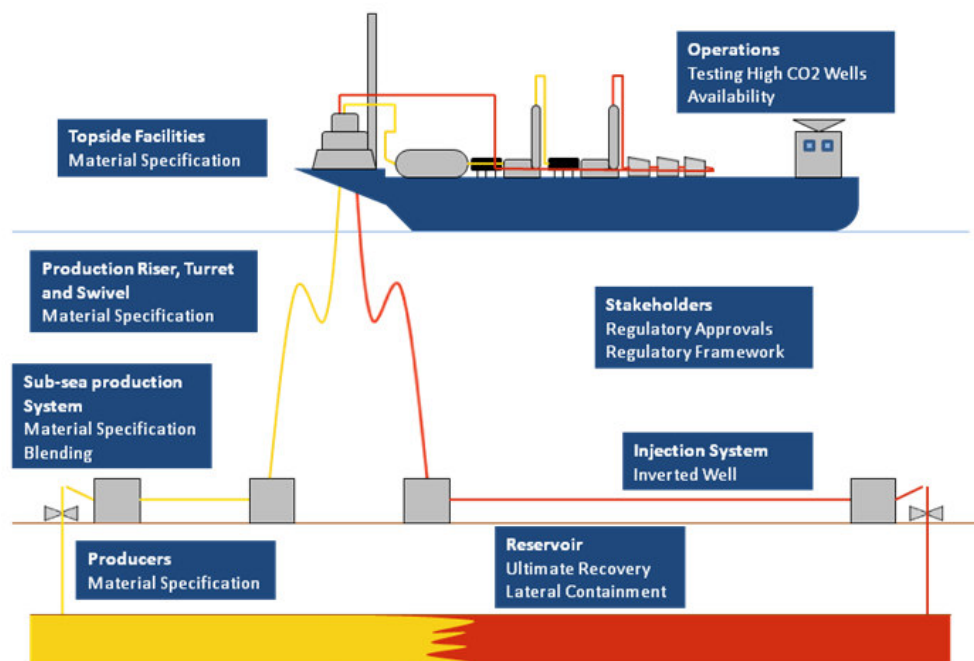


Figure 2.5: Integrated Prelude Geo-Sequestration System

Figure 2.5 show the key elements of the integrated geo-sequestration system for the Prelude Upper Swan Sandstone Member. Each of these is discussed in the next paragraphs, highlighting key issues for consideration to ensure successful geo-sequestration.

2.6 Reservoir

Breakthrough of injected CO₂ at the production wells has been assessed by reservoir simulation. The CO₂ concentration will increase and eventually reach the processing capacity of the AGRU. Injection is expected to reduce recovery of methane, but simulation showed that active well and reservoir management can limit the impact on ultimate recovery of methane and slightly increase recovery of condensate[9]. This is done by beaming back wells that produce at high CO₂ rates and shutting in producers when they reach 50% mass of CO₂.

The simulation results concur with literature as it is expected that recovery of methane will be reduced compared to depletion alone if injection is undertaken early in the life of a depleting life. Results from K12-B, the first reported site of CO₂ injection into the same reservoir as it originated, have so far not indicated evidence of measurable improvement in gas production performance. It has also been suggested by Turta (2003) that a relatively high number of wells (at least 4 to 5) should be used for enhanced gas recovery operations by CO₂ injection [10].

2.7 Production Wells

CO₂ injection modeling indicate that CO₂ breakthrough will be a given, not a risk. The anticipated time of breakthrough is five years, after which the CO₂ and H₂S concentration will increase significantly.

A consequence of the increased CO₂ and H₂S concentrations is upgrades of well materials compared to selection made without CO₂ injection. Considerations needs to be given to metallurgy, cement, packer fluid and elastomers.

2.8 Subsea System, Riser, Swivel and Turret

Indications from reservoir simulation show that the CO₂ content of individual wells can reach values of 70 mol % before they are shut in. The potential impacts of this high value are [9]:

- The requirement of more corrosion resistant alloys and negative effects on properties of non metallic components like the flexible production riser and the turret seals.
- Ensure that subsea equipment is designed to handle the change in PVT properties that this change will cause.

As the Joule-Thomson cooling effect is quite prominent in CO₂ the wellhead temperature may drop significantly at breakthrough. This occurred on Shell's Little Creek Field in Mississippi, USA, where CO₂ flooding was used for tertiary recovery. The temperature drop on breakthrough allowed ice to form on the wellheads. Field experience has also indicated that when CO₂ is subjected to a large pressure drop, such as depressurizing, the formation of solid CO₂ may be prominent in vent lines. Reduction in wellbore and flow line operating pressure would have a high impact on the flow assurance strategy, which relies on maintaining arrival temperature of at least 35°C or higher to prevent hydrates and wax formation. [9]

Examination of the temperature effects was done with flow assurance simulations, where changes of 5-10°C was observed in wellhead temperature when CO₂ content increased from 5-10%. Simulations failed to simulate the observations at Little Creek, and it was concluded that re-injection into the Swan reservoir was feasible from a flow assurance point of view. [9]

To date, there are no applications of CO₂ injection through flexible pipe. Because supercritical CO₂ is an excellent solvent for many organic materials there is a question whether the inner liquid barrier in the flexible pipe can maintain its long term integrity in contact with SC-CO₂. [11] Other material issues relates to explosive decompression and swelling of the elastomers and polymers due to uptake of gas. However based upon results on testing and evaluation it has been concluded that material solutions for risers and swivel seals can withstand the level of CO₂ during normal production, and during well testing when a single well will be produced by itself in the production riser. [9]

2.9 Topside

The utility (steam, power and cooling water) was designed for CO₂ content up to 9%. Recycling will increase this towards 13%, thus exceeding the gFLNG utility design [9].

One solution to this problem would be to replace the steam turbine with a gas turbine fueled by feed gas. This is a deviation from generic design and would require additional engineering scope[9].

The CO₂ will be compressed to a maximum of 255bar over 5 stages. Compressing gas generates heat, and thus an aftercooler is placed after each compression stage. The temperature after stage 5 is in the range of ~78°C [11]. Wellbore simulation have shown that reducing the temperature after the last stage of compression will significantly reduce the required discharge pressure, thus aftercooling to 40°C is assumed.

2.10 Injection System

The injection system has many of the same material challenges as described for the production wells. The partial pressure of CO₂ and H₂S is higher and thus the well will be more prone to corrosion. An additional challenge is the possibility of an inverted well. As the SC-CO₂ is denser than the hydrocarbon gas, it's possible that the wellbore will be displaced from SC-CO₂ to hydrocarbon gas when shut-in. As this will reduce hydrostatic head, additional injection pressure will be required over normal operating pressure to start up the injector. This injection pressure will exceed the current generic design of the compressor output and associated injection riser, if the well is fully displaced.

Reservoir simulation indicate that this can only occur in the first 1-1.5 years of operations. After this period the reservoir around the wellbore will be saturated with CO₂ and thus no methane gas will be available to displace the well. Also, CO₂ will be miscible with methane and thus a fully methane filled well would be a worst case scenario that is not very likely. [9]

2.11 Start-Up & Shut-Down

For start-up considerations should be given fluids in the wellbore post-completion as these could potentially cause damage to the reservoir, or corrode tubular. For shut downs mitigation should be taken to the formation of hydrates. Depressurization has been identified as a particularly important problem as many operators report problem with formation of solid CO₂ due to phase change [9].

2.12 Well & Reservoir Management

As the gFLNG is designed for a maximum of 13 mol % CO₂ in the inlet stream, blending has been adopted as a strategy to keep within this constrain. Even though materials at the gFLNG intake are expected to tolerate even high percentage CO₂, it is seen as a good precaution from a technical integrity point of view. The production manifold allows for blending production stream in almost any combination [9].

2.13 Existing Wells

Based on the injection modeling and the possible extent of the CO₂ plume migration, six wells was identified as a potential leakage risk. An investigation of the identified wells concluded that the risk of leakage from the Swan formation through the wells was low [12]. The investigation did not take into the account the effects of CO₂ on cement and casing. Before CO₂ injection, it is recommended to look at this as it may compromise the long term integrity.

2.14 Monitoring

The key observation regarding monitoring, measuring and verification (MMV) is that plume monitoring through 4D seismic is not feasible due to reservoir depth and limited impedance contrast between the CO₂ and reservoir gas. However, plume migration will be feasible through reservoir simulation and history matching. In addition CO₂ plume migration can be monitored through CO₂ breakthrough at the producers [9].

2.15 Stakeholders and Regulatory Landscape

In engagement with government and other stakeholders Shell has given an overview of what work has been done on geo-sequestration. It has been explained that feasibility cannot currently be confirmed, but that work will continue to resolve the identified challenges [9].

For injection of CO₂ into the Swan reservoir, no separate regulatory approvals will be necessary, as geo-sequestration would be within the existing petroleum license[9].

2.16 Conclusion

It is clear from the identified challenges, that material assessment is very important; as CO₂ injection systems are prone to corrosion. Challenges have been presented regarding the entire geo-sequestration system, but only challenges related to the well barrier envelope will be explored in the rest of the thesis.

Chapter 3

Evaluation of Industry Experience

3.1 Objectives

CO₂ injection in the oil and gas industry is not a novel subject. In fact they have been injecting CO₂ for enhanced oil recovery for 35 years[13]. However, injection into a producing gas reservoir has not been extensively explored, and literature review only point to one application K12-B, as reported by Van der Meer et al. [14]. An overview of industry experience with injection for different purposes is reviewed here and a comparison of different injection schemes to CO₂ injection for storage offered.

3.2 Methodology

A literature review was conducted to gather information regarding well design and experiences from other injection projects. Some of the information has been collected from Shell sources. The review is presented according to purpose of the injection. The relevance of different injection schemes to CO₂ injection is presented at the end, and a conclusion regarding applicability to Prelude is drawn.

3.3 Commercial CO₂ Geological Storage Operations

3.3.1 K12-B

K12-B was the first site in the world where CO₂ was injected into the same reservoir that it was produced from. The field is located in the Dutch sector of the North Sea, approximately 150 km northwest of Amsterdam. The produced gas contains some 13% CO₂, which was reinjected into the Upper Slochteren Member above the original gas-water contact. The reservoir is located at a depth of 3800 meters with approximately 105 bar bottom hole pressure, and a formation temperature of 132°C [14] [5]. The injection rate is approximately 0.9 MMscf/d [5]. This makes the injection rate and bottom hole pressure low compared to injection into the Swan formation.

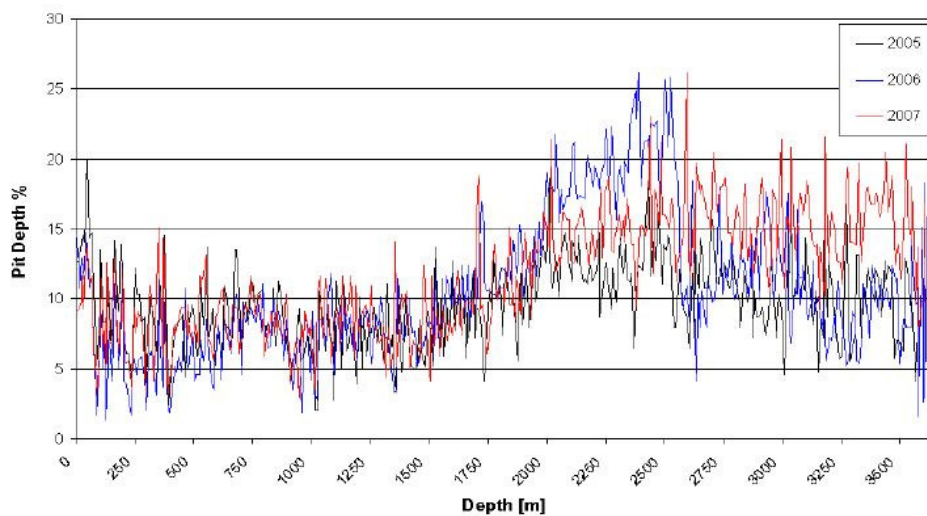


Figure 3.1: Time lapse pit depth chart of the injection tubing of well K12-B6 [15].

The injection well in the project is a converted gas producer, and the material used for tubing is 13%Cr stainless steel. To evaluate the integrity of the tubing, several time-lapse multi-finger caliper surveys have been conducted since the start of the CO₂ injection back in 2004. The result of the pit depth analysis is displayed in Figure 3.1. In the 2006 survey an anomaly can be seen between 1525 m and 2440 m, which is not seen in the 2007 survey. Absence of a film in the tubing during 2006 survey may be a possible explanation for this. Between 3050 m and 3500 m, an increase in pit depth can be observed from year to year, but the cause is concluded to be the same as for the other anomaly, thus no reason for concern. It seems that the CO₂ injection has had no negative effect on the tubing integrity [15].

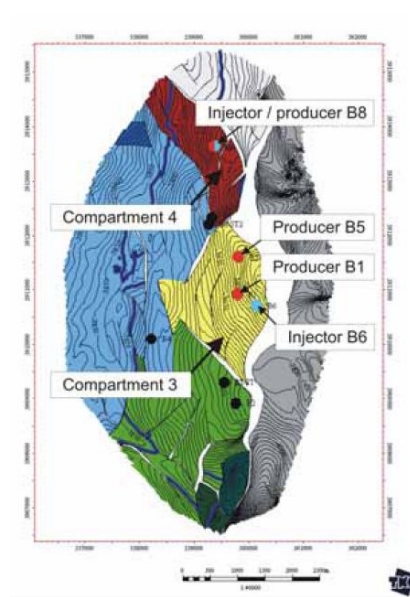


Figure 3.2: Map of the top reservoir depicting compartments, injection and production wells directly involved in the injection of CO₂ at K12-B [15].

The production well K12-B1, which is located near the CO₂ injection point, showed an increase in CO₂ concentration from 13% to 21% from 2005 to 2009. Also, the produced gas in well K12-B5 (until November, 2008) has remained constant at 13% even though the initial tracer breakthrough (at very low concentrations) occurred already in 2006 [15].

Another interesting observation was done in well K12-B8 which was used for injection in 2004 into a depleted single well reservoir compartment. In 2007, production was once again re-initiated. The reservoir had re-pressurized to 85 from 51.5 bar caused by likely water and/or gas influx. The possible cleaning effect caused by CO₂ injection made the well flow at high rates for an extended period of time with relatively low CO₂ concentrations [15].

So far, the project has not been able to conclude on a EGR effect through CO₂ injection, as the injected quantities are too small. However, the injection has not had a negative effect regarding the gas production [15].

3.3.2 Gorgon

The natural gas in the Gorgon field contains approximately 14% CO₂ [16]. The CO₂ will be separated from the hydrocarbon gases at Barrow Island LNG facility, compressed to supercritical state and then transported in a 12 km pipeline to the injection site [17]. Nine injection wells (low permeability) will store the CO₂ in the Dupuy Formation 2300 m below Barrow Island. Here 1.5-3.1 trillion standard cubic feet which is expected to be produced with the hydrocarbon gases, will be permanently stored. Injection rate will be up to 4.9 Mt/y. The injection is planned to commence in 2014 [16, 17].

The project will comprise of 4 specific well types [18]:

- CO₂ injection wells
- Reservoir surveillance wells
- Water production wells (pressure management)
- Water injection wells (pressure management)

There will be three injection centers (DC-A, DC-B and DC-C) strategically located to be able to control the injection. The average permeability is 25 mD, and modeling of CO₂ migration in the heterogeneous injection reservoir, predicts preferential CO₂ migration along high permeability layers resulting in a laterally non-uniform spread [17]. The CO₂ will be in supercritical state and be injected under matrix injection conditions [18].

The reservoir surveillance wells will monitor the migration of the CO₂ plume and observe the effect of injection on the reservoir. One well is planned at DC-A and one at DC-C. In addition two more will be drilled at later date [18].

Strategically located 5-7 km away from the CO₂ injectors, pressure management will be drilled from 4 drill pads. At each pad, one water injector and one producer will be drilled. The main functions of the water production wells is to provide pressure management in the Dupuy reservoir, assist in maintaining injection pressure below fracture initiation condition and re-direct the CO₂ plume away from potential leak points in the reservoir. To manage the anticipated increasing reservoir pressure, water will be produced from the western edge of the Dupuy reservoir and reinjected into the overlying Barrow Group [18].

For the injection wells it is anticipated that there will be no water condensation under all expected injection operating conditions so that carbon steel corrosion will be nil. However, in contrast to other CO₂ injection wells, the Gorgon injection wells are designed for backflushing. Corrosion rate during this operation is anticipated to be very high, and therefore CRA completion is required. The project looked at GRE lined tubing versus 25%Cr and found that from a NPV point of view, 25%Cr was the preferred choice, because of higher workover costs for GRE. 13%Cr was considered susceptible to sulfide stress corrosion cracking [18].

3.3.3 Sleipner

The Statoil operated Sleipner field in Norway was the first commercial CO₂ storage project to commence operations. It has since starting injection back in 1996, injected more than 10 Mt of CO₂ into the Utsira formation. The CO₂ is captured from the production stream which contains approximately 9% CO₂. The Utsira, a saline formation, 50 to 250 m thick sandstone that is located at a depth of about 1000 m, directly above the producing formation (See Figure 3.3) [17]. The permeability is between 1-8 D, and the porosity is 35-40% [19].

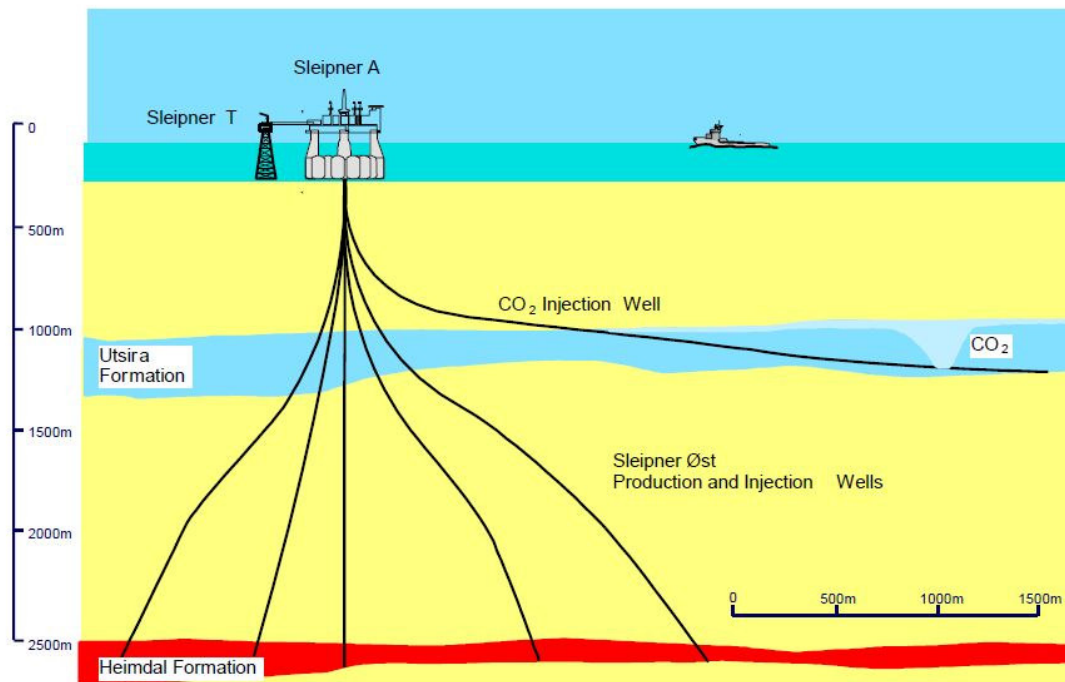


Figure 3.3: Simplified diagram of the Sleipner CO₂ storage project[17].

Before CO₂ is injected it is brought to a supercritical state, requiring compression to 80 bars and cooling to 40°C. This is done by a 4 unit compressor train, each with a knockout drum to remove water. The injection happens through a single well into the storage reservoir. The 3752 m long well were drilled to a vertical depth of 1163 m with a terminal inclination of 83 degrees. It is completed with 25%Cr duplex steel tubing [19].

Time lapse seismic has been used to monitor the movement of the CO₂ plume. This has revealed a “baffle” effect of inter formational layers with low permeability. Instead of forming a uniform plume below the main top seal, the injected CO₂ spreads out laterally along various horizons in the reservoir, as shown in Figure 3.4.

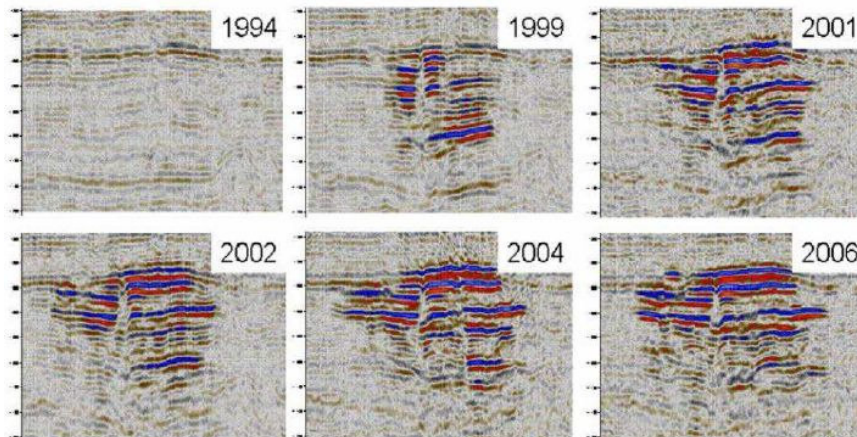


Figure 3.4: Time-lapse dataset visualizing the spread of the injected CO₂ in the Utsira Formation Sleipner [17].

The driver for selection of a horizontal well was the need to locate the injection point sufficiently far away from wells already penetrating the Utsira formation. Modeling showed a maximum extent of the CO₂ plumb of 3 km after 20 years [19]. The development wells have been completed with 13%Cr through the Utsira formation, just in case. To give the necessary service life, the tubing was completed with 25%Cr duplex steel, and also for exposed parts of the casing. The fact that the project relied on a single well was an important factor for metallurgy selection [19].

After the initial perforation in the reservoir, the well experienced injection problems. To counter the problem a 300 microns sand screen was installed, and injection improved, but the rate remained variable and there was a continuous influx of sand, and it was necessary to re-perforate on the low side in the interval 3102-3140 m MD RKB. A gravel pack containing 200 micron sand screens was installed. (See Figure 3.5) To prevent corrosion this was of high quality stainless steel (25%Cr and Duplex 125). Since then, the well has been injecting at stable rate of 1.4-1.6 MSm³/d with a wellhead pressure of 65 bar [20].

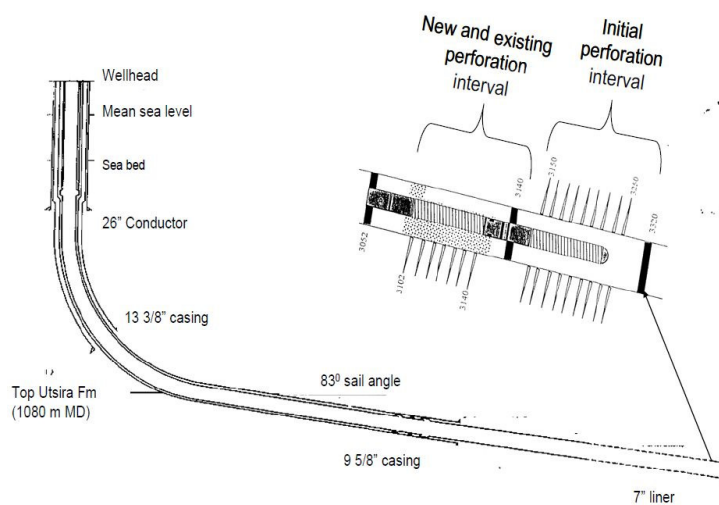


Figure 3.5: Injection well design and perforation interval [20].

3.3.4 Snøhvit

The Statoil operated Snøhvit field in the Barents Sea started injection of CO₂ in May 2008 [17]. CO₂ is captured onshore and transported in a 150 km subsea where it is injected into the Tubaaen formation at 2600 m below sea level with a sandstone having permeability of several hundred mD [21]. About 0.7 million ton will be injected annually [17].

This project is an interesting analogy for Prelude as it is the only CO₂ injection project in the world, currently, that uses a subsea injection well. This means that more considerations must be given to material selection, as interventions will be very expensive. However, an intervention on the CO₂ injection well was performed in 2010 due to reduced injectivity. The nature of the work is not known.

Literature review suggest AISI 4140 was selected for tubing, with all completion components being 25%Cr duplex stainless steel. The liner is 25%Cr 7%Ni 4%Mo [22]. The choice of 4140 has been deemed unusual, and is possibly driven by a low temperature fracture consideration, but this is not confirmed. The exact composition of the gas and aquifer is not known, but as for Sleipner there would be no oxidizing acid components [1].

3.3.5 In Salah

The In-Salah gas project, a Sonatrach, BP and Statoil joint venture, re-injects CO₂ separated from the produced gas in Algeria's Ahmet-Timimoun Basin. Seven proven gas fields is developed in the joint venture. The gas contains up to 10% CO₂ and needs to be decreased to CO₂ content of 0.3% to reach export levels. From July 2004 1.2 Mt/yr CO₂ have been reinjected into the aquifer section of the Krechba field, the Carboniferous Tournaisian sandstone reservoir at 1800m depth. Following separation from the natural gas stream, the CO₂ is compressed to 200 bars and dehydrated. It is injected using three injection wells, with 1500 m horizontal completion, due to moderate permeability and to combat potential high injection pressure. Further the wells are directed to intersect the main fracture orientation in the reservoir sandstone [23].

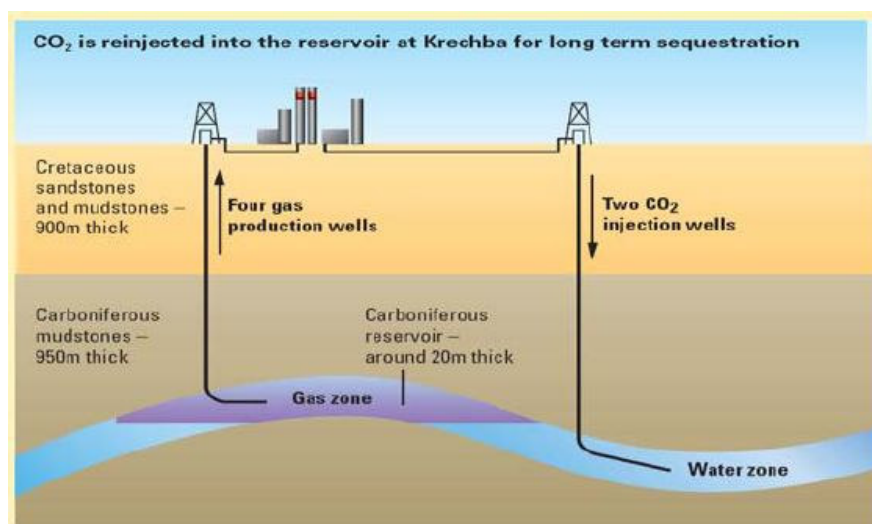


Figure 3.6: Schematic of CO₂ storage at Krechba [24].

Haigh (2009) indicate that the injector wells have been completed in carbon steel throughout [25].

3.4 Acid-Gas Injection

Oil and gas producers in the Alberta basin in western Canada have over the two last decades been faced with a growing challenge to reduce the emissions of hydrogen sulfide (H₂S), which they produce from “sour” hydrocarbon reservoirs. Surface storage of the sulphur is a liability, and it is expensive to desulphurize, thus more operators are turning to the storage of H₂S by re-injection. 48 operations for acid gas injection had been approved by 2007. Approximately 4 Mt CO₂ and 3 Mt H₂S had been injected in western Canada by the end of 2007 [17].

CO₂ stream with no H₂S is less corrosive and less hazardous than the injection in western Canada. Thus technology and experience in the engineering aspects of acid injection operation can be adopted for operations related to CO₂ injection. This includes well design, materials, leakage prevention and safety. Fines migration, precipitation and scale potential, oil or condensate banking and plugging, asphaltene and elemental sulphur deposition, or hydrate plugging all poses a major concern regarding the injection process as they can cause formation damage and reduce injectivity. Compared to what is expected from CO₂ projects, injection rates for acid gas are generally low (<100 kt/year). There are however a few larger ones: 1 Mt/year at LaBarge in Wyoming, Talisman’s Sukunka operation with up to 300 kt/year and Apache Canada’s Zama with injection of 120 kt/year. No matter the injection rate, problems related to reduced/loss of injectivity due to geochemical reactions with injected gas with and reservoir rock may be applicable to CO₂ injection projects [17].

The main remediation strategy is to stimulate and complete additional reservoir interval. At five injection sites acid gas showed up in nearby production wells. This had been anticipated for some sites, thus at a later stage. The deviation from modeling is likely to be caused by uncertainty in reservoir heterogeneity [17].

3.5 Enhanced Oil Recovery Projects

Carbon Dioxide has been used in commercial EOR projects since early 1970s, after the first field test at the Mead Straw Field in 1964. There are currently more than 1000 injection wells in the US in ten CO₂ EOR projects. The largest number being 537 at the Wason in Texas. The Weyburn EOR project is planning to increase the number of wells to 675 over the next 15 years [17].

A summary of the most common materials used in CO₂ EOR projects in the USA was given by Meyer (2007) and is reproduced in Table 3.1. One point to be made – most of the US experience is in shallow conditions, thus at lower pressure and temperatures. Most of the service is WAG, with water of possibly varying quality alternating with periods of dry CO₂ injection. Most of the CO₂ EOR projects has the purpose of miscible flood (tertiary oil production) and not designed for CO₂ sequestration. Thus compared to what can be expected from CO₂ sequestration, the CO₂ EOR projects see relatively short lifetimes and some of the projects tolerate frequent component replacement [1].



Component	Materials
Xmas Tree (Trim)	316 SS, Electroless nickel plate, Monel
Valve Packing and Seals	Teflon, Nylon
Wellhead (Trim)	316 SS, Electroless nickel plate, Monel
Tubing	Glass reinforced epoxy (GRE) – lined carbon steel; internally plastic coated carbon steel, Corrosion resistant alloys (CRA)
Tubing joint seals	Seal ring (GRE), Coated threads and collars
ON/OFF tool, Profile nipple	Nickel plated wetted parts
Packers	Internally coated hardened rubber, etc. Nickel plated wetted parts; corrosion resistant alloys particularly in old wells to improve sealing to worn casings.
Cement and cement additives	API cements and/or acid resistant cements

Table 3.1: Commonly used materials in CO₂ injection well design and construction – USA projects [13].

Chevron has provided the most complete record of materials and experience used for construction for a CO₂ EOR flood after operating at the SACROC (Scurry Area Canyon Reef Operators Committee) field. They used plastic coated tubing but tested other coatings with varying degree of success. One of the most successful was epoxy-modified phenolic coating. This would however blister if applied to thick (>0.17 mm). They reported an average service life of 50 months for coated tubing. Also, they tested 6 tubing strings with polyethylene liners – they all failed. The failure was caused by CO₂ permeation of the liner, followed by deterioration of the adhesive and collapse of the liner by pressure build up [1].

At the Dollarhide Unit (WAG) Unocal used plastic coated injection tubing, but damage during installation led to corrosion problems. They also had problems with leaking connectors. They tried various 8-round thread coupling and thread lubricants including modified seal rings and premium nose seal couplings, Teflon tapes and Teflon thread lubricants – but all developed leaks. Finally they established the use of a modified 8-round coupling with Ryton coating on the threads and a seal ring. To solve the leak problem they also introduced low-speed make-up of connections and rigorous helium testing of each connection [1].

There are few continuous CO₂ injection programs. In one of the few, Texaco ran bare carbon steel tubing as it would not be exposed to water and thus no corrosion was anticipated [1].

Even though US CO₂ floods have been in service since the 1970's, there is no experience of the abandonment phase of the projects indicating how well integrity is maintained over time [1].

Despite the differences between the purpose of CO₂ EOR and CO₂ sequestration, there are several problems related to CO₂ EOR wells that could occur similarly in CO₂ sequestration wells. These include: corrosion, channeling and early breakthrough, hydrate formation, scaling, asphaltene deposition and pressure fluctuations due to CO₂ phase changes along the well tubing [17].

3.6 Other Injection Schemes

Fluid injection for natural gas storage, waste water disposal, and geothermal operations have experience with general injectivity issues.

3.6.1 Natural Gas Storage

Natural gas consumption is prone to seasonal change in demand, thus in gas storage it has to be possible to extract the majority of the injected gas if needed. Geometrically constrained reservoirs like depleted reservoirs and salt caverns are frequently used. In contrast to CO₂ project which aims at long term storage and thus looks mainly at saline aquifers. There are however similarities regarding surface facilities like pipelines, and compressors etc.. Perry (2005) pointed at the following five technologies that could have relevance to CO₂ geological storage [17]:

- Application of all available techniques
- Observation wells
- Pump testing techniques
- Assessment of cap rock sealing
- Surface monitoring

To prevent negative impacts on reservoir and caprock integrity, it is expected that reservoir pressure associated with CO₂ storage in depleted oil or gas fields will not exceed initial pressure. This was also true in gas storage projects, however, according to Bruno et al. (1998) the pressure in gas storage reservoirs can be safely lifted if the geomechanical behavior of the reservoir is well understood. By doing so, the storage capacity will also be increased. Cooper (2009) referred to a storage field in Italy, Settala, where the initial reservoir pressure was increased with 7%. This resulted in a 45% increase in storage capacity. To ensure containment of the gas in such a case, testing of operating pressure and an efficient monitoring program is critical [17].

3.6.2 Liquid Waste Disposal

A comparison between liquid-waste and CO₂ injection was presented by Tsang et al. (2008) in a review of the history of liquid waste disposal by deep injection in the US. Apps and Tsang (1996) presented a comprehensive compilation of scientific research related to the underground disposal of liquid waste. Tsang and Apps (2005) included additional references on CO₂ geological storage. More evaluations on parallels between liquid waste disposal and CO₂ storage can be found in Wilson et al. (2008) and Apps (2005). Issues pointed at by the authors related to deep injection of liquid waste in the 1960s and 1970s included corrosion of well casing and cements, clogging from precipitation from mixing two incompatible waste streams, and triggering of seismic events [17].

CO₂ geological storage in saline aquifers have been found more complex compared to deep injection of liquid waste in the hydrologic area and in terms of technical approach [17]:

- The relatively high buoyancy forces, low viscosity and the large volumes of the injected supercritical CO₂ result in an extensive area that must be considered for the potential of CO₂ leakage i.e through abandoned wells or fractures in the overlying aquifers.



- The buoyancy pressure, which is higher in the case of CO₂ geological storage, requires that the hydromechanical effects on the overlying aquitards be assessed along potential leakage pathways extending from injection horizon to shallow groundwater aquifers.
- In contrast to liquid waste injection, CO₂ leakage into shallow aquifer systems may not present a serious environmental problem.
- Fiberglass lined tubing has been selected frequently for shallow CO₂ EOR projects, however, it is not suitable for service above 90°C and 34 MP, so the experience can't be generalized to every scenario of injection.

3.7 Conclusion

Sleipner, Snøhvit and In Salah was by the year 2009 the only three commercial-scale projects injecting more than 1 MtCO₂/year for the purpose of geological storage. Two of the projects have very good injectivity and thus the optimization of storage efficiency has been of smaller priority. In Sleipner and Snøhvit, full injection is achieved with only one well. The In Salah project however, has a low permeability (order of 5 mD) limits injectivity and thus resulting in the need of three injectors. In addition, these wells are completed horizontally. Most likely Gorgon is going to be the next large scale project injecting up to 4.9 MtCO₂/year via 9 CO₂ injector wells. To reduce the chance of overpressuring the heterogeneous injection horizon as predicted by modeling, four water production wells will be included to maintain pressure control in the reservoir. The produced water will be disposed in an overlying, pressure depleted, formerly hydrocarbon bearing unit. It is expected that the Gorgon field will provide invaluable information regarding multi well injection strategies in heterogeneous aquifers and pressure management [17]

The best analogue to large scale CO₂ geological injection is acid-gas injection. The main differences are lower injection rates and added complication from the H₂S in the stream. The technology and experience from acid gas injection projects can be adopted for large scale operations of CO₂ geological storage [17].

EOR projects provide important insight into optimization of sweep efficiency and geometry of well pattern. The EOR operations also have considerable experience combating well problems like corrosion, channeling and early breakthrough, hydrate formation, scaling and asphaltene deposition. Many of these can be directly applied for CO₂ storage operations. The drivers for EOR and CO₂ geological storage are very different; this should be kept in mind. EOR aims at maximizing oil production, thus the volume of injected fluid and sustainability flow rate in a single well is less important. For geological storage, maximizing injectivity in each well is a primary concern. This is due to two reason, expensive drilling and no redundancy [17]. The latter means CO₂ will be vented if Injectivity is lost, and a possibly CO₂ tax.

The experience from other cases of injection (i.e. natural gas storage, waste water disposal) is less applicable to the optimization of CO₂ geological storage, mainly due to difference in fluid properties, injection rates and the overall purpose of the project. Similarities can be seen between deep injection of liquid waste in terms of general purpose, time scale and use of injection wells without production wells for pressure maintenance. Injection volumes and fluid properties are however different. A comparison between different injection schemes and CO₂ geological injection is shown in Table 3.2.

The pressure and temperatures at Prelude are much higher than those seen in EOR operations in the US where polymeric lining is not unusual. Polymeric lining at high pressure conditions have shown mixed performance. When bottom hole conditions with >350 bar is expected, linings are not recommended because of concerns of blistering.

WAG which is typical for many USA wells cause a very aggressive intermittent wet and dry environment at the bottom of wells. The experience with corrosion in these cases indicates that an aggressive environment could occur in CCS wells if the aquifer flow back to the wellbore over time. This could be during prolonged well shut-in or at abandonment, and it is advisable to select CRA for bottomhole. This is also observed in several of the commercial projects injecting into an aquifer. Prelude injection is into a gas reservoir with a non mobile aquifer and only connate water left behind. This may give an opportunity for to use low alloy steels.

CO₂ injection well generally does not contain large amount of solids and is not expected to cause local pressure build up in the well. The experience from Snøhvit is thus a lesson learned and emphasize that not all is known about CO₂ injection. Prelude being dependent on a single wet injector should therefore have some redundancy to handle unforeseen events like pressure build-up.

Characteristics	CO ₂ Storage	EOR	Acid-gas injection	Natural gas storage	Liquid waste disposal (Class I)	Geothermal
Purpose	Reduction of CO ₂ emissions	Increase of oil production	Reduction of H ₂ S flaring and stripping of CO ₂ from natural gas	Storage of gas for seasonal and backup use	Disposal of liquid waste	Energy production
Time Scale	100s – 1000s of years	<100 years	100s – 1000s of years	Seasonal, <10 years	>10000 years	<100 years
Injection depth	>800 m	Variable	>800	Variable	>1500 m	<350 m
Total injection volume						
Injection rate	~4-20x10 ⁶ t/year	<2x10 ⁶ t/year	<1x10 ⁶ t/year		<25x10 ⁶ /year	
Injection fluid	CO ₂	CO ₂ (+water, NG)	H ₂ S (+CO ₂)	NG	Water, organics, other	Water
Reservoir geometry	Saline aquifers (open), depleted hydrocarbon reservoirs (closed)	Depleted hydrocarbon reservoirs (closed)	Saline aquifers (open), depleted hydrocarbon reservoirs (closed)	Depleted hydrocarbon reservoirs (closed), salt caverns (closed) & aquifers	Saline aquifers (open)	Saline aquifers (open)
Number of wells	10s to 100s	<675	1-3		1-3	~2 to 20
Well types	Injection (+monitoring pressure maintenance)	Injection & production	Injection	Injection & production	Injection	Injection & production
Well completion	Corrosion resistant	Corrosion resistant	Corrosion resistant			
Monitoring	Comprehensive; pre-, syn-, and post injection	Variable; syn-injection/production	At the wellhead, syn-injection	Comprehensive; syn-injection	Wellhead, annulus	Variable, syn-injection/production

Table 3.2: Comparing characteristics of CO₂ geological storage to other injection types (green = comparable, red = not comparable, yellow = comparable in some aspects). Well numbers, injection rates and volumes are "site scale" and refer to a single operation [17].

Chapter 4

Key Parameters

4.1 Objectives

This chapter provides the key data regarding flow rate, fluid composition and subsurface and environmental properties. These are necessary to perform the simulations conducted in the next chapters.

4.2 General

The key parameters that set the boundaries for the project is the required CO₂ injection rates [8]:

- Maximum Flow : 57 kg/s (93 MMscf/d)
- Nominal average flow: 40 kg/s (65 MMscf/d)
- Minimum flow: 28 kg/s (46 MMscf/d)
- Design life: 25 years

4.3 Injection Fluid Properties

The fluid composition:

- CO₂ = 99.98%
- H₂S = 200 ppm
- H₂O = 50 ppm
- C1 = traces
- C2 = traces

For all modeling purposes, the fluid has been modeled as pure CO₂.

4.4 Subsurface and Environmental Properties

Reservoir:

- Reservoir pressure: 415 bar
- Reservoir temperature: 155°C
- Chloride content: 20,000 ppm
- Top reservoir: 4010 mTVD

	Low	Base	High
Permeability [md]	21.4	36.5	69.5
Porosity [%]	11	12	13
Kv/Kh [frac]	0.19	0.33	0.8
Reservoir thickness [m]	40	60	80

Table 4.1: Reservoir properties.

Environment:

- Temperature sea (seabed/surface)
 - Base: 8/20°C
 - Winter: 4/15°C
 - Summer: 13/28°C

Chapter 5

Pressure & Temperature Predictions

5.1 Objectives

The objective of this section is to establish the operating envelope of the well. Temperature and pressures during transient operations will be estimated. Temperature and pressures are important factors for selection and recommendation of materials and to assess the loads acting on the well.

5.2 Methodology

CO₂ thermodynamics are dependent on pressure and temperature. The properties of CO₂ are thus introduced. The operating envelope is typically modeled with a wellbore simulator. Most of these are developed for use with hydrocarbons, so it is necessary to investigate how accurate results they give with CO₂. Results are compared with a reference value. The temperature and pressures are then predicted for different reservoir realizations. The closed-in tubing head pressure is estimated from reference data.

The wellbore simulator used in this instance (Prosper) is not capable of predicting behavior of transient operations. These operations are, however, found to be very dependent on reservoir pressure and the Joule-Thomson effect, and thus some high level conclusion can be stated.

5.3 CO₂ Properties and Behavior

In order to understand the CO₂ dynamics, it is useful to have an understanding of the CO₂ properties and how they change with pressure and temperature.

Carbon dioxide is a colorless, odorless gas. At standard temperature and pressure (STP), the density of carbon dioxide is about 1.98 kg/m³, nearly 1.5 times that of air. The CO₂ molecule is composed of two oxygen atoms covalently bounded to a single carbon atom. It has no electric dipole. As it is fully oxidized, it is not very reactive and, in particular, not flammable[26].

CO₂ can exist as a gas, liquid, solid or a supercritical fluid, as shown in the phase diagram in Figure 5.1.

The stable carbon dioxide at normal atmospheric pressure and temperature is gas. The point where three phases (gas, liquid and solid) can co-exist in thermodynamically equilibrium is called the triple point. It is at 5.18 bara and -56.6°C. At the critical point (pressure 73.9 bara, temperature 31.1°C) the liquid and gas can no longer exist as separate phases. The fluid in this region is called supercritical. Supercritical CO₂ has viscosity similar to gas and a density close to that of a liquid. Supercritical fluid is also has excellent solvent properties[26].



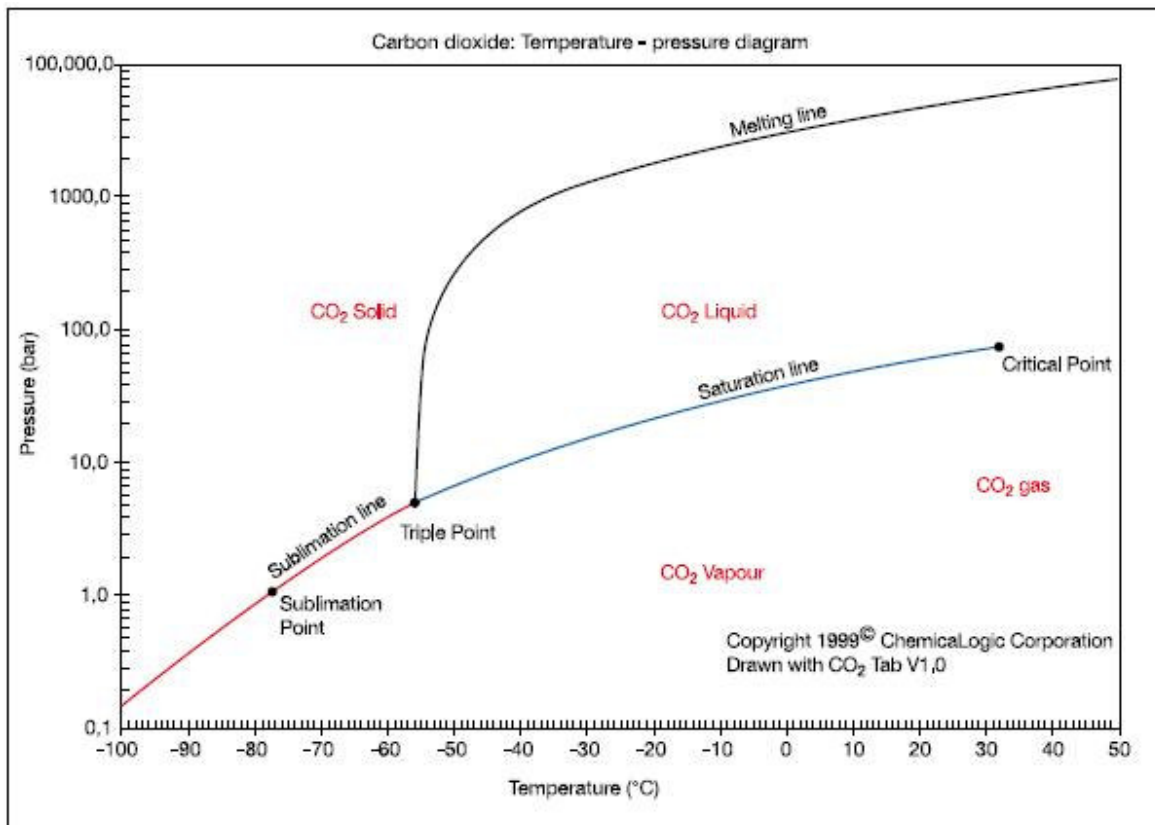


Figure 5.1: Phase diagram of CO₂. [27]

When one of the boundaries in Figure 5.1 is crossed a phase change occurs. For example if the operating conditions change from (T=20°C, p=100 bar) to (T=10°C, p=10 bar) there will be a phase transition from liquid to gas. The process corresponds to boiling.

Figure 5.2 shows how changes in pressure and temperature affect density. It indicates that even small changes can have a large impact on density, thus the chosen equation of state becomes very important aspect of wellbore modeling. The injection well's vertical lift performance (VLP) greatly depends on fluid density and viscosity, which depends on pressure and temperature at every point along the flow path, including the riser, flowline, and wellbore. These conditions, in turn, determine the fluid density and viscosity at the target injection depth[5].

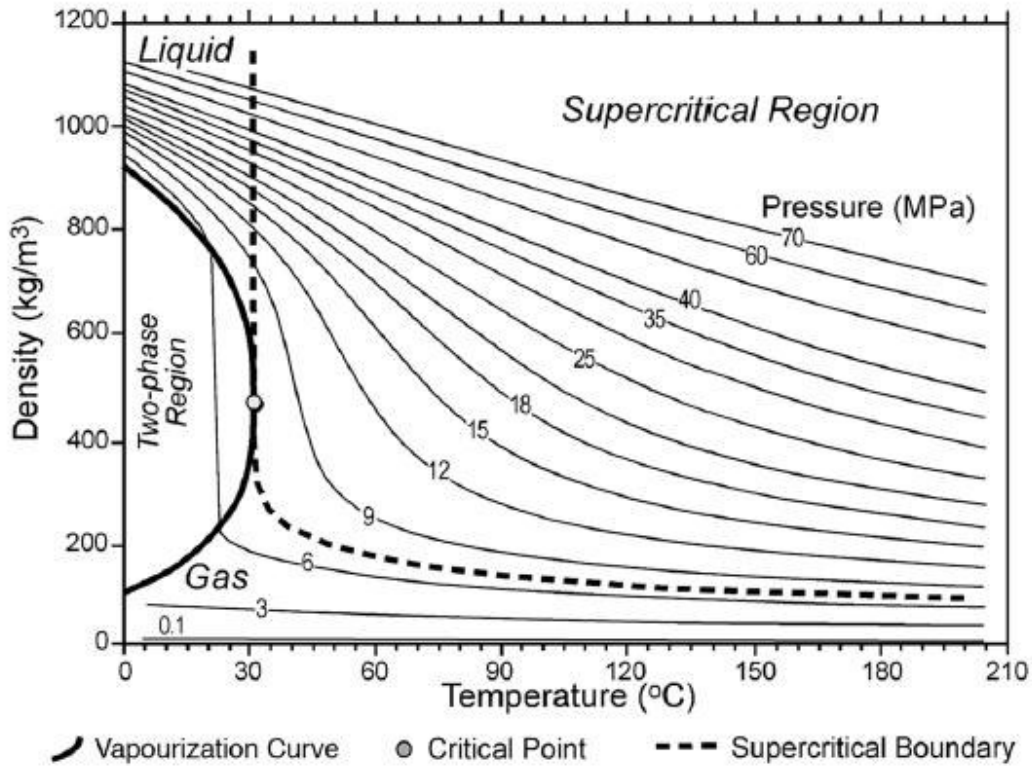


Figure 5.2: CO₂ density as a function of temperature and pressure[27].

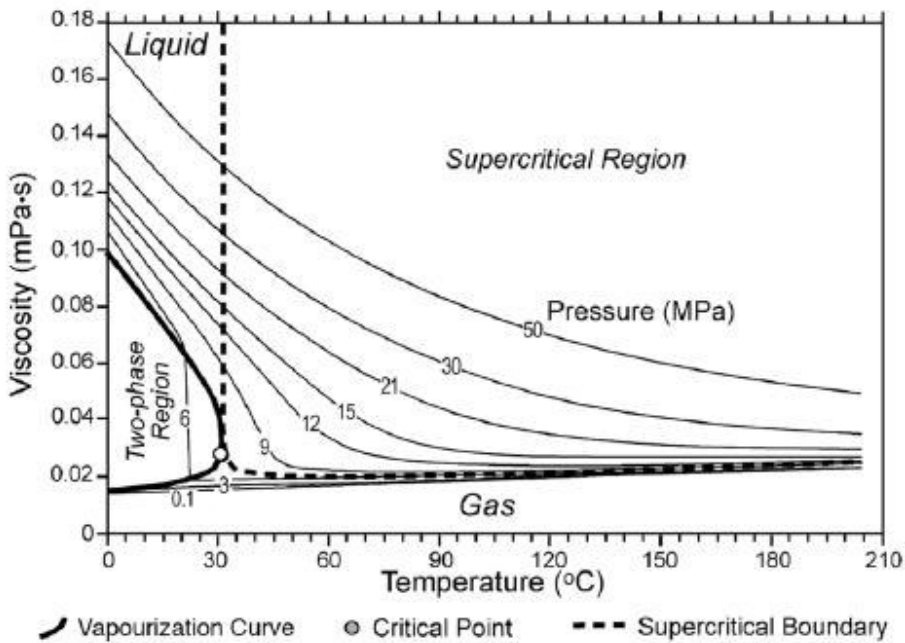


Figure 5.3: Variation in CO₂ viscosity as a function of temperature and pressure[27].

Figure 5.3 shows a pressure-viscosity plot for various temperatures. The condition in the Swan reservoir is at 41.5 MPa and 155°C (6020 psi, 311°F). The CO₂ viscosity for this case is on the order of 0.06 cp

The Figure 5.4 below show the Joule-Thomson coefficient for CO₂ at different pressure and temperatures. Through a throttling process the temperature will experience a large drop in temperature as a result of throttling. This process is described by the Joule-Thomson coefficient [28]:

$$\mu_{JT} = \left(\frac{\partial v}{\partial P}\right)_h = -\frac{1}{c_p} \left[v - T \left(\frac{\partial v}{\partial T}\right)_p \right] \quad \text{Eq. 5.1}$$

where c_p is the heat capacity at constant pressure. Thus the Joule-Thomson coefficient is a measure of the change in temperature with pressure during a constant-enthalpy process. The temperature can increase, decrease or remain unchanged [28]:

$$\mu_{JT} \begin{cases} < 0 & \text{temperature increases} \\ = 0 & \text{temperature remains constant} \\ > 0 & \text{temperature decreases} \end{cases}$$

For CO₂ the JT coefficient is very high (0.9-1.4 °C/bar) for vapor phase, while it is very low in the liquid phase (0.15 °C/bar). Very low temperatures can be produced at pressure let-down points, which may cause concerns for metallurgy and hydrate formation.

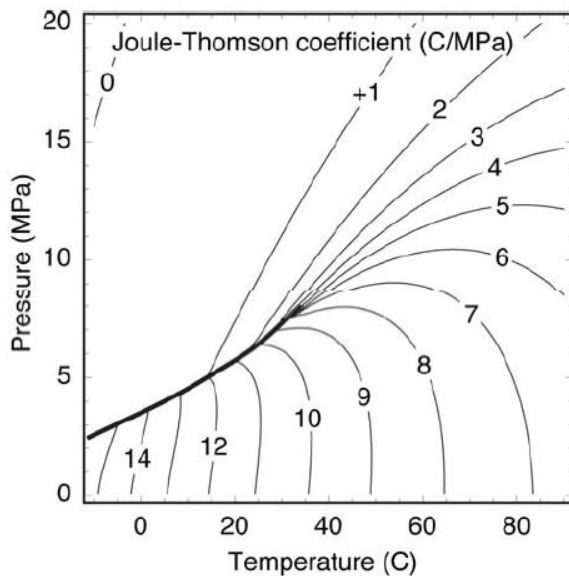


Figure 5.4: JT coefficient of CO₂ [29].

The figures show that small changes in temperature and pressure can have a significant impact on properties of CO₂, thus a full enthalpy balance becomes an important tool in accurately model the injection system. Heat transfer to and from the surrounding environment need to be included to get an accurate determination pressure and temperature along the injection system.

5.4 Numerical Simulation of CO₂ Flows

The purpose of simulating CO₂ transport is to form the basis of design for pipes and wells. It is useful in optimizing and verifying the design. The simulations need to encompass both normal steady state operation and transient operation such as start-up and shut-in. The oil and gas industry has considerable experience transporting hydrocarbons liquid and gases through pipelines and in wells. The flow of CO₂ may differ significantly to these for the following reasons [30]:

- CO₂ is usually transported as a single-component fluid, with only small impurities. The thermodynamic phase envelope of CO₂ flow is thus expected to be very narrow. The result is more abrupt phase changes in CO₂ fluids.
- The molar weight of CO₂ is 44 kg/kmol, versus 16 kg/kmol for methane. The density of CO₂ flow is thus much higher than that of natural gas.
- CO₂ is normally transported in dense phase, to optimize throughput at a low pressure (high density, low viscosity)

Most simulation software in the oil and gas industry is developed to model water, oil and gas flows. CO₂ have different properties than these fluids, and thus it is not self evident that they will also perform well with CO₂ flows. Simulations software use equation of state to calculate thermodynamic properties of the involved fluid. The standard EoS used in the oil & gas industry has been developed and improved for hydrocarbon system and are less accurate for modeling pure CO₂.

Reviews of the applicability of EoS to accurately determine thermodynamic properties of CO₂ have been published by Boyle et al. (2001) [31]. The results for pure CO₂ showed absolute average errors from SRK of 6.31% in the supercritical region and up to 13.38% in the liquid region. The PR EoS showed absolute average errors from 2.11% in the supercritical region up to 2.20% in the liquid region but 6.51% near the critical area.

In another study the SRK showed a deviation of 26% and BWRS EoS showed 12% within the considered temperature range from 0 to 37°C and pressure from 20 to 100 bar [32].

Sugianto (2007) also investigated the accuracy of the most common EoS used in the oil & gas industry to predict various thermodynamic properties. His result for CO₂ density is given in Table 5.1[33].

	Density [% error]		Near Critical Region [% error]	
	0<T>200°C & 1<P<400 bara			
	Min.	Max.	Min.	Max.
PR	-10	6	-1	13
TWU	-10	6	-1	13
BWRS	-5	4	0	12
PT	-12	3	-1	17
SRK	-18	0	0	35
TB	-1	15	-3	5

Table 5.1: Sugianto (2007) error for density [33].

The accuracy of various EoS in predicting density are reasonable accurate in the vapor phase (AAE less than 2%), and yield less accurate results for dense phase (liquid and SC) (AAE more than 2%) [31]. Transportation of CO₂ is primarily in dense phase.

There is no real consensus which EoS that should be used for simulating CO₂ flow, especially when impurities are present. For different CO₂ mixtures different EoS might be the preferred choice. Not one EoS covers all possible mixtures to the same degree of accuracy.

A reference equation for pure CO₂ has been introduced by Span and Wagner (2002) [34]. Deviation between measured and predicted values for density is in the range of ±0.05%.

5.4.1 Effect of Impurities

Generally there are no strong technical barriers to provide high purity of CO₂. However, higher purity requirements are likely to induce extra cost requirements. The purification of a CO₂ stream vary depending on the purification process. Prelude will utilize an amine solution and will be relatively clean, with the main impurity being H₂S. Impurities in the CO₂ stream affects the design of the compression system, flowline and well. Thermodynamic and transportation properties of the CO₂ stream will be affected, and can either be beneficial or detrimental. The relationship between source, requirements and pretreatment and their effect upon well/flowline design and operation are shown schematically in Figure 5.5.

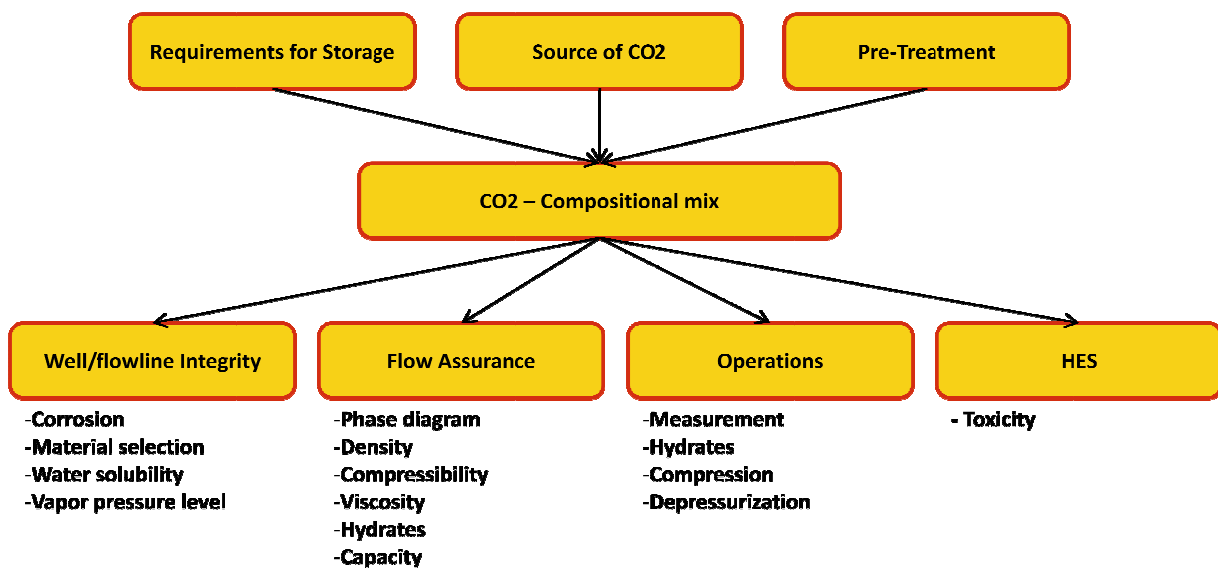


Figure 5.5: Schematic description of impurities effect upon well design and operation.

Most referenced studies focus on binary CO₂ mixtures, but most CO₂ flue gases are multi compositional. With more than one impurity, the changes in thermodynamic properties remain unclear. Further, the current binary studies are performed at pressures and temperatures not covering the complete operating envelope of Prelude. A list of binary data available can be found in [32].

Because of the lack of reference values for mixtures of CO₂ and impurities, and for binary CO₂ mixtures within the operating envelope, the composition for all modeling purposes will be pure CO₂.

5.4.2 Well Performance Simulations

A steady-state simulation software can tell how pressure, flow and temperature is going to be distributed along the well/pipe once some sort of equilibrium state has been established, and nothing about the way there. A fully transient simulator has the ability to say something about the way to steady-state condition. For this study, no fully transient simulation tool was available.

Prosper (version 11.1) was used to model inflow/outflow performance, utilizing Peng – Robinson Equation of State (PR). The PR is described by [35]:

$$p = \frac{RT}{v-b} - \frac{a}{v^2+2bv-b^2} \quad \text{Eq. 5.2}$$

where

$$a = \frac{0.45724R^2T_c^2}{p_c} \alpha \quad \text{Eq. 5.3}$$

$$b = \frac{0.07780RT_c}{p_c} \quad \text{Eq. 5.4}$$

$$\alpha = [1 + (0.37464 + 1.54226\omega - 0.26992\omega^2)(1 - \sqrt{T_r})]^2 \quad \text{Eq. 5.5}$$

where T_c and p_c are the critical temperature and pressure for the pure compound and T_r the reduced temperature:

For CO_2 , changes in pressure and temperature can have a significant impact on fluid density and therefore the column weight in the tubing and wellbore. The vertical lift performance (VLP) greatly depends on fluid density and viscosity, which depends on pressure and temperature at every point along the flow path, including the riser, flowline and wellbore. Thus to validate the simulated density and viscosity calculated from Prosper, they were compared to pure fluid property reference package (REFPROP) from NIST, Figure 5.6.

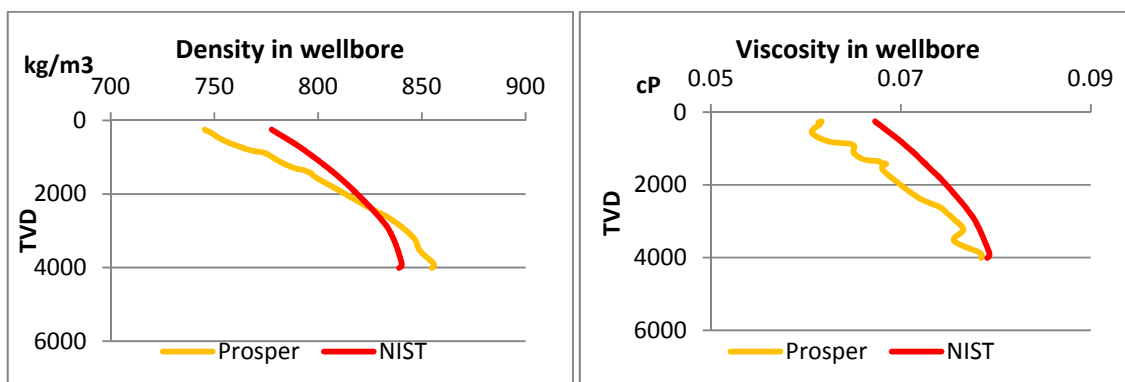


Figure 5.6: Comparison between values calculated by Prosper (PR) and REFPROP from NIST.

From Figure 5.6 it is observed that the density profile calculation from Prosper and NIST deviates at top and bottom of well. However, the average density in the tubing deviates with less than 1%, and can thus be used to calculate the injection pressure required. Viscosity is involved in pressure and temperature profile through the Reynolds number to estimate friction factor of flowing fluid.

Simple sensitivity calculation performed in connection to the thesis indicated that friction factor is only a weak function of Reynolds number. Reynolds number is given by [35]:

$$Re = \frac{\rho v d}{\mu} \quad \text{Eq. 5.6}$$

where μ is viscosity, ρ density, v is the flowing velocity and d the diameter of the pipe. The Reynolds number is used in calculation of friction factor. One common correlation to predict friction factor for single phase is the Colebrook and White equation [35]:

$$\frac{1}{\sqrt{f}} = 1.74 - 2 \log \left(\frac{2\varepsilon}{d} + \frac{18.7}{N_{Re}\sqrt{f}} \right) \quad \text{Eq. 5.7}$$

where ε is pipe surface roughness and f the friction factor.

Thus the observed viscosity error do not transform into an equally large error in pressure and temperature. Sugianto (2007) also showed that PR EoS deviates even higher for conceptual properties like enthalpy, entropy and thermal conductivity. Petroleum Experts (company) are developing a method for calculating CO₂ or CO₂ mixtures for implementation in Prosper[36].

To accurately model the CO₂ injection system, the pressure and temperature along the riser, flowline and tubing depend on heat transfer to and from the surrounding environment. This can be done using full enthalpy balance in Prosper. This thermodynamic model considers heat transfer by conduction, radiation, and forced and free convection. The model is described in the next section. Prosper input screens are shown in [Appendix B](#).

Description of fluid flowing requires three conservation equations:

- Continuity equation (mass balance)
- Momentum/Impulse equation
- Energy equation

Mass and momentum conservation are direct flow considerations and can not reveal anything about how the temperature develops in the fluid. Heat flow has a large impact on pipeline hydraulics for CO₂ flow. Heat flow is included in the model through energy conservation equation with states that net energy coming into an element has to accumulate within it.

The first law of thermodynamics for open system yields the following equation [33]:

$$\frac{dU_{cv}}{dt} = \dot{Q} - \dot{W} + \dot{m}_i \left(u_i + p_i v_i + \frac{v_i^2}{2} + g z_i \right) - \dot{m}_e \left(u_e + p_e v_e + \frac{v_e^2}{2} + g z_e \right) \quad \text{Eq. 5.8}$$

The subscript i and e refer to in and exit. U_{cv} (Joule) is the total internal energy of control volume. t (s) is time. \dot{Q} (J/s) is the heat rate exchanged between the system with surroundings (positive for the heat enters the control volume). \dot{W} (J/s) is work exchanged between system and surroundings (positive for work done by system). \dot{m}_i and \dot{m}_e (kg/s) are mass rate into and out of system respectively. u_i (J/kg) and u_e is specific internal energy of the fluid entering and exiting the system. v_i and v_e (m³/kg) are specific volume of fluid in and out of the system. V_i and V_e (m/s) are the



velocity of fluid in and out to/from the system. z_i and z_e (m) is the vertical distance from inlet and outlet of the system relative to reference spot.

The equation is solved in Prosper to give pressure and temperature gradient along the flowline and tubing.

The flow from the reservoir to the tubing is known as inflow performance (IPR). To calculate the pressure drop occurring in a reservoir an equation is needed to calculate the pressure losses as a function of flow rate. There are several forms of this equation depending on fluid and formation type, but all are based on the fundamental equation known as Darcy's Law [37]:

$$q = -\frac{kA}{\mu} \cdot \frac{\delta p}{\delta x} \quad \text{Eq. 5.9}$$

q = flow rate

k = permeability

A = area open to flow

μ = fluid viscosity

$\frac{\delta p}{\delta x}$ = pressure gradient in the direction of flow

The latter equations are solved simultaneously within Prosper to give the solution for the system. From the solution, the pressure and temperature profile along the flowline and in the well can be obtained.

Well performance simulators contain limitations to representing actual inflow performance. These limitations need to be understood such that the results can be judged fit for purpose or not. Limitations specific to CO₂ injection are [38]:

- Well performance simulators are stand-alone units, which analyse one well configuration at time. This means that they do not take into account well interference or other external behavior. They are also 'static' models, which assume a certain instantaneous pressure regime so time dependent variables will change.
- All reservoir inflow models available in well simulators assume a simple homogeneous radial 'pie' reservoir with the well positioned in the centre. Only basic variables like permeability, thickness, well bore size, drainage radius etc, can be adjusted.
- Like most standard petroleum engineering software, they are designed around hydrocarbon-water systems. This HC-water fluid is assumed to be present throughout the entire system. By the same token, when CO₂ fluid is selected, it is assumed to be injecting into a CO₂ reservoir. Therefore, relative permeability effects are not included and the initial calculation rate (when water is immediately around the wellbore) would be very optimistic. There is also more complex supercritical CO₂-water interaction affecting dissolution rates and front progress.
- For injection into an aquifer, CO₂ is a foreign fluid so there will be chemical rock interactions that could open or block pores. None of these behaviors are taken into account.

It is thus not possible to model injectivity with a well performance simulator because we are not able to account for geomechanical, geochemical, reservoir heterogeneity, skin increase, mobility and relative permeability over time. To model injectivity it is necessary to use a reservoir model and include coupled wellbore-reservoir responses.

A generic challenge in using simulation tools preventing utilizing them as 'black boxes'. There is no substitute for understanding what a simulation tool do, how they work, and their limitations. Interfacing with a simulation software means understanding it's possibilities and limitations and how to interpret and check the results.

5.4.3 Enthalpy Balance

Enthalpy balance temperature model in Prosper applies the general energy equation for flowing fluid [39]:

$$\Delta U + \Delta \left(\frac{mv^2}{2} \right) + \Delta(mgz) + \Delta(PV) - Q = 0 \quad \text{Eq. 5.10}$$

In terms of enthalpy [39]:

$$H = U + pV \quad \text{Eq. 5.11}$$

This is written [39]:

$$\Delta H + \Delta \left(\frac{mv^2}{2} \right) + \Delta(mgz) - Q = 0 \quad \text{Eq. 5.12}$$

In other terms [39]:

$$\frac{dT}{dz} = \frac{1}{c_{pm}} \left(\frac{dQ}{dz} - g \sin \theta - v \frac{dv}{dz} \right) + \mu_T \frac{dP}{dz} \quad \text{Eq. 5.13}$$

Prosper solves the general energy equation by considering the enthalpy balance across an incremental length of pipe. The enthalpy term includes the effects of pressure (including JT effect) and phase changes.

The algorithm commences by calculating the enthalpy at the known pressure and temperature of the first calculation node (H_1 at T_1, P_1)

For a given pipe increment, the enthalpy (H_2) at the other end of the pipe is estimated. The difference (H_2-H_1) is compared to ΔH , where [39]:

$$\Delta H = -\frac{\Delta Q}{\rho_l q_l + \rho_g q_g} + \Delta L \cos \theta + \frac{1}{2} \frac{\bar{V}_{tot}^2}{g} \quad \text{Eq. 5.14}$$

If previous calculation exist, then [39]:

$$P_2 = P_1 - G\Delta L; \quad T_2 = T_1 - \frac{dt}{dz} \Delta L \quad \text{Eq. 5.15}$$

To give the first estimate of H_2 . We now deal with a piece of tubing of length L , and [39]:



$$\bar{P} = \frac{P_1+P_2}{2}; \quad \bar{T} = \frac{T_1+T_2}{2} \quad \text{Eq. 5.16}$$

The total heat transfer coefficient is estimated for T, P of the iteration step to calculate the heat exchanged. Using the energy equation, dh can be found. If dh does not equal H₂-H₁, the iteration continues until convergence. The enthalpy balance method solves the energy equation simultaneously for both temperature and pressure. The solution temperature at the downstream side of the pipe increment is therefore the value T₂ when the iteration has converged.

The heat transfer coefficient is used to calculate dQ within the enthalpy balance iterations and not the temperature. The heat transfer coefficient is itself a function of the temperature of both the fluid and the surrounding; therefore iteration is required to find both the heat transfer coefficient and the enthalpy balance. The formation is a thermal sink at temperature T_e. The temperature profile near the wellbore is dependent upon injection/production time and the thermal diffusivity of the formation. The heat diffusivity equation accounts for localized heating (or cooling) of the formation by the well fluids.

For a pipe increment, the heat flow is calculated using [39]:

$$dQ = 2\pi \left[\frac{(T_f - T_e)}{\frac{f(t)}{k_e} + \frac{1}{r_{to} U_{to}}} \right] \Delta L \quad \text{Eq. 5.17}$$

where T_f-T_e is the temperature difference between the fluid and the formation at infinity, k_e is the effective thermal conductivity of the formation, f(t) is the solution of the heat diffusivity equation and U_{to} the overall heat transfer coefficient.

The exact solution of the heat diffusivity equation is [39]:

$$\frac{1}{f(t)} = \frac{4}{\pi^2} \int_0^\infty e^{-x^2 u^2} \frac{du}{u(j_0^2(u) + \gamma_0^2(u))} \quad \text{Eq. 5.18}$$

This integral poses numerical problems as u₀ and is slow. This equation is evaluated for very early times only. For intermediate times, Prosper uses a fit of the TD vs tD generated using the exact solution. At later times logarithmic approximations is used [39]:

$$f(t) = 0.982 \log_e \left(1 + 1.81 \frac{\sqrt{\alpha t}}{r_n} \right) \quad \text{Eq. 5.19}$$

where thermal diffusivity:

$$\alpha = k/(\rho C p) \quad \text{Eq. 5.20}$$

This formulation approximates the exact solutions with less than 1% error.

The overall heat transfer coefficient is [39]:

$$\frac{1}{U_{TO}} = \frac{1}{h_f} + \frac{1}{h_c} + \frac{1}{h_r} + \frac{1}{h_{co}} \quad \text{Eq. 5.21}$$



The overall heat transfer coefficient takes into account forced convection inside the pipe and free convection outside the pipe plus radiation and conduction.

Heat transfer from the pipe is in three terms [39]:

Conduction

$$\Delta Q = 2\pi k \Delta L \frac{(T_1 - T_2)}{\log_e\left(\frac{r_2}{r_1}\right)} \quad \text{Eq. 5.22}$$

Forced Convection:

$$\Delta Q = 2\pi r_2 h_f \Delta L (T_1 - T_2) \quad \text{Eq. 5.23}$$

Free Convection and Radiation:

$$\Delta Q = 2\pi r_1 (h_c + h_r) (T_1 - T_2) \quad \text{Eq. 5.24}$$

Examining the components of the overall heat loss coefficient individually. h_f is due to forced convection inside the pipe [39]:

$$h_f = \frac{0.023 k Re_{en}^{0.8} Pr_r^{\frac{1}{3}}}{r_{ti}} \quad \text{Eq. 5.25}$$

Where k is the average conductivity [39]:

$$k_{av} = k_{gas}(1 - holdup) + k_{liquid}(holdup); \quad \Delta Q = 2\pi r_1 (h_c + h_f) \Delta L (T_1 - T_2) \quad \text{Eq. 5.26}$$

Re_{en} = mixture Reynolds number

$$Pr_r = \frac{C_p \mu}{k} \quad \text{Eq. 5.27}$$

Mixture Prandtl number:

$$C_p = C_{p\ gas}(1 - holdup) + C_{p\ liquid}(holdup) \quad \text{Eq. 5.28}$$

In the annulus, the free convection term is [39]:

$$h_c = \frac{0.049(G_r Pr_r)^{\frac{1}{3}} Pr_r^{0.0074} k}{r_{to} \log_e\left(\frac{r_{ci}}{r_{to}}\right)} \quad \text{Eq. 5.29}$$

Where:

$$G_r = \frac{(r_{ci} - r_{co})^3 \rho_a^2 \beta g (T_{to} - T_{ci})}{\mu_a^2} \quad \text{Eq. 5.30}$$

i.e mixture Grashof number, and ρ_a is mixture density, and thermal expansion coefficient given by:

$$\beta = -\frac{1}{\rho} \left(\frac{\partial \rho}{\partial T} \right)_p \quad \text{Eq. 5.31}$$



The convection terms are themselves a function of temperature. Iteration is therefore required to find the annulus temperature for the convection term and determine the overall heat transfer coefficient.

The radiation term is given by [39]:

$$h_r = \frac{\sigma(T_{to}^2 + T_{ci}^2)(T_{to} + T_{ci})}{\frac{1}{\varepsilon_{to}} + \frac{r_{to}}{r_{ci}} \left(\frac{1}{\varepsilon_{ci}} - 1 \right)} \quad \text{Eq. 5.32}$$

Where σ is the Stefan-Boltzman constant and ε is emissivity.

The Conduction Terms. An example is for the tubing, where [39]:

$$h_{co} = \frac{r_{to} \log_e \left(\frac{r_{to}}{r_{ti}} \right)}{k_i} \quad \text{Eq. 5.33}$$

Similar expressions are used for each casing string and each term combined to find the total conductivity term U_{TO} .

5.5 Tubing Size

The tubing size is inherently important for pressure and temperature calculations. Considering the injection rates in [Chapter 4](#), the preferred tubing size for the injection well is a 7" tubing. This is based on the need to provide sufficient flow area to keep injection pressures as low as possible. Figure 5.7 show a sensitivity plot of gas injection rate as function of the host facility discharge pressure for the Swan injection well with a highly deviated well.

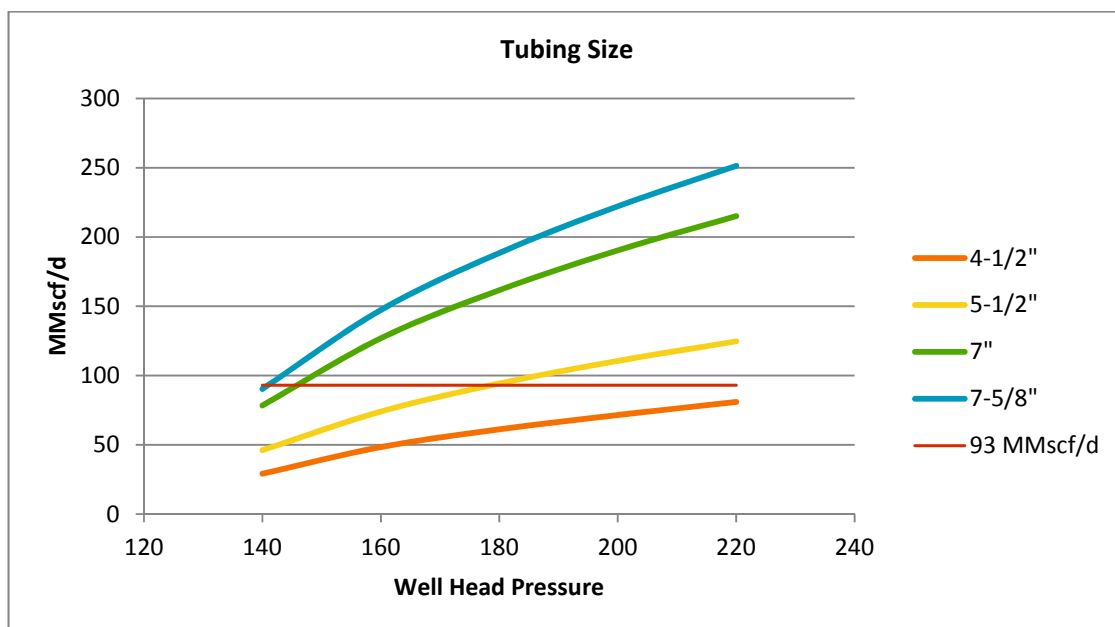


Figure 5.7: Tubing size sensitivity modelling.

The result shows that a 7" tubing provides significant lower injection pressures to meet the required injection rate, compared to the smaller tubing sizes. The 5-1/2" tubing is feasible, but offers limited flexibility and requires high discharge pressure at the full facility design rate. The 7-5/8" tubing only provides marginal increased tubing performance.

5.6 Deviation

Four different deviations were considered for the well:

- Vertical
- Slightly Deviated (55°)
- Highly Deviated (85°)
- Horizontal

Simulation was performed with Prosper with three different reservoir realizations:

- Base Case: Permeability of 36.5 mD and mechanical skin 1.
- Good Case: Permeability of 69.5 mD and mechanical skin 1.
- Bad Case: Permeability of 21.4 and mechanical skin 2.5.

These cases were constructed based on sensitivity analysis on the most important factors affecting injection pressure. The result from this exercise can be observed in Figure 5.8.

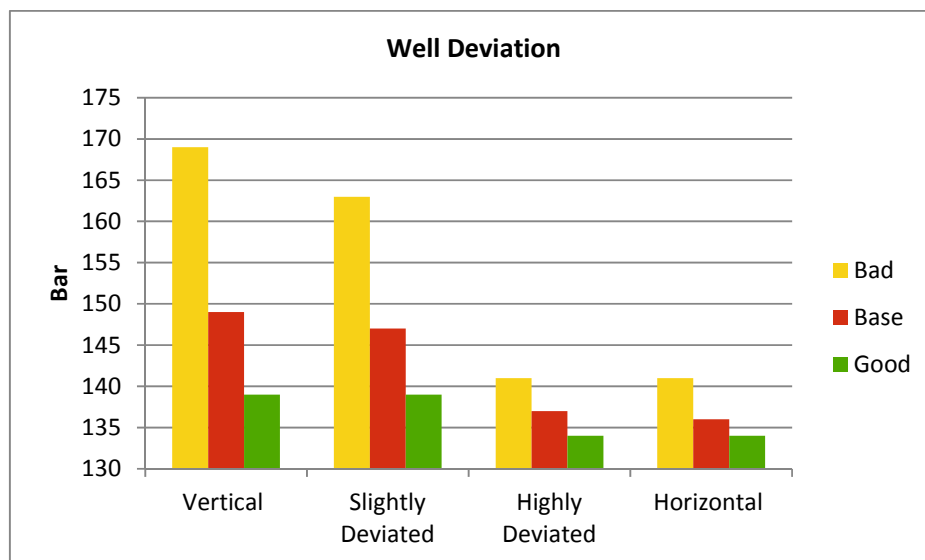


Figure 5.8: Well deviation and injection pressure for rate of 93 MMscf/d.

The objective for the well is to inject a maximum of 93 MMscf/d at as a low injection pressure as possible. With this in mind, the “Bad Case” gives a very high injection pressure for both vertical and slightly deviated well. Because of this, they are excluded from further discussion, and the choice stands between highly deviated and horizontal. The injection pressures for these two cases are similar. However, because of shale draping in the Swan reservoir, highly deviated well will be selected. By drilling highly deviated through the reservoir there is higher chance of intersecting

high quality horizons, and less chance of pressure build up caused by accumulating in “the shoe box”. Highly deviated well also gives redundancy if wellbore impairment should occur.

5.7 Operating Pressure

The objective of this section is to define the operating pressure for wellhead and bottomhole for the three reservoir realizations described in section 4.4. The pressures are calculated for initial reservoir pressure (415 bar) and expected abandonment pressure (136 bar). The lower completion is OHGP as recommended in [Chapter7](#). All calculation used a discharge temperature of 40°C. The results are tabulated in Table 5.2.

Rate	46 MMscf/d		65 MMscf/d		93 MMscf/d	
	WHP	BHP	WHP	BHP	WHP	BHP
415 bar						
Base [bar]	86	419	136	422	144	425
Good [bar]	130	417	134	418	141	420
Bad [bar]	135	427	142	432	154	442
136 bar						
Base [bar]	65	143	71	149	78	158
Good [bar]	64	140	69	142	77	148
Bad [bar]	68	156	75	167	80	189

Table 5.2: Injection pressure. Rounded to nearest bar.

As can be observed from the table, the pressures at well head and bottom hole is dependent on the reservoir realization and the injection rate. The expected wellhead operating envelope is 64-154 bar. For bottomhole it is in the range 143-442 bar.

5.8 Operating Temperature

The objective of this section is to define the operating temperature for wellhead and bottomhole. The pressures are calculated for initial reservoir pressure (415 bar) and expected abandonment pressure (136 bar). The lower completion is OHGP as recommended in [Chapter7](#). All calculation used a discharge temperature of 40°C. The results are tabulated in Table 5.3.

Rate	46 MMscf/d		65 MMscf/d		93 MMscf/d	
	WHT	BHT	WHT	BHT	WHT	BHT
415 bar						
Base [°C]	38	86	39	83	39	80
Good [°C]	39	86	39	83	39	80
Bad [°C]	38	85	39	82	39	79
136 bar						
Base [°C]	31	108	33	102	36	94
Good [°C]	30	107	32	100	36	91
Bad [°C]	32	109	35	105	37	95

Table 5.3: Injection temperature. Rounded to nearest °C.

As can be observed from the Table 5.3, the temperature at well head and bottom hole is dependent on the injection rate. When the rate is low, the velocity is low, and thus the time a certain mass CO₂ uses

from WH to BH is longer. Thus it will gain more heat from the surroundings. The expected wellhead operating envelope is 30-39°C. For bottomhole it is in the range 80-109°C.

5.9 Operating Envelope

The pressure and temperature calculated in the previous two sections can be put into a PT-diagram to obtain the operating envelope for the well, Figure 5.9.

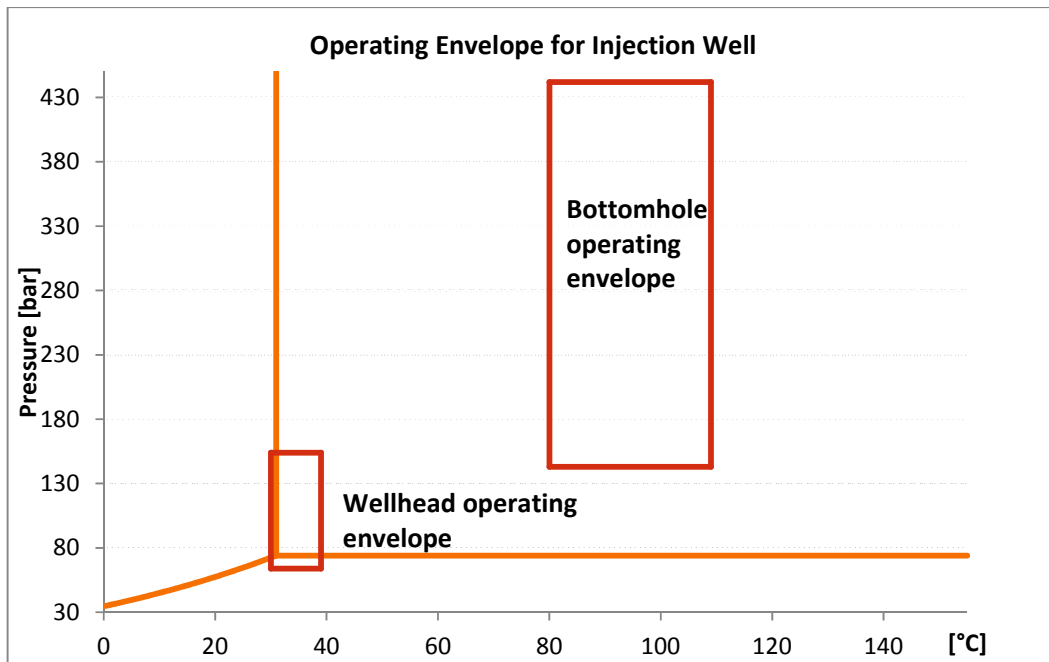


Figure 5.9: Operating Envelope for Well.

For majority of the field life, the well will be operated in the dense phase. The advantage of operating the well in single phase (above saturation line) is small variation in CO₂ density under steady-state condition.

To maintain dense phase late life, the discharge pressure could be increased.

5.10 Steady-State Behavior with Time

All the calculations performed so far with Prosper, have been at 100 days since production start. Prosper is capable of predicting transient state of energy balance between the fluid and the surrounding casing/annulus/cement/formation as function of time. The results can be observed in Figure 5.10.

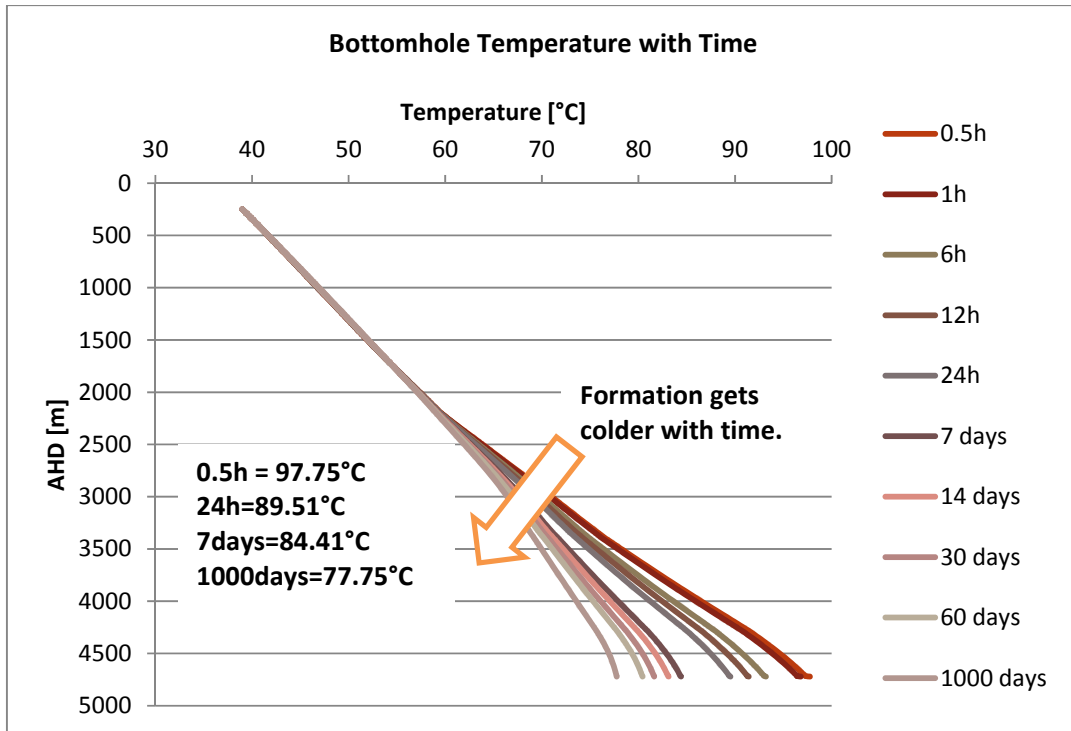


Figure 5.10: Fluid bottomhole temperature with time.

Prosper assumes the specific injection rate (93 MMscf/d) has commenced a certain amount of time. In Figure 5.10 the 1000 days case indicate steady state injection for 1000 days without any transient operations. As the cold injection commences over time, the colder fluid receives heat from the surrounding formation. The heat flow is calculated from Eq. 5.17:

$$dQ = 2\pi \left[\frac{(T_f - T_e)}{\frac{f(t)}{k_e} + \frac{1}{r_{to} U_{to}}} \right] \Delta L$$

Where $T_f - T_e$ is the temperature difference between the fluid and the formation at infinity, k_e is the effective thermal conductivity of the formation, $f(t)$ is the solution of the heat diffusivity equation and U_{to} the overall heat transfer coefficient.

The temperature near the wellbore is dependent upon injection time and the thermal diffusivity of the formation. The heat diffusivity equation accounts for localized cooling of the formation. The overall heat transfer coefficient accounts for forced convection inside the pipe and free convection outside the pipe plus radiation and conduction.

5.10.1 Quality Control of Model

In order to investigate the robustness of the model a hypothetical injection rate of 1 MMscf/d was considered, keeping all other parameters constant. If the model is robust, then due to such low flow rates and long exposure time, the flowing bottom hole temperature should reach the formation temperature of 155°C right from the start.

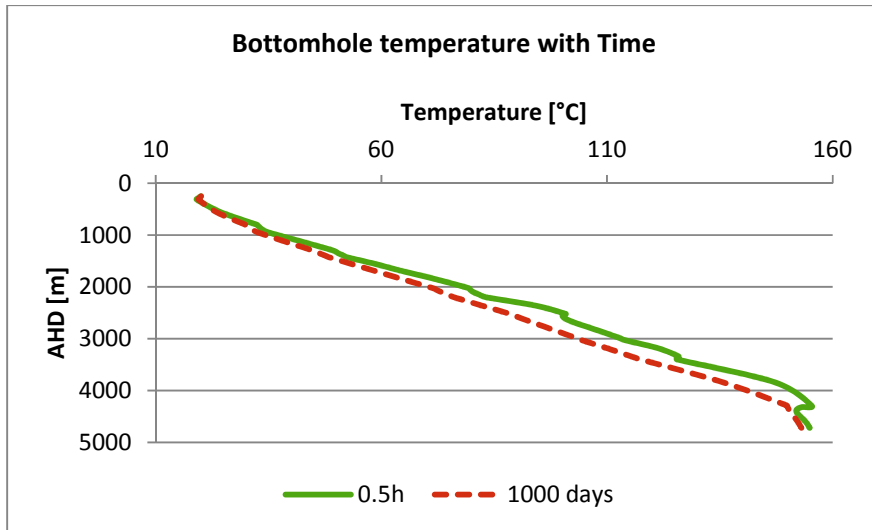


Figure 5.11: Temperature as function of time for hypothetical case of 1 MMscf/d injection rate.

Figure 5.11 show the transient temperature profile at 0.5h and 1000 days for an injection rate of 1 MMscf/d. As expected the fluid reached formation temperature from the beginning, due to low flow rate and high exposure time. Hence the model is robust in predicting the steady-state temperature as a function of time.

5.11 Closed In Tubing Head Pressure (CITHP)

The CITHP for different reservoir pressure was determined using data from NIST. In closed-in condition there are no frictional loss, and it is assumed that the CO₂ reaches equilibrium with the geothermal gradient. The pressure drop along the well can be calculated using the static head equation:

$$\frac{dp}{dz} = \rho g \quad \text{Eq. 5.34}$$

Where ρ is fluid density, g is the acceleration of gravity and z denotes the true vertical depth from the well head. By dividing the well pipe into small segments of length, the well head pressure can be calculated from reservoir to wellhead using NIST data for density at each segment.

Figure 5.12 below pictures the CITHP and its variation with the reservoir pressure. It is observed that the CITHP remains constant when reservoir pressure is depleted beyond ~ 220 bars.

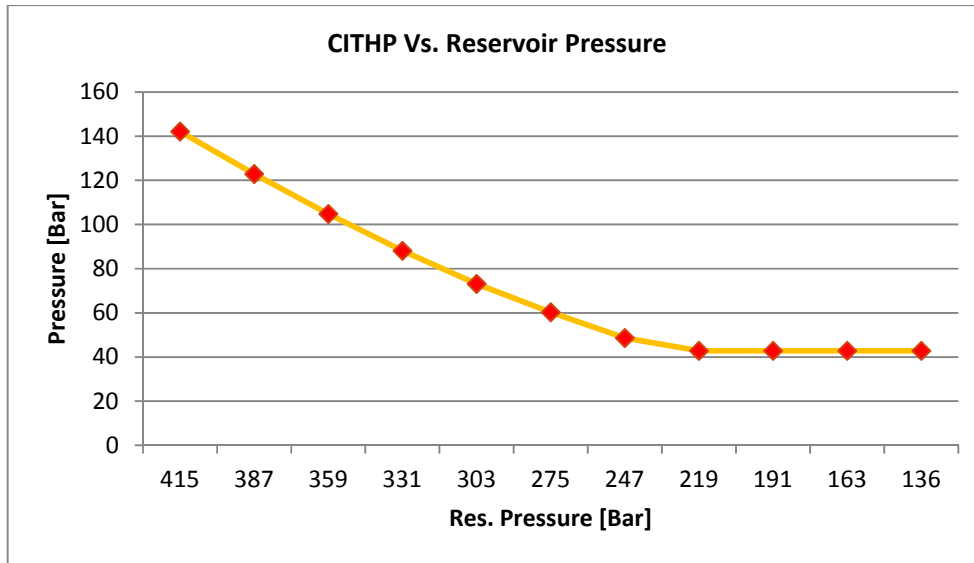


Figure 5.12: CITHP variation with change in reservoir pressure.

Under closed-in conditions, a gas-liquid phase boundary is present in the well depending on the reservoir pressure (see Figure 5.13). With decreasing reservoir pressure, the liquid hold-up depth increases, i.e. liquid level falls. It can be interpreted from the graph below that when the reservoir pressure is less than ~220 bars, under closed-in conditions, two phases will be observed in the well. Liquid and gas interface level depends on the reservoir pressure. From initial reservoir pressure to ~220 bars, the CO₂ in the well will be in dense phase (liquid only) and no interface is observed.

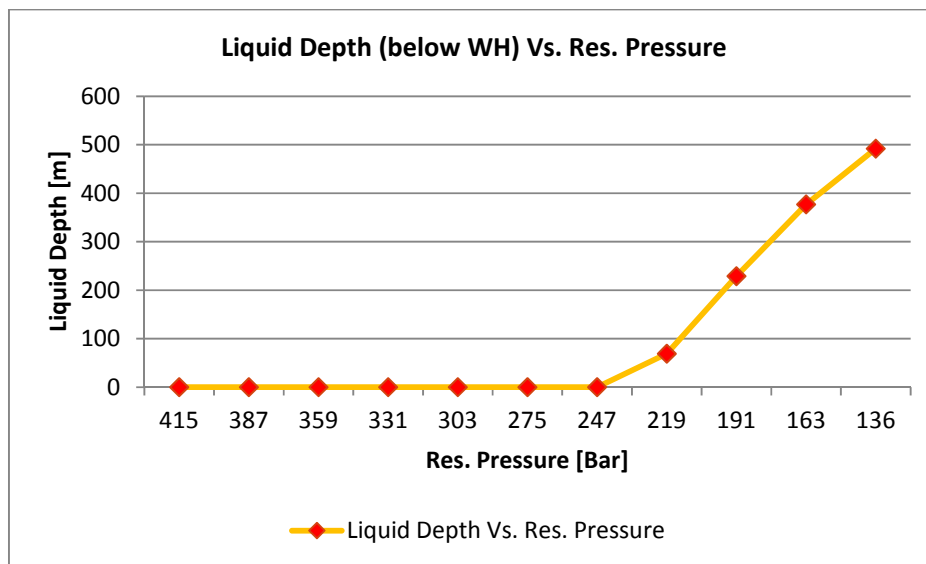


Figure 5.13: Liquid depth in the well during closed-in condition for different reservoir pressures.

Below is a graph depicting the change in density/phase for various reservoir pressure. The depth from which both liquid and gas density is observed is the interface of two phases of CO₂. It is observed that

density in the bottom of the well is lower than the density of the liquid CO₂ higher up in the well. This will introduce a flow instability.

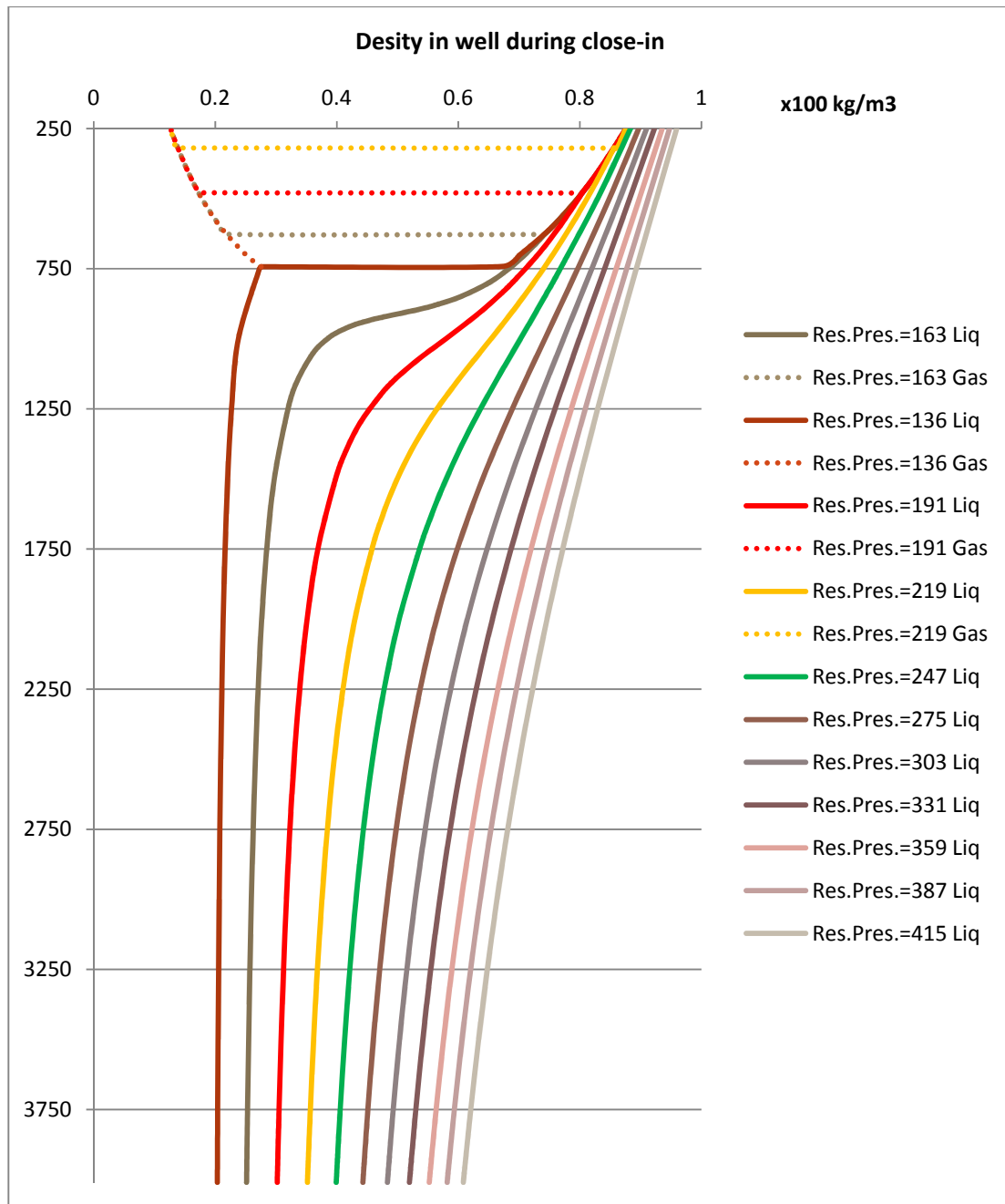


Figure 5.14: Density variation in the well during closed in condition for different reservoir pressure.

When two phases exist in the well, just after shut in, liquid can be expected above gas in many places which gives flow instabilities, illustrated in Figure 5.15 with a seabed temperature of 8°C and reservoir pressure of 136 bar.

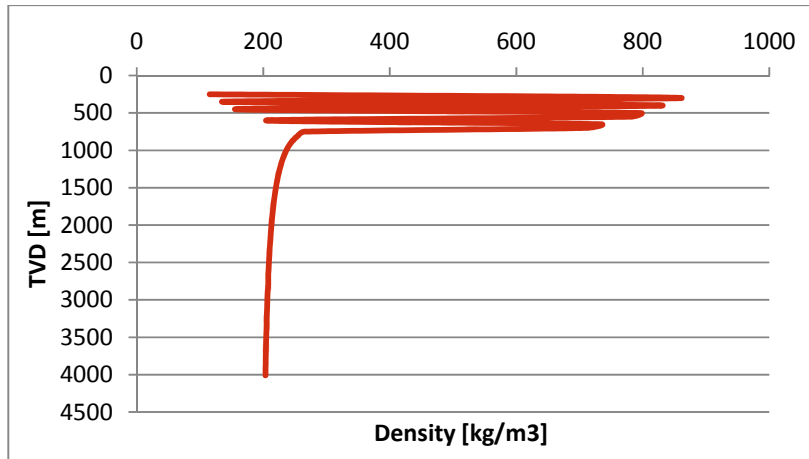


Figure 5.15: Mixture density as a function of depth when the reservoir pressure is 136 bar and has a temperature of 155°C.

Lord Rayleigh (1883) derived that an instability in the surface between two fluids on top of each other will propagate if the fluid situated on top has a higher density than the fluid on the bottom, and that it will go faster if the difference between the two fluids is larger [30]. More precise, a growth of a small perturbation at the interface is exponential and takes place at a rate $\sim \exp(\lambda t)$, where t denotes time and λ is the growth rate equal to [30]:

$$\lambda = \sqrt{R \cdot g \cdot \alpha} \quad \text{Eq. 5.35}$$

Here, g is acceleration of gravity, α is the spatial wave number of the perturbation and the ratio [30]:

$$R = \frac{(\rho_{heavy} - \rho_{light})}{(\rho_{heavy} + \rho_{light})} \quad \text{Eq. 5.36}$$

The well in Figure 5.15 will therefore experience that vapor rise through the well, cool down and form liquid, which in turn fall down. The result is a circulating flow which in principle can go on as long as the geothermal profile is transmitted to the fluids in the well.

A relatively stable column with gas above liquid can be obtained when the fluid and surrounding casing and formation is no longer at geothermal gradient due to prior boiling and condensation. A stable static column is obtained when gas over liquid has a thermal gradient that follows the saturation line. This indicates that overtime, the casing and rock in the vicinity of the well will approach these gradients above and below the gas-liquid boundary [29].

5.12 Transient Temperature Analysis

In this part we will do a simple analysis of what is to be expected during transient operations like emergency shut-in, shut-in and start-up of the injector well. Fully transient software can simulate these operations, but was not available for this study.

5.10.1 Emergency Shut-down

Upon closing in a well the frictional pressure drop is lost. Depending on the reservoir pressure, this will cause CO₂ to flash to gas near the top of the well. Due to the Joule Thomson effect the temperature will

drop. The chilling effect will increase as the pressure of the reservoir decreases with depletion. For ESD the amount of CO₂ is restricted to the tubing volume, which will restrict the thermal effects in the rest of the well (Annulus, tubing, casing, etc.).

When injecting the fluid pressure in bottom hole will be higher than the reservoir pressure. Once shut in, this will start equalizing with the reservoir pressure. When shut-in, the WH pressure will also fall, due to removal of the friction. A conservative approach is thus assuming compressed hydrostatic head from fluid reservoir depth to WH. Several mechanisms occur when the well is shut-in:

- Friction goes to zero.
- Bottomhole pressure goes towards reservoir pressure.
- Column of fluid start to expand due to reduced pressure.
- Expansion causes the column to lighten.
- Expansion causes mass flow out of tubing.
- Depending on conditions, gas may flash at WH.

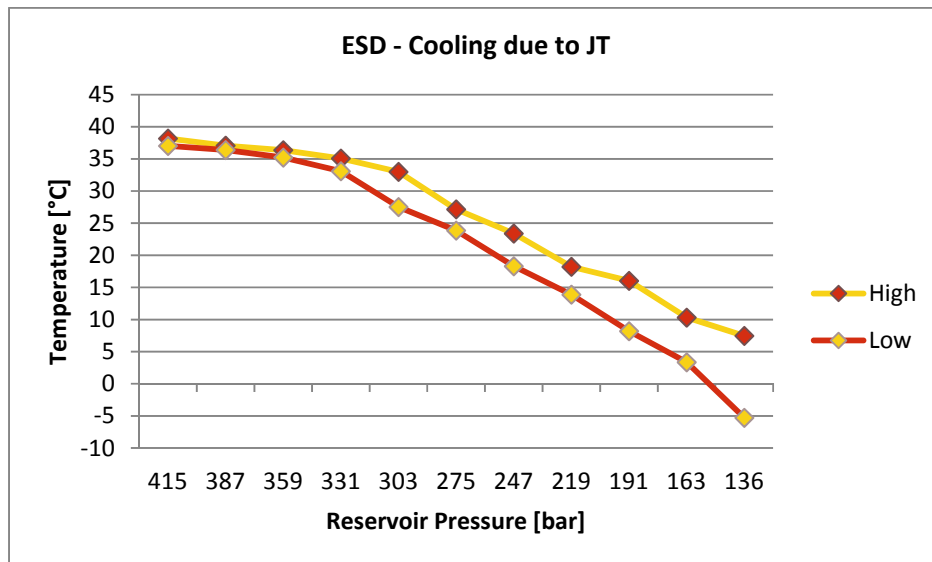


Figure 5.16: Conservative approach to ESD of JT cooling in the injector.

The temperature drop can thus be estimated by the JT effect. JT coefficient can easily be calculated from NIST data using:

$$\mu_{JT} = \frac{v}{c_p}(\alpha T - 1) \quad \text{Eq. 5.37}$$

where α is the coefficient of thermal expansion. The JT coefficient have to be calculated at various pressures and temperatures in steps as the JT coefficient will change with pressure and temperature. For example, if CO₂ at 70 bar, 39°C is taken down to 35 bar, the temperature will drop to approximately 1°C as shown in Table 5.4.

Pressure [bar]	Temperature [°C]	JT [°C/MPa]
70	39.00	8.922
65	34.53	9.486
60	29.79	10.093
55	24.749	10.746
50	19.37	11.45
45	13.65	12.214
40	7.54	13.049
35	1.02	

Table 5.4: JT cooling.

Figure 5.16 above indicate that the wellhead temperature during ESD depend on reservoir pressure. Late life, it may become below freezing. At 136 bar reservoir pressure, the WH pressure will drop from 76 bar to 30 bar. This is below the pressure required to keep CO₂ in dense phase, and thus CO₂ flashes and the temperature drop due to the JT effect.

5.10.2 Close-In and Start-Up

The well can be closed in by means of a choke. The choke will be gradually closed, and the injection ramped down and finally shut-in. If the CO₂ remains in liquid phase upstream and downstream of the choke, only small temperature difference is expected. If however, the CO₂ reaches the saturation line, a small change in pressure can provoke a very large change in temperature (follows saturation line). This happens as the CO₂ goes through an adiabatic flash were the vaporized gas will experience rapid Joule Thomson cooling. During late life, there is a possibility of this occurring. This is illustrated in Figure 5.17. The pressure drop down to the saturation line is illustrative, not real.

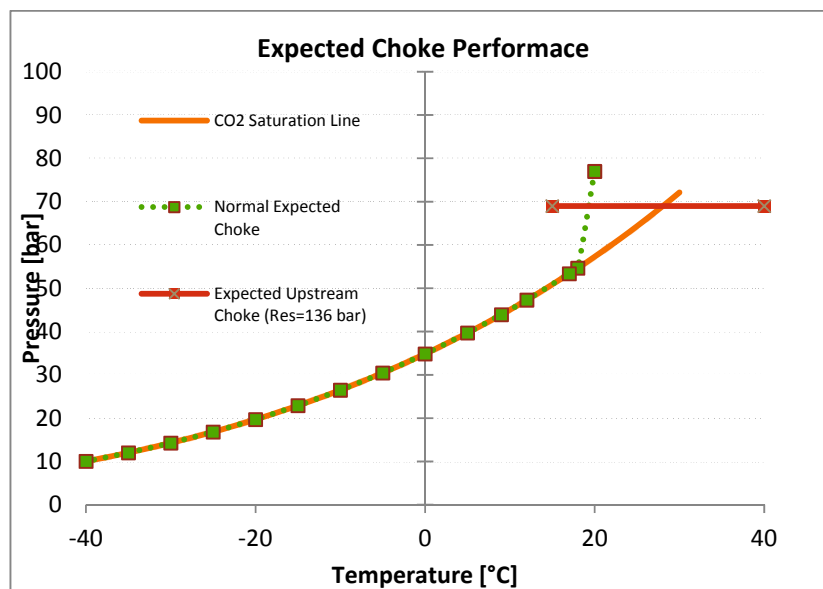


Figure 5.17: Expected choke performance and conditions upstream of the choke at reservoir pressure 136 bar.

When the reservoir pressure has been reduced to less than ~220bar, there will be two phases present in the wellbore after it has stabilized at CITHP. When injection is restarted, CO₂ will flash in the wellbore

causing a temperature drop. As frictional pressure build the CO₂ will be forced into single phase and the temperature drop will decrease approaching steady state injection condition. The well will begin to cool down again as the injected CO₂ is colder than the formation.

As opposed to the ESD, the mass of CO₂ during close-in/start-up will not be limited to the mass in the tubing, hence the temperature may be transmitted radially to the rest of the well components to a larger degree. This may have a consequence for well design.

5.13 Injection Under Matrix or Fracturing Conditions

It is of interest to know whether injection happens under matrix or fracture injection. Prosper can in general not be used for this work because fracturing depends on injection fluid quality, well length, reservoir permeability, injection rate, reservoir pressure, injection temperature, time and viscosity [40]. Prosper does not account for these effects, and instead it is recommended to use FRAC-IT. However, because we can adjust permeability and increase skin, we can get an idea about injection condition.

Skin is varied between 0 and 100, and permeability between 21.4 and 36.5. The injection pressure is set to 255bar which is the maximum case for the gFLNG[11]. These are considered to be extreme cases. The results are shown in Figure 5.18.

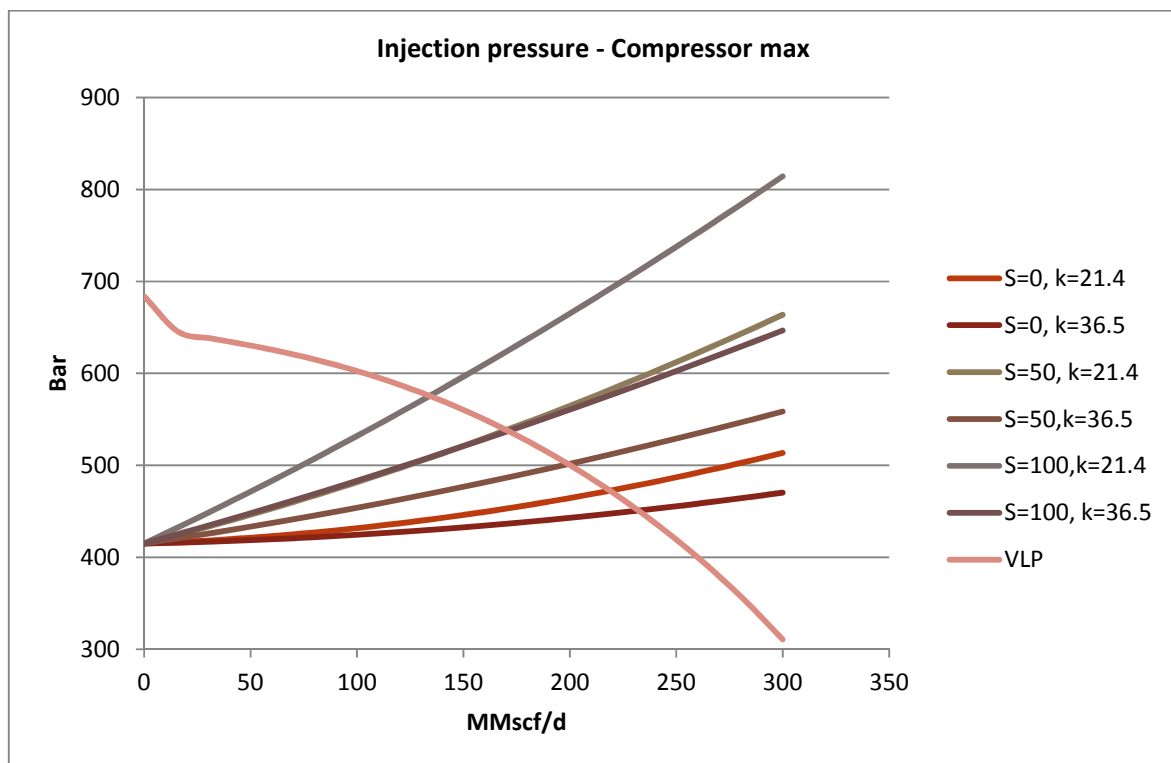


Figure 5.18: Injection pressure compressor max.

The formation breakdown pressure for the Swan reservoir is stated at 640 bar [5]. Keeping this in mind, it can be observed from the Figure 5.18 above that even in the extreme case with S=100 and k=21.4, the reservoir will not fracture.

The figure also show that the topside, most likely, does not have the capability to inject under fracture conditions. One of the reasons for this is the very low viscosity of the SC-CO₂, and the large reservoir contact.

The injected CO₂ is not expected to contain solid particle, but small particles and corrosion products may occur. Monitoring of bottom hole pressure can prevent mitigating fracturing.

A further study should be performed to account for thermal effects and reservoir depletion over time which could result in changes to formation breakdown pressure.

5.14 Conclusion and Recommendation

- Operating envelope is within single phase for majority of the field life, but may become two-phase late life.
- When reservoir pressure is depleted beyond ~220 bar, two-phases are expected in the well once it is shut-in. The well will be unstable until formation follows CO₂ saturation line.
- During transient operations, low temperatures can be expected resulting from a high JT effect.
- A fully transient model should be built to consider the impact of short time events (i.e. ESD, close-in and start-up)
- Thermal effects need to be studied more in detail. There is a possibility that the formation may experience thermal fracturing as the formation is cooled due to cold injection.
- It is observed that for transient operations, the temperature drop will increase with decreasing reservoir pressure.
- It is observed that current simulation software used in the industry has limitations in their capability to predict CO₂ properties.

Chapter 6

Material Selection

6.1 Objectives

The objective for this chapter is to review degradation mechanisms of CO₂ on cement, steel and elastomers and come with recommendations for material selection for the Prelude CO₂ injector. Dry CO₂ is by itself not corrosive but will in combination with water form carbonic acid which is known through the oil and gas industry as a highly corrosive environment. Corrosion rates exceeding 10 mm/y have been observed [26].

6.2 Methodology

As most degradation mechanisms of CO₂ are dependent on formation of carbonic acid, the amount of dissolved water that can be present in CO₂ is reviewed. When the amount of water rises above the solubility limit at specific conditions, free water will form. At this stage either hydrates or carbonic acid will form, and it is important to know which one.

Chemical degradation of cement is presented, and reported carbonation rates presented. The carbonation rate is found to be slow, but mechanically induced fractures can greatly enhance degradation.

CO₂ corrosion mechanisms are reviewed, and the effect of various parameters indicated. Corrosion is not a problem in dry CO₂, but becomes paramount if free water is formed. Models for predicting corrosion rate on carbon steels are provided in order to predict expected corrosion rate at Prelude conditions. As the corrosion rate is expected to be too high for carbon steel, feasibility of the most common alloys in the industry is reviewed and recommendation given.

Elastomers used for hydrocarbons will often be degraded by CO₂. The properties of various elastomers are reviewed, and feasibility for Prelude established. A leaking packer can give rise to corrosion in the annulus if a water based packer fluid is used. The pros and cons of water versus oil based packer fluid are presented.

6.3 The Free Water Issue

CO₂ is by itself only a weak corrosive agent, but become highly corrosive if free water is present. Occurrence of free water will lead to dissolution of CO₂, which again form carbonic acid, H₂CO₃. Water has a limited solubility in CO₂ in both gaseous and dense liquid phase. The solubility of water in CO₂ will be in effect a function of pressure and temperature, and also the purity of the CO₂.

During transport, if the solubility limit of water is exceeded, free water will precipitate inside the flowline and give rise to problems. The two negative effects free water will cause in the CO₂ system is corrosion and hydrate formation.

The maximum solubility of water in liquid CO₂ is important, as it dictates the maximum water content that can be tolerated in the injection system without causing corrosion and hydrate problems.

Spycher et al (2003) did a review on published data on H₂O solubility in CO₂ and developed a model to calculate the solubility limit [41]. The solubility limit for temperatures 35°C, 40°C, 60°C, and 75°C is pictured in Figure 6.1. Points are measured data, solid line calculated.

The water content in the CO₂-rich phase first decreases with pressure and then increases with pressure (see Figure 6.1 below). At sub-critical temperatures, the sharp change in the water content coincides with the phase change from the gaseous to liquid CO₂-rich phase. As the temperature increases above the critical temperature, the change in slope is progressively smoother.

The water content in the CO₂ rich phase increases with increase in temperature. This can be explained by the fact that the vapor pressure of water increases with temperature, thus the water molecules tries to be in the CO₂-rich phase.

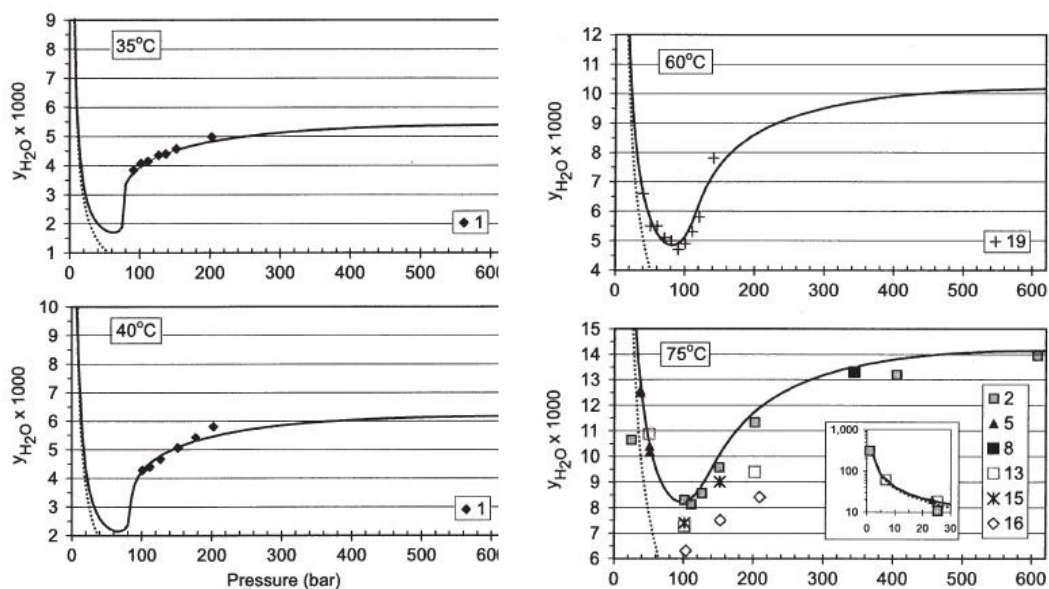


Figure 6.1: Mutual solubilities of H₂O and CO₂ at 35, 40, 60, and 75°C and pressures to 600 bar[41]. y-axis show y H₂O in ppm [41].

Impurities like H₂S and CH₄ will lower the water solubility in CO₂. Experiments and calculations for the solubility of water in pure CO₂ have been compared with that of a mixture containing methane. The water solubility in dense phase was shown to be as much a 30% lower for a mixture containing 5.3% CH₄ compared to pure CO₂ [32]. Another study indicated that small amounts (up to 200 ppm) of H₂S did not affect the water solubility significantly [32].

The expected water content to follow the injection stream at Prelude is 50 ppm. At initial injection state of 137 bar and 40°C, the CO₂ can contain up to ~4900 ppm without free water forming. It is also observed that the amount of dissolved H₂O that can be contained in the injection stream will increase towards bottomhole conditions to ~14,000 ppm. Thus, it is highly unlikely that a free water phase will form.

Even if free water is not expected during normal operation, it may be introduced in a number of other situations:

- Depressurizing the system will lower the temperature and pressure and thus the solubility limit. Water may condense.
- Fluids used during drilling and completions.
- Defect dehydration unit.
- Back flowing the well.
- Connate water around the lower completion.

6.3.1 Hydrates

Free water in the injection system can cause CO₂ hydrate to form. Hydrates (clathrate hydrates) are solids in which gas molecules occupy a vacancy in a cage made up of hydrogen bonded water molecules. CO₂ is just one of the light gas molecules that can form hydrate together with water.

The disassociation curve represents the conditions of pressure and temperature where hydrate separate into water and gas. The hydrate formation point will be on the inside of this curve. The disassociation curve for pure CO₂ with distilled water is pictured in Figure 6.2.

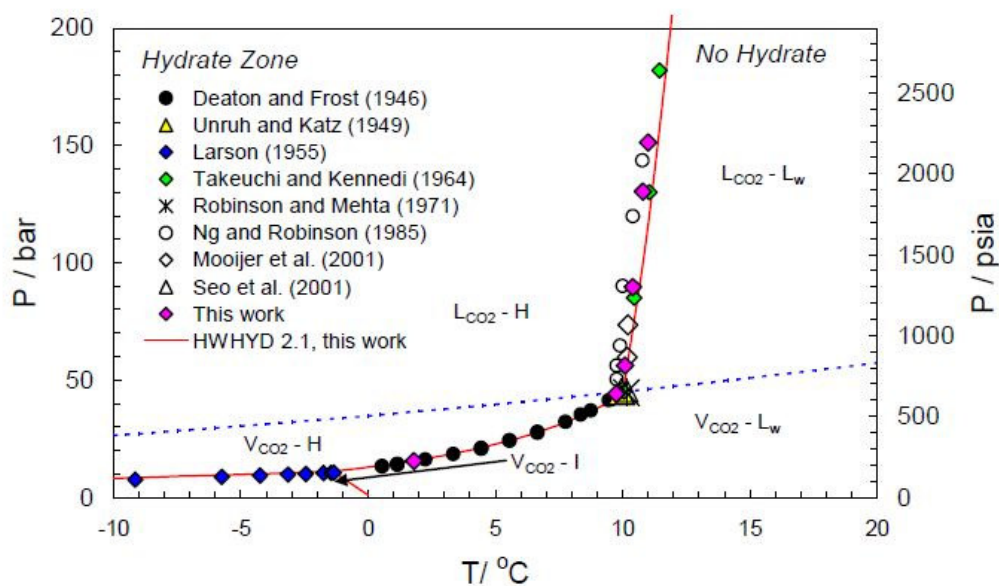


Figure 6.2: Hydrate stability in the presence of distilled water [42]

The phase transition point is highly pressure dependent, and become more stable with increasing pressure. When hydrates are formed they may plug pipelines or block valves and thus need to be controlled.

From Figure 6.2 it is observed that hydrate will mainly form at low temperatures. The injection temperature for Prelude will be at 40°C, thus far outside the hydrate formation curve. However, transient operations such as start-up, shutdown and blowdown are very susceptible to hydrate

formation because the conditions are more likely to drop into the hydrate formation zone. The well bore gradient for early and late life shut-in can be observed in Figure 6.3 (geothermal gradient). It is observed that the wellhead pressure is at hydrate formation conditions. Other operations like ESD will also be within this region. To mitigate hydrate formation a methanol cap could be pumped in the top of the tubing.

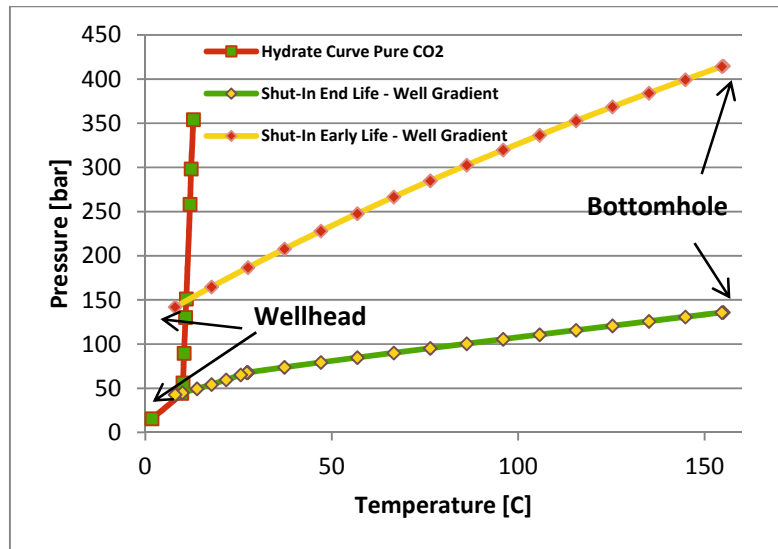


Figure 6.3: Pressure vs. temperature profile of tubing fluid during shut-in for early and late life plotted against the hydrate curve for pure CO₂ obtained from [42].

The amount of water in the injection stream is stated at 50 ppm, and as previously established, no free water is expected during normal operation. Chapoy et al (2009) performed experimental work on the equilibrium between liquid CO₂ with hydrates. For a system at -2°C and 50 bar this was measured to 600 ppm and at 4°C and 190 bar to 1000 ppm [42]. Chapoy concluded that the risk of hydrate formation in a pure CO₂ stream at temperatures between -2°C and 30°C at pressures up to 200 bar to unlikely with a water content below 250 ppm.

In CO₂ gas phase, given favorable combination of pressure and temperature, CO₂ hydrate may form. In dense phase however, it is not evident whether CO₂ hydrate will form under dense phase, even with free water. Gaseous CO₂ is able to contain less water than dense phase, so in any depressurizing operation, water may drop out. Combined with the possible hydrate condition, hydrates may form [26].

In addition there is uncertainty as to whether free water in dense phase CO₂ will form hydrates or carbonic acid. This will depend on the CO₂ pressure, temperature and the water content. At high pressure, there is a higher risk of hydrate formation, and at low pressure there is a higher likelihood of corrosion [26].

Hydrate formation is not likely to form under steady-state conditions due to high fluid temperature and absence of water. However, it is considered a potential risk in certain transient operations as the conditions for hydrate formations are apparently met.

6.4 Cement

Cementing is critical to a sound mechanical integrity. The cement anchors the casing to the formation providing structural stability and providing a seal between the casing and surrounding formation. Possible leak pathways through an abandoned well are pictured in Figure 6.4. The figure show leakage could occur because of poorly cemented casing, failure of casing (due to loads or corrosion) and improper abandonment. Properly set cement will have permeability in the order of 10^{-2} m^2 [43], being an effective barrier against flow. However, due to the corrosive environment provided by CO_2 , cement is known to degrade. The compressive strength of the cement decreases and the permeability and porosity increases, eventually leading to integrity failure [44]. Integrity can also be lost if the cement is not properly set, or if the casing fails due to corrosion, erosion or improper design [43].

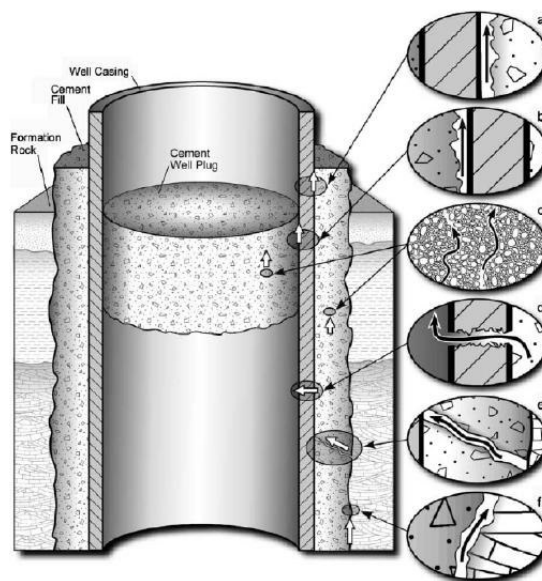
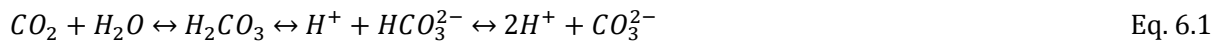


Figure 6.4: Schematic of possible leakage pathways through an abandoned well (a) between casing and cement (b) between cement plug and casing (c) through the cement pore space (d) through the casing (e) through fractures in cement (f) between cement and rock [43].

Currently, there is an ongoing discussion about degradation of cement by CO_2 as field observations show much lower carbonation than measured in laboratory tests. Based on the field results, Portland cement will be sufficient. From studies conducted to date, it seems that degradation rate is controlled by the diffusion of solution into the cement. If this is the case, the time to breach the seal could be thousands of years. If fractures exist within the cement, degradation could however occur very rapidly and cement integrity may be more important than degradation. Care should thus be taken when completing the wells and making sure the cement job is as sound as possible[23]. Here we will be discussing the degradation of cement, and methods used to improve cement integrity.

6.4.1 Chemical Degradation of Cement

In combination with water (wet supercritical CO₂ or CO₂ dissolved in water) CO₂ dissociates to form carbonic acid [45]:



After dissolution of CO₂, cement degradation commences with progressive consumption of the solid cement constituents Portlandite (Ca(OH)₂(s)) to produce carbonates (aragonite, vaterite and/or calcite). This stage is called 'carbonation'[45]:

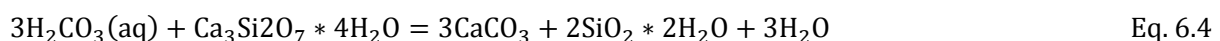


Carbonation reduces porosity due to the precipitation of calcium carbonate. According to Shen et al (1989) the molar volume increase from 33.6 to 36.9 cm³ as calcium carbonate has higher molar volume[23]. For cement sheath integrity, this reaction improves the cement's properties and the carbonation is therefore a self-healing mechanism in the carbonate.

In a CO₂ sequestration project, the supply of CO₂ around the wellbore will continue the carbonation as long as Ca(OH)₂ is present in the cement. The calcium carbonate is also soluble with the CO₂, even though it is more stable than Ca(OH)₂. Experiments by Kutcho et al (2007) showed that when all Ca(OH)₂ has reacted in the carbonation process, the pH will drop significantly (Zone 1 on Figure 6.5). When the pH drops, more of the CO₂ will react with water and form HCO₃⁻ (Zone 2), due to the following reaction:



The abundance of HCO₃⁻ will react with the calcium carbonate to form calcium (II) carbonate, which is soluble in water and can move out of the cement matrix through diffusion[23]. When CaCO₃ is dissolved and diffused out, the pH is not buffered inside the cement. Therefore, the final reaction that occurs in Zone 3 (close to cement surface) can occur. Calcium silicate hydrate reacts with H₂CO₃ to form calcium carbonate (CaCO₃) according to the following reaction:



The volume of Ca₃Si₂O₇·4H₂O is larger than that of CaCO₃(s), thus the reaction leads to an increase in porosity. Commonly the calcium silicate hydrate is generalized to the form C-S-H as the amount of calcium to hydrate varies. The latter reaction is however applicable for all types of C-S-H. The large difference in pH inside and outside the sample, 2.9 versus 12, will cause diffusion of acid and continue until the entire cement plug is reacted [23]. The final result of the total degradation process is an amorphous silica gel. This gel has extremely low strength and can easily be washed out by fluid flow or deformed if pressure is applied [45].



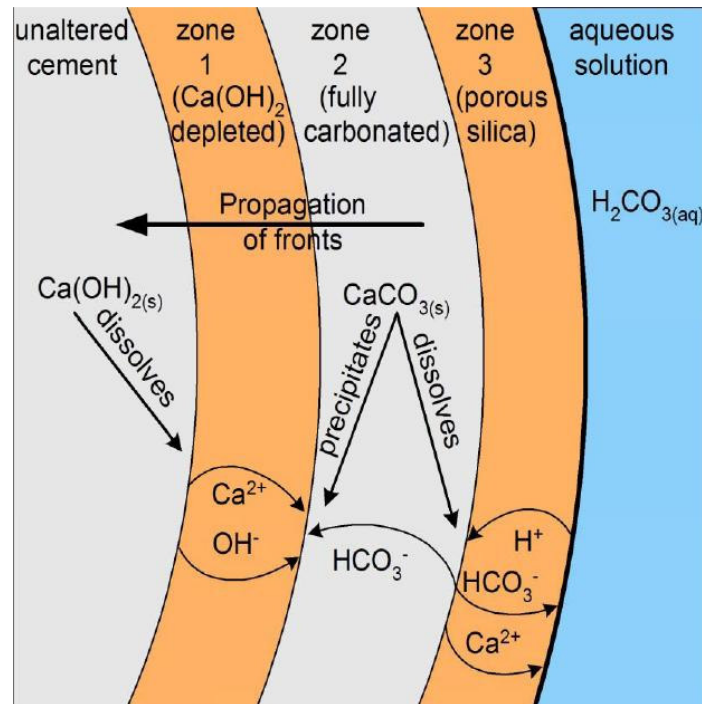


Figure 6.5: Illustration of the different Zones due to the chemical reactions occurring in the cement core. Zone 1–Dissolution of $\text{Ca}(\text{OH})_2$. Zone 2–Precipitation of CaCO_3 . Zone 3–Dissolution of CaCO_3 and decalcifications of C-S-H. Kutchko et al. (2007) [23]

It is likely that the reduction in porosity that is observed during carbonation by precipitation of calcium carbonates also reduces the permeability (Zone 1 & Zone 2). This will have a decelerating effect on the diffusion rate. Some experiments have reported a low permeability in the order of micro- to milli- Darcy (e.g. Barlet-Gouedard et al., 2006; Duguid et al., 2006; Lecolier et al., 2006) and in field observation with CO_2 exposure for 30 years. It is however uncertain how permeability will develop over longer time scales.

Onan et al. (1984) studied the effect of supercritical CO_2 . He reported that the rate of carbonation was influenced mainly by partial pressure of the CO_2 and the temperature, and that the water content level secondary in respect to rate. At low temperature and pressure, carbonation was only observed in the outer regions, whereas at high temperature and pressure complete carbonation was observed. A second observation was that at low temperature and pressure, dynamic systems lead to more carbonation than static systems [46].

Experiment and modeling work done by Huet et al. (2008) on carbonation of Class H cement by CO_2 . They found that content of dissolved CO_2 was highly important, and that pH was secondhand. From this follows that salinity will be a key parameter as it influenced the amount of dissolved CO_2 . At a given temperature and pressure, low salinity will give higher concentration of CO_2 .

Milestone et al. (1986) performed experiments on cement slurries with different amount of silicates at 150°C and 8 bar CO_2 pressure. The samples that did not contain silicate only had a small carbonation front. The carbonation depth seems to be closely related to the amount of $\text{Ca}(\text{OH})_2$. A

reason may be that silicate reacts with Ca(OH)_2 . Thus, when the Ca(OH)_2 is spent, the CaCO_3 could start dissolving and increase porosity. Thus the CO_2 can penetrate the sample further. Silicate increase the reaction because Ca(OH)_2 gets spent faster. 20% silicate is needed to get a permeability of 0.1 mD which is the API recommendation. It is also needed for compressive strength [47].

The conclusion drawn by Milestone et al. (1986) was that all calcium silicate based geothermal grouts are subject to carbonation by CO_2 fluids. Initial permeability is a factor, but the most important one is the phases present in the cement. With no Ca(OH)_2 , the attack is rapid and products are porous [47].

Adding different additives to the cement can make it more acid resistant. Beddoe et al. (2005) added quartz to Portland cement in order to make it more acid resistant. The reaction with CO_2 leaves only a paste affected by CO_2 , thus reducing the carbonation rate by the induced aggregate particles. It is reasonable to assume that additives to the Portland cement will change its properties, and possibly more resistant to acid attack. However, because Portland cement is thermodynamically unstable in contact with CO_2 , it is not assumed that the carbonation will be prevented, but instead a reduction in rate is expected [23].

CO_2 resistant cements have been introduced by cementing companies in response to the upswing of CO_2 injection projects. All three main suppliers to the oil industry have provided and used these special cements around the world in CO_2 environments. The products are:

- Schlumberger Well Service EverCRETE
- Halliburton ThermaLock Cement
- BJ Services PermaSet Cement

Experiments performed by the vendor them self have indicated that ThermaLock and EverCRETE are much more adapted to degradation from CO_2 compared to Portland cement (Brothers (2005), Barlet-Gouedard et al. (2006, 2008)) [23]. It is possible that these comparisons are biased to show the vendor product in a better light. Total (company) have performed experiments with CO_2 resistant cements which was presented on "1st Combined Network Meeting on Modelling and Wellbore Integrity" in Perth 28th of April, 2011 by Laudet et al. (2011). They tested three different CO_2 resistant cements (type not given, but likely to be Bj, SLB and Halliburton). All the cements showed high resistance to chemical attack by CO_2 . Mechanical properties were not testes.



Name	Description
ThermaLock™	ThermaLock cement is specially formulated calcium phosphate cement that is both CO ₂ and acid resistant. This cement is well suited for high temperature geothermal wells. ThermaLock has been laboratory tested and proven at temperatures as low as 60°C and as high as 371°C. It is however not compatible with Portland cement and must be handled separately, and cannot be added to Portland cement either [23].
EverCRETE™	EverCRETE is marketed as CO ₂ resistant cement that can be applied for CCS projects. EverCRETE has proven highly resistant to CO ₂ attack during laboratory tests, including wet supercritical CO ₂ and water saturated with CO ₂ environments at temperatures up to 110°C. Reported to be compatible with Portland cement.
PermaSet™	BJ CO ₂ resistant cement. Temperature range 4°C to 232°C.

Table 6.1: CO₂ resistant cements.

6.4.2 Degradation Rates

Experiments performed by Kutcho el al. (2007) with Class H cement in supercritical CO₂ at 50 °C, and further research by Kutcho el al (2008) gave the reaction rates are shown in Figure 6.6 and Figure 6.7 underneath.

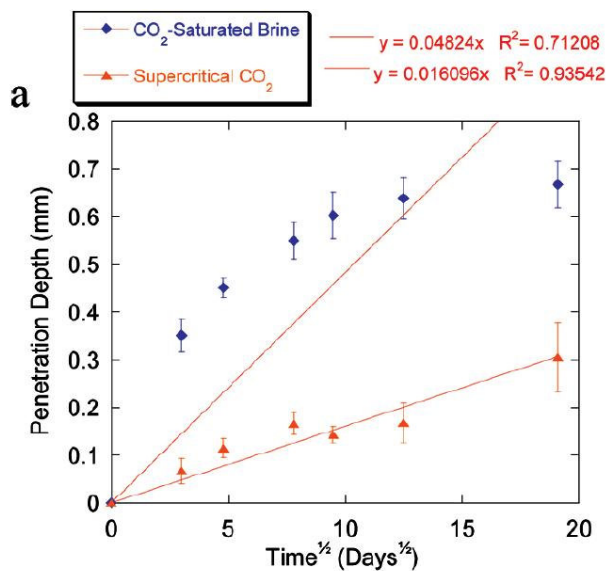


Figure 6.6: Carbonation depth (mm) vs time^{1/2} (days^{1/2}) at 50°C, Kutcho el al. (2008) [23]

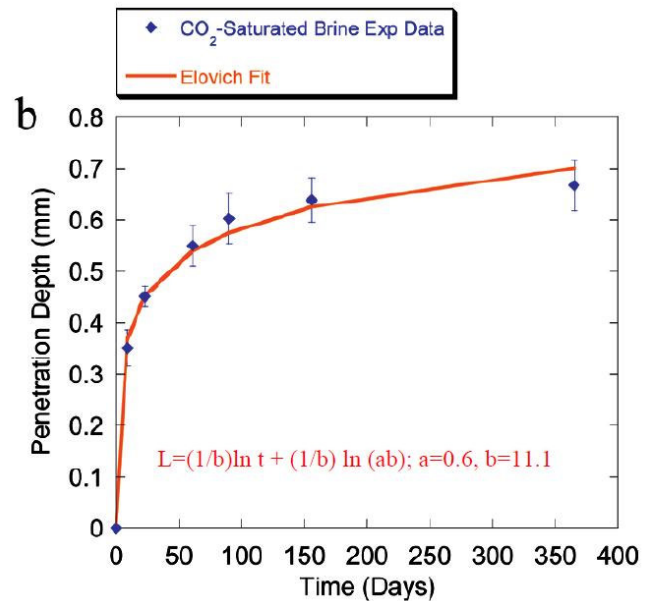


Figure 6.7: Carbonation depth (mm) vs time (days) at 50°C, Kutcho el al. (2008) [23]

Barlet-Gouedard et al. (2006) tested Portland Class G cement in an autoclave at 90°C and 280 bar. The samples were tested in CO₂ saturated water and in supercritical CO₂ atmosphere. Drawing of the apparatus is shown in Figure 6.9. Carbonation rate in respective medium is shown in Figure 6.8.

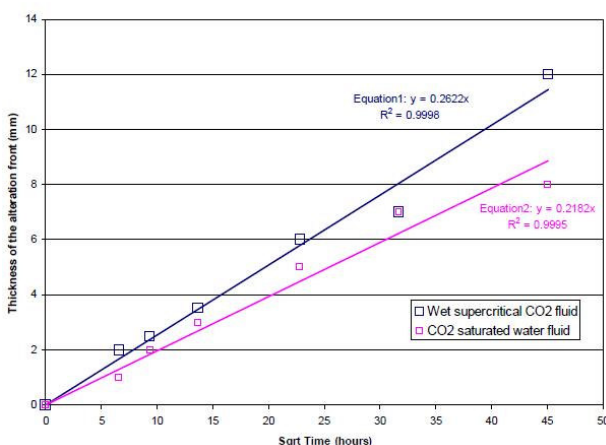


Figure 6.8: Rate of carbonation for Portland cement, Barlet-Gouedard et al. (2006) [33]

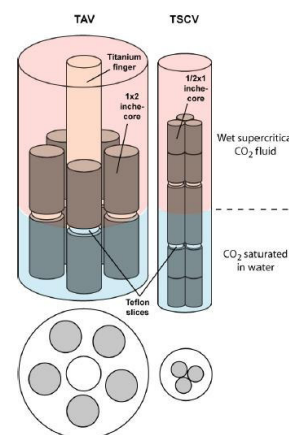


Figure 6.9: Experimental setup for testing cement at supercritical CO₂ conditions Barlet-Gouedard et al. (2006) [48]

It can be noted that the rate of carbonation in the Barlet-Gouedard et al. (2006) experiments was very rapid compared to that of Kuchkov et al. (2008).

For comparison the carbonation of the two respective experiments are shown in Figure 6.10. There is a huge difference, and there are more differentiators in the two experiments besides temperature. They also used different testing procedure and cement. Kutchkov et al. (2008) pointed out the main differences in the experimental procedure, see Table 6.2[23].

Barlet-Gouedard et al. (2006)	Kuchkov et al. (2008)
Class G cement	Class H cement
72 h curing time	28 day curing time
An antifoam agent, dispersant, and retarder added to the cement mix to optimize slurry properties	Neat cement
Deionized water	0,17 M NaCL
90°C	50°C

Table 6.2: Main differences between experiments of Barlet-Gouedard et al. (2006) and Kuchkov et al. (2008) [49].

Following, Barlet-Gouedard et al. (2008) preformed additional experiments with 4 molar NaCl brine solution, but keeping the same setup as Barlet-Gouedard et al. (2006). The reason for doing this was to simulate downhole conditions. Solubility of CO₂ in water is lower at increased salinity, and higher salinity leads to less precipitation as the kinetics are more stable [23]. Carbonation was measured after two days, and the result was compared to the previous experiment in pure water. The carbonation can be seen in Figure 6.10. The result from the 4Mmolar NaCL test compares much better with the results of Kutchkov et al. (2008) and field experience. It should also be pointed out that the molarities of the brine used in Kutchko et al. (2008) was only 0.17M, which is a closer to pure water[23]

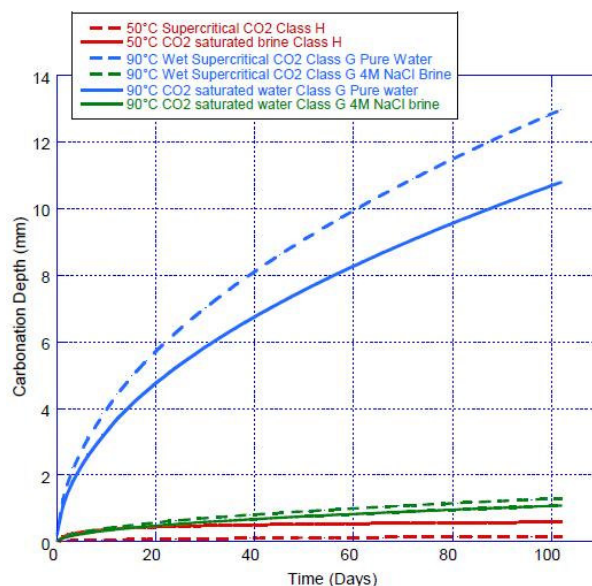


Figure 6.10: The carbonation depth (mm) versus time (Days) at 50°C and 90°C, based on results from Kuchkov et al. (2008) and Barlet-Gouedard et al. (2006, 2008) [23]

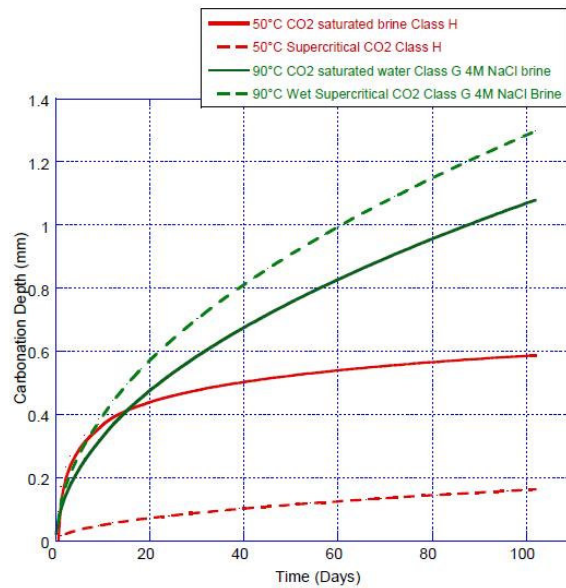


Figure 6.11: The carbonation depth (mm) versus time (days) at 50°C and 90°C, based on results from Kuchkov et al. (2008) and Barlet-Gouedard et al. (2008) [23]

Duguid (2008) found that initial degradation rates are reduced to significantly lower values after 2 to 3 months. The reduction in degradation rate has been concluded to be caused by a diffusive barrier of calcium carbonate which precipitates during CO₂ attack. The rate can be estimated from Fick's Law [45]:

$$d = C \cdot t^{1/2} \quad \text{Eq. 6.5}$$

where d is penetration depth (mm) and t represent time (h). The diffusion coefficients C result from experiments. Based on the result from reported experiments, it appears that diffusion-based chemical degradation rates are relatively low. In general degradation rates increase when cement is exposed to CO₂ at higher temperature and lower pH conditions. Even under very high temperature (204°C at 69 bar, $C=1.3199$) degradation rates would result in a maximum of 12.4 m of cement degradation after 10,000 years of exposure to CO₂ (Shen et al. 1989), assuming that diffusion define the degradation mechanism [45].

6.4.3 Field Experience

The SACROC unit in West Texas in the USA is a 240m thick reservoir located at 2100m depth and a temperature of 54°C and a pressure of 180 bar. The reservoir shows permeability of 10-100mD and porosity in the 10% range. Cementing to total depth was neat Portland cement. Well 49-6 was drilled in 1950 and not exposed to CO₂ until 1975. In the following years it was a producer for 10 years in a low pressure environment. The next seven years it was an injector at high pressure injecting 110 000 tons of CO₂ [23]. Carey et al. (2007) performed a study on the cement from this unit, whereas samples from 6-4 m above the caprock-reservoir contact was taken of casing and cement. Shale samples was also collected. Analysis of the cement showed partial carbonation. The cement in contact with the shale rock was heavily carbonated, and the cement close to casing pure carbonate. Direct proof of CO₂ interaction with shale was not found. The permeability of the cement was found to be higher than pristine Portland cement, and SEM imaging precipitation of CaCO₃ in the void spaces [23].

It was concluded that the structural integrity of the Portland cement was adequate to prevent any significant transport of fluids, even in the light of samples showing heavy carbonation. It was also found that CO₂ had been migrating along shale and casing interfaces for a while [23].

Carbonation of Class G cement in geothermal wells was examined by Shen et al. (1989). In high temperature, silica flour is added to stabilize Portland cement. In geothermal wells Ca(OH)₂ is normally not used, so the C-S-H phase can be directly attacked by CO₂ [23].

The temperature of the wells was between ~200-300°C and with a CO₂ content of 12,200ppm CO₂. Examination showed that carbonation rate was a function of temperature, CO₂ concentration and location. The fractures and fissures that were observed in both carbonated and uncarbonated cement was assumed to be due to thermal cycles in the wells. The number of shutdowns was found to correlate with the increase in permeability. Sharp changes in temperature will cause strains in the cement and likely fracturing, thus it fits the observation. No immediate correlation between carbonation and porosity was identified. The amount of calcium carbonate formed showed a linear relationship with temperature. Thus, increased temperature gave increased amount of CaCO₃ [23].

Wells exposed to 180°C and 22% CO₂ was studied by Krilov et al. (2000). After 15 years when the performance suddenly dropped, debris was found downhole. Following this Krilov et al. (2000) performed experiments simulating the downhole conditions of the wells. Loss of compressive strength and cement integrity was found to be caused by high temperature and CO₂ content [23].

Crow et al. (2009) published a field study of a 30 year old well from a natural CO₂ production reservoir (96% CO₂). Casing and cement sample was recovered from different side walls. The well was completed with a 50:50 ash Class H cement including 3% bentonite mixed at 14.2 ppg. Temperature was 140°F and pressure about 1500 psi. Analysis revealed greatest carbonation near the CO₂ reservoir, and original cement phases more abundant further from the reservoir. This showed that the cement-pozzolan system inhibited CO₂ migration although carbonation occurred. Evaluation of log information showed good bonding and no leak was ever detected [50].



6.4.5 Mechanical Considerations

Experiential data and field observation indicate that cement is expected to provide adequate resistance against any significant CO₂ migration through its matrix. However, if CO₂ is allowed to flow in the annulus through mechanically induced fractures, carbonation will progress more rapidly through the cement column than if the cement sheath remained intact. Thus it seems mechanical integrity and quality of placement is more important than chemical degradation. Migration pathways are most likely to form at the interface between both casing and formation, and thus they are very important for well integrity. Poor cement jobs or cement shrinkage can result in micro fractures and micro-annuli. This can give rise to debonding and enhanced permeability pathways resulting from e.g. cement shrinkage, poor mud removal or decentralized casing especially in deviated wells.

Tensile strength of normal cement is taken to 1/10th of the compressive strength. This is also typical for tensile bond strength in the formation. Axial deformation in wells under reservoir depletion, or injection can result in debonding of cement from casing. This is so because stiffness of steel is greater than that of formation and cement. In other words, casing will barely deform while cement and formation will [23].

An exothermic reaction could occur in the cement when setting if water flow into the cement. This will cause cement pore pressure diminishing and cement shrinkage. Such shrinkage can, according to Ladva et al. (2005), lead to fractures in the interface shale [51].

Fractures can develop as a result of cement failure under stress. Causes can be high injection pressure and/or temperature changes or cycles. These processes could enhance the widening of existing or develop pathways through the cement or rock. Fields producing CO₂ rich fluid at high temperature has shown that frequent shut ins causes tensile stresses in excess of the cement's tensile strength, provoking widespread fissuring and cracking, as reported by Shen et al. (1989) [23].

Unfortunately, many risks, even if flawless planned and executed cannot be engineered away. This was the case with the Otway CRC-1 well in Victoria, Australia, reported by Loizzo et al. (2008). This well is part of a CO₂CRC research program where every risk prevention was taken to construct a flawless well. Even so, small wash-out and break-outs across the caprock, coupled with a small (<2°) hole deviation led to the tail slurry being contaminated by the lead slurry. This in turn led to a high porosity solid channel along the narrow side of the annulus across some of the primary caprock .

6.4.6. Selection of Cement System

It is not a question whether the Portland cement is degraded due to CO₂ attack or not. The main question is how fast the degradation occurs and how it affects the integrity of the well. The reaction rate, from various experiments is not shown to be very high, but as temperature increases so do reaction rate. This is as expected since reaction kinetics usually increases with temperature. The slow degradation is likely due to the process being diffusion controlled, and that the permeability of the cement is very low. Cracks or channels present in the cement or cement interfaces can cause rapid loss of sealing capability. Especially at high temperature and if pure water exists. Prelude CO₂ stream is expected to be more or less free of water. However, connate water will be present in the formation.

Based on the previous discussion the following options were considered for cementing system:

- Reduced Portland cement
- Portland Cement with tail of CO₂ resistant cement
- CO₂ resistant cement

Swan reservoir is overlay by 1800 m of shale. The risk of CO₂ leaking through a properly cemented casing through this is very low. On the other hand, CCS projects are still novice, and thus it must be considered good practice to go the “extra mile” in terms of stakeholder engagement and select CO₂ resistant cements.

However, there are many things that speak against using a CO₂ resistant cement like cost and handling, as it usually not compatible with Portland systems. For example have Shell Canada tried out CO₂ resistant cements and since moved away from them, and now uses a Class G/pozzeland blend [52].

As described in the previous sections, Portland cement is thermodynamically unstable in contact with CO₂, thus even a reduced Portland cement will react with CO₂, however at reduced rate.

The best solution for Prelude would be to select a Portland cement system with a tail of CO₂ resistant cement. The only CO₂ resistant cement available for blending with Portland cement is EverCrete. The operating limit for EverCrete is 110°C, and thus not suitable.

6.4.7 Conclusion & Recommendation

- Selecting CO₂ resistant cement is considered the best alternative from a stakeholder engagement point of view.
- Selecting CO₂ resistant cement has the highest robustness and can provide integrity for long term storage.
- As CO₂ resistant cements are inert, or close to inert, to CO₂, testing of CO₂ resistant cement should focus on mechanical integrity (bonding to formation and metals, and triaxial properties).

It is considered crucial to employ good cementing practice to maintain wellbore integrity. A summary of good cementing practices include [53]:

- Centralize the casing. Take into account dogleg severity and inclination in centralization placement. Proper centralization is one of the major factors contributing to a good cement job.
- Circulate the hole and condition the mud prior to cementing. The mud should be thinned as much as possible while still maintaining adequate lifting capacity and density.
- Reciprocate (or rotate in critical situations) the casing while circulating and cementing. Unless the casing starts to stick, the casing should be reciprocated until the plug bumps.
- Pump a thin spacer fluid in front of the cement. The spacer should be compatible with both the drilling fluid and cement.
- Do not hold pressure on the casing after the plug is bumped unless the float equipment does not hold. Keeping pressure on the casing while the cement sets can cause micro annulus.
- In high angle directional wells, prevent the formation of a water channel on the high side of the hole. Minimize the cutting bed on the low side of the hole by cleaning the hole with adequate annular velocities.

6.5 Steel

Corrosion is caused by chemical or electrochemical reaction between a metal and its environment that produces a deterioration of the material and sometimes its properties[54]. Corrosion requires three conditions:

- 1) Metal
- 2) Water or electrolyte (saline solution)
- 3) A corrodent (something to create the corrosion such CO₂ or H₂S) [35]

If one of these elements is removed, corrosion cannot occur.

Corrosion mechanisms can be classified as:

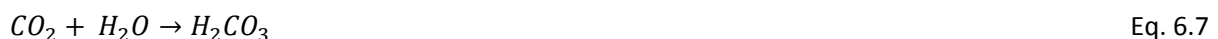
- 'Progressive'
- 'Immediate'

Progressive corrosion need time to accumulate and produce failure, such as CO₂ corrosion, pitting and stress corrosion cracking. On the other hand, immediate mechanisms can take place in a short amount of time. Sulphide stress cracking is such a mechanism, and will be considered here.

The terms 'sweet' and 'sour' are commonly referred to describe CO₂-containing fluids respectively lacking or containing hydrogen sulphide (H₂S). 'Sweet' environments cause corrosion which is dominated by the presence of CO₂, whereas a 'sour' one cause corrosion dominated by H₂S. Addition of H₂S to the CO₂ containing stream changes the form of corrosion, and affects the choice of material applied to prevent corrosion [17].

6.5.1 Carbon Dioxide Corrosion

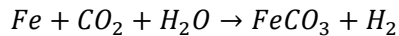
Crude and natural gas tend to contain some level of CO₂, thus CO₂ corrosion is one of the most studied form of corrosion and well understood. The major concern is that corrosion can cause failure on downhole tubing/equipment and lead to failure. The first step is CO₂ dissolution and hydration to form carbonic acid [55]:



The carbonic acid then dissociates into bicarbonate and carbonate in two steps:



When the solubility of a salt is exceeded, it will precipitate. This could lead to formation of a protective film on the surface. The most common type of film encountered in CO₂ corrosion is iron carbonate with the following overall reaction:



Eq. 6.10

When iron carbonate film $FeCO_3$ (and/or Fe_3O_4 particularly at higher temperature) precipitate the steel surface, it can slow down the corrosion by introducing a diffusion barrier or by covering a portion of the surface.

CO_2 corrosion is strongly dependent on the formation of a protective iron carbonate film. The protectiveness, rate of formation/precipitation, and the stability of the film control the corrosion rate and its nature (general or local). Precipitation rate depends on the iron and carbonate concentrations, and its subsequent formation and growth is extremely temperature sensitive. It is not the thickness of the film but the structure and its morphology that leads to low corrosion and protectiveness. Depending on conditions, corrosion up and beyond 10 mm/y have been observed [26].

6.5.1.1 Effect of Temperature

Temperature strongly influences the conditions to form protective iron carbonate layer. When the temperature is below 60°C the solubility of $FeCO_3$ is high and the precipitation rate is slow and protective film will only form if the pH is increased. The corrosion rate will increase with temperature up to about 60-80°C. Above this temperature the iron carbonate layer becomes more protective with increasing temperature. This is due to decreased iron carbonate solubility, thus the corrosion rate is reduced. At sites where breakdown in the formation of $FeCO_3$ occurs, significant increase in localized corrosion often results until a temperature where a very stable iron carbonate film is formed. Above 110°C magnetite (Fe_3O_4) may form through direct reaction between steel and water and at 130°C the steels are passivated [56].

6.5.1.2 Effect of pH

$FeCO_3$ formation strongly influenced by pH as increasing the pH decrease the $FeCO_3$ solubility and promotes precipitation and lower corrosion rates. Cathodic reduction of H^+ is slowed by an increase in pH, this in turn decrease the anodic dissolution rate of iron. At very high pH values protective carbonate scales are formed on the surface that reduces the corrosion rate significantly. This is caused by a reduction in solubility of iron carbonate in the solution. One study showed that protective scales could only be observed for pH's greater than 5 in flow loop tests with carbon steel. Another study found that protective scales are only formed when the pH is increased to at least 6 at low temperature, while at above 80°C protective scales are easily formed [56].

6.5.1.3 Effect of Flow

The impact of high flow conditions can be significant as wall shear stress may mechanically strip protective surface films from the underlying material allowing bare material to corrode freely. Also, high flow rate can influence mass transport leading to lower Fe^{2+} concentration at the material surface and decrease tendency to form $FeCO_3$. Given the importance of $FeCO_3$ and other corrosion product films in hindering corrosion reactions at high temperature, careful considerations should be given to the impact of wall shear stress on CO_2 corrosion [56].

In the presence of a protective CO_2 corrosion film, the flow can influence the transport of cathodic species towards the steel surface, resulting in a higher metal dissolution at higher flow rates. Flow may



also stimulate removal of Fe^{2+} ions from the steel surface at the bottom of pores and may cause lower surface supersaturation and slower film formation [56].

6.5.1.4 Influence of CO_2 Partial Pressure

By reducing the pH and by increasing the rate of carbonic acid reduction under film-free conditions, higher partial pressure causes higher corrosion. However, as the concentration of CO_3^{2-} generally increase with increasing CO_2 partial pressure, and that concentration of Fe^{2+} and CO_3^{2-} ions in solution dictate the stability of FeCO_3 films at a given temperature, greater partial pressure of CO_2 can actually reduce corrosion rate due to greater tendency to form FeCO_3 films.

When the conditions are favorable for protective film, high CO_2 partial pressure can reduce corrosion attack due to lower availability of cathodic sites. Increasing the CO_2 partial pressure from 4 to 18 bars under film-free conditions in a horizontal wet gas flow yielded an increased corrosion rate from 3 mm/y to 8 mm/y [56]. On the other hand, an increase of the CO_2 partial pressure in the same system when a semi protective film exist (pH range below 5.2), reduces the corrosion rate from 15 to 0.2 mm/y [56].

At high flow rates the relationship between corrosion rate and CO_2 partial pressure can be complicated. Higher CO_2 partial pressure tend to stabilize the FeCO_3 films, but high wall shear stress from high flow rates break them down causing higher corrosion rates.

6.5.1.5 Effect of Steel Type

Alloy composition is important in the resistance to CO_2 corrosion. The addition of different alloys gives the following benefits [35]:

- Chromium improves corrosion resistance, particularly in the presence of carbon dioxide. Chromium also improves strength under high temperatures.
- Nickel improves the toughness and provides corrosion resistance in conjunction with chromium, especially in the presence of hydrogen sulphide. Nickel is austenite stabilizer.
- Molybdenum and tungsten increase high temperature strength and make it easier to harden the metal and maintain hardness during heat treatment. They also improve resistance to localized corrosion (pitting).
- Manganese ties up and prevents free sulfide and also increase hardenability.
- Titanium strengthens the steels.
- Niobium and vanadium are added to improve hardening and increase strength. Nitrogen are used as strengthener in very low concentrations.

The temperature dependence of CO₂ corrosion have been found to relate to the chromium content of the alloy. With increasing Cr content, T_{max} have been found to increase. This is demonstrated in Figure 6.12.

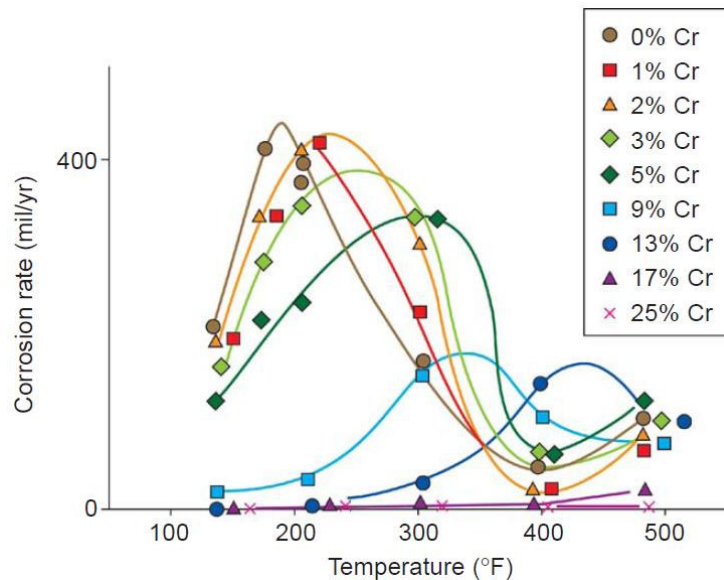


Figure 6.12: Corrosion rate as a function of chromium content [35].

6.5.1.6 Effect of H₂S

In the presence of H₂S in a primarily CO₂ system will for most concentrations decrease corrosion rate. The presence of H₂S enable the formation of FeS films on the material surface, providing an alternative mechanism for corrosion mitigation.

In a flow loop experiments at 120°C with 10 m/s with an aqueous solution of 5000 ppm chloride and 120 ppm bicarbonate under 0.69 MPa CO₂. At a CO₂/H₂S ratio above the NACE sour limit the corrosion rate was reduced from 30-40 mm/y with no H₂S, to 0.5-2.0 mm/y with H₂S. The iron sulfide film appeared to be more flow resistant [56].

It is however found that extremely small concentrations of H₂S in a primary CO₂ wet gas system can result in significant accelerated corrosion compared to the corresponding CO₂ concentration without H₂S. The effect is highly temperature dependent, and is observed to disappear above 80°C. The cause of accelerating effect is not well understood, though speculations of effect of adsorbed sulfide have been presented.

For corrosion inhibition by H₂S below 80°C is has been suggested at 15 ppm or 30 ppm, but is not well established. The stability of the corrosion product can often be estimated from the ratio of CO₂:H₂S. Estimation of carbonate and sulfide regime was suggested by Dunlop et al. for room temperature. Carbonate regime exists when ratio is above 500, while sulfide regime is reached below 500 [56].

The corrosion rate is observed to drop at the transition between sweet and slightly sour corrosion. At this point the corrosion mechanism shifts from CO₂ controlled to slightly sour controlled, as verified by

experiment by Smith and Pacheco when testing steel in an environment of 14 MPa total pressure containing 10 Mole-% CO₂ and 2 to 30 ppm H₂S at 50°C. Figure 6.13.

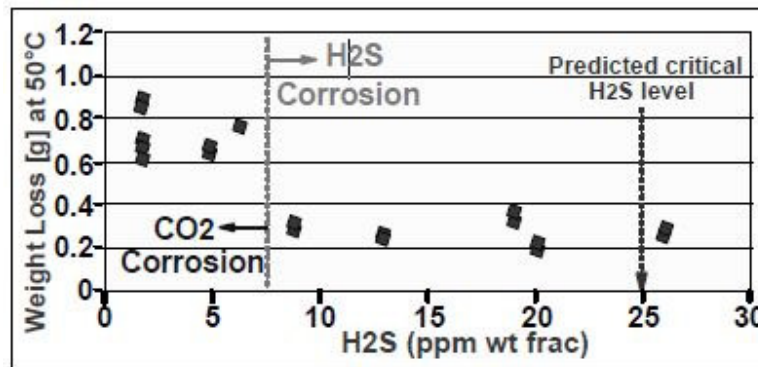


Figure 6.13: Effect of H₂S concentration in a slightly sour environment [56].

The primary concern regarding CO₂/H₂S system is cracking of high strength steels by SSC. Both carbon steel and CRA's are susceptible to SSC. The most significant factors affecting SSC are:

- Partial pressure of the H₂S
- pH-value
- Chloride ion concentration
- Total tensile stress

The role of hydrogen sulfide is to provide hydrogen at the metal surface by corrosion and prevent hydrogen escaping into the production fluid. Usually, with the formation of hydrogen at the cathode, hydrogen would either react with any oxygen in the fluid or bubble of a hydrogen gas. Sulfide in the well fluid prevents hydrogen from escaping through the well fluid. The hydrogen then finds an alternative route by migrating through the metal structure, which is possible due to the small size of hydrogen molecule. Away from the sulfide, the hydrogen combines to form the much larger hydrogen molecule, and migration becomes severely restricted [35].

The migration is temperature dependent and becomes easier with higher temperature. At lower temperature, migration is restricted and hydrogen can build up. This preferentially happens at dislocations or grain boundaries where it generates high pressure. Under low stress, blistering can occur below the exposed metal surface. Under high stress, the pressure can cause the material to catastrophically crack. Environmental cracking is expected to occur during the initial phase of production and is not expected to have a time dependent development similar to 'sweet' corrosion [54]. Brittle materials (strong and hard) are particularly prone to SCC.

Below a critical partial pressure of H₂S no SSC is expected to occur. Above this limit, there is an increasing risk for SSC and the environmental conditions are termed sour. SSC is controlled by specification of the material properties and manufacturing process.

SSC is generally a much reduced risk at operating temperatures above 80°C. However, it is strongly recommended to follow ISO 151562 / MR0175 requirements for all the facilities exposed to H₂S, irrespective of the operating temperature, because of the risk of cracking of hydrogen saturated materials during, for example, shut-downs at ambient temperature [57].

6.5.1.7 Stress Corrosion Cracking

Stress corrosion results from the presence of aqueous conditions and chloride salts, usually in combination with sulfur compounds or oxygen at temperatures above 60°C. It usually result in local anodic (pitting) attack, which, in combination with tensile stress, provides sites for initiation of SCC.

SCC of low alloy steel has formerly been encountered in 3-component system CO-CO₂-H₂O. It has been shown that SCC is possible in CO₂-H₂O by Schmitt and Schlerkmann. Favorable conditions for SCC are higher strength steel, high CO₂ partial pressure and temperature above 60°C. Rhodes and Kapusta also confirmed that SCC can occur in some steels used for casing and tubing. Quenched-and-tempered, high strength low alloy steel study was followed up Mack. He suggested that the cracking mechanism is controlled by active dissolution, and probably further controlled by the electrode potential at the interface of the steel and corrosion product, and not hydrogen controlled. The steels showed highest susceptibility to SCC at temperatures between 66°C and 177°C at CO₂ partial pressure of 6,9 MPa in aqueous solutions [56].

It is well established that martensitic 13%Cr stainless steels are susceptible to SCC in chloride containing solutions at elevated temperature. Ibrahim et al. found that the presence of oxygen, CO₂, and H₂S in CaCl₂ brine was the most likely cause for intergranular cracking. Reservoir condition was 140°C to 156°C, CO₂ partial pressure 4.4 to 9.6 MPa, H₂S partial pressure 0.0004 to 0.0014 MPa and chloride concentration 3000 to 8000 mg/L. Test in the laboratory under simulated downhole conditions showed that in CaBr₂ and NaBr brines cracking did not occur because they promote passivity on super 13%Cr stainless steels. This indicates that CaBr₂ and NaBr brines would be better selections for completion fluids than CaCl₂ brine. High susceptibility of CRA's to SCC in CaCl₂-CaBr₂ brines at elevated temperatures was also suggested by Ikeda et al [56].

6.5.1.8 Effect of Supercritical CO₂

Propp et al. (1996) did experiments on AISI 1080 with dry supercritical CO₂. At 160-180°C, and 90-120 bars, corrosion rates of around 0.01 mm/y was observed [58]. Short term test has also confirmed this. Schremp et al. (1975) conducted test at 3 and 22°C at 140 bar CO₂, 800-1000 ppm H₂O and 600-800 ppm H₂S, the corrosion rate for X-60 carbon steel was measured to less than 0.5 µm/y [59]. Very few problems have been experienced with transportation of high pressure dry CO₂ in carbon steel pipelines. One operating pipeline showed corrosion rate of 0.25-2.5 µm/y during a 12 year period. More than 3000 km of pipelines carrying CO₂ is in operation internationally, mostly in the US for EOR projects [60].

At pressures above 50 bar with wet CO₂, quantitative measurements on corrosion rate is sparse. Propp et al. (1996) concluded that it was unacceptable [58], and others that carbon steel develops evident corrosion attacks in 24 hours at 50°C and 240 bar CO₂ as soon as the water solubility limit is exceeded. One study showed that the pH was changed in the test solution during testing by the corrosion process

and that this affected the corrosion rate at high CO₂ pressure. This study was performed in an autoclave with 1 M NaCl solution at 80°C and CO₂ pressure up to 50 bar. Further it showed small changes in corrosion rate under floating pH conditions at 5 and 50 bar. At constant pH corrosion rate increased with CO₂ partial pressure and at pH of 3.5 a corrosion rate increased from 10 to 15 mm/y at 5 and 50 bar respectively. Generally corrosion rate tends to decrease as pH increase, and lowest corrosion rate of 2.5 mm/y was observed during floating pH. This fact is explained by a more protective carbonate scale formed under floating pH conditions [61]. Experience with wet CO₂ in field is limited. One CO₂ pipeline reported accumulation of corrosion products due to insufficient drying and a leak at a low point due to water build up [60].

More recently Thodla et al. (2009) performed experiments with supercritical CO₂ at 31°C at 1150 psi with the addition of impurities of water and MEA. This experiment showed that a very small amount of water (~100 ppm) in SC-CO₂ is sufficient to form a second phase of water, and will cause a high corrosion rate (1-2 mm/y). The presence of amine with water in SC-CO₂ lead to significant decrease in corrosion rate [62]. Ayello et al. (2010) looked at the impact of impurities of O₂, SO₂ and NO₂ in wet supercritical CO₂. The test conditions was 1000 ppm water, 75.8 bar, 40°C and 100 ppm of impurity. Conclusion from this work was that NO₂ significantly increased the corrosion rate, SO₂ gave a small increase in rate and O₂ showed a slight increase in corrosion rate [63].

Zhang et al. (2011) investigated the influence of temperature (50, 80, 110, and 130°C) on the performance of two carbon steels and three CRA's in a CO₂/water system where the CO₂ where in supercritical state. They tested in pure CO₂, CO₂ containing dissolved water, and water saturated with CO₂. Their results confirmed that dry SC-CO₂ is not corrosive, and that water saturated with CO₂ is very corrosive for carbon steels and yielding intense localized corrosion in the whole temperature range of 50-130°C. The results from water saturated with CO₂ is pictured in Figure 6.14. Notice that both the austenitic-ferritic (1.4462) or the austenitic CrNi steel (1.4539) surpassed the target of 0.1 mm/y at 110°C [64].

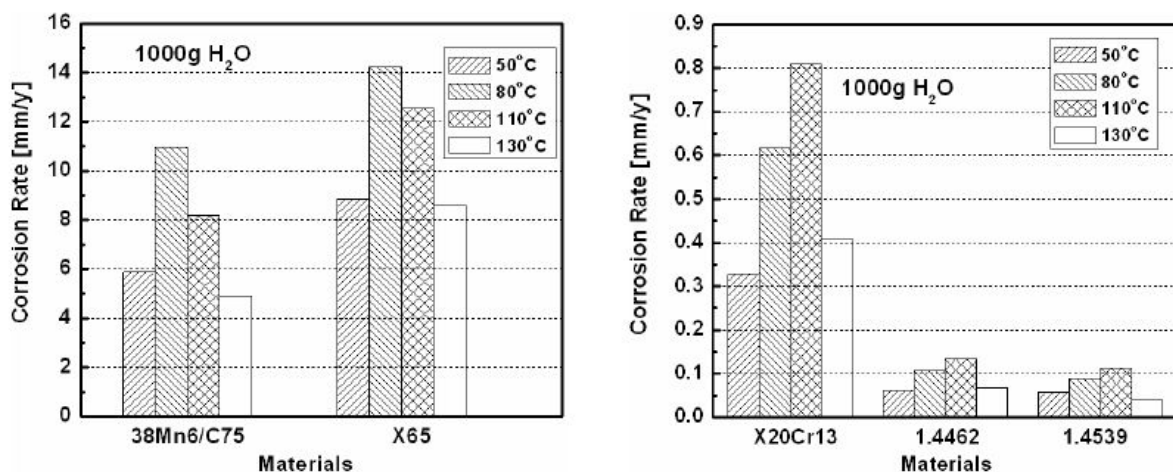


Figure 6.14: Effect of temperature on corrosion rate of steels in the system. 450g CO₂/1000g H₂O [64].

They also found that equilibrium exist between CO₂ and carbonic acid even under supercritical phase when water is dissolved in SC-CO₂. For CO₂ containing dissolved water at SC conditions they concluded that propagation of corrosion is significantly retarded by formation of a thin, protective iron carbonate film which cannot be dissolved due to lack of solvent [64].

Experiment indicate that the corrosion rate that can be expected if water drops out of a CO₂ rich fluid is hard to anticipate, but expected to be high. A study by Seiersten (2001) found that corrosion of carbon steel in wet CO₂ at high pressure were considerable, but smaller than expected from model developed for CO₂ corrosion at low pressure. Seiersten also found that the rate decreased with increasing pressure above 20 bar [60].

It is appreciated that material issues associated with supercritical CO₂ have to a very little degree been explored. So is the case also of impurities in relation to supercritical CO₂.

For corrosion rate prediction of carbon steel in aqueous environment that have dissolved CO₂, there exist several models. None of which are capable of predicting corrosion in condensed phase CO₂. At critical point (31°C/1070psi) the density of the CO₂ increases dramatically to about 0.4 g/cc². If water is added, a condensed phase consisting of liquid CO₂ and water will precipitate. All of the dense phase CO₂ present, precipitates out as liquid CO₂ along with water that is present. Published literature on supercritical CO₂ corrosion focus on CO₂ in equilibrium with an aqueous environment (water + salt) [62].

Seiersten (2001) stated that if corrosion is limited, short periods of water wetting may be accepted [60].

6.5.2 Injection Well Metallurgy Assessment

Sumitomo Metals have published a schematic (Figure 6.15) to be used as a first pass in selecting metallurgy. The schematic uses two primary corrosion mechanisms, one for each axis. Carbon dioxide and hydrogen sulphide corrosion. The bottom hole condition for Prelude injector is marked with a star in Figure 6.15.

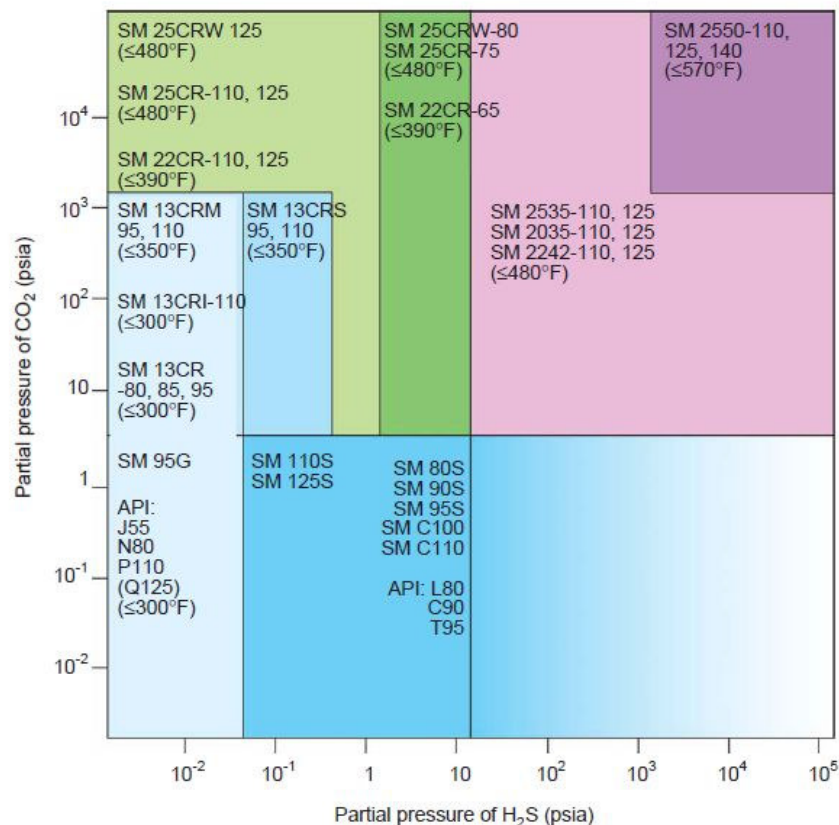


Figure 6.15: First pass material selection [35].

From the figure it appears higher grade steels will have to be considered.

6.5.2.1 Corrosion Considerations

During normal injection, free water will not be present in the system and dry CO₂ is not corrosive. Therefore, there is no risk of degradation mechanisms affecting the integrity of the injection well during normal operation. However, process upsets and injection well flow back could introduce free water and condensate water from the reservoir into the wells. The risk of having free water flowing back into the wellbore during long shut-ins is very low as the aquifer is not mobile. Dry conditions cannot be fully assured in any operation and materials should be evaluated in a scenario that includes presence of both formation and condensate water.

Table 6.3 indicates the expected partial pressure of the CO₂ and H₂S. These are considered to be the worst expected condition during the injection phase.

Partial Pressure	Maximum Expected (Int. Reservoir Pressure 415 bar)
ppCO ₂	414.17
ppH ₂ S	0.091

Table 6.3: Partial pressure CO₂ and H₂S.

6.5.2.2 Carbon Steel Feasibility

Carbon steel is the most commonly used material in a non-corrosive environment. In fact, it is even the preferred material in moderate corrosive environments owing to its lower price, strength and high availability internationally [17].

Bare carbon steel is however vulnerable to CO₂ corrosion. The limit of H₂S concentration at which an environment is considered to be “sour” for carbon steel and low alloy steels is defined by ISO 15156/ NACE MR0175. In oxygen free, sour environments, the corrosion product (iron sulphide) can be very protective and carbon steel can be highly successful as long as the guidance of ISO 15156 / NACE MR0175 is followed for avoiding SSC cracking [17].

If CO₂ is injected in a dry supercritical state, there is no significant risk of corrosion, because the corrosion rate of metals in the presence of dry supercritical CO₂ is very low. In that case, carbon steel is sufficient if dry conditions can be maintained. However, carbon steel is susceptible to high corrosion rate if wet conditions are present.

To estimate the corrosion rate for carbon steel, several models have been developed over the years. Shell currently uses the Hydrocor for estimation of corrosion rate. This software was not available, thus the NORSOK model was used instead. Table 6.4 show some of the models used to estimate CO₂ corrosion.

	Modell	Developer	Temperature [°C]		Pressure [bar]	ppCO ₂ [bar]		pH	
			Min	Max		Min	Max	Min	Max
1.	De Waard-Milliams	De Waard and Milliams, 1975 / Shell, IFE	0	140			10		
2.	Hydrocor	Shell	4	150	200	0.05	20		
3.	Cassandra	BP		140	200		10		
4.	NORSOK	Statoil, Hydro, Saga, IFE	5	150	1000	0.1	10	3.5	6.5
5.	Cormed / Lipucor / Corpos	Total / Elf	20	150	250		50		
6.	KSC	IFE (JIP)	5	150	200	0.1	20	3.5	7
7.	Tulsa	University of Tulsa	38	116			17		
8.	Predict	InterCorr International / Honeywell	20	200			-	2.5	7
9.	SweetCor	Shell	5	121		0.2	170		

Table 6.4: Corrosion models [65, 66].

From Table 6.4 it is observed that there is currently no model that estimate corrosion at the high pressures anticipated in the injection well at Prelude. However, literature available for laboratory and field applications have shown that corrosion rates in high CO₂ partial pressures are lower than the corrosion predicted by the models [61]. Hence, the Norsok model for CO₂ corrosion will not under predict the rate. The corrosion rate obtained from NORSOK has been used as a conservative approach. The Norsok M-506 model is an empirical model fitted to data from experiments at IFE [67]. The Norsok Standard for CO₂ corrosion rate calculation (M-506) is freely available at:

<http://www.standard.no/PageFiles/1178/M-506d1r2.pdf>

The input used in the model for flowing and static condition can be observed in Table 6.5.

	Static			Flowing		
	WH	CSG	LC	WH	CSG	LC
Temp [°C]	8	140	155	39	78	80
pCO ₂ [bar]	140	400	414	143	419	425
pH	3.5	3.5	3.5	3.5	3.5	3.5
Shear stress [Pa]	0	0	0	30	30	30

Table 6.5: Input to NORSOK M-506.

Corrosion rate assuming permanent wet conditions was estimated for wellhead, lower completion and casing below packer. The results are shown in Table 6.6 and 6.7. With the unconventional high partial pressure of CO₂, a pH value lower than 3.5 is expected if free water is present. An estimated wall thickness loss based on different wet event scenarios per year is also indicated.

Static	Corrosion rate 100% wet conditions [mm/year]	Wall thickness loss per year for 5 days wet conditions [mm]	Wall thickness loss per year for 48 hours wet conditions [mm]	Wall thickness loss per year for 24 hours wet conditions [mm]	Wall thickness loss per year for 8 hours wet conditions [mm]
Wellhead	4.08	0.056	0.022	0.011	0.004
CSG	131.62	1.803	0.721	0.361	0.120
LC	110.58	1.515	0.606	0.303	0.101

Table 6.6: Corrosion rate and wall thickness loss estimation static condition.

Flowing	Corrosion rate 100% wet conditions [mm/year]	Wall thickness loss per year for 5 days wet conditions [mm]	Wall thickness loss per year for 48 hours wet conditions [mm]	Wall thickness loss per year for 24 hours wet conditions [mm]	Wall thickness loss per year for 8 hours wet conditions [mm]
Wellhead	262.88	3.601	1.44	0.720	0.240
CSG	648.76	8.887	3.555	1.777	0.592
LC	659.77	9.038	3.615	1.808	0.603

Table 6.7: Corrosion rate and wall thickness loss estimation flowing condition.

It is clear that the corrosion rate is highly over estimated. Even if the corrosion rate is overestimated with a factor of ten the corrosion rate is still too high. Considering the availability of the system have been estimated at 89% [7], the system will be static for 40 days a year with an estimated corrosion rate 12.12 mm/year.

Further, because the pCO₂:pH₂S is about 4500, it should be considered a mixed corrosion regime according to DEP 30.10.02.14-Gen[68](Shell standard). With a pH₂S of 0.091 bar (1.32 psi) and a pH of 3.5 in the near wellbore area, it can be observed that reservoir conditions are in region 3. Region 3 is highly sour service, and sulphide stress cracking needs to be considered.

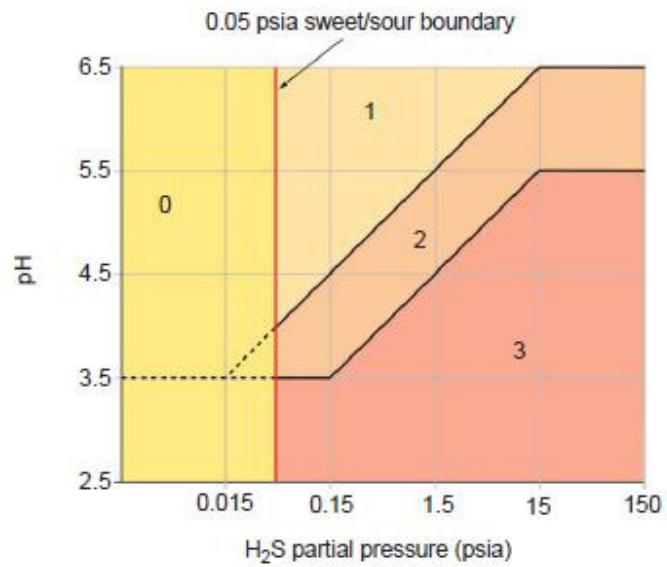


Figure 6.16: NACE MR 0175 Sour service definition [35].

The challenges of estimating carbon steel corrosion, makes corrosion allowance a non suitable way to deal with the danger of CO₂ corrosion of carbon steel. Unless dry conditions can be guaranteed, carbon steel is not feasible.

6.5.2.3 Corrosion Resistant Alloys

When the corrosion rate is too high for carbon steel and lining is not practicable, corrosion resistant alloys can be assessed in place. CRA have been essential for providing long term resistance in highly corrosive environments [17]. There are many CRAs to choose from, and the following discussion will only be limited to common options.

The following parameters influence the corrosion properties of CRAs [17]:

- Temperature
- Chloride ion concentration
- Partial pressure CO₂
- Partial pressure H₂S
- Environment pH
- Presence of other contaminants, principally oxygen and other acidic or oxidizing contaminants

Between them these parameters influence

- The stability of the passive film (initiation of pitting).
- Ease of repassivation of initiated pits.
- Rate of dissolution of metal from pits (pitting rate).
- The risk of stress corrosion cracking (SCC) initiating and propagation (or SSC in ferritic & martensitic CRAs).

One wants to choose a CRA that is the most cost-effective for which there is no risk of passive film breakdown. The expected operating conditions should be within the safe operating envelope of no pitting or cracking.

6.5.2.3.1 Martensitic Stainless Steel Sweet Conditions

13% chromium grades typically have good resistance to CO₂. The safe operating envelope for API 13 Cr stainless steel exposed to wet CO₂ containing NaCl, without contaminants, is represented in Figure 6.17. The corrosion resistance of 13Cr has been defined for CO₂/NaCl environments for CO₂ partial pressure up to 136bar (2000 psi). The partial pressure of CO₂ for the Prelude injector will be more than 400 bar. At such high partial pressure, a very low pH can be expected. Low pH level will increase the tendency for breakdown of the passive film, which could lead to localized corrosion and hydrogen related cracking mechanisms.

Published data suggest that S13Cr (Super 13Cr) are generally stronger than the basic API 13Cr grade and are suitable to about 30°C higher operating temperature than standard 13Cr grades in a H₂S free environment [57].

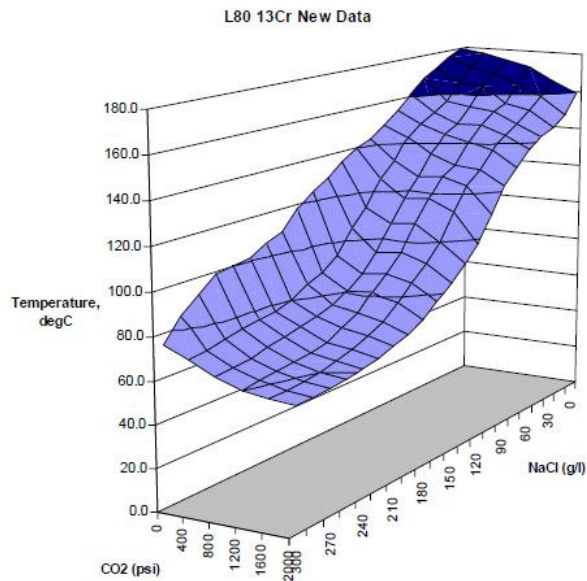


Figure 6.17: Safe operating envelope for 13Cr stainless steel in sweet service (based on limiting corrosion rate of 0,05 mm/yr) [57].

Sour Conditions

NACE MR0175 / ISO 15156-3 specify a maximum H₂S content of 0.1 bar (1.5 psi) and a minimum pH of 3.5 for martensitic stainless steels in tubing and general equipment. This limit also applies for super 13Cr grades. Recent laboratory work and field data do however suggest that the limit is a bit higher than the earlier publications suggested and what NACE MR0175 / ISO 15156-3 allows. Figure 6.18 show the range of different conditions where data indicates that the material is resistant to SSC and where it is susceptible to SSC (low pH, higher H₂S). The figure is based on a variety of data with chloride levels >50 000 ppm, and one can expect to see different service ranges for extremely high- or low chloride contents [57].

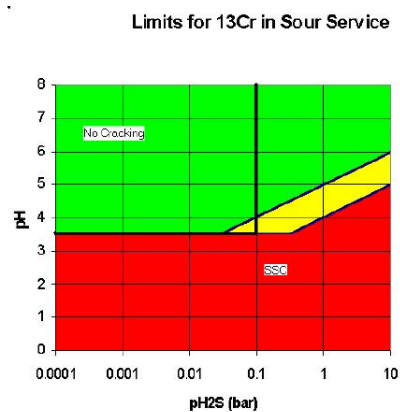


Figure 6.18: API L80 13Cr; sulphide stress cracking (red); resistant (green), and yellow represents conditions requiring further checking of alloy behavior. ISO 151156-3 limits shown by heavy black lines [57].

The critical feature to take away from Figure 6.18 is the transition between cracking and no cracking which is seen at pH 3.5 (test data established at room temperature). This has also been confirmed by recent publications, where 13Cr family of materials has shown a tendency to depassivate below a pH of about 3.5, depending upon heat treatment conditions and composition of alloying [57]. This indicates that the well possibly will be susceptible to SSC during short periods of wet operation. This cracking mechanism can jeopardize the integrity of the well and it is noted that this could potentially start within hours.

Though to be caused by their higher strength, Super 13Cr grades have been found to be more susceptible to H₂S than standard 13Cr grades. Higher strength material has a greater risk of enhanced initiation of pitting, hydrogen embrittlement and sulphide stress cracking, as shown in Figure 6.19.

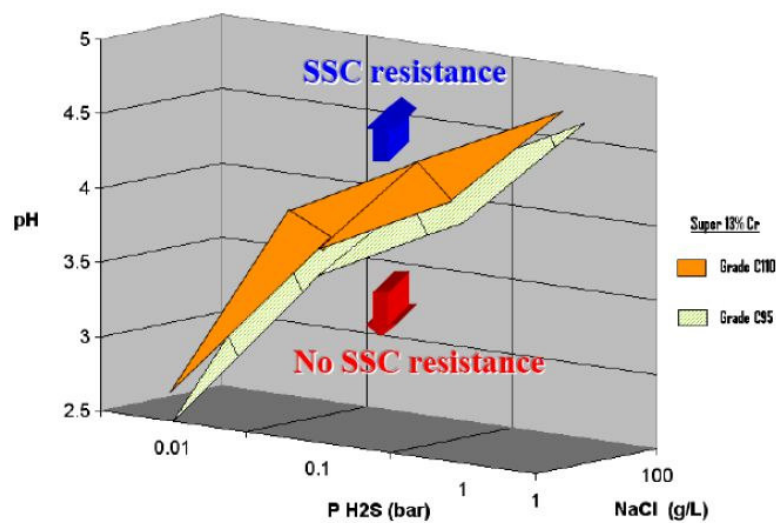


Figure 6.19: Dimensional SSC susceptibility diagrams of a Super 13% Cr SS (specimens were stressed at 90% AYS) [57].

6.5.2.3.2 Austenitic Stainless Steel Sweet Conditions

The 300 series of stainless steels are a broad range of materials based around the standard AISI 304L grade and the higher Molybdenum-containing Alloy 316L. These materials have all shown resistance to corrosion in sweet environments [57]. The grades containing more Mo have a more stable passive layer and are therefore more suitable for CO₂ environments with chloride ions present. The graph in Figure 6.20 show the operation envelope for Alloy 316L in terms of NaCl%, partial pressure of CO₂ and temperature. There is a high sensitivity to chloride content when partial pressure of CO₂ is very high.

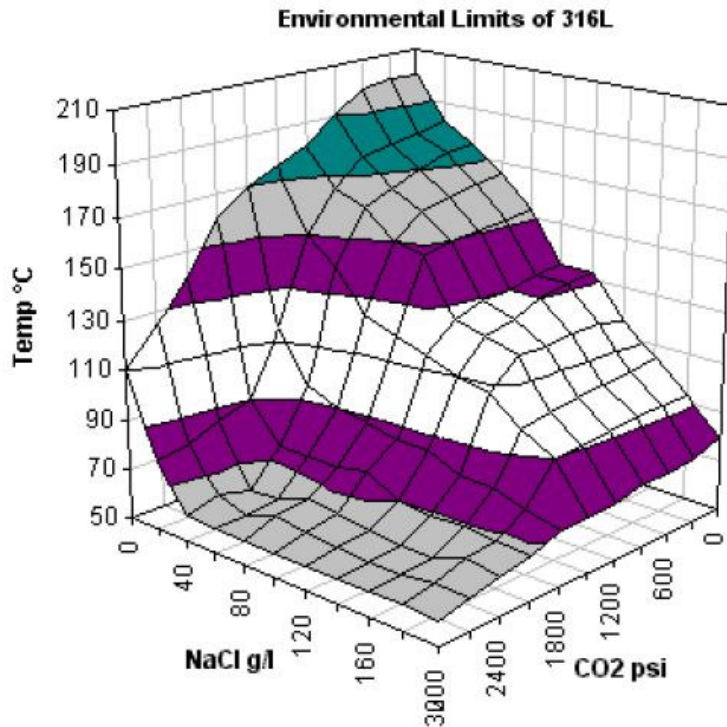


Figure 6.20: Limits of use of AISI 316L stainless steel in sweet environments.

Sour Conditions

ISO 15156-3 was first published 15/12/2003. Technical Corrigenda is published from time to time, and have frequently affected the limits of austenitic steel. Table 6.8 summarizes published operating limits of austenitic stainless steels as of 15/12/2007. The stated values are maximum limits [57].

Material Type	Temperature (°C)	Partial pressure H ₂ S (psi)	Chloride conc. (mg/l)	pH
Austenitic stainless steels (including 304L)	60	15	Any	Any
	Any	Any	50	Any
S31600, S31603	93	1.5	5000	≥5
	149	1.5	1000	≥4
S20910	66	15	Any	Any

Table 6.8: Safe operating limits 15/12/2007 [57].

An extensive review set the limits for use of Alloy 316L in environments containing H₂S and high chloride levels. In principle these test were preformed with oxygen purging, but pre-dated rigorous laboratory controls and it is considered that the low limits they obtained are indicative of the impact of some air. For chloride concentration of 10 g/l this indicated that the limiting partial pressure of H₂S above which there was a likelihood of sulphide stress cracking was 0.9 bar, over a range of temperatures from room temperature up to 225°C [57]. This indicates that it is feasible for Prelude injector from a sour corrosion stand.

6.5.2.3.3 22 Cr and 25 Cr (Duplex Stainless Steel)

Sweet Conditions

Resistance of the 22Cr duplex stainless steel is very good in sweet environments. Up to 200°C there is no risk of pitting or stress corrosion cracking, even at sodium chloride content in the brines of 200 g/l (200 000 ppm)[57].

Greater resistance to pitting still, 25Cr steels add probably about 30°C at any set of condition compared to 22Cr grade, as shown in Figure 6.21.

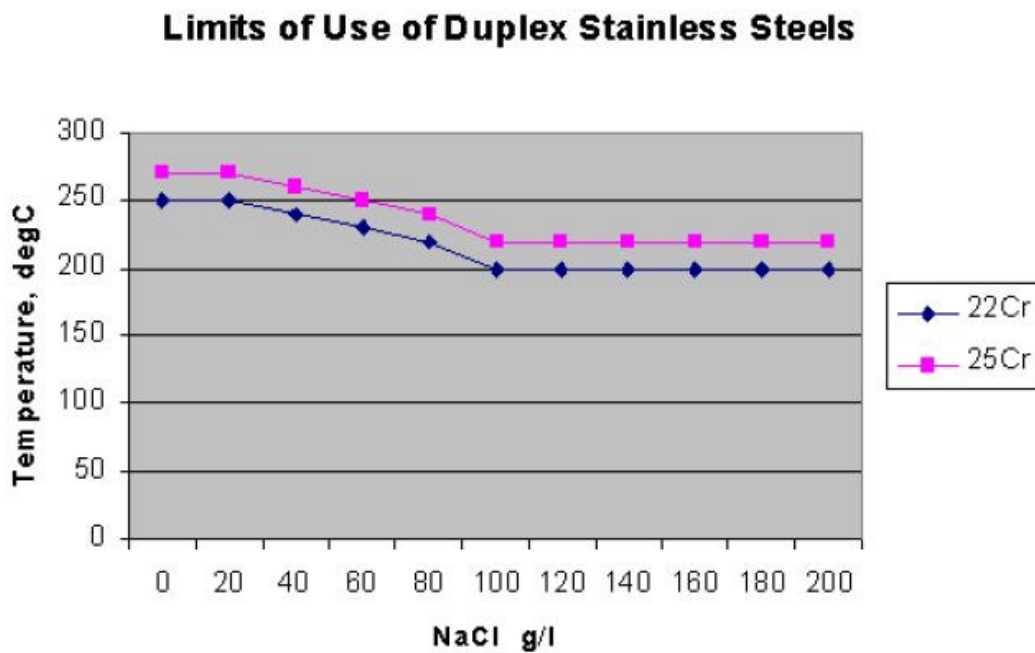


Figure 6.21: Temperature limits for duplex stainless steels as a function of sodium chloride concentration (<0,05 mm/yr corrosion and no SCC or SSC) [57].

Sour Condition

ISO 15156-3 / NACE MR0175 allows 22Cr duplex alloys with up to 0.1 bar H₂S and 25Cr superduplex alloys with up to 0.2 bar and without limits on chloride content or pH [57].

At around 80-100°C the duplex stainless steels show the highest sensitivity to sulphide stress cracking, and so test data at that temperature has been checked to establish safe environmental limits. pH and chloride content also influence cracking. The pH is taken at room temperature because this is the value reported for the laboratory test data on which the limits are based. Figure 6.22 shows limits of H₂S as a function of pH and chloride content.

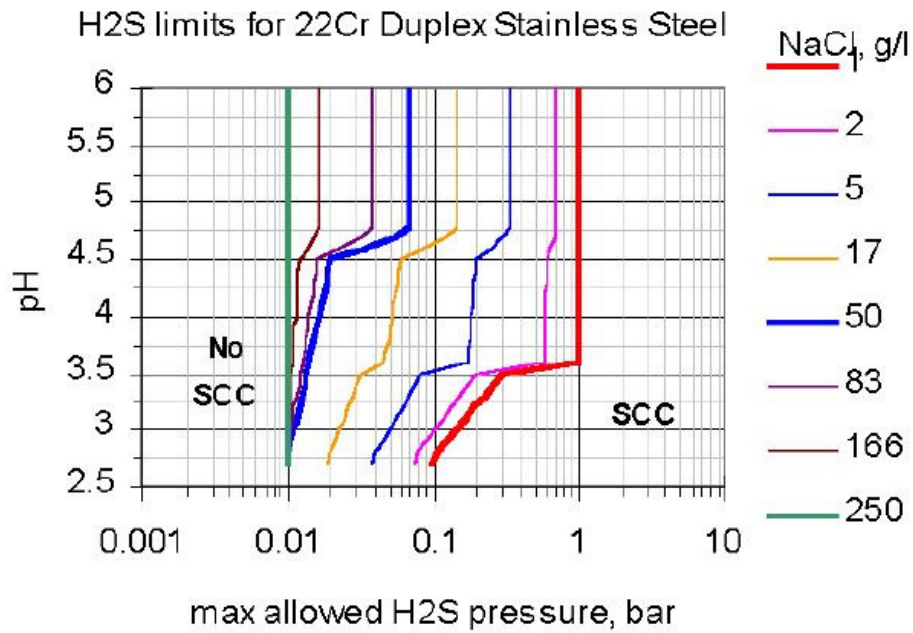


Figure 6.22: Safe operating envelope of 22Cr duplex stainless steels in CO₂ environments containing H₂S and chloride ions [57].

25Cr superduplex stainless steel is more resistant to hydrogen sulphide in general, but as shown in Figure 6.23 the limits of H₂S all converge together at higher chloride content and low pH, as for 22Cr grade.

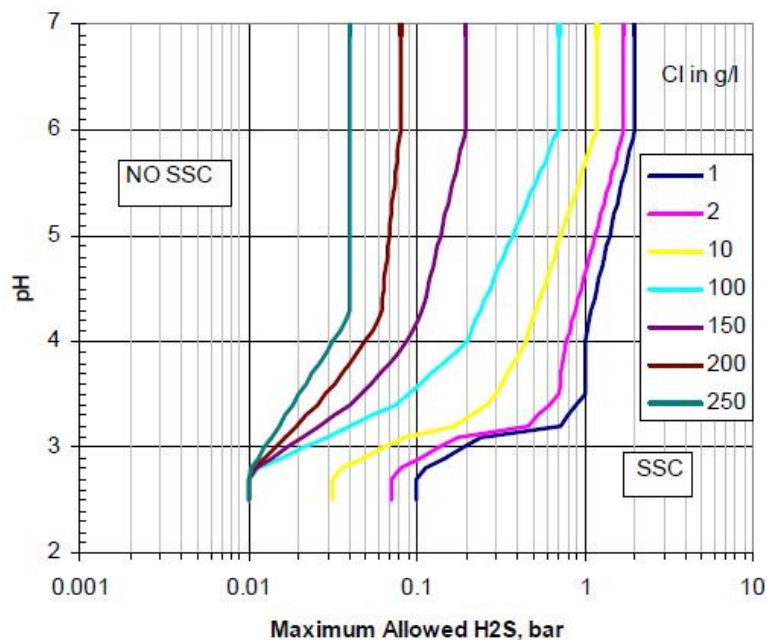


Figure 6.23: Safe operating envelope of 25Cr duplex stainless steels in CO₂ environments containing H₂S and chloride [57].

6.5.2.3.4 Nickel Alloys and Titanium

The nickel alloys are effectively immune to CO₂ corrosion and very resistant to the presence of H₂S, caused by a strong passive layer which is relatively pitting resistant. Nickel alloys are generally considered to include 40%Ni containing Alloy 825 and more highly alloyed grades [57].

Even these materials have limits regards to pitting and SCC in the presence of oxygen and chlorides. In fully aerated brines, Alloy 625 is resistant to about 60°C and Alloy C276 up to about 80°C. For temperatures above 90°C it becomes necessary to consider pure titanium or its alloys for handling hot aerated brines [57].

Formation of elemental sulphur may occur in the combined presence of H₂S and oxygen, which will introduce a significant pitting risk. If this is the case, highly pitting resistant alloys such as Alloy C22, Alloy C276 and Alloy 59 need to be considered [57].

6.5.3 Selection of Metallurgy

The injection well is forecasted to operate for about 25 years. Wet conditions are not likely to occur. However, due to the offshore nature of the project, and the fact that a workover in case of barrier breach will take many months to schedule and execute, robustness of solution should be very good. Wet conditions can be introduced as a function of back-flowing, depressurization and injection upsets. SC-CO₂ can contain a certain amount of dissolved water without being wet. When the flowline is depressurized, water will potentially drop out of the injection stream and accumulate in the bottom of the flow line. Upon start-up, there is a possibility that this water could be injected into the well.

A key differentiator for Prelude CO₂ injection well compared to other injection projects is the high bottom hole temperature of 155°C which renders materials used for many onshore projects useless (i.e GRE and plastic coated steel tubular).

Table 6.9 list the possible corrosion risk. It should be emphasized that a prequalification test should be performed on the recommended materials as no data is available for the partial pressures seen at Prelude.

Component	Corrosion Risk	Comment
13-3/8" Casing	Very Low	No threat if dry conditions. Not expected to be exposed to corrosive environment. Only risk is leak through cement to B-annulus, which is very unlikely.
9-5/8" Production Casing	Low for joints above the production packer. High for casing joints below the production packer.	No threat if dry conditions. The production casing will be exposed to the injected fluid below the production packer. 50m above the packer should be included for additional safety.
7" Production Liner	High	No threat if dry condition. Possible wet CO ₂ near wellbore and during injection upset.
7" Production Tubing	High / Medium	No threat if dry condition. The severity of the environment is lower at WH than at bottom hole. However worst has formed basis.
9-5/8" x 7" Production Packer	High	No threat if dry condition. Injection upsets may introduce wet conditions.
SCSSV	Medium	No threat if dry condition. Wt conditions in case of back-flowing, venting and injection upset.

Table 6.9: Corrosion threats for tubing and completion components.

In Table 6.10 the feasibility of different materials according to the corrosion risk above is assessed. A wet condition has been anticipated. Solutions that are on the borderline of what can be accepted will require further study.

		Sweet	Sour
13Cr		÷	Borderline
316L		÷	OK
Duplex	22Cr	OK	÷
	25Cr	OK	Borderline

Table 6.10: Feasibility of common metals.

From the latter table it is recognized that 13Cr is not feasible for Prelude CO₂ injector due to susceptibility of SSC. 25Cr has highest susceptibility to SSC between 80-100°C, which is in the expected temperature range of the injected CO₂, a upgrade to 25%Cr Super Duplex is required.

Technical specifications from Sumitomo metals states the maximum applicable H₂S level for SM25CRW (Super Duplex 25%Cr) to 3.0 psi with any combination of temperature and pH. Chlorides are restricted to 120 kppm. Thus the operating conditions will be beneath the maximum levels for the tubing.

6.5.4 Conclusion & Recommendation

The recommended metallurgy is tabulated in Table 6.11. Robustness is the key driver for the recommendation.

Component	Material Recommendation
13-3/8" Casing	Carbon Steel
9-5/8" Production Casing	All joints down to 50m above production packer: Carbon steel Rest: 25%Cr Super Duplex
7" Production Liner	25%Cr Super Duplex
7" Production Tubing	25%Cr Super Duplex
9-5/8" x 7" Production Packer	Nickel Alloy
SCSSV	Nickel Alloy

Table 6.11: Metallurgy recommendation.

- Dry conditions cannot be fully assured for all operation. Materials selection was based on a worst case scenario with a wet environment.
- Since a small amount of corrosion on a valve gate, flapper, or seat may completely destroy its function, a nickel alloy should be selected.
- The material recommendation is based on literature review only.
- A qualification process, which include autoclave testing, should be carried out to assure that the recommended metallurgy can actual operate under operating conditions.
- A model to predict CO₂ corrosion at high partial pressure does not exist.
- There is a general lack of experimental data of corrosion at high partial pressure CO₂.

6.6 Elastomers

Elastomers have the ability to be stretched easily to high extension and then reverse back to original shape when the stress is released. Most elastomers are made from long chained molecules known as base polymer, which provide basic and physical characteristics. Between the long chains molecules a small amount of free space exist, termed “free volume”. This allows the molecules to move more or less independently from one another, and give elastomeric components the ability to deform and change shape [69].

Perfect elastomers are strong, resilient, chemically inert, cheap and easily manufactured. However, this type of elastomers does not exist, and properties are trade-off between physical and chemical properties. Elastomers are affected by temperature and some chemical can soften, harden or swell the elastomers [35]. Table 6.12 list different elastomeric materials and their physical and chemical limitation. As you are getting closer to the limits, the properties of the elastomers will generally become weaker or more prone to degradation. For example, as the temperature rises, the elastomers will become softer and therefore more prone to extrusion [35].

Additives are included in the elastomers to manipulate the physical and chemical properties. Viton® is one additive that is available to improve chemical resistance. Hardness in another property that can be engineered for different purposes. At high temperature hard elastomers are stronger and resist extrusion better than softer elastomers, which are better at filling gaps. Standard design often uses a “sandwich” design with hard-soft-hard slabs. The harder slab mitigates extrusion of the softer element. This design is called multi-durometer [35].



Name	Nitrile	Hydrogenated Nitrile	Fluoro elastomers	Fluoro elastomers	Perfluoro elastomers	Ethylene Propylene
Material code	NBR	HNBR	FKM	FEPM or TFE/P	FFKM	EPDM
Common name		Therban®	Viton®	Aflas®	Chemraz® Kalrez®	Hydrocarbon rubber
Temp. range [°C]	-30 to 110	-20 to 150	-20 to 170	-20 to 200	-20 to 280	-40 to 150
S. Gravity	1.31	1.24	1.9	1.62	1.98	1.2
Hardness (Shore A)	60-90	70-75	75	55-95	65-95	70
Physical prop	Excellent	Good	Some more chemically inert grades have poor resilience	Poor extrusion resistance	Poor extrusion resistance	Good
H ₂ S	Poor (<10 ppm)	Poor when hot (<20 ppm)	Depends on grade, but can be poor	Good	Good	Poor
Amine inhibitors	Poor	Poor	Not recommended	Good	Good	
Methanol	Good	Good	Poor	Good	Good	
Zink bromide brines	Not recommended	Poor at high temperature	Good	Good	Good	
Hydrochloric acid	Poor with dilute acid. Not recommended for concentrated or hot acid	Poor with dilute acid. Not recommended for concentrated or hot acid	Some swelling with hot concentrated acid	Some swelling with hot concentrated acid	Good even with hot concentrated acid	Good
Aromatic hydrocarbons	Not recommended	Poor	Good	Poor	Good	Poor
Solubility parameter	8.5-11	8.5-11,5	9-12.5	8.5-10	Not measurable	7.5 - 9

Table 6.12: Common elastomers [35].

6.6.1 Degradation of Elastomers

Elastomers are prone to the phenomena of explosive decompression. Gas is absorbed upon exposure to the elastomers. If the gas pressure suddenly is reduced, gas expands but is not able to migrate out of the elastomers quick enough. This results in blistering [35]. With higher pressures these issues are expected to be more severe. Before choosing elastomers, it's important to have good knowledge about the explosive decompression properties of seals and gasket materials.

The most important factors affecting ED failure is decompression rate, which is defined as change of pressure with respect to time. However, the operator has very little control over this factor. If the rate can be controlled, it is possible to control the rate of CO₂ release from the elastomer and thus avoid damage [70].

An indicator of how well CO₂ dissolves in an elastomeric material is the solubility parameter. For liquid CO₂ this is 10-11 (cal cm³)^{1/2}. Gross swelling is unlikely if the difference in solubility is more than 1-2 units. However, many elastomers are optimized for service with hydrocarbons (iso-octane 6.9, toluene 9), but do not perform well with CO₂ [57].

One example with elastomers that have been demonstrated to work more successfully with CO₂ is EPDM. This is consistent with solubility parameter (7.5-9 (cal cm³)^{1/2}) being lower than CO₂. On the other hand, it is closer to hydrocarbons and thus not used in oilfield applications.

There are also other factors to consider. While swelling is reversible, chemical ageing permanently changes polymer properties. Typical degrading is embrittlement and loss of ductility. Chemical ageing is accelerated by high temperature. In tests at 120°C on a range of elastomers it was shown that the presence of small amounts of H₂S (e.g., 0.5%) in a gas mixture had little or no effect towards degradation. However it should also be noted that many elastomer do react with H₂S; including NBR, HNBR and several FKMs. TFE/P and FFKM are little affected by H₂S even at high temperature [71].

Hydrocarbon gases are not chemical aggressive to elastomers, but will as with other gases cause explosive decompression [71].

6.6.2 Selection of Elastomers

Elastomers need to meet three basic requirements [72]:

- Be chemically resistant to the environment.
- Withstand the temperature in service and during storage.
- Withstand mechanical loads as pressure, stress or abrasion.

Because the well is completed in a hydrocarbon reservoir, the elastomer solubility parameter should preferentially be distant from that of hydrocarbons and injected CO₂. With CO₂ and HC having widely different solubility parameter, this is hard to obtain.

Nitrile Butadiene Rubber (NBR), Hydrogenated Nitrile Butadiene Rubber (HNBR) and Ethylene Propylene rubber (EPDM) all have good properties for CO₂ service. This is consistent with their solubility parameter. However, NBR and HNBR have been reported to react with H₂S, but HNBR to less extent.



EPDM has been shown to react with fluid typically present in hydrocarbon reservoir, and need to be avoided if there is a chance of contact. If the well will be choked upon closure, a very low temperature could arise at well head. FFKM has extreme high temperature resistance and wide chemical resistance but its use is limited below 0°C.

FEPM (Aflas) is considered a good choice for Prelude application. There is however evidence for excessive swelling. Ender (1985) reported results of an investigation into swelling of well elastomers in carbon dioxide. He reported a linear swelling of elastomer with pressure at a temperature of 100°C. From this work it was observed that FEPM had a 20% volume swell at 106 bar, which is the maximum allowance criteria set in DEP 30.10.02.13 [73]. High swell of elastomers could potentially lead to failure if explosive decompression rate occur. Explosive decompression rate is less likely to occur in liquid environments and is a much reduced risk here. Swelling is normally only a concern when running the tool in the well when element swell can cause the packer to become stuck or damage the seals. After the packer is set and seals are in place, swelling is usually not a concern [74].

All elastomer have specialty grades available for extremely low or high temperatures.

6.6.3 Conclusion & Recommendation

Rapid decompression generally has relevance when the environment is gas, and thus is only a concern in the upper part of the well where gas flashing will occur during shut-downs. Further down where the CO₂ will be in dense phase, this is less of a concern. Here high temperature is the driver. Aflas (FEPM) would have been preferred at downhole conditions, but considering the work of Ender (1985), it is not recommended for Prelude CO₂. Instead, FFKM is recommended at bottom hole condition as the lower limit for its temperature range will not be reached.

For top hole conditions where JT-cooling reduces the temperature during shut downs and start-ups, HNBR is preferred over NBR due to its higher H₂S resistance. Further it is recommended that a high hardness is selected to be more resilient to rapid decompression.

Further recommendation:

- The material selection is based on literature review only. Testing of elastomer material should be performed at operating conditions before a final selection.
- The suppliers should provide qualification data based on testing in CO₂ as the behavior of an elastomer in CO₂ and natural gas can be very different.
- The results found by Ender should be confirmed. There is an opportunity to use FEPM.
- Thermoplastic materials like Nylon and PTFE, are practically unaffected by explosive decompression, and could potentially be used.

6.7 Packer Fluid

6.7.1 Introduction

Control and management of annulus pressures is a key requirement in safeguarding well integrity over the lifecycle of a well. As control of B- and C-annulus pressures (i.e. annuli between various casing strings) usually is not possible on subsea wells, maximum expected pressures in these annuli with appropriate safety factors are accounted for in the well design. For the A-annulus (tubing-production casing annulus) however, failure to control the pressure increase due to thermal expansion may lead to tubing collapse.

In subsea production systems A-annulus pressure management is conventionally done through a dedicated vent line to the host or through the cross-over valve in the Xmas tree.

The potential risk of a CO₂ leak into the A annulus can potentially cause a corrosion risk to the secondary barrier. If an aqueous packer fluid is selected a subsequent CO₂ leak would produce general corrosion caused by the formation of carbonic acid and lowered pH.

CO₂ corrosion requires replenishment to continue its corrosion attack on carbon steel. The reaction between steel and CO₂ creates a layer of protective iron carbonate which protects the casing against further attack. Iron carbonate is slightly soluble in a flowing system, but the annulus is more likely to be a static system, thus the layer will serve to inhibit further corrosion [75].

Two solutions typically used are base oil/diesel and buffered clear brine. One of the main differentiators between the two is heat expansion. If base oil/diesel is used the danger of CO₂ leak is less, as CO₂ and water would migrate to the bottom of the well, and CRAs would only be needed in this area. On the other hand, the much higher expansion factor would potentially cause integrity issues [75].

6.7.2 Selection of Packer Fluid

The basic packer fluid requirements for Prelude CO injection well in the “A” annulus:

- Avoid/minimize corrosion in tubing/production casing.
- Compatibility with material. Metallurgy and elastomers.
- Maintain positive pressure for indication of tubing to annulus communication.
- Avoid freezing at low temperature.
- Have favorable rheological properties to allow pumping/ bleed off through the umbilical from the FLNG.

The required density of the packer fluid will depend on the activities planned in the well. In general terms it can be stated that normal injection wells where activities involving well killing is not anticipated, there are no specific density requirements. Density ranges from 0.8 s.g. for base oil to 2.3 s.g for clear brines. A lighter fluid will allow for a higher MAASP. For Prelude an oil based mud packer fluid will not be considered as suspended particles may become unstable and settle.

Salt solutions are often highly corrosive and dissolved oxygen is a primary agent causing it. Even though brines may initially contain oxygen this will be quickly depleted and consequently the corrosion will only be superficial. A leak of CO₂ into annulus containing brine will be susceptible to CO₂ corrosion.

Formate brines are basically non-corrosive to well materials due to their high pH (>9) and lack of oxidizing power. They have typically found application as drilling, completion and packer fluids in HTHP wells due to their high specific gravity. Experiments performed by Leth-Olsen (2004) showed that an influx of CO₂ in this brine caused CO₂ corrosion on carbon steel. This was observed to be high initially, and then reducing as a protective layer was built (0.05-0.2 mm/y between 120°C and 180°C) [76]. CO₂ corrosion also occurred on 13% Cr steel, but at a higher rate due to less protective carbonate layer. Higher grade steel like Super 13% Cr and upwards showed very low corrosion rate with CO₂ ingress up to 180°C.

For formate brine to be non corrosive requires the pH to be above 7. Formate brines are usually heavily buffered in field application (pH 9.5-11), and can therefore tolerate a high influx for acid before a pH drop is experienced [77].

As described in chapter 3, the temperature of the injected CO₂ during transient operations can become below 0°C. Both oil based and water based packer fluid can be selected with a low freezing point. Base oil can be selected with freezing point as low as -20°C. Water based fluid can have salt added to depress the freezing point (but also increase the density).

Depending on annulus management, it would be preferential to have a fluid with low viscosity that can be easily pumped in/bleed off from the annulus through the umbilical. There will be a threshold pressure, strong function of viscosity, needed to bleed off the pressure when it builds.

For monitoring purposes the “A” annulus needs to maintain a positive pressure. In production wells, thermal expansion will occur after the wells are put on-stream. This pressure build up can then be bleed-off, either through X-over valve to production string or through a dedicated annulus line. Afterwards, a positive pressure can be maintained for monitoring. Injection wells are cold during operation and experience thermal expansion when they are shut-in. Assuming the annulus is topped up when injection starts, it will experience a gradual pressure build-up as it is warmed up to geo-thermal gradient during shut-in.

A first-order approximation of the thermal effects was investigated using a basic model for annular pressure build up [78]. The model and its shortcomings is described in [Appendix 3](#). Prosper showed average annulus temperature increase of 37°C when the well went from full injection to geothermal gradient. Therefore based on the following coefficients [79]:

Base Oil

- Vol. Coeff. Of thermal expansion: 8.64E-4 1/°C
- Compressibility: 6.45E-05 1/bar

Water

- Vol. Coeff. Of thermal expansion: 2.07E-4 1/°C
- Compressibility: 4.0E-05 1/bar

and assuming that 9-5/8" casing balloon and 7" production tubing reverse balloon, the annulus pressure will increase ~268 bar with for base oil and ~40 bar with water based packer fluid.

As base oil is considered a better solution from a corrosion point of view, a third option is to install nitrogen on top of the base oil. A N₂ cushion can absorb the volume increase by being compressed and allow for a positive pressure monitoring.

The annular volume per meter is 0.0121 m³/m. The annular length is 4370m. With a 150m nitrogen cushion, the unconstrained fluid contraction of the base oil would be [78]:

$$\Delta V_f(\Delta T) = V_{ann} C_T \Delta T \quad \text{Eq. 6.11}$$

which causes a contraction in volume of 1.632 m³. This equates to 135m drop down to 285m. The new nitrogen pressure under WH will be ~11 bar.

The comparison of installing the N₂ cushion and without the compressible cushion is presented in Table 6.13.

The N₂ cushion will likely prevent any well integrity problems related to fluid expansion in the annulus. However, a nitrogen cushion has specific challenges:

- Initial placement of the nitrogen.
- Will the nitrogen remain in place for the lifecycle of the well.
- Will the N₂ cushion mask any tubing to annulus communication?
- Complex and costly system with potential reliability problems.

	N ₂ Cushion	No Cushion
Initial condition	Installation (@ geothermal) N ₂ cushion: 20 bar, 150m of N ₂	Positive pressure 10-20 bar. Base oil to top of well
Thermal contraction (from geothermal to injection)	N ₂ level drop down to ~285m as base oil contract. Positive pressure maintained after cooling (~11bar).	Top of the well to vacuum. Positive pressure not maintained. Change in height: ~140m. To keep positive pressure, top up with ~15 bb base oil.
Thermal expansion (from injection to geothermal)	N ₂ level rise as base oil expands. Back to ~initial condition.	If the well is topped up during injection, change in pressure ~268bar.

Table 6.13: Comparison between N₂ cushion or not in the A-annulus.

6.7.3 Conclusion & Recommendation

Robustness is a primary driver and corrosion rate of carbon steel is too aggressive should the packer experience a leak. It is recommended to select base oil as a packer fluid. Base oil greatly reduces the corrosion risk. The downside associated with base oil is the low hydrostatic head and higher expansion.

- An opportunity exists to select water based packer fluid. For this option to viable, the risk and volumes of influx of CO₂/H₂S need to be quantified.
- The selected fluid must be tested for compatibility with elastomers.
- A multistring WellCat study should be performed to get more accurate numbers for annular pressure build up.
- More investigation will be required for the annulus pressure management. Currently, the umbilical design for the project is not known. The most straight forward solution is likely to be annulus management through an umbilical line.

6.8 Chapter Conclusion

The formation of free water in the CO₂ stream creates a highly corrosive environment. The amount of water that can be dissolved in the CO₂ stream before formation of free water is thus highly important. The expected amount of water for Prelude is below the solubility limit during normal operation, and no free water is expected. However, there is no guarantee that free water does not form during transient operations or can be introduced through completion operations. Free water is expected to cause very high corrosion of carbon steel calling for the need of CRA's. The environment at Prelude is of such nature that selection of super duplex steel and titanium/nickel alloys are required.

The degradation rate of cement is likely to be diffusion controlled making it a slow process. Mechanical induced fractures in the cement can excel degradation and pose a danger to the well integrity. Even though Portland cement is expected to provide sufficient barrier for the Prelude field, it is recommended to use acid resistance cement as this has a better robustness.

Elastomers used for hydrocarbon service are often not suitable for CO₂ service. A review showed that elastomers fit for Prelude can be obtained. A leaking packer seal can cause corrosion in the annulus. It is recommended to select an oil based packer fluid to leave this concern moot.

There is a general lack of measurements and experimental results from high partial pressure of CO₂. CO₂ is optimally injected in shallow aquifers, and transported in dense phase at pressures much lower than what is observed at Prelude and thus there has not been an incentive to expand the pressure envelope for testing. Before any selection is made, it would be recommended to establish corrosion rates at the higher pressure and temperature conditions seen at Prelude.

Chapter 7

Well Hardware Selection

7.1 Objectives

The main objective of this chapter is recommendation of sand completion for the CO₂ injector. Considerations regarding other completion components are highlighted and the inverted well case is introduced and possible barriers identified.

7.2 Methodology

The requirement for sand control in the Prelude field has previously been established for the development wells. This work has been reviewed and the industry experience with sand control in injection wells examined.

A methodology sand control selection has been adapted from the Sakhalin project. A recommendation is given based on reliability, cost, installation and productivity. A wellbore simulator was used to model the productivity of the various completions. The skin factors for the various completions were established through assessment of reported values in the literature. A sensitivity analysis was performed to evaluate the robustness of the recommended completion.

The closed-in tubing head pressure for the inverted well is established by the use of a wellbore simulator. Considerations for completions components relating to CO₂ are identified.

7.3 Selection of Lower Completion

7.3.1 Requirement for Sand Control

To decide whether to use downhole sand control and what type to use, it is fundamental to accurately predict when a reservoir will fail and start to produce sand. The production of sand depends on three main components [35]:

- The strength of the rock and other intrinsic geomechanical properties of the rock.
- Regional stress imposed on the perforation or wellbore.
- Local loads imposed on the perforation or wellbore due to the presence of hole, flow, reduced pore pressure and the presence of water.

7.3.1.1 Rock Strength

UCS, TWC, sonic log and porosity gives a fair estimate of rock strength. The UCS and TWC are core-derived strength tests and sonic and porosity can be taken from logs and be performed on cores.

For the unconfined compressive strength (UCS) a cylindrical sample (50 mm long, 25 mm diameter) is compressed in axial direction by a steel piston without lateral support (confining stress zero) up to and beyond failure. The axial stress and axial and radial deformation are measured. The resulting index properties are the unconfined compressive strength UCS and the elastic parameters Young's modulus E and Poisson's ratio ν (at zero confining pressure) [80].

The thick-walled cylinder strength (TWC) test addresses the stability of underground cavities such as boreholes and perforations. A hollow cylinder sample (50 mm long, 25 mm outer diameter and 8.5 mm inner diameter) is subjected to isostatic compression at its outer surfaces (circumference and flat ends) the inner circumference is not loaded.

The compression causes a stress concentration at the inner hole wall. At high enough stress the inner wall starts to fail, producing grains or slivers of material. Increasing stress first results in the creation of two diametrically opposite breakout zones where material has been disaggregated and, subsequently, leads to collapse of the sample. The stress (i.e. the TWC strength) is recorded and constitutes an index property [80].

The sonic log records the time required for sound waves to travel through the formation in microseconds. The porosity is related to the sonic log travel time. Short travel times (50 microseconds) are indicative of low porosity and hard dense rock, while long travel times (95+ microseconds) are associated with softer rock.

Porosity of a formation can be used as a guideline for the need for sand control. The rule of thumb being that if porosity is higher than 30%, there is a higher probability for sand control requirements. Porosity of less than 20% has a low probability of sand control, and porosity between 20-30% is more uncertain [81].

7.3.1.2 Sand Failure Prediction

Sand failure prediction was based on Shell's proprietary [FIST](#) (Fully Integrated Sand Production Tool). The basis of sand production in FIST is as follows: The strength of the sand at any point is compared with the stresses acting over the lifetime of the well (or field). Consequently, rock strengths have to be estimated along with the stresses. When the stresses exceed the strength, the rock fails and sand production is predicted [82].

The rock strengths are usually measured from laboratory strengths tests from a few specific locations which have been cored. Sand production will occur in the weaker zones and may not have been intersected by coring. Core data from a limited number of depths are used to determine the strength along with the corresponding petrophysical parameter for which field e-logs are available across the entire reservoir interval. Then a correlation is constructed between measured strength and a petrophysical parameter [82].

To obtain a full strength profile versus depth the rock strength correlation is applied to the full data log. This is also required as rock strength measurements are sparse and expensive and it is common to only obtain a limited number of point by point strengths. Using log data, a synthetic, continuous strength vs. depth log can be created. This process is used to derive TWC and UCS strength profile through the reservoir [82].

It is thought that the TWC test captures some of the geometric aspects of the collapse problem, and are thus preferred to other tests. The strength estimates obtained from TWC strengths are considered to be equivalent to the initial failure of the borehole [82].

After initial failure, the perforation or borehole will produce some sand and will stabilize through the formation of a stable breakout. This is referred to as the zone of “transient” sand production. The breakout size will vary with the stresses acting on the borehole. The larger this stress is, the larger the breakout will be. At a certain stress, breakout will become unstable and catastrophic failure will occur [82].

For predicting sand production, both TWC and UCS are used. This can be summarized in the “FIST” diagram, Figure 7.1, which pictures the evolution of the sand prediction tendencies of a particular depth interval during depletion and drawdown as the field produces[82].

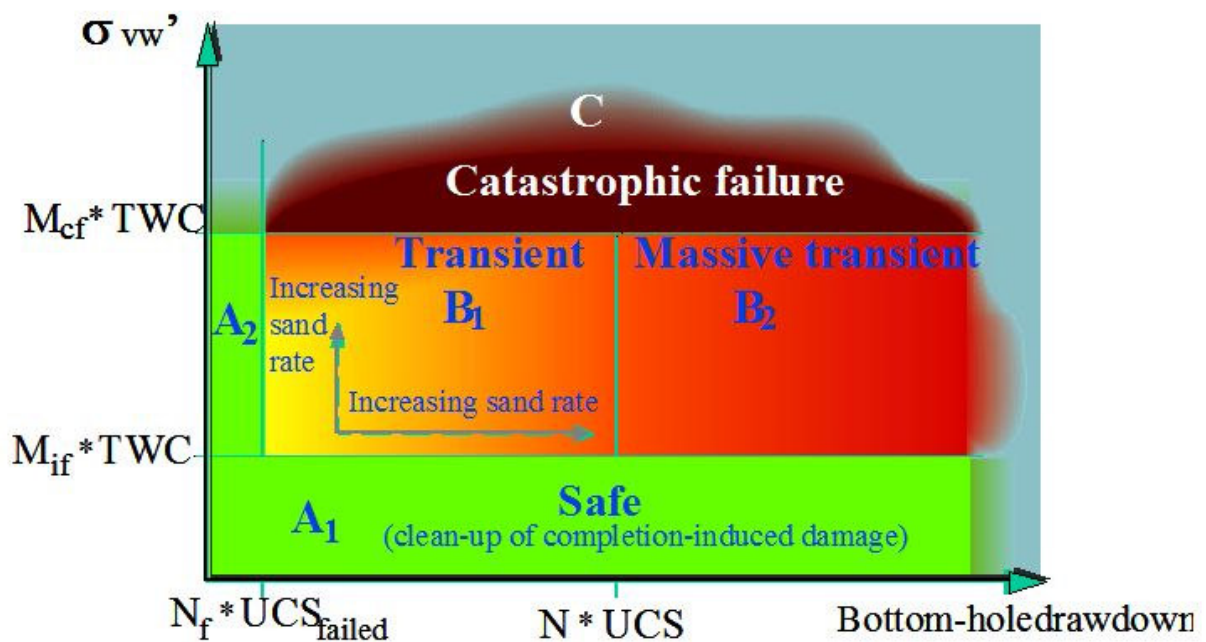


Figure 7.1: Conceptual FIST diagram, showing tendencies for sand at a specific depth [82].

Drawdown is plotted on the horizontal axis and effective stress on the vertical. The critical UCS and TWC values are used to distinguish between the different sand tendency areas; safe, transient, massive transient and catastrophic failure [82].

The near wellbore vertical effective stress includes the combined effects of in-situ far field stress, depletion and drawdown [80]:

$$\sigma_{v_w} = \sigma_v - P_{wf} = \sigma_v - P_{res,i} + \Delta P_{de} + \Delta P_{dd} \quad \text{Eq. 7.1}$$

where σ_{v_w} is (future) near wellbore vertical effective stress at perforation depth, σ_v is the far-field vertical total stress (overburden), P_{wf} is the near wellbore pore pressure at flowing conditions, $P_{res,i}$ is initial reservoir pressure, ΔP_{de} is field-wide depletion, and ΔP_{dd} drawdown applied at the wellbore.

Where the boundary criteria is described by [80]:

$$\sigma_{v_w} = M \cdot TWC \quad \text{Eq. 7.2}$$

$$\Delta P_{dd} = N \cdot UCS \quad \text{Eq. 7.3}$$

where M and N are factor depending on rock, fluid and operational parameters such as deviation, completion type and hole size.

During reservoir depletion, the near wellbore stresses increases and the point depicting the sanding tendency (actual drawdown and near wellbore vertical stress) moves vertically up the diagram. Initially, only perforation clean up sand may be produced (in the A1 safe area). Increasing depletion will move the sanding tendency vertically up the diagram until the boundary between A1 and B1 is crossed and indicating the onset of sand production. With continued depletion the perforations will enlarge and merge and lead to the tendency for catastrophic failure. The exact boundary between transient and catastrophic sand production is a function of rock strength, in-situ stresses and well and completion type. The sand tolerance at the surface facilities will dictate whether transient or catastrophic sand production will be manageable [82].

The effect of flow on sand production tendencies is delineated by the vertical boundary between the transient and massive transient zone (B1 to B2). The effect of flow is expressed as a function of the drawdown for this specific location. This boundary is probably gradual and the location will depend upon well, completion and produced hydrocarbons [82].

A better view of the total of a well is given by the “Sand Prone” plot which show the sanding tendencies for all the depth intervals in the producing zones (Figure 7.2) [82].

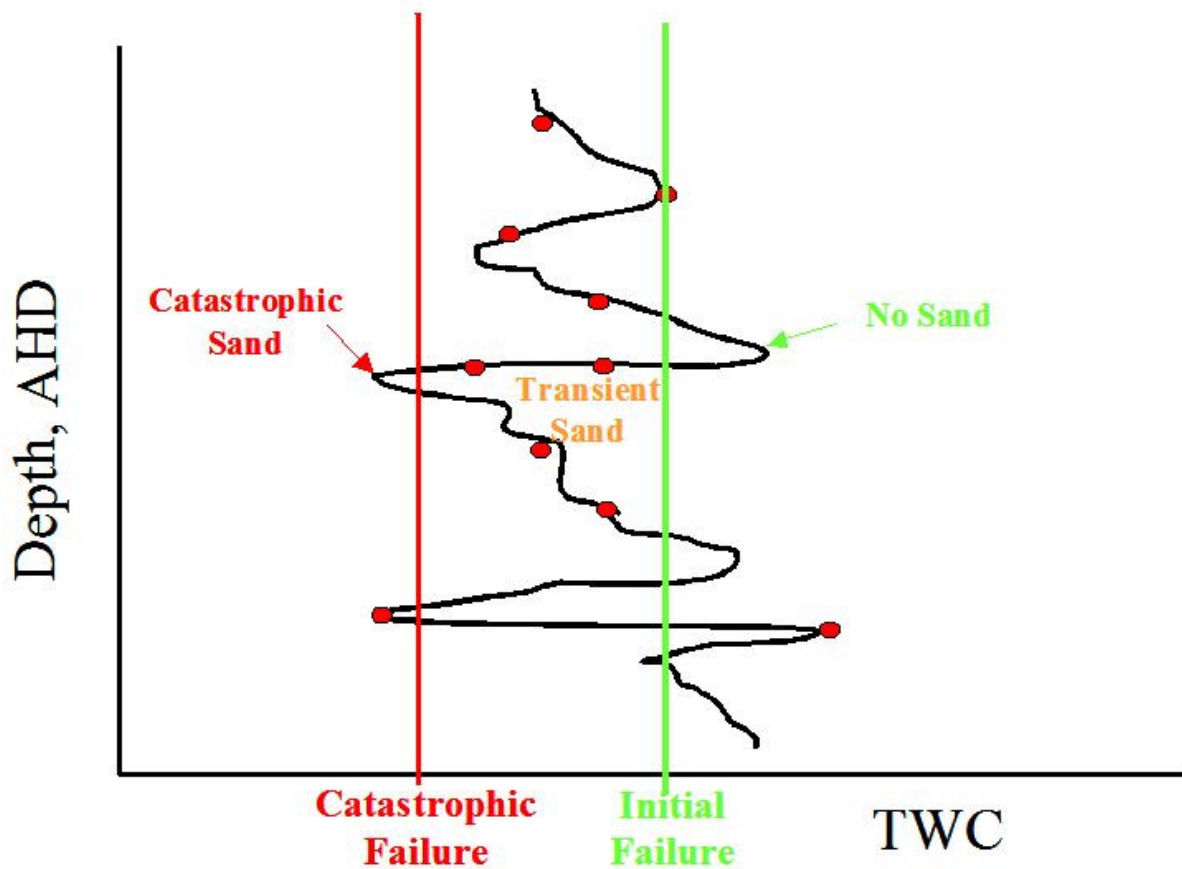


Figure 7.2: Illustration of the sand prone plot showing different sanding tendencies for different depths in the completion interval [82].

The sand prone plot shows measured formation strength (red dots), predicted formation strength (black line) and red and green failure lines (red for catastrophic and green for initial failure). Sections where the predicted strength is higher than the critical initial failure line (at the right of the green line) will not show any sand failure. Intervals that cut through the green line to the left will show initial failure and if they cross the red line there will be catastrophic failure predicted for these sections [82].

7.3.1.3 Sand Failure Analysis for Prelude Swan Reservoir

The requirement for sand control has been defined previously in EP 2010-5402 – Sand Failure Prediction for the Prelude Field, and this section only summarizes the results.

For the Swan injector well a FIST analysis was performed to assess the sand failure. Table 7.1 lists the Swan reservoir rock characteristics that founded the basis for the FIST study:

Parameter	Value
UCS	>5400 psi
TWC	>14000 psi
Sonic time	<76 microsecond /ft
Porosity	2-16 %

Table 7.1: Prelude Swan reservoir - Rock characteristics [83].

Based on the properties in table, the following high level observations was made[83]:

- The rock has good strength as UCS and TWC from core sample are high. Also, the compressional sonic time and porosity values are also low further corroborating the competency of the formation.
- Being a CO₂ injector well the onset of water is not a risk and is not likely to cause the resulting strength degradation and capillary cohesion damage.
- Since the gas producers and CO₂ injector are in the same reservoir, reservoir pressure will deplete over time.

A FIST analysis have been conducted for open hole completion. For strength criteria in open hole the TWC becomes more important, and it was observed that increasing the inner diameter of a core i.e. hole size, decreases the TWC strength. Increasing hole size from 8mm to 170 mm gives a reduction of 30-60% depending on sand type [83].

FIST has enabled inclusion of this “size effect factor” which can be described by [83]:

$$\frac{TWC \text{ perforation}}{TWC \text{ borehole}} = \text{Size effect factor} \quad \text{Eq. 7.4}$$

As the size effect factor plays an important role in sand prediction, sensitivities with different size effect factors was conducted with size effect factor of 2 and 2.5 [83].

With size effect factor 2, initial failure is seen after one year of injection for the case of 50% TWC certainty (meaning 50% probability) and from the beginning with 95% TWC (5% probability). However in later life of injection due to reduction in reservoir pressure, initial/transient sand failure is predicted as shown in Figure 7.3. Analysis suggest that no massive catastrophic failure is predicted over the injection period even with 95% TWC certainty plot [83].

Increasing the size effect factor to 2.5 predicts sand failure right from the beginning (Figure 7.5). There are however, no massive or catastrophic sand failure observed during the lifetime of the well. Sensitivities with size effect factor also showed there might be transient failure initially or late life due to reservoir pressure depletion. It is difficult to quantify and estimate the total time to remove transiently failed sand during clean up as it may vary from hours to days depending upon other parameters like rock strength and in-situ stresses [83].

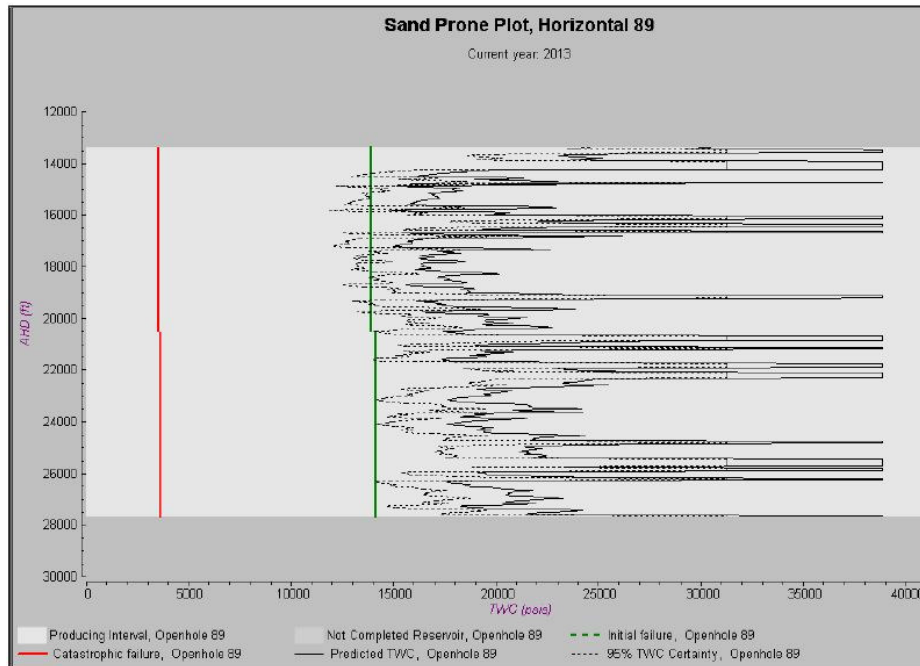


Figure 7.3: Initial sand failure profile for size effect factor 2. (open hole- first year of injection)[83]

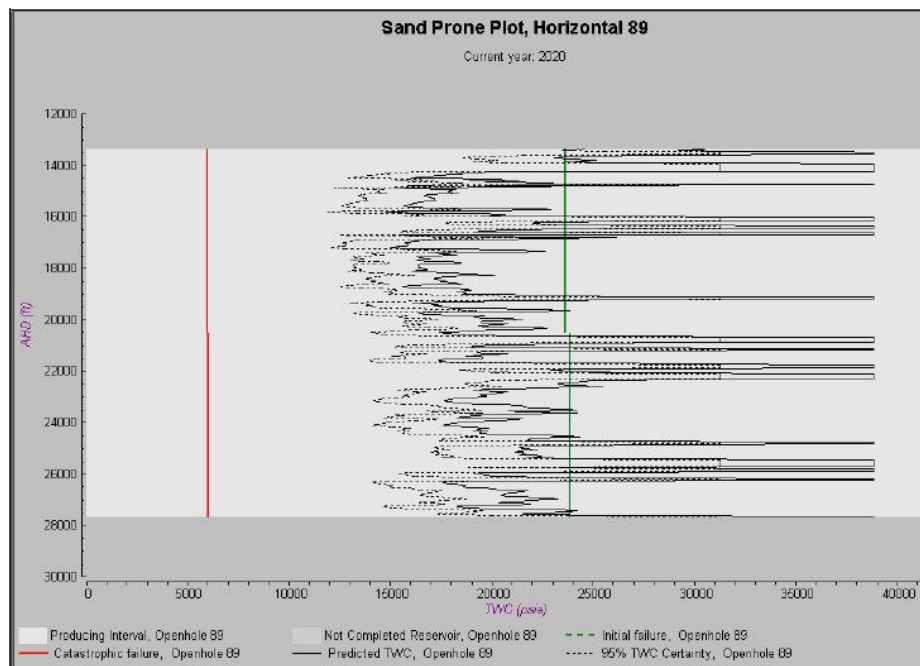


Figure 7.4: Initial sand failure profile for size effect factor 2 (open hole - late injectionlife) [83].

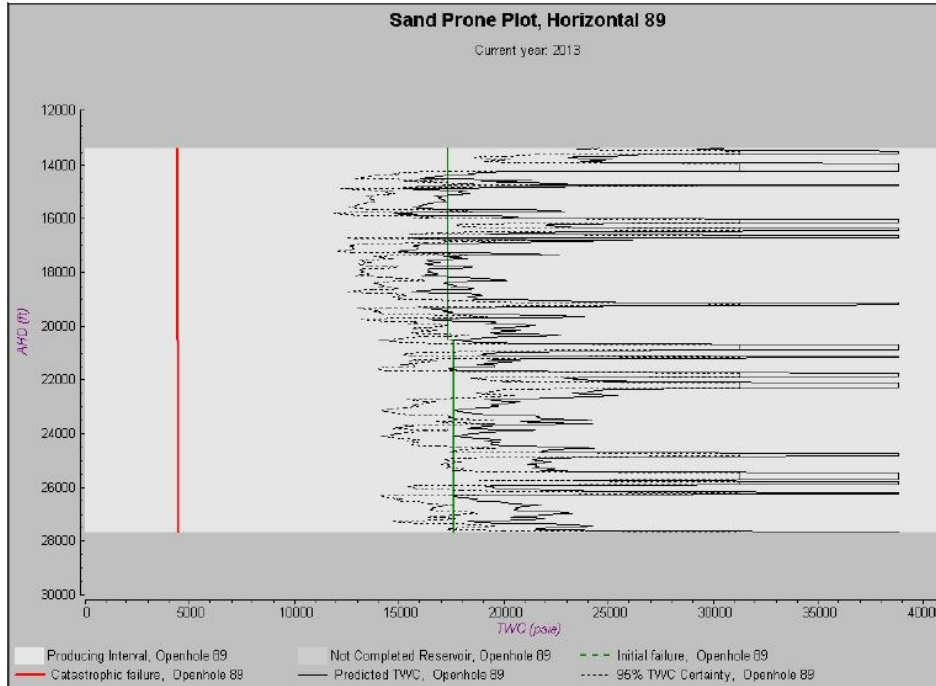


Figure 7.5: Initial sand failure plot for size effect factor 2.5 (open hole - first year of injection) [83].

7.3.1.4 Sand Entry Into Wellbore

In the past, the industry has typically assumed that in even relatively unconsolidated sands, sand control would not be necessary as the force and pressure of injectors would prevent sand failure. However, over the years, as the industry gained more experience with injectors, they have realized that injectors have specific challenges.

7.3.1.5 Fluid Hammer

In an emergency shutdown, the injection will stop up very quick. The flow velocity drops to zero as it meets this barrier, this causes a strong pressure pulse known as fluid hammering. The pressure pulse will travel down the tubing and hit the wellbore-reservoir interface crating a cyclic pressure wave. The velocity and magnitude of the initial pressure pulse created depend on the fluid, geometry, stiffness of the pipe material, and frictional effects. The rock quality at the wellbore-reservoir interface affects the amplitude of the reflected waves and energy dissipates faster in a well with high PI. The pressure created by the fluid hammer effect can reach 90 bar and 3280 ft/s [84]. At Foinaven, studies conducted showed a pressure rise of about 500 psi. These cyclic pressures may break rocks into individual sand grains, causing rock liquefaction creating a slurry which can then pass through the screens more easily [84].

CO₂ in liquid and supercritical state have a high density, and comparatively near to water at high pressures. It is thus anticipated that a water hammering effect can be observed in a CO₂ injection well.

The maximum WH pulse pressure, ΔP , that can be calculated from [85]:

$$\Delta P = -\rho a \Delta V \quad \text{Eq. 7.5}$$

where ΔV is the change flow velocity, and a is the wave velocity given by [85]:

$$a^2 = \frac{\frac{K}{\rho}}{1 + \left(\frac{K}{E}\right)\left(\frac{D}{e}\right)} \quad \text{Eq. 7.6}$$

Where K is fluid bulk modulus, ρ is fluid density, E , D and e are modulus of elasticity, diameter and thickness of the tubing respectively.

Analyzing the fluid hammer effect for Prelude CO₂ injector showed that the pressure wave amplitude could reach as high as 35 bar for maximum injection rate of 93 MMscf/d. ($E=200\text{GPa}$, $D=0.1778\text{m}$, $e=0.0092\text{m}$, $K=1.49\text{GPa}$, $\rho=778.02\text{ kg/m}^3$ and $\Delta V=3.5\text{m/s}$)

Following previous discussion the following conclusion can be drawn:

- The pressure amplitude could be high enough to cause sand failure.
- Sand liquefaction phenomenon occurs in high porosity sands (~50%) [86]. Whereas, Swan reservoir is a low porosity reservoir and is unlikely to have liquefaction.
- The effect can be minimized by taking operational measures like shutting-in the well slowly and reducing shut-in frequency.

7.3.1.6 Initial Well Cleanup

Perforation debris and transient failed sand will be brought into the wellbore during initial cleanup and then transported to the surface (if the well is back flushed).

7.3.1.7 Flow-Back

A well is mainly flowed-back due to plugging of formation near sand face. This is a common operation in water injectors. Flow back brings the failed sand into the wellbore and after shut-in, the suspended sand may settle in the wellbore and plug it. If the flow velocities are not high enough, then it cannot be transported to surface and settles at the bottom of the well. Sometimes flow-back is required to lower reservoir pressure to keep the injection pressure within limits [83].

As almost pure CO₂ is planned to be injected, there will be minimal injection of solid content. CO₂ EOR case studies has indicated that clean-up is not normally required in CO₂ injection wells due to absence of plugging materials in the CO₂ stream [83]. Further, at Prelude CO₂ injection will be performed into the Swan reservoir, where the pressure will reduce over time due to production. This will reduce the possibility of flow-back.

7.3.1.8 Cross Flow

Vertical wells with permeability contrast and multizone commingled production, cross flow phenomenon has been observed. The flow from high pressure low permeability to high permeability low pressure brings sand into the wellbore and sometimes plugs the perforations or settle down in the bottom. For horizontal wells, this effect is normally not as severe. However, the wells will be highly deviated intersecting the entire reservoir, and may therefore see some cross flow during shut-in. This can be simulated in a near well bore simulator, for example NETool.

7.3.1.9 Sand Control Recommendation

Based on the previous discussion, it was recommended to have some form of sand control method. This is based on the possibility of transient failure of open hole case, and the critical nature of the project [83].

7.3.2 Screening for Lower Completion

7.3.2.1 Screening Methodology

There are a variety of different sand control options available, and so the question arises: How to choose an appropriate method? A screening matrix was developed that considered aspects of reliability, cost, installation and productivity. These categories was further subdivided into sub-categories, for example is reliability a result of several issues including sand control exclusion, plugging resistance, well uptime, etc..

The ranking of the different options is obtained by the following method:

- Assigning a technical score, high(5) for poor options, low(1) for good options or characteristics.
- The ranking under each sub-category is then multiplied with a weight factor where importance is ranked from one to five, five being most important.
- Further the score under each aspect is normalized by dividing the minimum score achievable by the actual score, giving a value of maximum one.
- This value is then multiplied with a project rank factor, which adds to one, based on project drivers given in [Chapter 1](#).
- Final step is to add the different scores to give a final ranking.

The project drive ranking, ranks reliability highest (0.4) followed by cost (0.25), installation/do-ability (0.2) and productivity (0.15).

The screening matrix was completed based literature review, simulations and discussions with well engineers.

7.3.2.2 Evaluated Sand Control Methods

Slotted Liner

The major advantage of the slotted liner is that it is a cheap solution. The flow area of a slotted liner is typically 3%. With even a small amount of plugging, flow may be so restricted that an intervention will be needed to increase injectivity again. This brings up the life cycle cost of the solution. Installation is relatively easy, but the liner is more susceptible to collapse. Because slotted liners are primarily used in shallow onshore and low cost projects where minimizing cost requires reduction in quality [87].

The well has a 688m long reservoir section. This requires a long inner string to be able to pump.

Wire Wrap Screen

The major advantage of wire wrap screen over slotted liner is the increased inflow area, which allows full productivity even if an amount of the area is plugged [81]. Wire wrap screens can't be rotated during installation.

Premium Screen

Premium screens were developed to deal with the shortcomings of the other stand alone screens, namely, plugging, erosion and robustness. A general trend for design is that they have a woven mesh with some form of shroud for protection. The more robust build gives them an advantage in terms of reliability and installation [35].

Some points regarding stand-alone-screens as a whole is that they generally have a higher failure rate than other sand completion. 20% failure rate is reported by Shell [35]. BP's industry database contains more than 2000 wells (2003), and indicates SAS have three times the failure rate than open hole gravel packs [35].

Cased & Perforated

C&P has been selected as sand completion for the development wells. Carrying the solution over to the injector well could give positive replica effects regarding installation. Perforating is considered a mature technology, but handling explosives makes it more complex than SAS. Further, the completion can't be pulled, and thus if it fails, a sidetrack will need to be drilled. It has higher score for stimulation options as it can isolate and treat individual zones (No open annulus).

Expandable Screen

The merit of expandable screens is based on avoiding the open annulus (compliant) which historically has caused the failure of many SAS. It stabilizes the sandface and minimizes sand movement, reducing the risk of sand failure and screen erosion caused by sand production. Costs are expected to similar to OHGP. The productivity of expandable screen is expected to be close to, or better, than OHGP. It offers the largest internal ID of all the sand screens.

Open Hole Gravel Pack

OHGP prevent the formation from collapsing, therefore reduces fines production. Operationally they are challenging and during installation the integrity of the filter cake must be retained, as failure can cause excessive leak off of carrier fluid and consequently premature screen-out, resulting in failure to place required amount of gravel. However, considering installation is successful, they are considered very reliable.

The decision matrix is found in Figure 7.6.

Prelude CO2 Injector - Sandface Scening Criteria	Technical Importance Weighted Factor Project Drive Ranking	Slotted Liner	Wire Wrap Screen	Premium Screen	Cased & Perforated	Expandable Screen (compliant)	Open Hole Gravel Pack	Comments
Reliability	0.4							
Sand control (exclusion effectivity)	5	3	15	2	10	2	10	
Plugging resistance	5	4	20	3	15	2	10	
Well uptime	5	5	25	3	15	3	15	
Damage reistance	4	3	12	3	12	2	8	
Workover (retrievability)	2	2	4	2	4	5	10	
Hole stability	3	5	15	4	12	3	9	
Lifetime expectancy	5	3	15	3	15	3	15	
Wellbore access	1	3	3	3	3	3	3	Internal diameter
Sub-Total		109	86	78	75	67	40	
Norzd		0.28	0.35	0.38	0.40	0.45	0.75	
Productivity	0.15							
Skin	5	4	20	3	15	2	10	Mechanical damage
Flow restriction	4	2	8	2	8	1	4	Pressure loss accross
Sub-Total		28	23	23	14	9	17	
Norzd		0.32	0.39	0.39	0.64	1.00	0.53	
Cost	0.25							
Overall cost	5	2	10	2	10	4	20	Installation and equipment
Life cycle cost (OPEX)	5	3	15	1	5	1	5	Likelihood of intervention, cost of maintenance
Sub-Total		25	15	20	25	30	30	
Norzd		0.40	0.67	0.50	0.40	0.33	0.33	
Installation / Do-ability	0.2							
General installation risk	5	2	10	3	15	2	10	
Complexity	3	1	3	2	6	1	3	Handeling risk
Stimulation options	5	3	15	3	15	2	10	
Optimum drilling fluids	3	2	6	3	9	2	6	
Sub-Total		34	45	37	38	46	62	
Norzd		0.47	0.36	0.43	0.42	0.35	0.26	
Assessment Rankin (high is better)		0.35	0.44	0.42	0.44	0.48	0.51	

Figure 7.6: Prelude CO₂ injector – sandface screening criteria.

7.3.2.3 Productivity Modeling

A comparison of surface injection pressure between the different completions under consideration was undertaken in Prosper. Low injection pressure is favorable. Prosper has the capability to model slotted liner, open hole gravel pack, wire wrap screen and cased & perforated completion. Further, expandable screens are considered to have similar or somewhat better performance than OHGP [35]. Premium screen is about the same as WWS [35].

For this exercise, data presented in [Chapter 4](#) regarding high, low and base case for permeability and skin was used to design reservoir cases regarded as Good Case, Bad Case and Base Case. The cases are as follows:

- Good Case: High case permeability and base case skin.
- Base Case: Base case permeability and skin.
- Bad Case: Low case permeability and high skin.

The cases were based on sensitivity analysis to individual parameters affecting IPR and VLP, where it was highlighted that permeability and skin was two of the most influential parameters. Input values for Prosper is presented in [Appendix 2](#). The values are taken from various sources [35, 81, 87-89].

The skin value for cased & perforated case was calculated using Karakas & Tariq model. Published sand control skin data is predominantly the total skin and therefore it is impossible to evaluate the effect of the individual skin effects caused by mechanical, anisotropy, completion and rate dependent skin. The total skin factor (S') comprises of a rate-independent term (S) and a rate-dependent term (D) [35]:

$$S' = S + Dq \quad \text{Eq. 7.7}$$

where D is the non-Darcy coefficient and q , the flow rate. Further, the rate-independent term is a function of mechanical, anisotropy and completion skin and is given by [35]:

$$S = \frac{h}{h_m} F(S_m + S_a) + S_c \quad \text{Eq. 7.8}$$

where h_m is the measured length of the completion interval. S_m , S_a , and S_c are the mechanical, anisotropy and completion skins respectively. The anisotropy skin is given by [35]:

$$S_a = \ln\left(\frac{2}{1+F}\right) \quad \text{Eq. 7.9}$$

and F by [35]:

$$F = \frac{1}{\sqrt{\cos^2\theta + \left(\frac{k_v}{k_h}\right)\sin^2\theta}} \quad \text{Eq. 7.10}$$

where θ is the hole angle – corrected for dipping formation.

In Prosper, literature reported skin was entered as mechanical skin, and because deviation comes into play, a reduction in the effect of mechanical skin is observed (depending on k_v/k_h) [35]. It was observed that the total skin calculated in prosper was less sensitive to the mechanical skin entered for highly deviated well compared to vertical well and that the results from Prosper are accurate enough for high level use.

The results from Prosper can be observed in Figure 7.7.

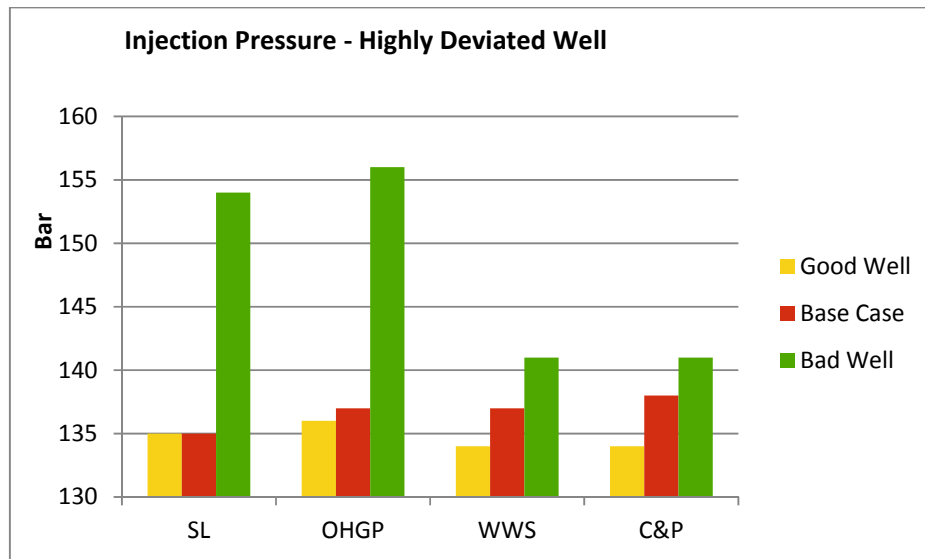


Figure 7.7: Injection pressure for different completions for good, bad and base case injecting at 93 MMscf/d.

The reported pressures are the pressure required to inject at least 93 MMscf/d for the given case. The most dominating feature from figure 7.7 is the required pressure to inject in the bad case for SL and OHGP. In selecting skin factor for the different completions, the highest one that was reported in the literature was selected as the high case. For SL and OHGP, this value was 40 and 11 respectively [35, 90].

In the rest of the cases, the results are comparable for the different completions.

7.3.2.4 Recommendation for Sand Control Method

It is observed from the screening matrix (Figure 7.6) that open hole gravel pack solution have the best overall score. The installation cost is relatively high, and the operation is complex compared to the alternative solutions. Once a successfully installed, the solution is considered very reliable.

The recommended sand face completion is open hole gravel pack.

7.3.2.5 Open Hole Gravel Pack Sensitivity Analysis

Upon selection of OHGP as the best matched sand completion, a sensitivity analysis was performed to investigate the effect of various reservoir and tubing parameters on the injection rate. A base case was established, and a high and low value obtained. The data is given in Table 7.2.

	Low	Base	High
Discharge Temperature [°C]	30	40	78
Permeability [mD]	21.4	36.5	69.5
Reservoir Thickness (assuming well completed through) [m]	40	60	80
Skin	0	1.5	11
Tubing roughness [inch]	0.000492	0.0006	0.0021
Sea Temperature (top/bottom) [°C]	15/4	20/8	28/13
k_v/k_h	0.19	0.33	0.8

Table 7.2: Low, base and high case for sensitivity analysis.

The sensitivity analysis was performed by establishing the base case injection pressure with corresponding well head pressure/temperature and bottom hole pressure/temperature. The base case is reported in Table 7.3.

Inj. Pres [bar]	WHP [bar]	WHT [°C]	BHP [bar]	BHT [°C]	Inj. Q [MMscf/d]
137	143.76	38.99	425.36	79.79	93.60

Table 7.3: Base case injection.

After establishing the base case, one parameter was adjusted at a time, maintaining the injection pressure at 137 bar. The result was recorded and given in Table 7.4.

		WHP [bar]	WHT [°C]	BHP [bar]	BHT [°C]	Inj. Q [MMscf/d]
Discharge temp [°C]	30	147.81	30.45	434.23	65.95	140.95
	78	147.75	51.05	416.01	106.11	14.80
Permeability [mD]	21.4	145.39	38.96	431.16	80.08	86.35
	69.5	142.42	38.95	420.71	79.47	98.81
Reservoir thickness [m]	40	145.89	38.95	432.94	80.20	84.12
	80	142.68	38.96	421.62	79.52	97.83
Skin	0	143.55	38.99	424.66	79.67	94.50
	11	144.91	38.96	429.49	79.97	88.47
Tubing [in]roughness	0.000492	143.83	39.04	425.55	79.70	94.83
	0.0021	143.23	38.66	424.07	79.89	85.29
Sea Temp top/btm [°C]	15/4	143.47	38.68	425.59	79.01	95.08
	28/13	144.13	39.40	425.05	80.66	91.63
k_v/k_h	0.19	144.02	38.99	426.29	79.78	92.43
	0.33	143.44	39.00	424.25	79.66	94.98

Table 7.4: Sensitivity analysis.

To visualize the effect of each parameter on injection rate the results was normalized, and the injection rate increase/decrease is reported in percent compared to the base case injection rate of 93.60 MMscf/d given in Figure 7.8.

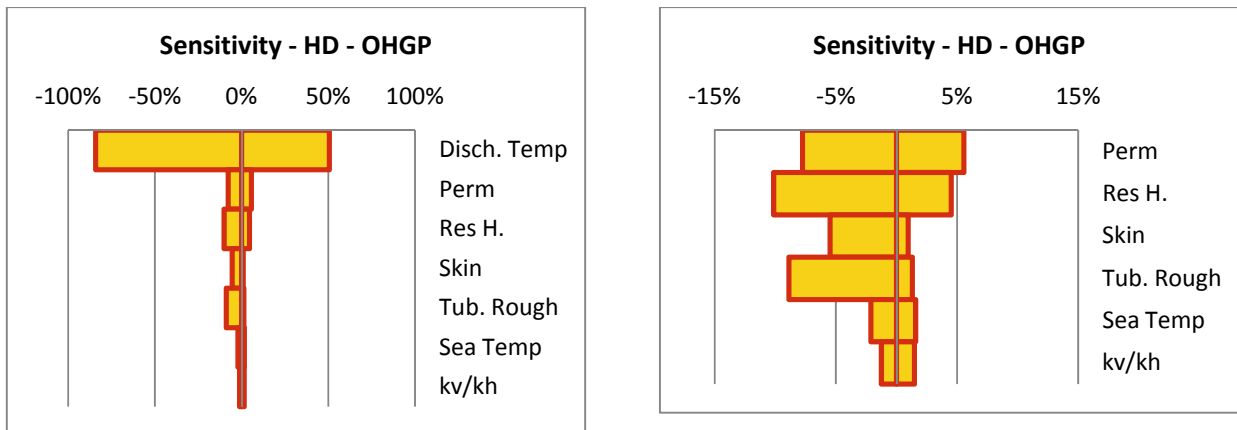


Figure 7.8: Sensitivity for OHGP parameters.

The sensitivity shows that discharge temperature have a very high effect on the injection rate, compared to other parameters. The discharge temperature from the compression facilities are expected to be 78°C without aftercooling [6]. Aftercooling has been added to the design basis for the FLNG. The aftercooler can be used to adjust discharge pressure and wellhead injection pressure by controlling density. This is done at Sleipner [20].

The average density at 137 bar reduces from 757.59 kg/m³ at 40°C to 381.77 kg/m³ at 78°C for pure CO₂ as illustrated in Figure 7.9. When no aftercooling occurs, and injection pressure is 137 bar, the bottom hole pressure is reduced, and injection rate of 93 MMscf/d can't be sustained. Further investigation showed that injection pressure would have to be increased to 197 bar at 78°C to maintain full injection at 93 MMscf/d. This is an increase of 60 bar and indicate the importance of maintaining aftercooling.

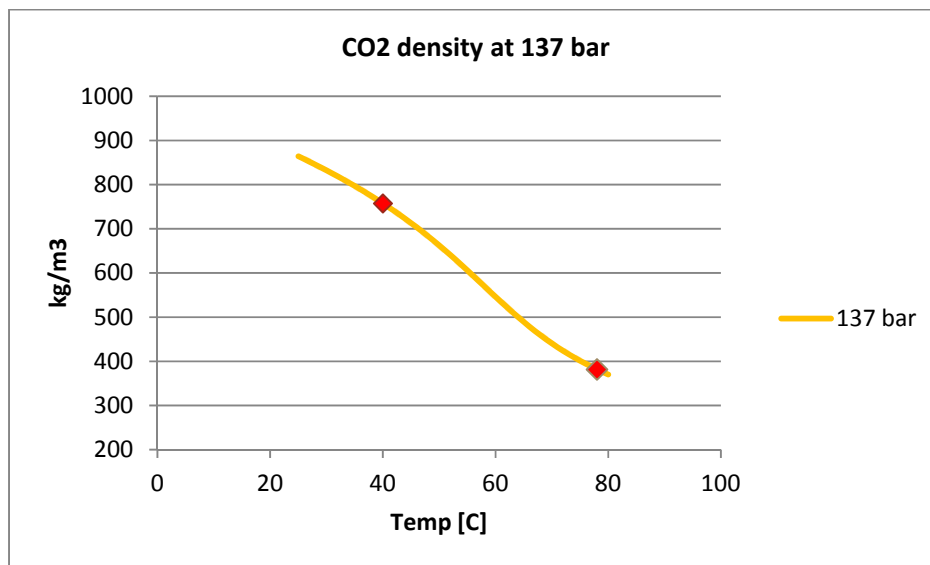


Figure 7.9: as a function of temperature at 137 bar [NIST].

Following comments can be given regarding the other sensitivities:

- Because the reservoir is contained in a dome structure, and the injection well will be located on the flank, there is a higher probability that the reservoir thickness will be towards the low side. The downside at maintained injection pressure is about 10%.
- Permeability showed to have an upside of 5.5% and downside of 7.7%, and is not considered major.
- Skin damage showed a downside of 5% with mechanical skin 11. This parameter is in the engineers control and proper planning and preparations should be conducted to minimize this.
- Tubing roughness depends on the material, where the base case was selected as “Well Tubing” and the high value was “Bare 13Cr”. Values taken from [35].
- Seasonal differences in ocean temperature from surface to mudline was tested, and found to have limited impact. However, this could have an impact for hydrate formation, and should be explored further.
- The range of vertical to horizontal permeability only have limited impact.
- Most of the parameters tested, only shows limited sensitivity, and it is expected that injection can be maintained by increasing injection pressure or decreasing temperature.

7.3 Inverted Well

One identified challenge with injecting into a producing gas reservoir is that due to density differences between the injected fluid and the reservoir fluid, in-situ gas will migrate in to the tubing and displace CO₂, causing a inverted well. By assuming the tubing is completely inverted and contains 91% methane and 9% CO₂, the closed-in tubing head pressure was estimated at ~325 bar. Restarting the well will require some incremental pressure to overcome friction, and completion pressure loss.

As the gFLNG design, contains a compressor specified for a maximum discharge pressure of 255 bar, it will not be possible to restart the well should the inverted well occur. Inverted well is recognized as an early life problem due to reservoir depletion and CO₂ flooding in near wellbore area.

However, being a very real threat, barriers to prevent reservoir fluid entering the wellbore should be put in place:

- Check valve: Automatic valve that open with forward flow and close with reverse flow.
- Hydraulic controlled valve: Surface controlled valve that is closed on demand.
- Deep set TRSSSV

Most valves have a potential to leak. SCSSSV, for example, shall according to NORSOK D-010, meet API RP 14B requirement for accepted downhole leak rate of 15 scf/min. Some points for consideration:

- Rate of flow reversal: If only a seep, will a check valve close?
- Space limitations: With a valve in the 7" tubing, will it be possible to install? Consider installing in 9-5/8" casing.
- Allowable pressure leak rate?
- Flow restriction?
- Closing time

7.4 Packer

The packer shall seal different pressures effectively and anchor the packer to the casing over a large variety of operating conditions. The metallurgy and elastomeric seals needs to be compatible with both CO₂ and hydrocarbons.

7.5 PDHG

PDG are sensors permanently installed in the well and connected to surface by means of a cable. They allow for real time monitoring and enable engineers to observe ongoing changes and make adjustment accordingly.

There may be a perception that injection a single phase fluid removes the need for any down hole pressure and temperature readings as this can easily be calculated from surface pressure. This is not so, and through this thesis, small changes in pressure and temperature have proved to cause large variations in CO₂ density.

Further, during shut-in it has been observed that at lower reservoir pressure, the tubing does not contain a full column of fluid, thus rendering any surface measurement meaningless. A PDHG will also give good information on pressure fall-off.

One of the main concerns regarding PDHG is reliability. They have since their introduction gone through the learning stages, and thus reliability has improved as well. A main concern for Prelude is the high temperature, as electronics fail more often [91]. Improved reliability can be gained through:

- Dedicated electronic circuits.
- Splice-free cables.
- Protective cap for cable in tubing section immediately below the tubing hanger to prevent crushing on installation.
- Bumper to prevent failure of cable in areas of high dogleg.
- Corrosion resistant alloys
- Metal-to-metal sealing

7.6 Safety Valve

The function of the surface-controlled subsurface safety valve is to provide closure of the well flow in the event of loss of the primary flow control safety equipment provided by the subsea tree. It is recommended that all wells capable of sustained natural flow to equipped with a sub-surface safety valve.

The valve will be a “failsafe”, indicating that if hydraulic control of the valve is lost, it will automatically close. The maximum setting depth is controlled by the hydrostatic pressure in the control line. The maximum fail safe setting depth is thus given by [35]:

$$D_{max} = \frac{p_{vc} - p_{mc}}{\rho_f \cdot 0.0981} \quad \text{Eq.7.11}$$

where D_{max} is the maximum fail safe setting depth (m), p_{vc} the recorded valve closing pressure (bar), p_{mc} the closing safety margin (bar) and ρ_f the control line or annulus fluid density (whichever is greater) (bar/m). This ensures that the valve remains fail safe if the control line leaks or parts. The maximum depth that hydrate will form also needs considerations.

The possible formation of hydrate will affect the setting depth of safety valves. The safety valve should be placed below the hydrate formation point under shut-in condition.

7.6.1 Safety Valve Testing

The critical nature of the TRSSSV requires it to be tested on a regular basis. Testing is usually performed by closing in the well at XM-tree, then closing the TRSSSV and bleeding off the pressure to a given value, normally 10% of the CITHP. The tubing pressure is then monitored for a period of 30 minutes for any increase in pressure. This is a relatively easy procedure for hydrocarbons and water injection wells, but becomes more complex for CO₂ injection wells.

Venting a full column of dense phase CO₂ from above the closed TRSSSV will cool the CO₂, the wellhead and the upper completion as the CO₂ falls below the gas liquid phase boundary. The faster this pressure is bleed off, the colder it will become. It was observed in a transient analysis for GoldenEye CCS that the CO₂ temperature just above the TRSSSV fell to around -40°C with a sudden pressure drop [79].

The implication is that the rate at which CO₂ is vented must be strictly controlled to prevent challenging the low temperature limitations of well components. Depending of the low temperature limitations, this operation has a potential to be very time consuming. A transient model should be built to assess the operation.

7.7 X-mas Tree

The basic types of subsea trees available are vertical and horizontal. Each type has advantages and disadvantages that can be weighted for selection. Simple solutions should be selected to enhance reliability and reduce the need for intervention. Over the years subsea trees have become very reliable thus reducing the chance of retrieval for repairs. However, there are a few additional concerns regarding CO₂ injection:

- Corrosion
- Explosive decompression
- Low temperature performance

Corrosion is discussed in Chapter 6, and recommendation was made for nickel alloy. Alloys C-276, 825, 718, 925 etc. are all very resistant to CO₂ related corrosion and chlorides at all temperatures and CO₂ partial pressure.

Elastomers need to be compatible with the injection fluid, as discussed in chapter 6. Subsea trees contain several gate valves in which metal-to-metal seals are used. However, the stem that operates the valves goes through a stem seal. Care should be taken when selecting stem seals for compatibility with the injected fluid.

Low temperature will affect the toughness of the material. The minimum service temperature is the temperature above which metals will show acceptable toughness if subjected to shock loading. 410 stainless steel, commonly used in xmas trees for gates and seats, have a very low Charpy impact value and could generate cracking.

7.8 Conclusion & Recommendation

- OHGP is recommended as sand control. This recommendation is based on reliability, installation, cost and productivity.
- When the well is shut-in, there is a possibility of an 'inverted well'. This will require a restart pressure that is higher than the current compressor is designed for. Barriers will be required.
- All selected completion components needs to be compatible with the encountered fluids. Special considerations for elastomers.
- Testing of TRSSSV may have implications for the overall well design, due to JT cooling. A fully transient model should be built to further assess the situation.

Chapter 8

Other Considerations

8.1 Objectives

The objectives of this chapter is to offer discussion on operating philosophy for the injector and provide an overview of in-well monitoring

8.2 Methodology

Operating philosophy is usually established with the help from a fully transient simulation tool. A suitable tool have not been available for the work conducted in this thesis. Instead, results from another CCS project within Shell is reviewed, and the conclusion regarding applicability to Prelude drawn. Industry literature was cited as well.

The purpose of monitoring is established and in-well monitoring techniques are identified from a literature review.

8.3 Operating the Well

Transient operations like close-in, start-up and emergency shut-down have been discussed in [Chapter 5](#). Simplified assumptions were made to investigate these operations. It was recommended to build a fully transient model to explore the subject in more detail. The results from such a study will be very important for the operating philosophy that will be adopted for the well.

Shell have recently (spring 2011) passed FEED for the GoldeEye CCS. Part of the work performed for the FEED was transient modelling of closing-in and starting-up. CO₂ is transported in a 103 km log pipeline to the offshore GoldenEye platform. The pressure before the wellhead is 115 bar, and the well is closed and opened by means of a choke. The results from their simulations highlight operational concerns that are applicable to Prelude. The result from GoldenEye CCS transient simulations is pictured in Figure 8.1. The simulation is performed with OLGA's single component module for CO₂.

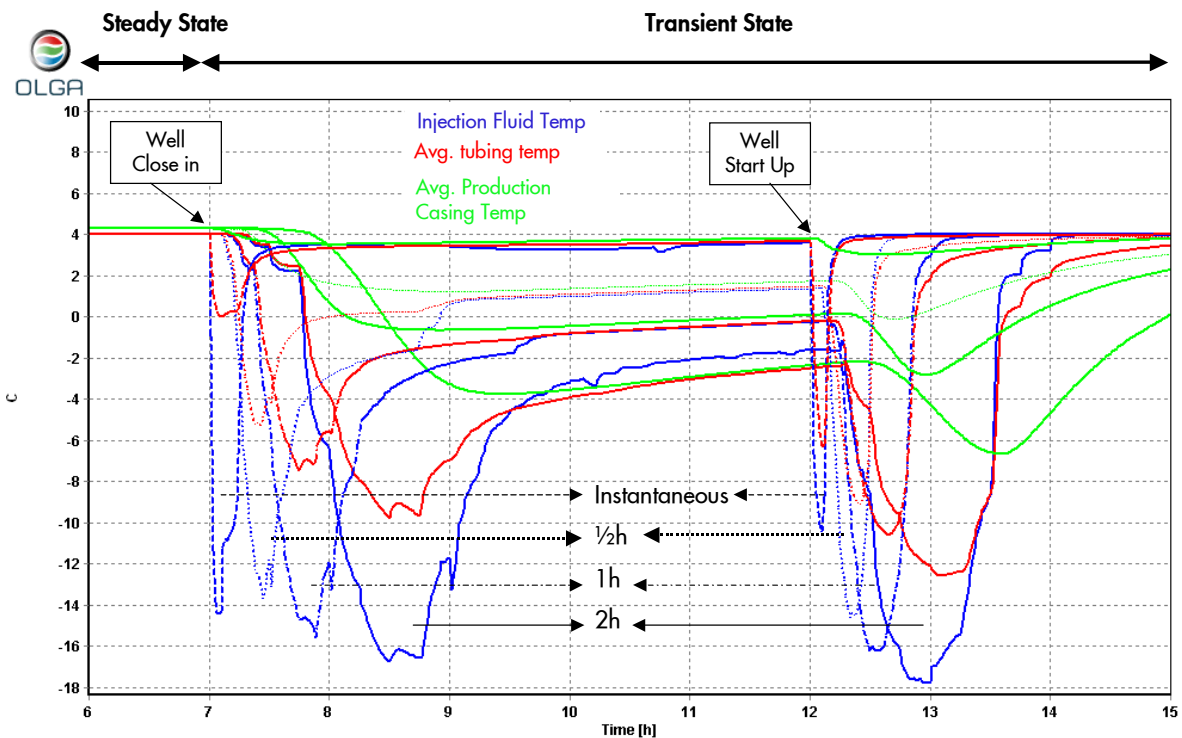


Figure 8.1: WH component temperature variation for close-in and start-up scenarios instantaneous, 1/2 hour, 1 hour and 2 hours [92].

From the simulations it is observed that fluid and well component temperature drops more with longer close-in/start-up times. This is observed as more CO₂ mass is involved during a slow close-in/start-up operation.

Choking the CO₂ upon delivery will create low temperature in and around the wellhead due to the Joule-Thomson cooling effect of the CO₂ when it expands across the choke. The hazard associated is the risk of hydrate formation at the wellhead which may lead to a possible loss of well integrity and inability to function surface tree valves. The main mitigation for this is to ensure that dry CO₂ is injected.

The temperature drop experienced at GoldenEye CCS will be different from that of Prelude. However, the general trend will be the same, and temperature drop can be managed by starting and closing the well quickly. In order to reduce the hammer effect described in [Chapter 7](#) the operations should not be instantaneous.

GoldenEye CCS simulations also investigated safety valve testing. Simulations showed that a sudden drop of pressure would result in ~-40°C in the fluid just above the safety valve, where the temperature drop would be largest. The temperature at this point can't be detected by the wellhead. To manage this temperature drop the pressure has to be bleed gradually followed by a close-in period. For Prelude the same approach should be taken. However, the GoldeEye project has dry trees while Prelude wet trees. This will further complicate the situation as the entire flowline have to be bleed down.

When the dense phase CO₂ inventory is vented to atmosphere the pressure in the inventory will quickly drop along with the temperature until the remaining inventory becomes a two-phase liquid-vapour mixture. The pressure and temperature will then continue to decrease as dictated by the release rate.

The depressurization rate need to be relatively slow to make sure all liquid CO₂ will be vented, or in vapor phase, before pressure falls beneath the triple point pressure of 5.18 bar. If, however, liquid exist when the pressure is reduced beyond 5.18 bar, a large proportion of this will likely freeze into solid CO₂ [26].

Solid CO₂ deposits will likely form plugs in pipelines, and effectively subdivide the volume causing safety issues. It may not be necessary to depressurize the flowline below the triple point in order to test the safety valve. The time to depressurize will be longer if lower pressures for testing are required.

Another potential issue for subsea pipelines is cooling of the pipe wall below freezing point of the ambient seawater which can cause ice to build up on the outside of the pipeline. The positive buoyancy of the ice layer can cause instability of the pipeline. This is also the case for freezing of liquefied masses surrounding trenched pipelines [26].

8.4 Adjacent Wells

In the case of CO₂ injection into the Swan reservoir, production wells would have to be redesigned. By injecting CO₂ and displacing in-situ hydrocarbons with CO₂ it is estimated to have a CO₂ breakthrough after 5 years of production. From the time of breakthrough, the CO₂ level will rise in the production well, thus the material selection done without CO₂ injection will no longer be valid. It is expected that the material in the producer needs to be upgraded, thus making them more costly. Also abandonment procedure should account for the possibility of exposed CO₂.

8.5 Well Monitoring

There are currently more than 40 technologies [93] that can be applied to a measurement, monitoring and verification program for a CCS project. None of these technologies are generic and should be tailored for each development. It is beyond the scope of this thesis to give a review of all these technologies; instead it states the purpose of the MMV program for the CCS project and gives a summary of in-well monitoring techniques.

The specific aims of a MMV program are to detect early warnings of seepage emissions, so that remediation actions can be taken. Knowledge of CO₂ migration through time is a fundamental requirement. Placement of sensors and detectors to provide pressure, temperature and fluid composition throughout an array of monitoring points would facilitate the correlation of observed data with predictive modeling forecast. It is best if these sensors are installed prior to CO₂ injection to get a baseline measurement [25].

There are four main ways containment (Figure 8.1) can be breached. In order of significance, these are:

- 1) Wells (Legacy and future wells) that punctuate the seal.
- 2) Faults and fractures

- 3) Cap-rock / seal properties (of primary and secondary seals)
- 4) Lateral boundaries (extent of plume migration)

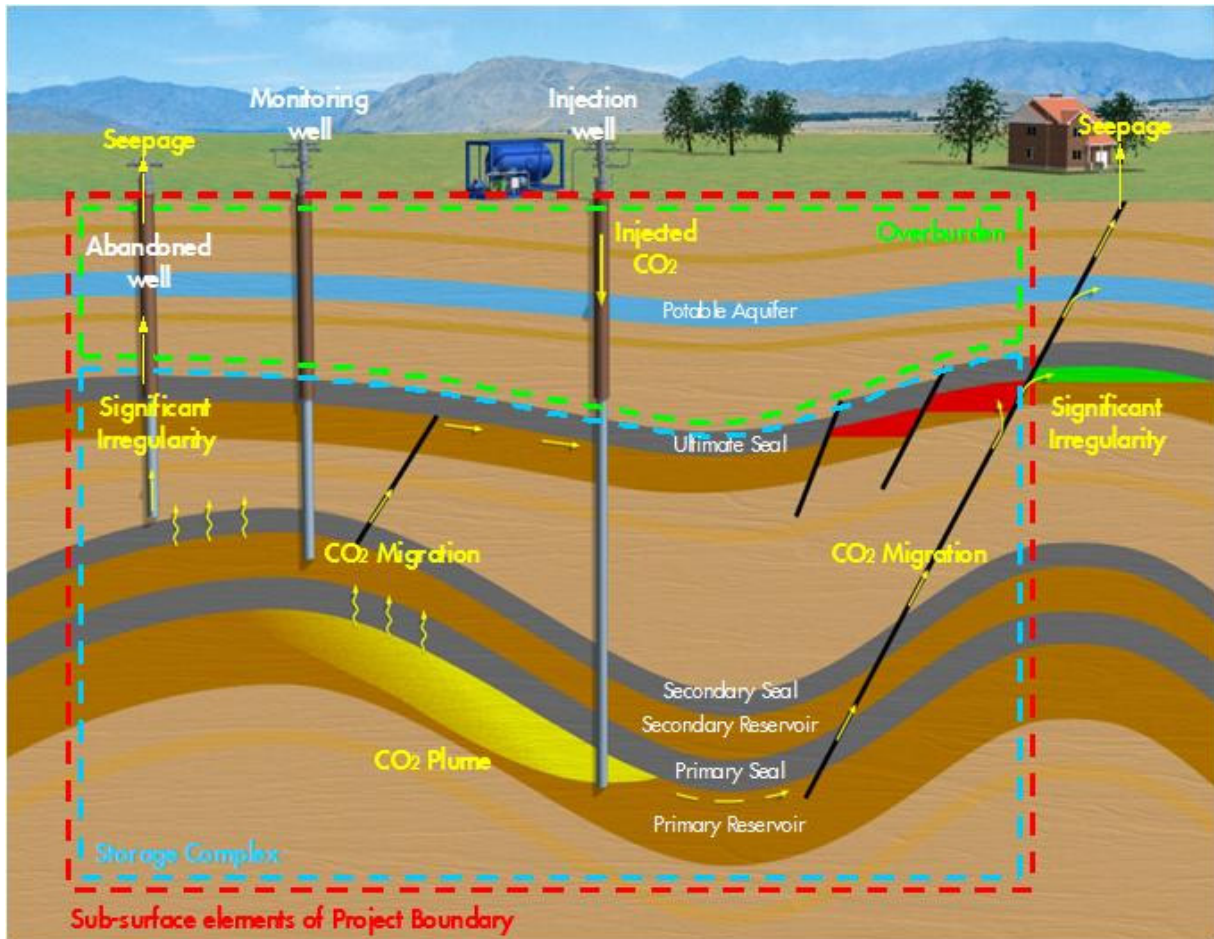


Figure 8.2: Schematic of primary migration & seepage pathways [93].

Generally the injection has four phases where the monitoring requirements will differentiate. The four phases are:

Pre-Operation: The main objective is to establish baseline conditions for comparison to future readings [25].

Operations: This is the period of time during which CO₂ is injected into the storage reservoir. All injection wells should have meters and pressure sensors to accurately measure injection and production rates, surface casing pressure, bottomhole injection pressure, and annulus pressure to verify that no casing, tubing, or packer leaks exists. Verification monitoring is required for additional measurements that improve the understanding of complex processes occurring in-situ. Environmental monitoring refers to monitoring aimed at safeguarding against risk to health, safety, and the environment [25].

Closure: This is the period of time immediately after injection has stopped, during which wells are abandoned and plugged, equipment and facilities removed, and agreed site restoration is accomplished. Only necessary monitoring equipment is retained [25].

Post-Closure: This is the period during which ongoing monitoring is used to demonstrate that the storage project is performing as expected and that it is safe to discontinue further monitoring. Once it is satisfactorily demonstrated that the site stable, monitoring will no longer be required except in the event of leakage, or legal disputes, or other matters that may require new information about the status of the storage project [25].

A summary of the in-well specific MMV monitoring techniques follows in Table 8.1.

Measurement Technique	Measurement Parameter	Example Application
Pressure (fibre optics)	Formation pressure Wellbore pressure gradient Behind wellbore pressure gradient Annulus pressure Groundwater aquifer pressure	Control of formation pressure below fracture gradient. Wellbore and injection tubing condition. Leakage out of the storage formation.
Temperature gradient (fibre optics)	Formation temperature Wellbore temperature gradient Behind wellbore temperature	Control of formation pressure below fracture gradient Wellbore and injection tubing condition Leakage out of storage system
Water composition	CO ₂ /H ₂ O/CO ₃ ²⁻ Major ions Trace elements Salinity	Quantifying solubility and mineral trapping. Quantifying CO ₂ -rock-interactions. Detecting leakage into shallow aquifer.
Well logs	Brine salinity Sonic velocity CO ₂ saturation	Tracking CO ₂ in and above storage formation. Tracking brine migration into shallow aquifers. Calibrating seismic velocities for 3D surveys.
Vertical seismic profiling and cross well seismic profiling	Brine salinity Sonic velocity CO ₂ saturation	Detecting detailed distribution of CO ₂ in the storage formation. Detecting leakage through faults and fractures.
Passive seismic monitoring	Location, magnitude and source characteristics or seismic events	Development of micro fractures in formation / cap rock. Locate CO ₂ migration pathways.
Electrical and electromagnetic techniques	Formation conductivity Electromagnetic induction	Tracking CO ₂ in and above storage formation. Tracking brine migration into shallow aquifers.

Table 8.1: Summary of in-well direct and indirect monitoring techniques [25].

In terms of performance and reliability, fibre optic technology should be chosen over conventional electronic monitoring systems. For fibre optics the probability of failure is highest at installation, but once installed they outperform other technologies. This is due to removal of the vulnerable electronic parts of the monitoring system from downhole to less harsh topside location [25].

Fibre optic can measure the temperature well gradient, which can be important in controlling transient operations.

It would be very useful to have information regarding injection profile across the sandface, but the fibre optic cable would have to penetrate the packer and potentially cause an integrity issue. Also, the fibre optic cable would have to be mounted on a base pipe, such as a slotted tailpipe extending across the sandface [25].

The offshore location of the Prelude field depth and pressure of the Swan reservoir bring some limitations. It is technically impossible to monitor the atmospheric domain accurately. The FLNG will have a number of exhaust emissions, making accurate flux maps of natural CO₂ variation impossible. On the Sleipner field in Norway 4D seismic has been utilized to successfully monitor CO₂ plume migration. For Prelude this the seismic response is estimated not to show before the reservoir was depleted to 3000 psi (50 %) [93].

8.6 Conclusions & Recommendations

- To avoid excessive cooling of the fluid and wellbore, start-up and close-in operations should be performed quickly. To avoid hammer effect, the operations should not be instantaneous.
- Safety valve testing will be complex due to depressurization of the flowline. The operations will cause cooling of flowline. The bleeding down will need to be operationally controlled to avoid extremely low temperatures.
- Safety valve testing is likely to be a slow process.
- Fibre optic temperature gradient will be a critical tool in controlling the bleed down.
- The inclusion of CO₂ injection into the Swan reservoir calls for redesign of the planned development wells.
- It is recommended to build a fully transient model to verify, and establish the exact operational procedures for the well.

Chapter 9

Tubing Stress Analysis

9.1 Objectives

The first objective of performing a tubing analysis of the Swan CO₂ injector was to identify whether the modelling software used within Shell had any limitations in terms of modelling CO₂. [WellCat](#) is the standard software used within Shell for casing and tubing design.

The second objective was to establish the weight grade required to withstand the loads experienced in the well.

9.2 Methodology

The existing WellCat model for the Prelude development wells was modified for CO₂ injection, and the different load cases were built from the Shell tubing and casing design guide. The capability of WellCat to model CO₂ properties was established by comparing results from a simulation with reference values.

Once the load cases were built and the temperature and pressure profiles were correct, all load cases were simulated to establish the required weight grade to withstand the load cases experienced in the well.

9.3 Design Assumptions

- The directional profile has been assumed to be the same as the producer wells.
- Casing scheme has been assumed to be similar to the development wells.
- Input parameters used for tubing stress analysis have been summarized in Table 9.1.
- Injection fluid has been assumed to be 100% CO₂.
- Diesel oil has been assumed as packer fluid.
- Well schematic is found in [Appendix D](#).

Parameter	Value
Material properties (25CrW-125)	Young's Modulus: 200 GPa Yield Strength: 125 ksi Ultimate Tensile Strength: 130 ksi Poisson's Ratio: 0.22 Thermal Expansion: 13.00 E-06 /°C Radial Anisotropy: 100% Hoop Anisotropy: 100%
Temperature Deration	1.00 @ 25°C 0.940 @ 100°C 0.857 @ 150°C 0.821 @ 200°C 0.758 @ 250°C
Corrosion	No allowance for corrosion was considered in this analysis (CRA material)

Table 9.1: Design data for WellCat model [94].

Weight kg/ft (lb/ft)	Top (m MD)	Bottom (m MD)	OD(in)	Grade	Burst (bar)	Collapse (bar)	Axial (lbf)
34.228 (23)	261.30	4620	7	SM25CRW-125	683	320	831937
38.692 (26)	261.30	4620	7	SM25CRW-125	779	444	943639

Table 9.2: Tubing performance properties.

Design Factors	
Triaxial	1.25
Burst	1.15
Collapse	1.00
Axial Tension	1.40
Axial Compression	1.10

Table 9.3: Design factors.

9.4 Modelling CO₂ in WellCat

As described in Chapter 4 Prosper does not estimate CO₂ properties very well. It is of interest to know whether WellCat have the same weakness. WellCat uses the calculated pressures and temperatures to perform stress analysis.

WellCat have two equations of state built in, SRK and BWRS. For pure CO₂ both of them give the same density profile which is pictured in Figure 9.1. It is observed that the calculated density is very poor compared to NIST data. The implication is that internal pressure profiles will be underestimated, causing a possible well failure if gone unnoticed.

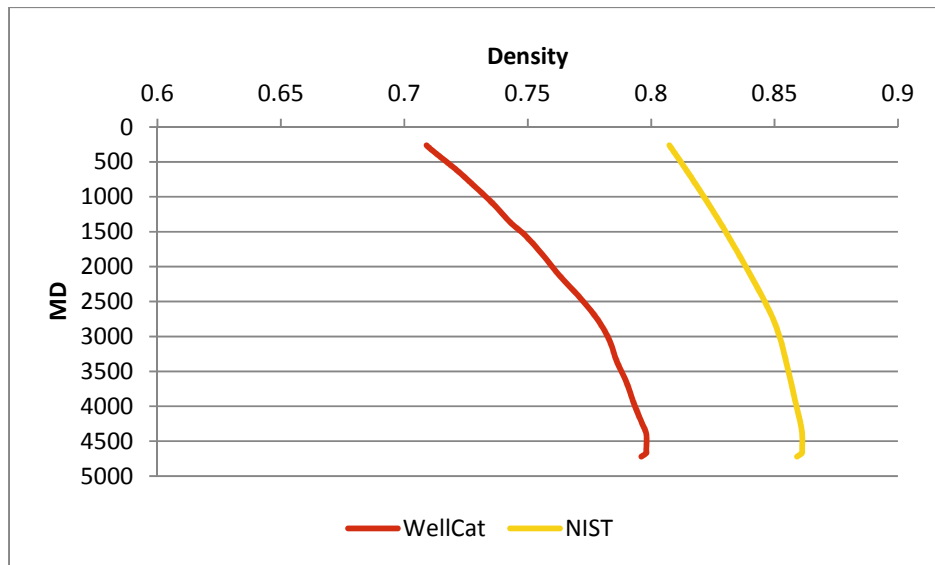


Figure 9.1: Wellbore density WellCat vs. NIST.

Considering how poor WellCat models CO₂ the approach to modeling will be slightly different from that of normal hydrocarbons. There are two options:

- Adjusting input parameters (for example rates) in an exercise to reproduce the same pressure profile obtained from a well performance simulator.
- Model a particular case in a well performance simulator then importing the resultant pressure and temperature gradient to WellCat.

The latter approach was chosen to eliminate potential issues with the CO₂ phase behavior inconsistencies in WellCat.

9.5 Design Load Cases

The design of tubing is based on calculation of the capacity of the pipe to withstand stresses caused by a combination of internal pressure loading, external pressure loading, mechanical axial loading, bending and temperature. Hanging the tubing in the well will cause small initial stresses. Larger stresses will be induced by changes in pressure and temperature compared to the initial reference state of the pipe. The initial state of the tubing is thus an important reference state from which each subsequent change of loading, and related stress, is determined.

The initial condition for the tubing is as hung at the top and latched at bottom. Subsequent changes in pressure and temperature will then generate axial stresses along the tubing.

9.5.1 Thermal Operations

The injection well undergoes a variety of operations that are unique to the injection process and which define the temperature changes along the tubing. These thermal operations determine the temperature changes which are used by various loading events:

1. **Initial Condition:** Corresponding to the in-situ conditions in which the string was run.

2. **Cleanup production:** The well is assumed cleaned up for two weeks. The preceding operation is: Initial condition.
3. **Shut-in from cleanup production:** The well is assumed shut-in just one minute after cleanup production. The preceding operation is: Cleanup production.
4. **Steady cold injection:** The injection of cold CO₂ into the well steady-state. The well is cold. The preceding operation: Initial condition.
5. **Long term shut-in from injector:** The well is shut-in for 6 months after cold injection. Preceding operation: Steady cold injection.

9.5.2 Load Cases for Tubing

1. **Running the tubing:** This is a running load case.
 - a. Packer fluid gradient inside and outside the tubing, making differential pressure zero.
 - b. The axial load is the buoyed hanging weight of the tubing, plus drag forces.
 - c. Frictional drag is accounted for and has been set to 0.3.
 - d. Reference thermal operation: Initial condition.
2. **Initial condition:** This is the reference case, using the installation temperature and the internal and external packer fluid gradient at the time the tubing was set in place.
3. **Tubing overpull:** This is a running load case. It assumes the tubing is stuck at bottom while running or pulling it out of the well. The top tubing joint will experience the full buoyed weight of the tubing string plus the overpull load which in this case was assumed to be 100000 lb. (45359.24 kg). The fluid density in the well is assumed to be packer fluid.
4. **Pressure test inside the tubing:** This is a burst load case. The test pressure is applied to the top of the fluid column inside the tubing. The pressure will not drive the design, but is intended to test connections for any gross makeup error.
5. **Pressure test outside the tubing (packer test):** This is a collapse load case for the tubing. Test pressure is applied on top of the A annulus fluid column behind the tubing. The pressure test load will not drive the design but test tubing connections for gross makeup error and the packer for isolation.
6. **Early life hot kill:** This is a burst load case, with a column of produced reservoir fluid assuming the injection well is placed on production for cleanup. The temperature is hot, the well is shut-in, and the kill pressure slightly exceeds the shut-in pressure to pump kill the well.
7. **Early life ambient kill:** This is a burst load case, with a column of produced reservoir fluid. This load case is the same as early life hot kill, except that the temperature has been allowed to reach ambient from wellhead along the well. The well is shut-in and the kill pressure slightly exceeds the shut-in pressure pump killing the well.
8. **Early life hot collapse – evacuation, with gas in the produced reservoir fluid:** This is a collapse load case. The tubing is hot corresponding to prior cleanup production. The internal pressure is 100% evacuated.

9. **Early life hot collapse – tubing leak, with gas in the produced reservoir fluid:** This is a collapse load case. The tubing is hot corresponding to prior cleanup production. The well is shut-in and a tubing leak to casing scenario is assumed.
10. **Early life ambient collapse – evacuation, with gas in the produced reservoir fluid.** This is a collapse load case. Same as early life hot collapse, but ambient temperature.
11. **Early life ambient collapse – tubing leak, with gas in the produced reservoir fluid:** This is a collapse load case. Same as early life hot collapse, but ambient temperature.
12. **Ambient injection:** This is a burst load case, corresponding to start of injection. The temperature is ambient at the wellhead and ambient formation temperature along the well.
13. **Cold injection:** This is a burst load case, corresponding to long term injection. The temperature is significantly colder than the ambient formation temperature along the string due to long term injection of cold CO₂. The external pressure is determined from the long term cold packer fluid gradient. The internal pressure is the maximum injection pressure.
14. **Early life cold collapse after injection:** This is a collapse load case. This load case occurs after cold injection. The temperature is cold. The fluid inside the tubing is a column of CO₂ supported by the reservoir pressure at bottom hole (415 bar).
15. **Late life cold collapse after injection:** This is a collapse load case. This load case occurs after cold injection. The temperature is cold. The fluid inside the tubing is a column of CO₂ supported by the reservoir pressure at bottom hole (136 bar).
16. **Maximum injection pressure:** This is a burst case. The injection compressor is run of maximum injection pressure. The temperature is cold.

A summary of the design loads is given in Table 9.4.

Injection Tubing					
Load case	Thermal operation	Internal pressure at wellhead	External pressure at wellhead	Internal pressure gradient	External pressure gradient
1. Running	Initial condition			Packer fluid	Packer fluid
2. Initial	Initial condition			Packer fluid	Packer fluid
3. Overpull	Initial condition			Packer fluid	Packer fluid
4. Internal pressure test	Initial condition			Packer fluid	Packer fluid
5. External pressure test	Initial condition			Packer fluid	Packer fluid
6. Early life hot kill	Cleanup production	Early shut-in + 500 psi		Hot production fluid	Packer fluid
7. Early life ambient kill	Initial condition	Early shut-in + 500 psi		Cold production fluid	Packer fluid

8. Early life hot collapse - evacuation	Shut-in from cleanup			Zero	Packer fluid
9. Early hot collapse – tubing leak	Shut-in from cleanup		Early shut-in + 500 psi	Hot production fluid	Packer fluid
10. Early life ambient collapse – evacuation	Initial condition			Zero	Packer fluid
11. Early life ambient collapse – tubing leak	Initial condition		Early shut-in + 500 psi	Cold production fluid	Packer fluid
12. Ambient injection	In-situ	Injection pressure		CO ₂	Packer fluid
13. Cold injection	Steady cold injection	Injection pressure		CO ₂	Packer fluid
14. Early life cold collapse after injection	Steady cold injection		Late shut in + 500 psi	CO ₂	Packer fluid
15 Early life cold collapse after injection	Steady cold injection		Late shut in + 500 psi	CO ₂	Packer fluid
16 Maximum Injection Pressure	Steady cold injection	Injection Pressure		CO ₂	Packer fluid

Table 9.4: load scenarios for injection tubing in injection wells.

9.6 Failure Criteria

Analyzing pressure loads in isolation is insufficient for rigorous design. Applying tension to a pipe will tend to reduce its diameter; applying collapse loading will have a similar effect. Compressing the tubing will balloon it, as will applying internal pressure. The combination of external pressure and tension or the combination of internal pressure and compression will generate higher stresses than either the pressure or axial loads alone.

A widely accepted method of predicted tubing failure due to pressure and tension limits is based on the von Mises stress. If the von Mises stress exceeds the yield strength of the material, the tubing is assumed to fail.

The von Mises stress is a combination of the three principal stresses in the tubing. The three principal stresses are:

- Axial stress (σ_a)
- Radial stress (σ_r)
- Tangential or hoop stress (σ_t)

These stresses are determined by the geometry of the tubing and the three variables:

- Internal pressure (p_i)

- External pressure (p_o)
- Axial force (tension or compression) (F_a)

The axial stress is caused by the axial force applied to the tubing. When the tubing is in tension, the axial stress is the axial force divided by the cross-sectional area [35]:

$$\sigma_a = \frac{F_a}{A} \quad (\text{tension}) \quad \text{Eq. 9.1}$$

Further it should be noted that the total axial force comprise the sum of many components that will add up for a specific case. A more detailed discussion of this can be found in [35]. The most common components:

- Weight of tubing
- Ballooning
- Temperature changes
- Fluid drag
- Bending stresses

According to the Lamé's equation, the hoop stress at a given location in the tubing wall is the stress through the tubing due to internal and external pressures. The radial stress is given by Lamé's equation [35]:

$$\sigma_r = \frac{p_i A_i - p_o A_o}{(A_o - A_i)} - \frac{(p_i - p_o) A_i A_o}{(A_o - A_i) A} \quad \text{Eq.9.2}$$

The maximum stress always occurs at the inner or the outer surface. Since yielding occurs first at the inner surface, the radial stress is [35]:

$$\sigma_r = -P_i \quad \text{Eq. 9.3}$$

Lamé's equation for the hoop stress at a given location in the tubing is given by [35]:

$$\sigma_t = \frac{p_i A_i - p_o A_o}{(A_o - A_i)} + \frac{(p_i - p_o) A_i A_o}{(A_o - A_i) A} \quad \text{Eq. 9.4}$$

As with the radial stress, the maximum stress always occurs at the inner or outer surface. Again, because yielding occurs first at the inner surface, the equation reduces to [35]:

$$\sigma_t = \frac{p_i(A_i + A_o) - 2p_o A_o}{A_o - A_i} \quad \text{Eq. 9.5}$$

The von Mises yield condition is commonly used to describe the yielding of steel under combined states of stress (triaxial). The initial yield limit is based on the combination of the three principle stresses (axial, radial and tangential stress), and described mathematically [35]:

$$\sigma_{VME} = \frac{1}{\sqrt{2}} [(\sigma_a - \sigma_t)^2 + (\sigma_t - \sigma_r)^2 + (\sigma_r - \sigma_a)^2]^{0.5} \quad \text{Eq. 9.6}$$

Yielding occurs when the VME stress (σ_{VME}) exceeds the yield stress (Y_p) of the material.

It is useful to be able to visualize the three dimensional failure criteria. To simplify the presentation of the limits, the pressure difference $p_i - p_o$ is calculated. A positive differential pressure represents a burst condition, and a negative collapse condition. By holding the external pressure constant at zero for top of the plot, and the internal pressure constant zero at the bottom part of the plot, the von Mises equation only have two variables. The von Mises stress (σ_{VME}) is set equal to yield stress of pipe. For burst this is real axial force and internal pressure, while for collapse it is external pressure. The resulting plot of pressure difference versus axial force are elliptical, and used to judge whether a tubing will fail or not. If the resulting von Mises stress (σ_{VME}) along the wellbore falls outside the ellipse, the tubing will be assumed to have failed.

9.7 Results from Load Analysis

Sensitivity analysis on tubing of SM25CRW-125 grade was conducted to find the right weight that could perform satisfactory for all load cases observed in the well.

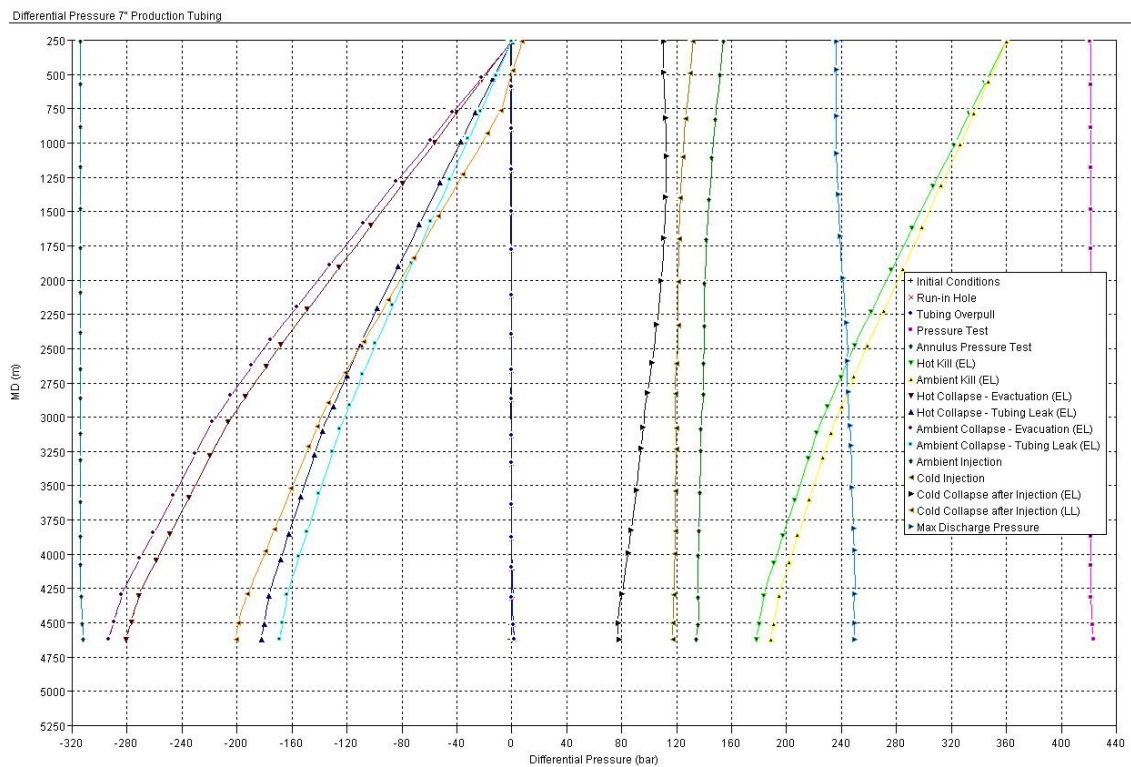


Figure 9.2: Differential plot for the different load cases.

Design Limits 7" Production Tubing Section 1 - OD 7.000 in - Weight 34.228 kg/m - Grade SM25CRW-125

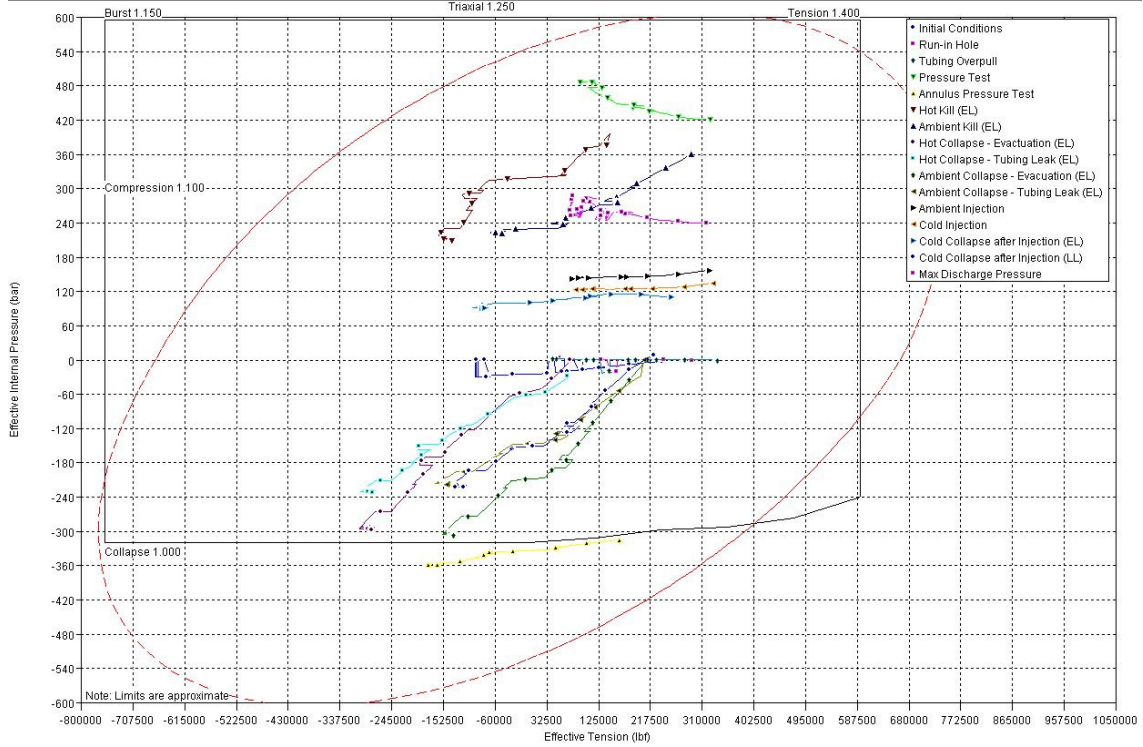


Figure 9.3: 7" SM25-CRW # 34.228 kg/m production tubing – VME plot.

Design Limits 7" Production Tubing Section 1 - OD 7.000 in - Weight 38.692 kg/m - Grade SM25CRW-125

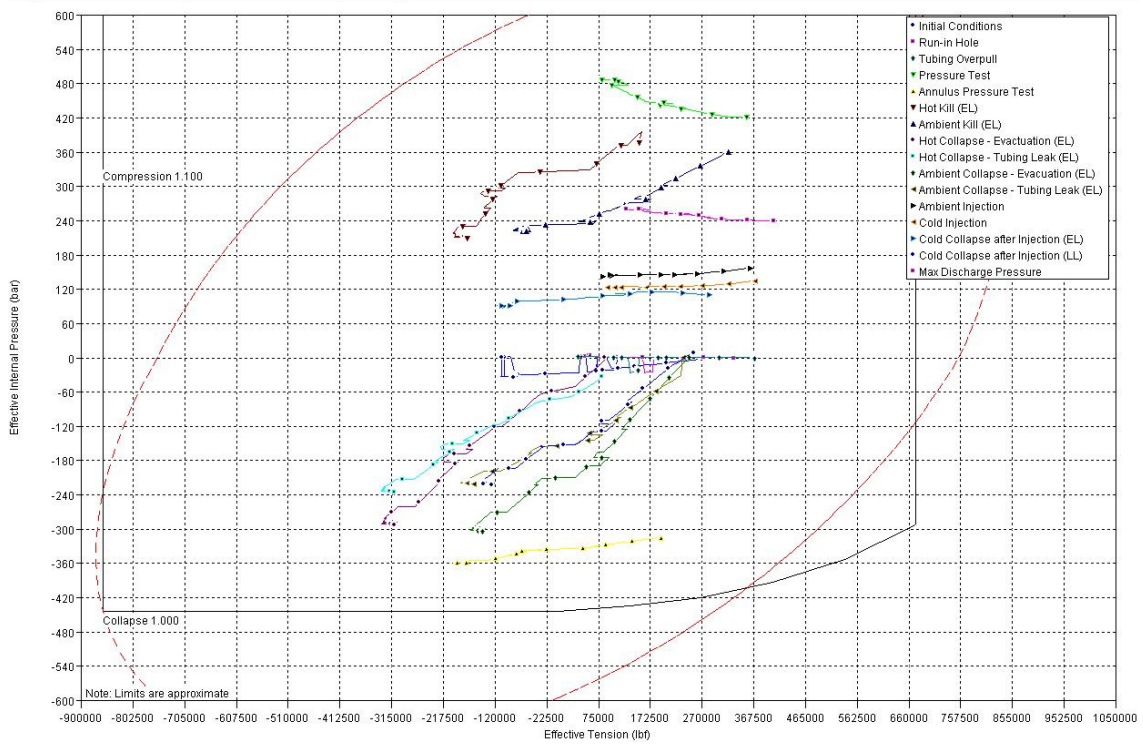


Figure 9.4: 7" SM25-CRW # 38.692 kg/m production tubing – VME plot.

It can be observed from the above plots that 7" SM25CRW-125 # 38.962 tubing will be recommended as the 7" SM25CRW-125 # 34.228 tubing cannot withstand the collapse pressures (Figure 9.4) associated with cold injection and ambient collapse evacuation.

9.8 Safety Factor Plots

The convention is for safety factor (SF) greater than 1 to represent a rating that is greater than the load. Given than more than one failure mechanism is possible, safety factor will be calculated for each failure mechanism.

$$SF = \frac{Rating}{Load} \tag{Eq. 9.7}$$

If all the safety factors are greater than 1, the tubing should remain intact. To account for uncertainty SF greater than one is normally used. SF used in these calculations are given in Table 9.3. The next figures (Figure 9.5 –Figure 9.8) show the triaxial, burst, collapse and axial safety factors for the SM25CRW -125 # 38.692 tubing.

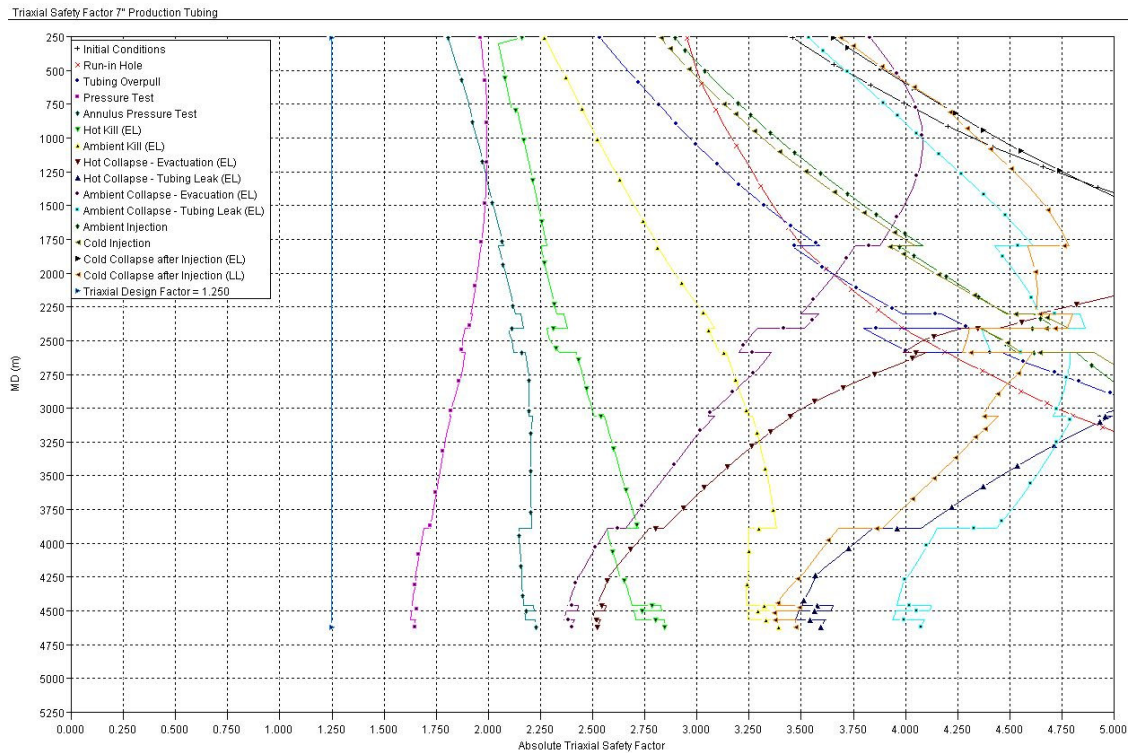


Figure 9.5: Triaxial safety factor plot for 25CrW -110 # 26 tubing.

Burst Safety Factor 7" Production Tubing

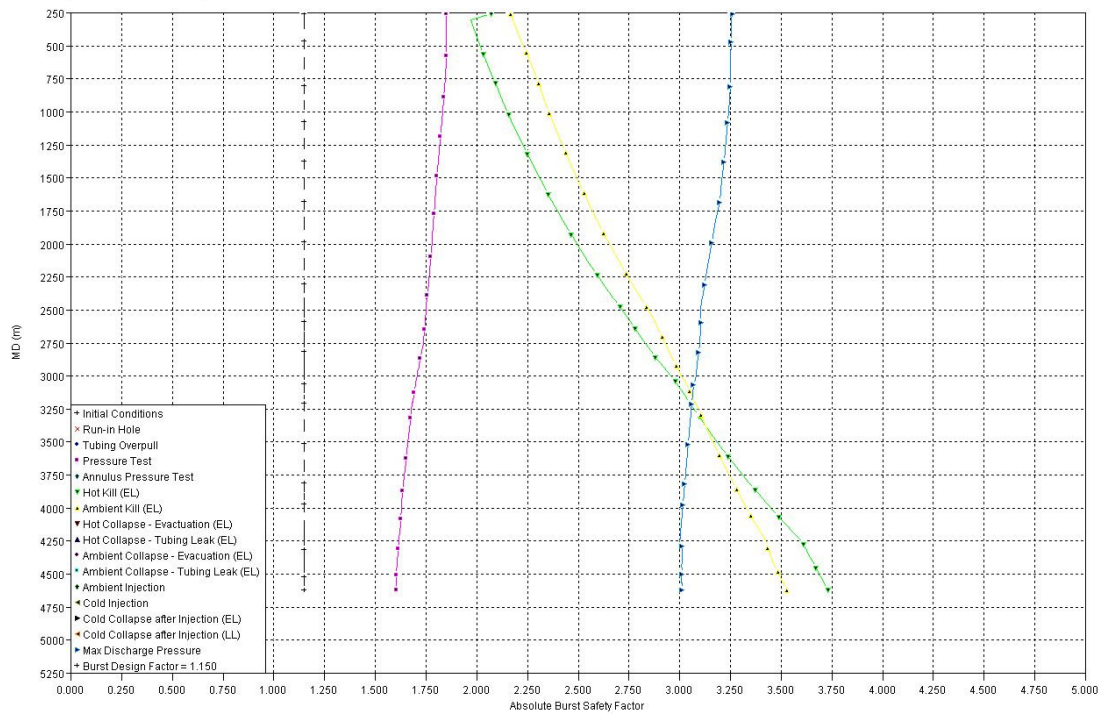


Figure 9.6: Burst safety factor plot for SM25CRW -125 # 38.691 kg/m tubing.

Collapse Safety Factor 7" Production Tubing

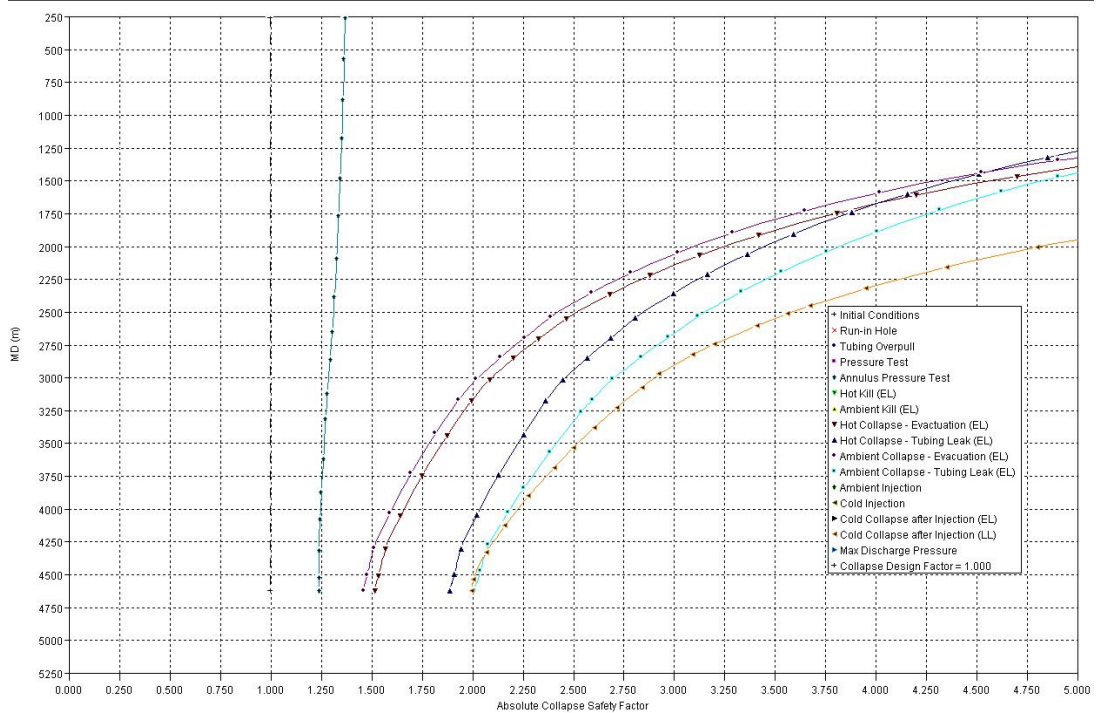


Figure 9.7: Collapse safety factor plot for SM25CRW -125 # 38.691 kg/m tubing.

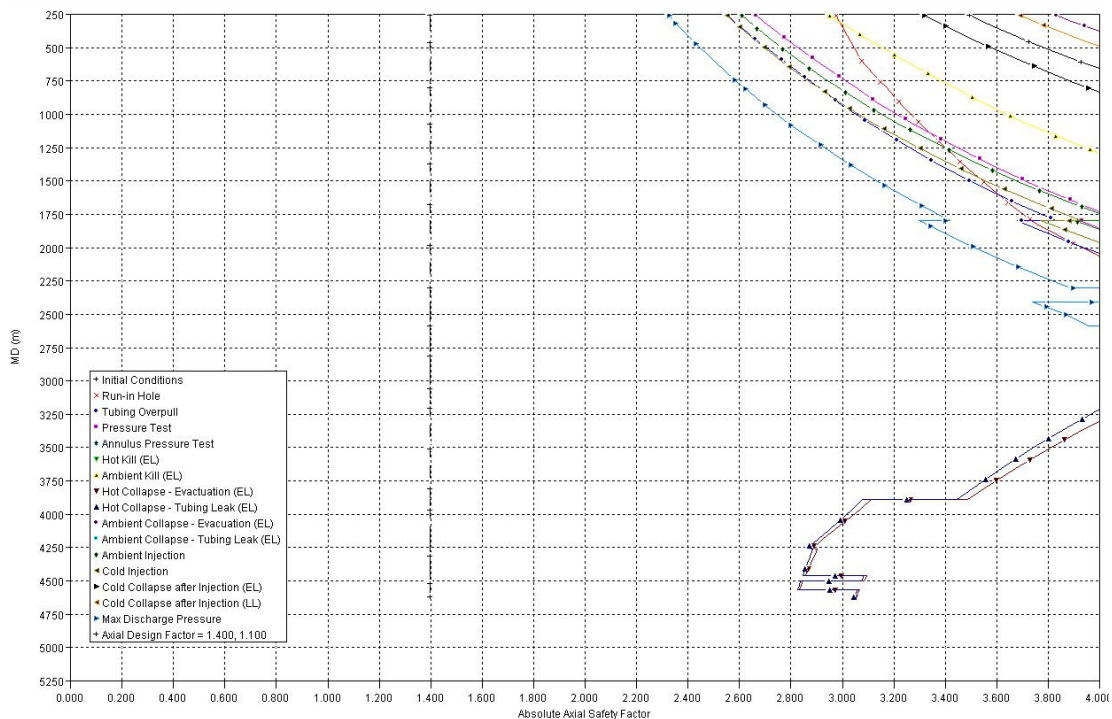


Figure 9.8: Axial safety factor plot for SM25CRW -125 # 38.691 kg/m tubing.

- It is observed from Figure 9.5 that the annulus and tubing pressure tests are the worst load case for triaxial loading. This is as expected as these tests are performed to check integrity of packer, tubing and connections.
- Figure 9.6 indicated that hot kill and ambient kill are the worst load cases, except from pressure test. This is as expected as we use a high injection pressure. The tubing would fail at well head.
- Figure 9.7 reveals that evacuation of tubing is the highest collapse load, except from pressure test. This load is highest at bottom hole, and is therefore a much less severe load case, and also the reason a smaller SF is used.
- In Figure 9.8 maximum injection pressure is the highest axial load case. This is because of higher injection rate – thus higher fluid drag, and more ballooning caused by a higher fluid pressure.

9.9 Conclusion & Recommendation

- 7" SM25CrW-125 # 38.692 kg/m tubing is recommended as it will be able to withstand expected operating loads.
- The modelling capability of WellCat in estimating CO₂ properties is very poor.
- To eliminate potential issues with the CO₂ properties in WellCat, it is recommended to import pressure and temperature profile from an appropriate wellbore performance simulator.

Chapter 10

HSE issues related to CO₂ Injection

10.1 Objectives

This chapter discusses HSE issues that are related to CO₂ injection.

10.2 Methodology

A literature review was conducted to identify HSE issues. However, issues are mostly related to phase characteristics and corrosion, and have thus been covered extensively in previous chapters.

10.3 Discussion

The nature of CO₂ wells is different than that of hydrocarbon wells due to the very corrosive environment which can lead to loss of integrity. In the US, many CO₂ wells have been in operations for years and CO₂ blowouts have been observed as these wells loose integrity. Most of the HSE issues are related to phase characteristics when dense phase CO₂ is depressurized, either through a planned operation of by an accidental release.

When pressure containment is lost, CO₂ converts from a supercritical fluid to a vapor with significant expansion. This vapor continues to expand with decreasing confining pressure as it moves up the wellbore. Flow velocities increase accordingly. Any mud or other fluid in the well will be expelled quickly leaving little hydrostatic pressure to resist influx from reservoir. This results in higher influx of CO₂ into the wellbore which quickly expands. This flow behavior is almost explosive in violence, BLEVE (boiling liquid/expanding vapor explosion). The violence of the surface flow is usually not expected by field workers. Often only a small volume of supercritical CO₂ in the wellbore is enough to trigger the process causing the well to blowout in a matter of seconds. Reaction time is very limited and equipment like manual BOPs and stab in safety valves cannot be handled fast enough to prevent complete expulsion of all liquid from the well and loss of pressure control [43]. The expansion will also cause rapid cooling of the wellbore and the fluid stream. When the CO₂ stream falls below the triple point, solid ice can form quickly [43].

Several special problems results from the unique CO₂ phase behavior:

- Intervention work is complicated due to high flow rates and workers are exposed to gas moving at high velocities, which can injure exposed skin due to high rate blow-by [95].
- Well control intervention methods has increased complexity due to possible formation of CO₂ hydrates that can collect in BOP, wellhead and other equipment around the wellhead [43].
- Expelled CO₂ will condense water in the atmosphere forming a white cloud around the wellbore and potentially be a cold hazard for workers [43].
- Fluids expelled from the wellbore by the expanding CO₂ may form a ground fire hazard [43].
- Dry ice formation results in a pea- to marble-size projectiles that are expelled from the well at very high speeds [43].



- High rate gas flow can cut grooves in tubular good very fast, damage rubber sealing elements and strip paint off equipment [43].

Well integrity studies, performed by SINTEF and Petroleum Safety Authorities Norway, identified injection wells to be 2–3 times more prone to leak than production wells. The studies had limited overlap. Two explanations for this trend can be:

1. Large cycling load on the injector wells due to injection of cold fluids. This can cause leakages if the well is not design to manage these loads (i.e. conversion of producers to injectors)
2. Injectors have a low status compared to producers.

Integrity issues with injection wells can have serious consequences, and should be given the same status as production wells. Good design is the most effective means of preventing CO₂ releases. When it is not practical to eliminate the hazard by design, prevention measures should be achieved through procedural controls and training.

The effect of high CO₂ exposure to humans is presented in Table 10.1.

CO ₂ Concentration in Air (% v/v)	Exposure	Effect on Humans
17-30	Within 1 minute	Loss of controlled and purposeful activity, unconsciousness, convulsions, coma, death.
>10-15	1 minute to several minutes	Dizziness, drowsiness, severe muscle twitching, unconsciousness.
7-10	Few minutes	Unconsciousness, near unconsciousness.
	1.5 minutes to 1 hour	Headache, increased heart rate, shortness of breath, dizziness, sweating, rapid breathing.
6	1-2 minutes	Hearing and visual disturbance.
	≤ 16 minutes	Headache, difficult breathing (dyspnea).
	Several hours	Tremors
4-5	Within a few minutes	Headache, dizziness, increased blood pressure, uncomfortable breathing.
3	1 hour	Mild headache, sweating, and difficult breathing at rest.
2	Several hours	Headache, difficult breathing upon mild exertion.

Table 10.1: Acute health effects caused by high concentrations of CO₂ [26].

10.4 Conclusion

The HSE issues related to CO₂ are mainly due to phase characteristics and corrosion. An effective management of water content will help prevent rapid internal corrosion. Depressurizing CO₂ will result in a significant expansion and temperature drop. The loss of containment can cause a flow behavior that is almost explosive in violence.

HSE issues are handled through good design, procedural controls and training. As CO₂ injection wells have different behavior than hydrocarbon wells, staff should be trained to be attuned to the hazards associated with CO₂ injection.

Chapter 11

Conclusion & Recommendations

Well design considerations for Prelude CO₂ injection are investigated through this thesis. A key differentiator for the project compared to other carbon dioxide injection schemes is the high temperature and pressure experienced (155°C, 415 bar). Temperature and pressure gradients through the injection system are important for material selection. These gradients are typically obtained from a wellbore simulator. Current wellbore simulators do not predict CO₂ properties as accurate as it predicts hydrocarbons, mainly due to the lack of a fit for purpose equation of state.

Carbon dioxide is not corrosive by itself, but form carbonic acid in the presence of free water. Free water is not expected during normal operations, but no guarantee can be given regarding transient operations. Carbon steel is therefore ruled out as an option and CRA is required. Based on literature review, the recommended metallurgy for the tubing is a 25%Cr Super Duplex, as the combined conditions of CO₂ and H₂S is too severe for common alloys.

The expected degradation rate of cement is slow, but in the presence of cracks or channels in the cement can cause rapid loss of sealing capability. The Swan reservoir is overlaid by 1800m of shale which will be cemented. The chance of a leak is very small. However, acid resistant cement exists on the market and is recommended for the project to provide long term integrity. It is considered crucial to employ good cementing practice during installation to maintain well integrity.

The solubility parameter of CO₂ and common elastomers are so close that they are incompatible and swelling is observed. To prevent gross swelling the solubility difference should be 1-2 units. Elastomers used in the industry are for the most part optimized for hydrocarbons, which have quite different solubility compared to CO₂. Rapid decompression generally only has relevance when the environment is gas, which occurs during transient operations. At bottomhole conditions, high temperature is the driver and FFKM (Chemraz) is recommended. HNBR is recommended for wellhead conditions.

A leaking packer can cause a corrosive environment in the annulus as water and CO₂ form carbonic acid. To prevent corrosion, it is recommended to use base oil. Base oil has its own challenges as low density and thermal expansion but leaves the corrosion issue moot.

A sand control study indicated that sand control would be needed in the injection well. The recommendation was to use open hole gravel pack as they are considered very reliable once installed. Fluid hammering in a CO₂ injection well can be as high as in a water injector due to the high density of the CO₂.

A sensitivity study on the effect of different injection parameter was conducted. The study demonstrated the sensitivity of temperature on injection rate. Without aftercooling (78°C) the injection pressure would need to be raised 60 bar for base case. The density of CO₂ is sensitive to changes in temperature, especially around the critical point (31.1°C).

Extra injection pressure is also required in the case of well inversion. If methane is allowed into the wellbore during a shut-in, the wellhead pressure will creep towards ~325 bar. The maximum discharge pressure for the compressor topside is 255 bar, and thus barriers should be installed as mitigation. Most straightforward solution is assumed to be some kind of a downhole valve.

During transient operations a temperature drop has been observed caused by the Joule-Thomson cooling effect. This occurs as pressure is lost and CO₂ flashes. To prevent massive cooling, closing and starting up the well should be done quickly to minimize the mass involved. Cooling of the wellbore is also expected during testing of the safety valve. This is expected to be highest in the gas-liquid interface, and cannot be measured at wellhead. These operations can be optimized if fibre optic measurement is installed.

The JT cooling is most severe for gas expansion. At shut-in conditions, before ~220 bar reservoir pressure, only one phase will exist in the wellbore, and only minor cooling will be expected. Once depleted beyond ~220 bar the cooling will become much more severe as two phases will exist in the wellbore. The cooling effect will thus become more severe as the reservoir pressure is depleted.

Tubing analysis confirmed that a SM25CrW-125 – 38.692 kg/m will be sufficient to withstand the loads experienced the injection well. The limitation of the well design software, WellCat, in modeling CO₂ can be overcome by importing results from a wellbore simulator capable of handling CO₂ streams.

Fields with high pressure and temperature are less suitable for CO₂ injection as the high temperature and pressure worsens the degradation of cement and steel. It is not anticipated that any of the identified challenges represents a showstopper for the Prelude injection well.

During the process of finishing this thesis, gaps have been identified in understanding and in the work process regarding CO₂ injection wells. A better understanding of these topics will provide safer design and operations.

- Current wellbore simulators are designed and improved for hydrocarbons and water and lack equation of state capable of predicting CO₂ properties satisfactory.
- There is a lack of knowledge regarding the impact impurities have on CO₂ thermodynamics. Especially for multi component systems.
- There is a general lack in experimental data for thermodynamics properties at higher pressure and temperatures.
- There is a general lack of corrosion and material performance data at the higher CO₂ pressure encountered in Prelude.
- Current models for predicting carbon dioxide corrosion are limited to 50 bar partial pressure CO₂.

Abbreviations

AGRU	Acid gas removal unit
CCS	Carbon Capture & Storage
CITHP	Closed-In Tubing Head Pressure
CRA	Corrosion Resistant Alloys
EGR	Enhanced Gas Recovery
EOR	Enhanced Oil Recovery
FLNG	Floating Liquid Natural Gas
gFLNG	Generic Floating Liquid Natural Gas
GRE	Glass Reinforced Epoxy
JT	Joule-Thomson
MMV	Monitoring, Measuring and Verification
MMV	Measurement, Monitoring & Verification
NIST	National Institute of Standards & Technology
NPV	Net Present Value
OHGP	Open Hole Gravel Pack
PDHG	Permanent Downhole Gauge
PVT	Pressure, Volume, and Temperature
SCC	Stress Corrosion Cracking
SC-CO ₂	Supercritical CO ₂
SCSSSV	Surface Controlled Subsea Safety Valve
SDA	Shell Development Australia
SSC	Sulphide Stress Corrosion
SSC	Sulfide Stress Cracking
STP	Standard Temperature & Pressure
STP	Standard Temperature & Pressure
TRSSSV	Tubing Retrievable Subsea Safety Valve
TVD	True Vertical Depth
TWC	Thick Walled Cylinder
UCS	Unconfined Compressive Strength
VLP	Vertical Lift Performance

References

1. Smith, D.L., et al., *CO₂ Sequestration Wells - The Lifetime Integrity Challenge*. 2010.
2. Prado, M., M. Sumrow, and H.-P. Bjoerndal, *Prelude Acid Gas Reinjection Project Investigation of Formation Fracturing Risks During Acid Gas Injection* S.I.E.a.P. INC. 2008, EP 2008-3191.
3. Stassi, M., *Prelude Development Concept Selection Report*. 2009.
4. *Prelude Floating LNG Project - Draft Environmental Impact Statement*. S.D.A.P. Ltd. 2009.
5. Prado, M., M. Sumrow, and H.-P. Bjoerndal, *Prelude Acid Gas Reinjection Project Investigation of Formation Fracturing Risks During Acid Gas Injection* S.I.E.a.P. INC. December 2008, EP 2008-3191.
6. Sumrow, M., *Produced Acid Gas Reinjection Modeling to Determine Compression Discharge Pressure Requirements Prelude CO₂ Sequestration Project*. SIEP. December 2008, EP 2008-3189.
7. Winkler, M. and E. Quint, *Prelude CO₂ Sequestration Options*. Shell. 2008, EP 2008-3192.
8. Nevels, H.F., T. Lovell, and N. Johnston, *Prelude CO₂ Injection Concept Summary for the Swan Injector*. SIEP. December 2008, EP 2008-3190.
9. Collins, M., *Prelude CO₂ Geo-Sequestration Feasibility*. 2010.
10. Landbrook, B., et al., *CO₂ Storage in depleted gas fields*. 2009, 2009/01.
11. Dresen, C., et al., *Prelude Floating LNG. Pre VAR3 Technical CTRs FB-SK-26 CO₂ Reinjection*. S.G. Solutions. November 2008, GS.08.53704.
12. Meena, P.P., *CO₂ Leakage Potential Assessment of the existing Prelude wells for CO₂ Injection*. Shell. 2009, EP200908313546.
13. Meyer, J.P., *Summary of Carbon Dioxide Enhanced Oil Recovery (CO₂EOR) Injection Well Technology*. API. August 2007.
14. Meer, L.G.H.v.d., et al., *K12-B A Test Site for CO₂ Storage and Enhanced Gas Recovery*. 2005, SPE 94128.
15. Vandeweyer, V.P., et al., *CO₂ Storage and Enhanced Gas Recovery at K12-B*. 2009.
16. Hilditch, D., et al., *A Technical Appraisal of the Feasibility for CO₂ Sequestering Operations for the Gorgon Gas Field Development Proposal - Phase IV: Executive Summary*. CO₂CRC. 2009.
17. Michael, K., et al., *Injection Strategies for CO₂ Storage Sites*. I. GHG. June 2010.
18. Lee, G., et al., *Gorgon Project: Basis of Design - CO₂ Wells*. Chevron. April 2009.
19. Baklid, A., R. Korbol, and G. Owren, *Sleipner Vest CO₂ Disposal, CO₂ Injection into a Shallow Underground Aquifer*. 1996, SPE 36600.
20. Hansen, H., O. Eiken, and T.O. Aasum, *Tracing the Path of Carbon Dioxide from a Gas/Condensate Reservoir, Through an Amine Plant and Back into a Subsurface Aquifer - Case Study: The Sleipner Area, Norwegian North Sea*. 2005, SPE 96742.
21. Wright, I., et al., *An Overview of Active Large-Scale CO₂ Storage Projects*. 2009.
22. Carcagno, G., T. Castineiras, and D.J. Eiane, *First Gas Field Development Using Exclusively Dope-Free Casing and Tubing Connections - Statoil Snohvit*. 2007, SPE/IADC 105855.
23. Randhol, P. and P. Cerasi, *CO₂ Injection Well Integrity*. SINTEF. 2008, 31.6953.00/01/08.
24. Wright, I.W., *The In Salah Gas CO₂ Storage Project*. 2007.
25. Haigh, M.J., *Well Design Differentiators for CO₂ Sequestration in Depleted Reservoirs*. 2009.
26. Johnsen, K., et al., *Mapping of potential HSE issues related to large-scale capture, transport and storage of CO₂*. DNV. January 2009, 2008-1993.
27. Metz, B., et al., *IPCC Special Report on Carbon Dioxide Capture and Storage*. IPCC. 1995.
28. Cengel, Y.A. and M.A. Boles, *Thermodynamics - An Engineering Approach 5th edition*. 2005.
29. Paterson, L., et al., *Numerical Modeling of Pressure and Temperature Profile Including Phase Transitions in Carbon Dioxide Wells*. 2008, SPE 115946.



30. Ijzermans, R., R. Bikatshev, and G. Haandrikman, *Modeling of CO₂ transport in pipeline and wells*. A. Shell Global Solutions International B.V. 2011.
31. Boyle, T.B. and J.J. Carrol, *Calculation of Acid Gas Density in the Vapor, Liquid, and Dense-Phase Regions* 2001.
32. Oosterkamp, A. and J. Ramsen, *State-of-the-Art Overview of CO₂ Pipeline Transport with relevance to offshore pipelines*. 2008.
33. Sugianto, *Study of CO₂ Properties and Transportation for Injection well into Reservoir*. 2007,
34. Span, R. and W. Wagner, *Equation of State for Technical Applications III. Results for Polar Fluids*. 2002.
35. Bellarby, J., *Well Completion Design*. 2009: Elsevier.
36. Sommerdijk, H., *Personal Communication*. 2011.
37. Experts, P., *Integrated Production Modelling - Prosper Online Help*. P. Experts. 2011.
38. Bouts, M., et al., *Production Technology CO₂ Guidelines*. Shell. 2009.
39. *IPM Prosper Version 11 - User Manual*. 2009.
40. Suri, A. and M.M. Sharma, *Fracture Growth i Horizontal Injectors*. 2009.
41. Spycher, N., K. Pruess, and H. Ennis-King, *CO₂-H₂O mixtures in the geological sequestration of CO₂. I. Assessment and calculation of mutual solubilities from 12 to 100C and up to 600 bar*. 2003.
42. Chapoy, A., et al., *Effect of Common Impurities on the Phase Behaviour of Carbon Dioxide Rich Systems: Minimizing the Risk of Hydrate Formation and Two-Phase Flow*. 2009, SPE 123778.
43. Randhol, P., et al., *Ensuring well integrity in connection with CO₂ injection*. SINTEF. December 2007, 31.6920.00/02/07.
44. Syed, T. and T. Cutler, *Well Integrity Technical and Regulatory Considerations for CO₂ Injection Wells*. 2010.
45. Benedictus, T., et al., *Long term integrity of CO₂ storage - Well abandonment*. November 2009,
46. Onan, D.D., *Effects of Supercritical Carbon Dioxide on Well Cements*. 1984, SPE 12593.
47. Milestone, N.B., L.E. Kukacka, and N. Cariello, *Effects of Carbon Dioxide Attack on Geothermal Cement Grouts*. 1986.
48. Barlet-Gouedard, V., et al., *Mitigation Strategies for the Risk of CO₂ Migration Through Wellbores*. 2006, SPE 98924.
49. Kutchko, B.G., et al., *Rate of CO₂ Attack on Hydrated Class H Well Cement under Geologic Sequestration Conditions*. Environ. Sci. Technol, 2008.
50. Brandl, A., et al., *Cementing Solutions for Corrosive Well Environments*. 2010, SPE 132228.
51. Ladva, H.K.J., et al., *The Cement-to-Formation Interface in Zonal Isolation*. 2005, SPE 88016.
52. Shell, *Cement Concept Select for GoldenEye CCS*. Shell. 2011.
53. Carden, R.S. and R.D. Grace, *Horizontal and Directional Drilling*. 2007: PetroSkills.
54. Lonvik, K., et al., *Material Risk - Ageing Offshore Installations*. DNV. November 2006, 2006-3496.
55. Koteeswaran, M., *CO₂ and H₂S Corrosion in Oil Pipelines*, University of Stavanger, 2010.
56. Schmitt, G. and M. Horstemeier, *Fundamental Aspects of CO₂ Metal Loss Corrosion - Part II: Influence of Different Parameters on CO₂ Corrosion Mechanisms*. 2006, NACE 06112.
57. Lee, C.-H., et al., *Corrosion and Materials Selection in CCS Systems*. April 2010, 2010/03.
58. Propp, W.A., et al., *Corrosion in Supercritical Fluids*. I.N.E. Laboratory. 1996, DE96014006.
59. Schremp, F.W. and G.R. Roberson, *Effect of Supercritical Carbon Dioxide (CO₂) on Construction Materials*. 1975.
60. Seiersten, M., *Material Selection for Separation, Transportation and Disposal of CO₂*. 2001, NACE 01042.
61. Kongshaug, K.O. and M. Seiersten, *Baseline Experiments for the Modelling of Corrosion at High CO₂ Pressure*. 2004, NACE 04630.

62. Thodla, R., A. Francois, and N. Sridhar, *Materials Performance in Supercritical CO₂ Environements*. 2009.
63. Francois, A., et al., *Effect of Impurities on Corrosion of Steel in Supercritical CO₂*. 2010, NACE 10193.
64. Zhang, Y., K. Gao, and G. Schmitt, *Water Effect on Steel Under Supercritical CO₂ Conditions*. 2011, NACE 11378.
65. TWI, *Materials Integrity in Supercritical CO₂/H₂S - JIP Launch Meeting TWI 6 Oct 2009*. 2009,
66. Nyborg, R., *CO₂ Corrosion Models for Oil and Gas Production Systems*. 2010, NACE 10371.
67. Nyborg, R., *Field Data Collection, Evaluation and Use for Corrosivity Prediction and Validation of Models. Part II: Evaluation of Field Data and Comparison of Prediction Models*. . 2006, NACE 06118.
68. Shell, *Carbon Steel Corrosion Engineering Manual for Upstream Facilities*. 2011, DEP 30.10.02.14.
69. Ho, E., *Elastomeric seals for rapid gas decompression application in high-pressure services*. 2006.
70. *Component Selection*. 2010, SP-CW030D3-RT 059.
71. Campion, D.R.P., D.B. Thomson, and D.J.A. Harris, *Elastomers for fluid containment in offshore oil and gas production: Guidelines and review*. H.a.S. Executive. 2005.
72. Shell, *Selection of Materials for Life Cycle Performance (Upstream Facilities) - Equipment*. 2011, DEP 39.01.10.12-Gen.
73. Rincon, P.R., *Material Assessment: Barendrecht CO₂ storage project. Material selection and corrosion assessment*. S.G. Solutions. 2009.
74. Clegg, J.D., *Volume IV: Production Operations Engineering*. Petroleum Engineering Handbook. 2007: SPE.
75. Bracewell, B., *Well Engineering - Swan Injector Initial Feasibility Statement*. Shell. 2010,
76. Leth-Olsen, H., *CO₂ Corrosion of Steel in Formate Brines for Well Applications*. 2004, NACE 04357.
77. Leth-Olsen, H., *CO₂ Corrosion in Bromides and Formate Well-Completion Brines*. 2005, SPE 95072.
78. Forum, W.E., *Shell Casing and Tubing Design Guide - Volume 2*. H. Shell International Exploration and Production INC. 2009.
79. Competition, S.C.U.D., *Completion Concept Select*. S.U. Limited. 2010,
80. Kroon, M.d., *Sand Management Guide - Sand Prediction*. Shell. 1997.
81. William, K., P.E. Ott, and J.D. Woods, *Modern Sandface Completion Practices Handbook*. W. Oil. 2001.
82. Hertogh, G. and I. Foo, *Sand failure prediction for the Prelude field (Australia)*. Shell. 2010.
83. Mena, P., et al., *Prelude CO₂ Injector Completion Philosophy & Material Selection*. Shell. 2010.
84. Murray, L.R. and D.J. Wood, *Designing Effective Sand Control System to Overcome Problems in Water Injection Wells*. 2005, SPE 93564.
85. Vaziri, H., et al., *Computation of Sand Production in Water Injectors*. 2007.
86. Eriksen, J.H., et al., *Orienting Live Well Perforating Technique Provides Innovative Sand Control Method in the North Sea*. 1999, SPE 56472.
87. Team, C.a.M., *Sand Management Guide: Sand Control Methods - Other Methods of Sand Control*. Shell. 1997.
88. *Production Handbook Volume 5: Production Technology*. 1991: Shell International.
89. Kumar, A., A.K. Srivastava, and R. Kumar, *Design Optimization of Slotted Liner Completions in Horizontal Well of Mumbai High Field*. 2010, SPE 133321.
90. Furui, K., D. Zhu, and A.D. Hill, *Optimization of Horizontal Well-Completion Design With Cased/Perforated or Slotted Liner Completions*. 2004, SPE 90579.



91. Gisbergen, S.J.C.H.M.v. and A.A.H. Vandewijer, *Reliability Analysis of Permanent Downhole Monitoring Systems*. 2001, SPE 57057.
92. Competition, S.C.U.D., *Flowline Well Interactions*. 2010, SP-PT060D3.
93. Mackie, E. and S. MacDonald, *Monitoring, measuring and verification screening Project Prelude, Western Australia, SDA*. Shell. August 2009.
94. Sumitomo Metals, *SM25CRW-125 Technical Specifications*. 2011.
95. Skinner, L. *CO₂ blowouts: An emerging problem*. January 2003 [cited 2011 08.02]; Available from: [http://www.worldoil.com/January-2003-CO₂-blowouts-An-emerging-problem.html](http://www.worldoil.com/January-2003-CO2-blowouts-An-emerging-problem.html).



Appendix A: Software Description

Prosper

Prosper is an application by Petroleum Experts. Prosper is a well performance, design and optimisation program which is part of the Integrated Production Modelling Toolkit (IPM).

It is designed to simulate well production and injection, as well as pipelines, including the effects of PVT (fluid characterisation), well outflow VLP correlations (for calculation of flowline and tubing pressure loss) and inflow, IPR (reservoir inflow into the wellbore).

WellCat

WellCat is part of the Engineer's Data Model (EDM) integrated suite of well engineering and data analysis computer applications.

WellCat provides precise solutions for both wellbore temperature and pressure analysis, and integrated casing and tubing design. The software calculates downhole temperature and pressure profiles which can be used for pipe-body movement and casing and tubing load analysis.

The software integrates five modules into a common environment to provide more accurate and reliable solutions to complex design problems. Thermal effects are modeled for drilling, completion and production operations. A comprehensive analysis of loads and stresses on casing and tubing is provided, including service life analysis. Detailed analysis of the entire casing system is provided to understand the effects of annular pressure buildup and the interaction in the casing and tubing systems within a well. Loads and their resulting wellhead movement are evaluated to determine the integrity of the well tubulars.

FIST

FIST (Fully Integrated Sand prediction Tool) is a user-friendly computer application which predicts the probability of sand failure for a single producing interval or a group of producing intervals during the production lifetime of any gas or oil producing well.

The FIST program provides a quantitative measure of the risk of sand production by combining the physical information on the cause of rock failure (the FIST failure criteria) with various types of information on local and reservoir-wide rock strength (core data, log data, knowledge of past failures, layering) and knowledge of the field conditions (reservoir pressure, production drawdown, in-situ stresses). The FIST sand failure prediction methodology has been implemented in the computer program as the comparison of the actual or estimated rock strength of a sand reservoir unit (TWC, UCS) with the critical rock strength needed to withstand the increased effective stresses exerted on the rock under the influence of progressing reservoir depletion and near-wellbore production drawdown. FIST helps the user to obtain a reliable and continuous strength profile over the pay zone intervals, to quantify the uncertainty on the basic strength input parameters and to assess how the uncertainty in the input propagates through the FIST criteria to a quantifiable uncertainty in the predicted outcomes.

Appendix B: Prosper Input

System Summary (Base Case HD- OHGP.Out)

Done Cancel Report Export Help Dalestamp

Fluid Description

Fluid: Retrograde Condensate
 Method: Equation of State
 Eq. of State: PROSPER Internal EOS model
 Separator: Multi-Stage Separator
 Hydrates: Disable Warning
 Water Viscosity: Use Pressure Corrected Correlation

Calculation Type

Predict: Pressure and Temperature (offshore)
 Model: Enthalpy Balance
 Range: Full System
 Output: Show calculating data

Well

Flow Type: Tubing Flow
 Well Type: Injector

Well Completion

Type: Open Hole
 Sand Control: Gravel Pack

Artificial Lift

Reservoir

Inflow Type: Single Branch

User information

Company: Shell Australia
 Field: F-Block
 Location: Australia
 Well: Swan Injector
 Platform:
 Analyst: Stig B. Haugstad
 Date: Wednesday, 2 March 2011

Comments [Ctrl-Enter for new line]

Appendix B 1 System summary.

Main Equation of State Options

OK Cancel Help

General

EOS Model: Peng Robinson
 Optimisation Mode: None
 Optimise Repeat Calculations: No

Volume Shift

Full Composition: No

Lumping

Allow Lumping: No

Reference Data for Standard Conditions

Reference Temperature: 15.5556 (deg C)
 Reference Pressure: 1.01325 (BARa) Set As Default

Phase Check

Phase Detection Method: Advanced

Path to Surface and Recycle

Separator Calc. Method:
 Flash Straight to Stock Tank
 Use Separator Train
 Use K Values

Target GOR Method: Use Separator fluids

Appendix B 2 Main equation of state options.

Edit Composition

Done Cancel Generate BI Coeffs... Phase Env... Help DLL Info Save Export Mole Weight
 Export...PRP Import...PRP Fill in Table Reset Comp Properties Target GOR Interpolate Recall Report 44.01

Options
 Change
 EOS Model : Peng Robinson
 Optimisation Mode : None
 Separator Calc Mode : No Separators
 Volume Shift
 Full Composition: No Volume Shift

	Name	Mole Percent (percent)	Critical Temp. (deg C)	Critical Pressure (BARa)	Critical Volume (m ³ /kg.mole)	Acentric Factor	Molecular Weight	Specific Gravity (sp. gravity)	Boiling Point (deg C)	Volume Shift	Omega
1	CO2	100	30.94	73.9777	0.0939	0.239	44.01	1.101	-78.45	-0.1002	0.45724
2											
3											
4											
5											
6											
7											
8											
9											
10											
11											
12											
13											
14											
15											
16											
17											
18											
19											
20											

Calculation Type: Calculated From EOS Model Reservoir Temperature: 155 (deg C) Salinity: 7900 (ppm)

Appendix B 3 Composition 1.

Edit Composition

Done Cancel Generate BI Coeffs... Phase Env... Help DLL Info Save Export Mole Weight
 Export...PRP Import...PRP Fill in Table Reset Comp Properties Target GOR Interpolate Recall Report 44.01

Options
 Change
 EOS Model : Peng Robinson
 Optimisation Mode : None
 Separator Calc Mode : No Separators
 Volume Shift
 Full Composition: No Volume Shift

	Acentric Factor	Molecular Weight	Specific Gravity (sp. gravity)	Boiling Point (deg C)	Volume Shift	Omega A	Omega B	Parachor	Costald Volume (m ³ /kg.mole)	Costald AF
1	0.239	44.01	1.101	-78.45	-0.1002	0.45724	0.077796	78	0	
2										
3										
4										
5										
6										
7										
8										
9										
10										
11										
12										
13										
14										
15										
16										
17										
18										
19										
20										

Calculation Type: Calculated From EOS Model Reservoir Temperature: 155 (deg C) Salinity: 7900 (ppm)

Appendix B 4 Composition 2.

Inflow Performance Relation (IPR) - Select Model

Done Validate Calculate Report Transfer Data Sand Failure Select Model
 Cancel Reset Plot Export Input Data
 Help Test Data Sensitivity

Model and Global Variable Selection

Reservoir Model

- Jones
- Forchheimer
- Back Pressure
- C and n
- MultiRate C and n
- MultiRate Jones
- External Entry
- Petroleum Experts**
- Hydraulically Fractured Well
- Horizontal Well - No Flow Boundaries
- MultiLayer Reservoir
- SkinAide (ELF)
- Dual Porosity
- Horizontal Well - Transverse Vertical Fractures
- Modified Isochronal
- Forchheimer With Pseudo Pressure
- MultiRate Forchheimer With Pseudo Pressure
- SPOT

Mechanical / Geometrical Skin

Enter Skin By Hand

Deviation and Partial Penetration Skin

Wong-Clifford

Reservoir Pressure	415	BARa
Reservoir Temperature	155	deg C
Water Gas Ratio	0	Sm3/Sm3
Total GOR	177200	Sm3/Sm3
Compaction Permeability Reduction Model	No	

Appendix B 5 Inflow performance relation – select model.

Inflow Performance Relation (IPR) - Input Data

Done Validate Calculate Report Transfer Data Sand Failure Select Model
 Cancel Reset Plot Export Input Data
 Help Test Data Sensitivity

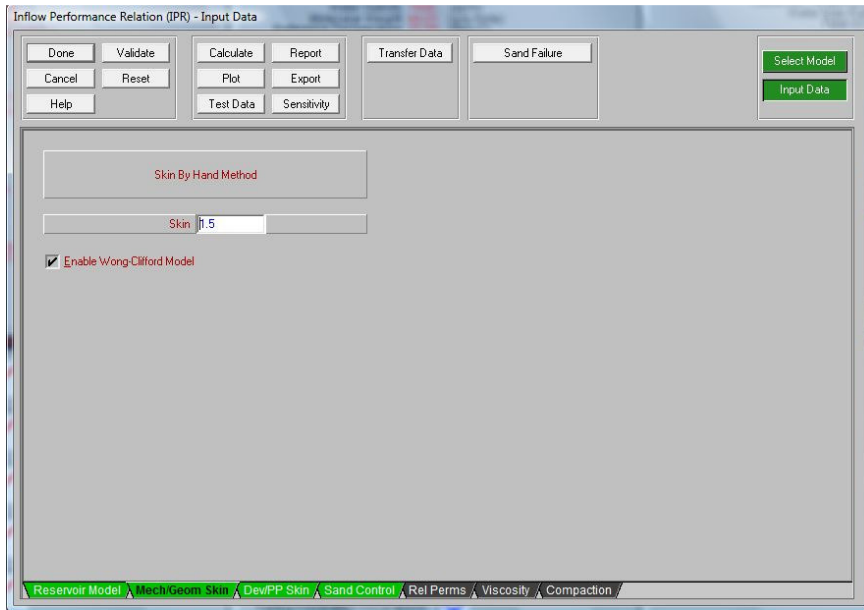
Petroleum Experts Reservoir Model

Reservoir Permeability	35.6	md
Reservoir Thickness	60	m
Drainage Area	404690	m2
Dietz Shape Factor	31.6	
WellBore Radius	0.2032	m
Production Interval	60	m
Time Since Production Started	100	days
Reservoir Porosity	0.12	fraction
Connate Water Saturation	0.2	fraction
Non-Darcy Flow Factor (D)	7.2868e-7	1/(Sm3/d)
Non-Darcy Flow Factor (D)	Calculated	
Permeability Entered	Total Permeability	

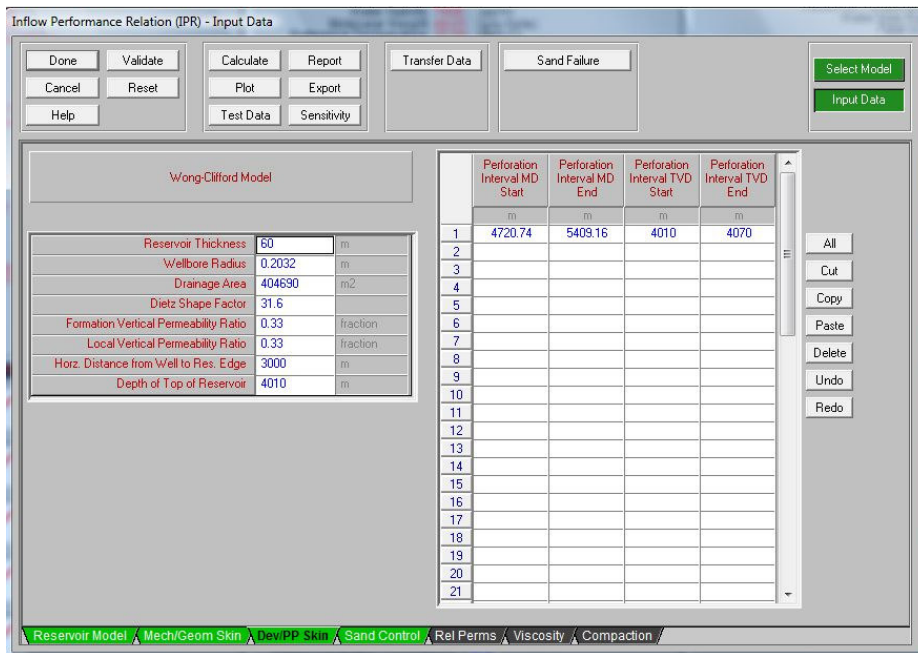
Calculate Dietz

Reservoir Model Mech/Geom Skin DevPP Skin Sand Control Rel Perms Viscosity Compaction

Appendix B 6 Reservoir model input.



Appendix B 7 Mechanical skin.



Appendix B 8 Deviation and partial penetration skin.

Inflow Performance Relation (IPR) - Input Data

Done Validate Calculate Report Transfer Data Sand Failure Select Model
 Cancel Reset Plot Export Input Data
 Help Test Data Sensitivity

Gravel Pack - Open Hole

Gravel Pack Permeability	350000	md
Gravel Pack Length	0.1143	m
Production Interval	60	m
Wellbore Radius	0.2032	m
Beta (Turbulence)	Calculated	
Beta (Turbulence)		1/m

Typical Values		
Gravel Type	Mesh Size	Lab Permeability
		mDarcy
Ottawa Sand	12/20	500000
	20/40	150000
	30/50	90000
	40/60	60000
Carbolite	50/70	30000
	20/40	350000
Isopac	16/20	500000
	20/40	110000

Reservoir Model Mech/Geom Skin DevPP Skin Sand Control Rel Perms Viscosity Compaction

Appendix B 9 Sand control data.

EQUIPMENT DATA (Base Case HD- OHGP.Out)

Done Cancel All Edit Summary
 Report Export Reset Help

Deviation Survey
 Surface Equipment
 Downhole Equipment
 Temperature Data
 Drilling And Completion
 Lithology
 Databases

Disable Surface Equipment No
 Injected Fluid Temperature 40 deg C

Appendix B 10 Equipment data.

DEVIATION SURVEY (Base Case HD- OHGP.Out)

Done Cancel Main Help Filter

Input Data

	Measured Depth	True Vertical Depth	Cumulative Displacement	Angle
	(m)	(m)	(m)	(degrees)
1	0	0	0	0
2	2520	2520	0	0
3	2550	2549.96	1.54868	2.95907
4	2610	2609.53	8.71911	6.86366
5	2670	2668.27	20.9507	11.7628
6	2730	2725.73	38.2235	16.731
7	2790	2781.48	60.4032	21.6947
8	2850	2835.08	87.3668	26.7048
9	2910	2886.13	118.893	31.6976
10	2970	2934.24	154.746	36.6945
11	3030	2979.05	194.647	41.6832
12	4290	3844.79	1110.12	46.5994
13	4350	3882.05	1157.15	51.6108
14	4410	3915.06	1207.25	56.6215
15	4470	3943.58	1260.04	61.6189
16	4530	3967.4	1315.11	66.6092
17	4590	3986.33	1372.05	71.609
18	4650	4000.22	1430.42	76.6146
19	4710	4008.98	1489.77	81.6048
20	4720.74	4010	1500.46	84.5503

Copy Cut Paste Insert Delete All Invert Plot Import Export

MD <> TVD
 4794.99 4009 Calculate

Appendix B 11 Deviation data.

SURFACE EQUIPMENT (Base Case HD- OHGP.Out)

Done Cancel Main Help Insert Delete Copy Cut Paste All Import Export Report Plot

Input Data

	Label	Type	Pipe Length	True Vertical Depth	Pipe Outside Diameter	Pipe Inside Diameter	Burial Depth	Roughness	Insulation	Rate Multiplier
			(m)	(m)	(m)	(m)	(m)	(m)		
1		Manifold		0					Enter	
2		Flexible	475	250	0.2286	0.2032	0	1.524e-5	Enter	1
3		Line Pipe	5800.01	250	0.2032	0.18732	1.27	1.524e-5	Enter	1
4									Enter	
5									Enter	
6									Enter	
7									Enter	
8									Enter	
9									Enter	
10									Enter	
11									Enter	
12									Enter	
13									Enter	
14									Enter	
15									Enter	
16									Enter	

Choke Method ELF
 Coordinate System TVD, Length
 Casing Database Pipe Types Insulation Types
 Total Pipe Length 6275.01 (m)

Appendix B 12 Surface equipment.

DOWNHOLE EQUIPMENT (Base Case HD- OHGP.Out)

Done Cancel Main Help Insert Delete Copy Cut Paste All Import Export Report Tubing DB

Input Data

	Label	Type	Measured Depth (m)	Tubing Inside Diameter (m)	Tubing Outside Diameter (m)	Tubing Inside Roughness (m)	Insulation	Rate Multiplier
1		Xmas Tree	250					
2		St. Steel (25%)	799.999	0.15707	0.1778	1.524e-5	Enter	1
3		SSSV		0.12			Enter	1
4		St. Steel (25%)	4720.74	0.15707	0.1778	1.524e-5	Enter	1
5							Enter	
6							Enter	
7							Enter	
8							Enter	
9							Enter	
10							Enter	
11							Enter	
12							Enter	
13							Enter	
14							Enter	
15							Enter	
16							Enter	
17							Enter	
18							Enter	

Appendix B 13 Downhole equipment.

Temperature Data (Offshore) (Base Case HD- OHGP.Out)

Done Cancel Main Help

Air Temperature 20 deg C
 Humidity 70 percent
 Air Velocity 0 m/sec

Mean Sea Level wrt Origin 0 m
 Sea Bed Depth wrt Origin 250 m

Formation Gradient

	Formation TVD (m)	Formation Measured Depth (m)	Formation Temperature (deg C)
1	0	0	20
2	250	250	8
3	4010	4720.74	155
4			
5			
6			
7			
8			
9			
10			
11			
12			
13			
14			
15			
16			
17			
18			
19			
20			

Sea Gradient

	TVD From Mean Sea Level (m)	Sea Temperature (deg C)	Sea Velocity (m/sec)
1	0	20	0
2	250	8	0
3			
4			
5			
6			
7			
8			
9			
10			
11			
12			
13			
14			
15			
16			
17			
18			
19			
20			

Copy Cut Paste Insert Delete All Invert Plot Import Export

Depth Reference RKB Enter Measured Depth

Appendix B 14 Temperature data.

Lithology (Base Case HD- OHGP.Out)

Done Cancel Main Help Insert Delete Copy Cut Paste All Import Export Report

Lithology

	Formation Type	Bottom Depth (m)	Shaliness (fraction)	Porosity (fraction)	Permeability (md)	Rock Consistency	In Situ Fluid	Salinity (ppm)
1	Limestone	940	0.16	0.2	0.1	Consolidated	Water	30000
2	Sandstone	1425	0.2	0.29	1000	Unconsolidated	Water	100000
3	Sandstone	1687	0.28	0.24	357	Unconsolidated	Water	95000
4	Sandstone	2025	0.53	0.22	195	Consolidated	Water	98000
5	Shale	3341						
6	Sandstone	3400.01	0.25	0.15	100	Consolidated	Water	30000
7	Shale	4716.5						
8	Sandstone	5062.5	0.22	0.12	40	Consolidated	Gas	8000
9								
10								

Reservoir Parameters:

Reservoir Temperature: 155 deg C

Reservoir Pressure: 415 BARa

Dry Rock Properties

In Situ Fluids Properties

Appendix B 15 Lithology.

TEMPERATURE DATABASES - DATA ENTRY (Base Case HD- OHGP.Out)

Done Cancel Save Reset Export Report Main Help

Cement Conductivity: 0.86537 W/m/K

Casing Conductivity: 44.9991 W/m/K

Pipes: Insulation Fluid Rock

Pipe Type	Pipe Conductivity W/m/K	Pipe Emmissivity
Mild Steel Tubing	44.9991	0.65
Coated Tubing	34.6147	0.65
St. Steel (13%)	31.1532	0.4
St. Steel (25%)	25.961	0.3
Line Pipe	46.7298	0.9
Coated Pipe	34.6147	0.9
Flexible Pipe	0.51922	0.95

Appendix B 16 Temperature database - pipes.

TEMPERATURE DATABASES - DATA ENTRY (Base Case HD- OHGP.Out)

Done Cancel Save Reset Export Report Main Help

Cement Conductivity 0.86537 W/m/K Reset

Casing Conductivity 44.9991 W/m/K Reset

Pipes **Insulation** Fluid Rock

Insulation Type	Insulation Conductivity	Insulation Emmissivity
	W/m/K	
Concrete	1.03844	0.95
Foam	0.034615	0.8
Bitumen	0.17307	0.9

Appendix B 17 Temperature database - insulation.

TEMPERATURE DATABASES - DATA ENTRY (Base Case HD- OHGP.Out)

Done Cancel Save Reset Export Report Main Help

Cement Conductivity 0.86537 W/m/K Reset

Casing Conductivity 44.9991 W/m/K Reset

Pipes Insulation **Fluid** Rock

Fluid Type	Fluid Specific Gravity	Fluid Conductivity	Specific Heat Capacity
	sp. gravity	W/m/K	KJ/Kg/K
Water (salinity < 10000.0)	1	0.60576	4.1868
Water (salinity < 200000.0)	1.08	0.5971	4.27054
Water (salinity > 200000.0)	1.15	0.58845	4.35427
Heavy Oil	0.96	0.14365	2.05153
Medium Oil	0.9	0.14279	2.0934
Light Oil	0.84	0.14105	2.0934
Gas	0.01	0.037211	1.08857

Appendix B 18 Temperature database - fluid.

TEMPERATURE DATABASES - DATA ENTRY (Base Case HD- OHGP.Out)

Done Cancel Save Reset Export Report Main Help

Cement Conductivity 0.86537 W/m/K Reset

Casing Conductivity 44.9991 W/m/K Reset

Pipes Insulation Fluid **Rock**

Rock Type	Rock Density	Rock Conductivity	Specific Heat Capacity
	g/cc	W/m/K	KJ/Kg/K
Sandstone	2.65	1.83458	0.76618
Shale	2.4	1.21151	0.93784
Limestone	2.71	0.9346	0.84573
Dolomite	2.87	1.73073	0.91691
Halite	2.17	4.84606	0.91691
Anhydrite	2.96	1.29805	1.1095
Gypsum	2.32	1.29805	1.08438
Lignite	1.5	3.46147	1.25604
Volcanics	2.65	2.76918	0.83736
Fixed Value	2.61	1.90381	0.83736

Appendix B 19 Temperature database - rock.

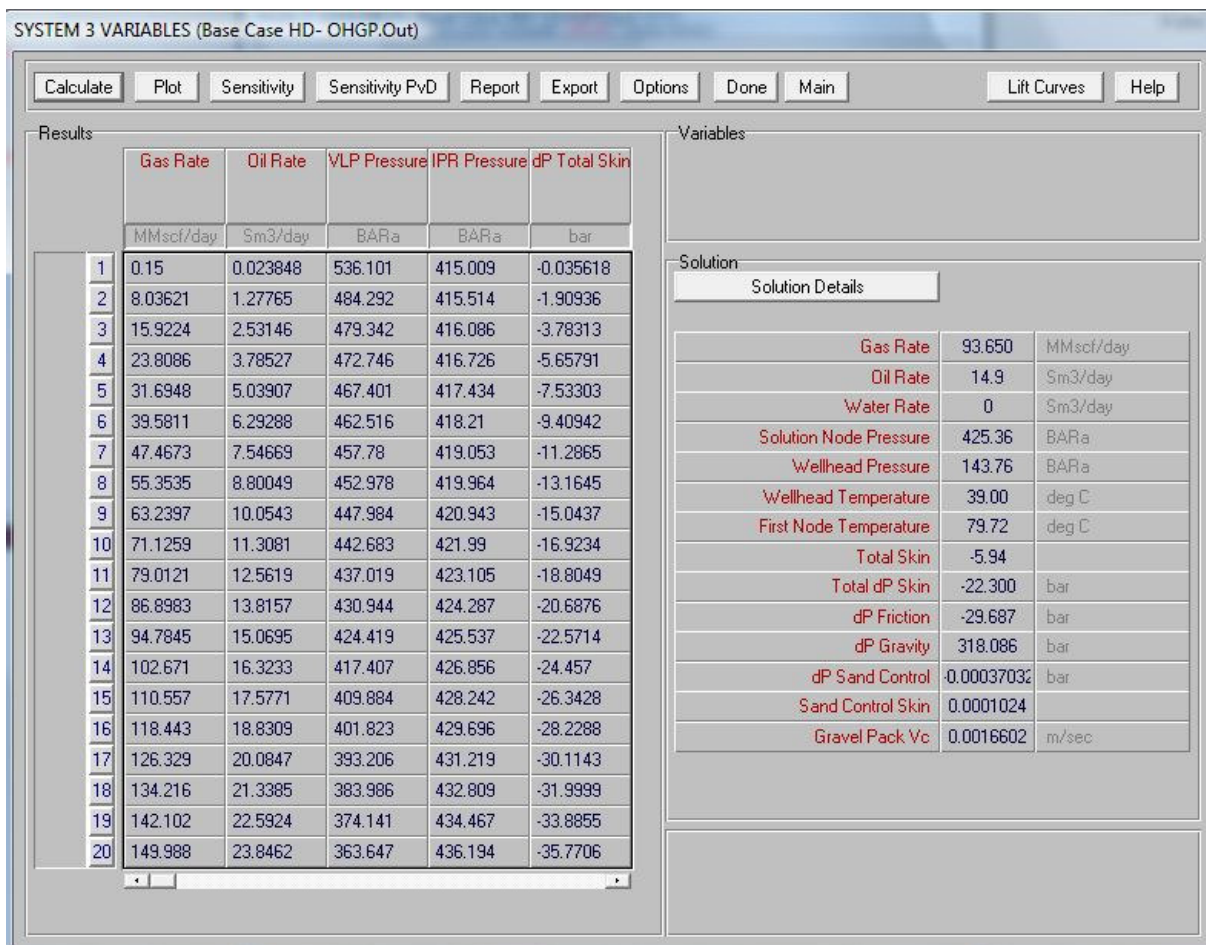
SYSTEM 3 VARIABLES (Base Case HD- OHGP.Out)

Continue Cancel Report Export Help

Input Data

Top Node Pressure	137	BARa
Water Gas Ratio	0	Sm3/Sm3
Total GOR	1000000	Sm3/Sm3
Time Since Production Started	100	days
Surface Equipment Correlation	Petroleum Experts 4	
Vertical Lift Correlation	Petroleum Experts 4	
Solution Node	Bottom Node	
Rate Method	Automatic - Linear	
Left-Hand Intersection	DisAllow	

Appendix B 20 System analysis - 3 variables.



Appendix B 21 Results Base Case OHGP - High Deviation.

Appendix C: Basic Model for Annular Pressure Buildup [78]

Wells with one or more trapped annuli, closed in at the mudline wellhead or hanger system and sealed by the cement between the casings, usually exhibit no axial displacement and consequently no transfer of axial forces between casings. This gives rise to a key simplification in the underlying models. Namely, the effect of casing axial stress/displacement on annulus volume change is substantially smaller than its radial counterpart and may be neglected. Consequently, three partially coupled models may be utilized to represent the annular pressure buildup problem adequately:

- Wellbore thermal model – Used for predicting temperature changes in the tubing, casing, and annular fluids, mainly after a prolonged production period. Relative to the setting temperatures, this prediction establishes the driving thermal “loads” in the well. The setting or packer setting, may conservatively assumed to be those of the undisturbed geothermal gradient. However, it should be noted that owing to circulation of drilling fluids prior to cementation, actual setting temperature might be considerably different from geothermal gradient.
- Fluid expansion model – Used for estimating the volume behavior, i.e., compressibility and thermal expansion, of annular fluids due to the imparted thermal loads, as described above., and any associated change in annular pressure.
- Annular expansion model – Used for calculating changes in the annular space between casing, mainly from radial strains, due to the imparted thermal loads, as described above, and any associated change in annular pressures.

Note that the fluid expansion model and the annulus expansion model are coupled through pressure and must be solved simultaneously.

Consider an annulus between two casings, filled with a drilling fluid, closed in at the mudline. At bottom, the annulus is sealed by the cement between the casing, which allows no radial or axial movement of the strings. At the mudline, the wellhead of a subsea well is axially fixed by cemented foundation pile, which, likewise, allows no axial displacement and consequently no transfer of axial forces between the casing.

Initially, at the time the annulus becomes sealed, the casing and fluid temperature are assumed to be those of the undisturbed geothermal gradient. When the well is produced over a prolonged period, the hot well effluent, in particular in HPHT or high-rate well, will increase the temperature of the annulus. Since axial displacement are not allowed in this case, both the annular fluid and the annulus walls will tend to expand. Thermal expansion of the base fluid of which the drilling mud consists, $\Delta V_{\text{fluid}}(\Delta T)$, is considerably larger than the thermal expansion of carbon steel, $\Delta V_{\text{cas}}(\Delta T)$; i.e. the pressure in the annulus will rise to the extent that volume increase of the annulus fluid is suppressed by compression, $\Delta V_{\text{fluid}}(\Delta P)$. In itself this pressure increase will give rise to some ballooning of the casing walls, which creates some extra volume for the liquid to expand, $\Delta V_{\text{cas}}(\Delta P)$. Eventually, a new equilibrium between the casing is obtained. Mathematically this can be expressed as follows:

$$\Delta V_{\text{fluid}}(\Delta T) + \Delta V_{\text{fluid}}(\Delta P) = \Delta V_{\text{cas}}(\Delta T) - \Delta V_{\text{cas}}(\Delta P) \quad (\text{C-1})$$

In order to evaluate the resulting pressure increase, ΔP , the volume changes, ΔV , have to be expressed as function of the (known or estimated) temperature change, ΔT , the unknown pressure change, ΔP , the properties of the annular fluids and the casing steel, and the annulus geometry.

Basic Fluid Expansion Model

The first term of the left-hand side of equation (C-1) is simply the thermal expansion of the initial volume of the annular fluids, expressed in terms of the isobaric coefficient of thermal expansion, C_T :

$$\Delta V_{fluid}(\Delta T) = V_{fluid} \cdot C_T \cdot \Delta T \quad (C-2)$$

Similarly the fluid volume change caused by the increase in the annular pressure can be expressed in terms of the isothermal fluid compressibility, C_p :

$$\Delta V_{fluid}(\Delta P) = -V_{fluid} \cdot C_p \cdot \Delta P \quad (C-3)$$

Note that in a completely rigid, non-expanding casing string, the terms on the right-hand side of the equation (C-1) would vanish. By inserting equation (C-2) and equation (C-3), we can then obtain for pressure increase:

$$\Delta P = \Delta T \cdot \frac{C_T}{C_p} \quad (\text{completely stiff casing}) \quad (C-4)$$

In practice, both terms of the right-hand side of equation (C-1) are non-vanishing.

Basic Annulus Expansion Model (Temperature Effects)

If the thermal volume expansion of the annular fluids equals the thermal expansion of the casing steel, the two terms depending on ΔT in equation (C-1) cancel. Since the remaining terms are both linear in the pressure increase, this pressure increase would effectively vanish. However, thermal expansion of steel is considerably less than that of the annular fluid. In addition, expansion of the inner casing reduces the annulus volume while that of the outer casing increases it, typically with a positive net effect. Hence, even in the absence of casing elastic effects (ballooning), a pressure rise would develop in a sealed annulus that is heated by the well effluent.

To evaluate the casing steel expansion, first note that all casing have been considered fixed at both ends. This implies that only radial expansion has to be taken into account. In general, the increase in diameter, d , of a cylinder that is raised in temperature is given by:

$$\Delta d = d \cdot \alpha \cdot \Delta T \quad (C-5)$$

where α is the coefficient of linear thermal expansion of steel. A typical value for carbon steel is $1.24 \times 10^{-5}/^\circ\text{C}$. In terms of the resulting volume change of the cylinder:

$$\Delta V_{cyl} = \frac{\pi \cdot L \cdot [(d + \Delta d)^2 - d^2]}{4} \quad (C-6)$$

By neglecting the quadratic term, Δ^2 , in equation (C-6) and inserting equation (C-5), we obtain the volume change of a cylinder fixed at both ends:

$$\Delta V_{cyl} = 2 \cdot V_{cyl} \cdot \alpha \cdot \Delta T \quad (C-7)$$

The total change in the volume of an annulus between an outer and inner cylinder on heating is given by:

$$\Delta V_{cas} = \Delta V_{cyl,o} - \Delta V_{cyl,i} \quad (C-8)$$

By inserting equation (C-7) and assuming that the temperature change and steel properties in both casings will be the same, which is correct in most cases, the change in annular volume caused by thermal expansion by a corrected coefficient, $C_T - 2 \cdot \alpha$:

$$\Delta P = (C_T - 2 \cdot \alpha) \cdot \Delta T / C_p$$

Basic Annulus Expansion Model (Pressure Effect)

With increasing pressure in the annulus, the confining casing will tend to balloon, which gives the fluid additional volume to expand. Again no axial displacement is allowed: fixed-fixed casing. This implies that only radial expansion has to be taken into account. The change in diameter corresponding to a tangential strain change, $\Delta \epsilon_t$, caused by the pressure change, is given by:

$$\Delta d = d \cdot \Delta \epsilon_t \quad (C-10)$$

This strain has to be expressed as a function of the pressure change in and outside the cylinder. Assuming that most casings can be treated effectively in a thin-walled cylinder and neglecting the effect of axial stress, the change in casing diameter can be written as:

$$\Delta d = \frac{d^2}{2 \cdot E \cdot t} \cdot \Delta P \quad (C-11)$$

where E is Young's modulus and t is the casing wall thickness. In the case considered so far, the pressure change is the increase inside the cylinder. If pressure also builds up outside, this pressure change has to be subtracted from the inside to obtain an effective pressure change. This applies to both the inner and outer casing of the annulus. At this stage, only pressure change inside the annulus is assumed. Similar to equation (C-7), the change in diameter can be converted to change in cylinder volume:

$$\Delta V_{cyl} = V_{cyl} \cdot \frac{d}{E \cdot t} \cdot \Delta P \quad (C-12)$$

For the resulting total volume change of the annulus, the contraction of the inner cylinder and the expansion of the outer cylinder have to be added:

$$\Delta V_{cas}(\Delta P) = \left(V_{cyl,i} \cdot \frac{d_i}{t_i} + V_{cyl,o} \cdot \frac{d_o}{t_o} \right) \frac{1}{E} \cdot \Delta P \quad (C-13)$$

assuming that the elastic properties of both casing are equal. This expression can be inserted for the second term of the right-hand side of equation (C-1), which can now be solved for the case of a single annulus in which pressure buildup occurs.

Shortcomings of the Basic Model

Annular fluid heat-up may give rise to considerable pressure increase in closed annuli. The equations presented to provide a first-order approximation of the magnitude of the pressure rise are, however, based on a number of assumptions the validity of which is hitherto unknown:

- The cement closing off the annulus at the casing shoe is considered perfectly sealing and impermeable. Obviously, leak-off of annular fluid to the surrounding formations could have a large impact on pressure build-up.
- Similarly, the casing have been considered perfectly leak tight. Again, transfer of limited amounts of annular fluids between casings would have a large impact on eventual pressure.
- The annuli were assumed to be filled completely with liquid, so that small temperature changes give large pressure rises, due to the low compressible nature of liquids. The presence of more compressible fluids or components would be beneficial.
- The derivation of equation (C-13) is based on thin-walled cylinder equations, neglecting the effect of axial stress.
- The fluid compressibility and coefficient of thermal expansion are assumed to be independent function of pressure and temperature.
- The cemented sections of the annulus walls are assumed to be fully rigid.

Values used in calculations:

Casing: OD – 9.625", ID – 8.535"

Tubing: OD – 7", ID – 6.18"

Annular volume: 52.83 m³

Water based mud: $C_T=2.07 \cdot 10^{-4}$ 1/°C, $C_p=4 \cdot 10^{-5}$ bar

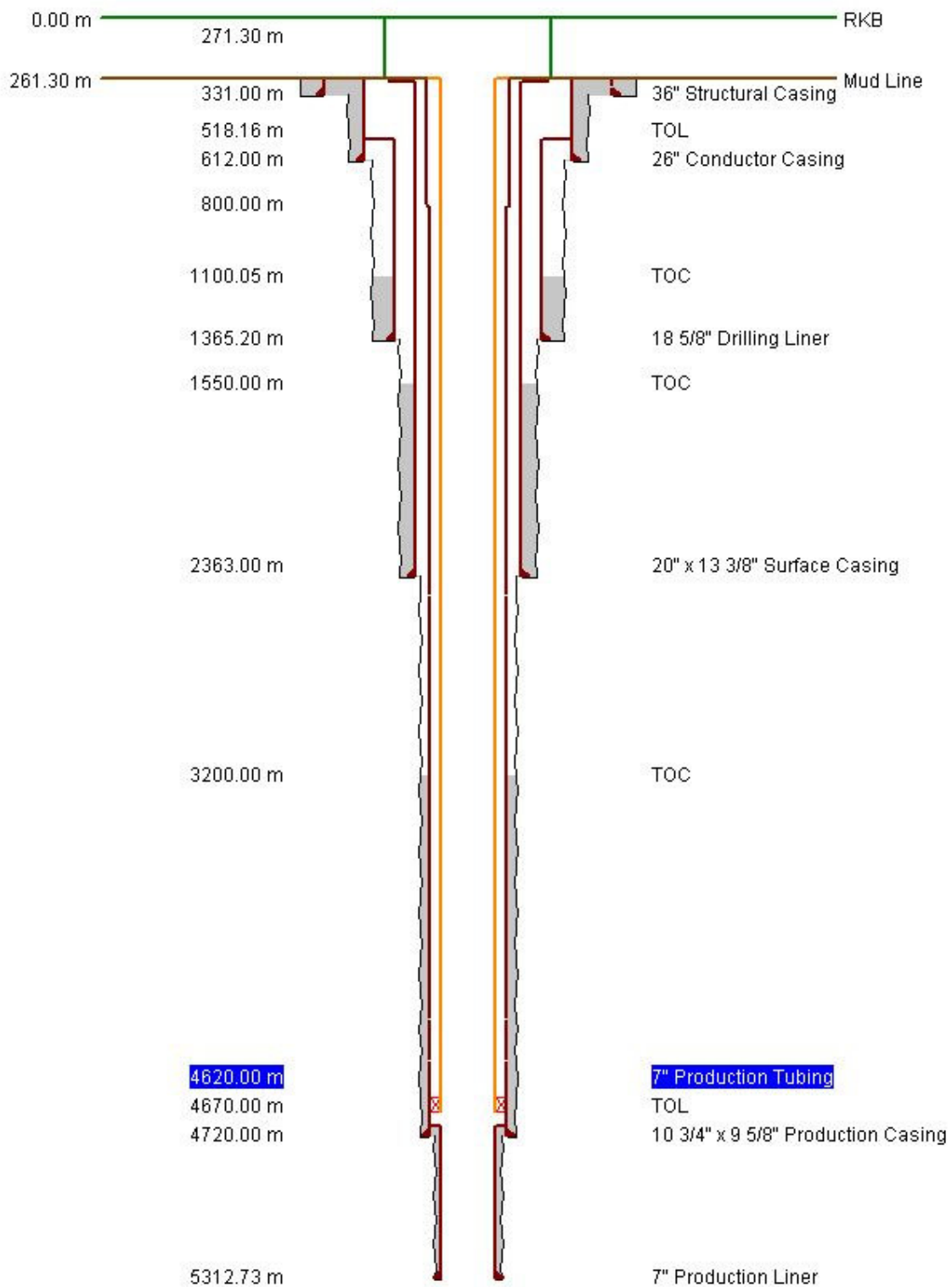
Base oil: $C_T=8.64 \cdot 10^{-4}$ 1/°C, $C_p=6.45 \cdot 10^{-5}$ bar

Carbon steel: $\alpha=1.24 \cdot 10^{-5}$ 1/°C, $E=2.1 \cdot 10^{11}$ Pa

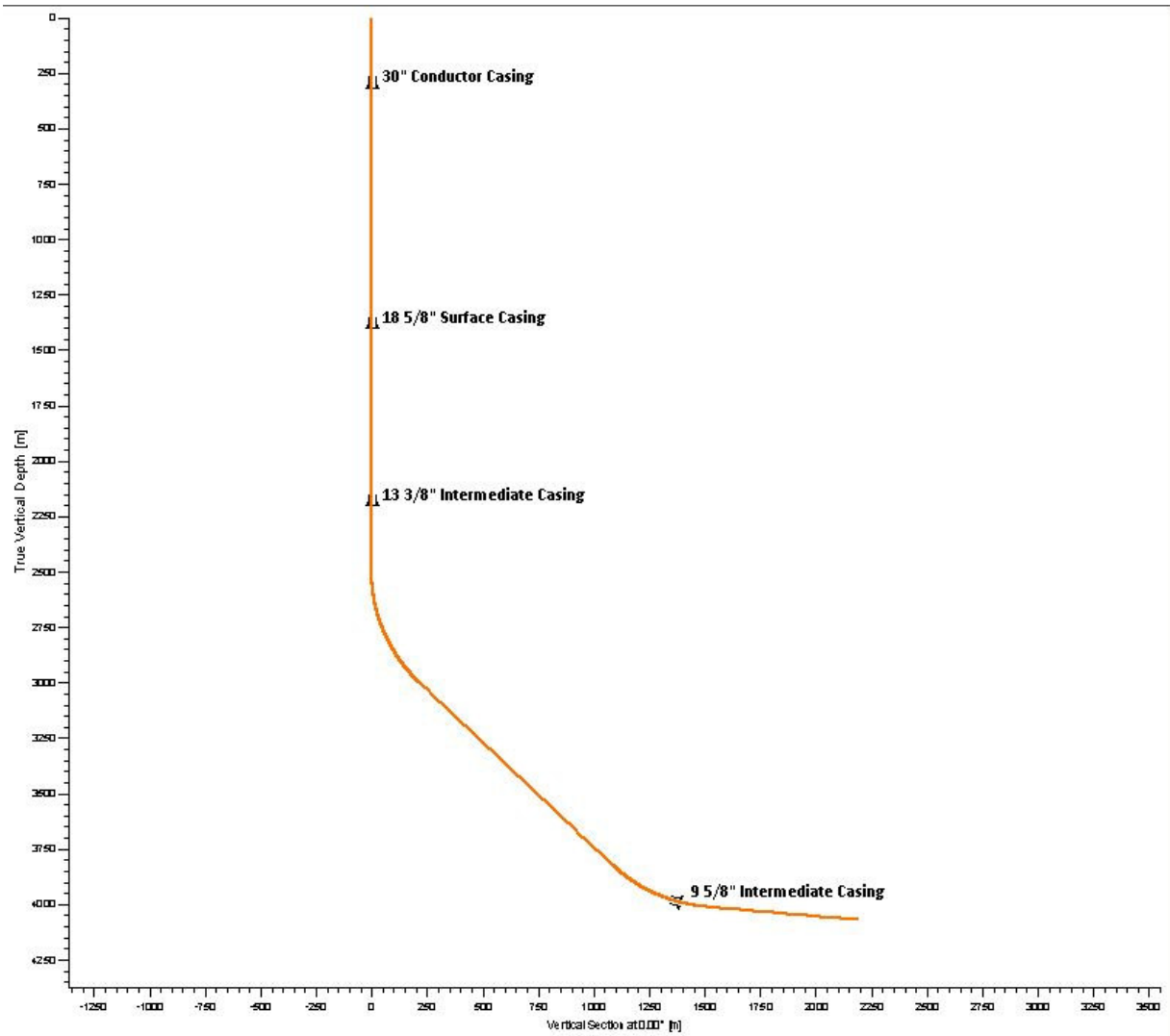
Stainless steel: $\alpha=1.5 \cdot 10^{-5}$ 1/°C, $E=2.1 \cdot 10^{11}$ Pa

Depths: Tubing – 4620 mAHD, Casing cemented up to 3000 mAHD, WH at 250m

Appendix D: Well Schematic



Appendix D 1 Well schematic (depth is MD)



Appendix D 2 Section view.